Structure and Regulation of NHX Exchangers in the Uptake of Potassium into the Vacuoles of *Arabidopsis thaliana*

Memoria que presenta

la Licenciada en Biotecnología **María Belén Rombolá Caldentey**

para optar al título de Doctora en Biología

por la Universidad de Sevilla

Sevilla a 25 de octubre de 2018

Structure and Regulation of NHX Exchangers in the Uptake of Potassium into the Vacuoles of *Arabidopsis thaliana*

Visado en Sevilla, a 25 de octubre de 2018

EL DIRECTOR

Dr. José Manuel Pardo Prieto

Profesor de Investigación del CSIC

Universidad de Sevilla - Instituto de Bioquímica Vegetal y Fotosíntesis (IBVF, CSIC)

EL TUTOR

Dra. Cristina Echavarría Ruiz de Vargas

Catedrático de la Universidad de Sevilla

Universidad de Sevilla, Facultad de Biología

Memoria que presenta

la Licenciada en Biotecnología María Belén Rombolá Caldentey

para optar al título de Doctora en Biología

por la Universidad de Sevilla

DOCTOR D. FRANCISCO JAVIER CEJUDO, DIRECTOR DEL INSTITUTO DE BIOQUÍMICA VEGETAL Y FOTOSÍNTESIS (IBVF), CENTRO MIXTO DEL CONSEJO SUPERIOR DE INVESTIGACIONES CIENTÍFICAS Y LA UNIVERSIDAD DE SEVILLA

CERTIFICA: Que la presente Memoria de Investigación titulada "Structure and Regulation of NHX Exchangers in the Uptake of Potassium into the Vacuoles of *Arabidopsis thaliana*", presentada por la Licenciada en Biotecnología María Belén Rombolá Caldentey para optar al grado de Doctora en Biología, ha sido realizada en el Instituto de Bioquímica Vegetal y Fotosíntesis, bajo la dirección del Profesor Dr. José Manuel Pardo Prieto, reuniendo todas las condiciones exigidas a los trabajos de Tesis Doctorales.

En Sevilla, a 25 de octubre de 2018.

Dr. Francisco Javier Cejudo

El presente trabajo se ha realizado en el marco de los proyectos BFU2012-35060 y BFU2015-64671-R del Plan Nacional de I+D+i y dentro del Programa Nacional de Formación de Personal Investigador con una Ayuda para Contratos Predoctorales para la Formación de Doctores del Ministerio de Economía y Competitividad (BES-2013-064466). También se ha disfrutado de una Ayuda para Facilitar la Movilidad de Investigadores en Formación del Ministerio de Economía y Competitividad y de una Beca para la Movilidad de Estudiantes en Grados Superiores Erasmus Plus+ en Prácticas de la Comisión Europea.

Agradecimientos.

INDEX

INTRODUCTION

I.1. Salt stress in plants

Salt stress is one of the major abiotic stresses that causes serious constraint to agriculture production around the world, leading to food crises. According to the Food and Agricultural Organization (FAO), soil salinity will destroy 50% of the arable lands throughout the world by the year 2050 (FAO, 2017). Soils are regarded as salt-affected, if they have salt concentrations above the thresholds of toxicity.

Salinity stress causes osmotic stress and ionic toxicity in plants cells. High salt concentration in soil reduces the soil's water potential, hampering the uptake of water (Munns et al. 2006; Pardo 2010; Roy et al. 2014), and the excess of sodium (Na^+) ions accumulated in plant tissues produces cellular toxicity.

Once Na^+ overcomes the root-soil boundary, either through non-selective cation channels (NSCC), including cyclic nucleotide-gated channels (CNGCs) and glutamate receptors (GLRs), high affinity K^+ transporters (HKTs), K^+ channels (Tester and Davenport 2003; CRAIG PLETT and MØLLER 2010; Hanin et al. 2016), or even aquaporins (Byrt et al. 2017), the ion moves to the xylem, and it is finally delivered to the shoot, specially to the leaf blade, where its effects are more dramatic (Munns and Tester 2008). Na^+ interferes with K^+ homeostasis and generates ion imbalance in the cytosol (Munns and Tester 2008; Assaha et al. 2017). K^+ is an essential macronutrient that plays important functions related to enzyme activation, osmotic adjustment and turgor generation, regulation of membrane electrical potential, and cytoplasmatic and vacuolar pH homeostasis (Barragán et al. 2012). Due to the similar physico-chemicals properties displayed by Na^+ and K^+ (i.e., ionic radius and hydration energy), Na^+ competes with K^+, inhibiting enzyme activity in key metabolic processes, and finally leading to malfunction of plant cells and tissues (Almeida et al. 2017; Munns 2005; Munns and Tester 2008).

The increase of osmotic soil potential, induces water loss and reduction in turgor pressure of plant cells, as a consequence of this cellular response, mechanosensitive receptor kinase cyclase might be activated, resulting in the accumulation of cGMP (Shabala et al. 2015). The accumulation of this compound deactivates NSCC, inhibiting Na^+ influx (Maathuis and Sanders 2001) and activating cyclic nucleotide-gated channels (CNGC) (Mäser et al. 2001) that facilitate calcium (Ca^{2+}) entry. The increase of this cation in the cytosol is sensed by different calcium binding proteins or calcium sensors, such as Ca^{2+}/calmodulin (CaM)-dependent kinases, which stimulate plasma-membrane H^+-ATPases, restoring membrane voltage and inhibiting depolarization-activated NSCCs (Shabala et al. 2006; SUN et al. 2010). Moreover,

the salt overly sensitive (SOS) pathway which is essential for salt tolerance is activated by Ca2+.

Salt stress tolerance mechanism

The sessile nature of plants has obliged them to develop mechanisms to overcome the detrimental effects of high salt concentration in soil. The mechanisms of salinity tolerance consist of 3 main processes: osmotic stress tolerance, Na^+ exclusion of the cell and Na^+ compartmentalization in the vacuole. The first one, involves biosynthesis and accumulation of compatible organic solutes to maintain water uptake (Munns and Tester 2008) helping to maintain protein structure or increasing scavenging of reactive oxygen species. The other two processes are more important since they contribute to maintain a balanced cytosolic K^+ /Na^+ ratio, a physiological trait considered essential for a successful adaptation of the plant to a saline environment

Na^+ exclusion of the root is mainly achieved by transporters that mediate Na+ extrusion out of the cell at the epidermis and transporters of the parenchyma cells surrounding the vessels that control the net Na+ flux into the xylem sap (Figure 1). Two main proteins have been described to be involved in this process: SOS1/AtNHX7 and HKT1(Shi et al. 2002; Shi and Zhu 2002; Sunarpi et al. 2005; Pardo 2010; Kronzucker and Britto 2011; Conde et al. 2011).

The High Affinity Potassium Transporter family (HKT) (Munns and Tester 2008; Roy et al. 2014) is divided in two distinct classes (Platten et al. 2006). In Arabidopsis, class I HKTs are localized mainly to the xylem/symplast boundary of roots and shoots, where they unload Na^+ from the xylem to the xylem parenchyma cells in both roots and shoots, reducing Na^+ transport from root to shoot and avoid excessive Na+ accumulation in the shoots (Mäser et al. 2002; Berthomieu et al. 2003; Sunarpi et al. 2005; DAVENPORT et al. 2007). Disruption of AtHKT1;1 causes a higher accumulation of Na+ in the shoots but reduced concentration in roots, with little effect on the net Na^+ uptake (Pardo 2010; Kronzucker and Britto 2011). It is

also true for rice OsHKT1;5 (Horie et al. 2012; Cotsaftis et al. 2012) and wheat TmHKT1;5D (Munns et al. 2012)

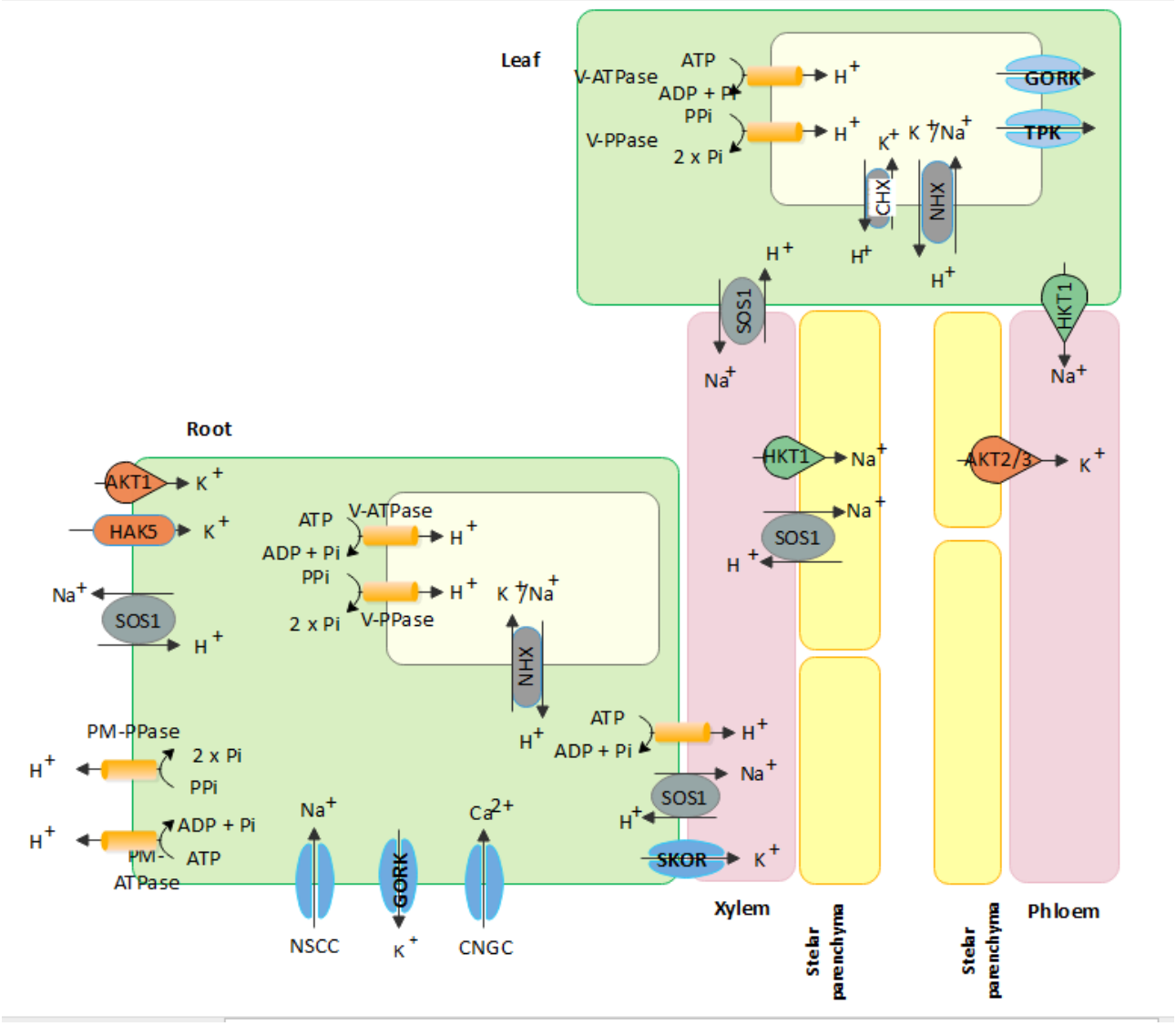

Figure 1. Schematic representation of key transporters, channels and pumps mediating Na^+ and K^+ homeostasis in plants under salt stress (adapted from Roy et al, 2014). Na^+ ions enter the cells via Non Selective Cation Channels (NSCCs) and possibly via other cation transporters not shown. The extrusion of K+ is induced. SOS1 reduces net influx of Na^+ by extruding it at the root soil interface. At the xylem parenchyma cells, HKT1 and SOS1 retrieve Na^+ from the xylem sap. To translocate Na^+ back to the root, HKT1 proteins also load Na^+ into phloem from shoot. SOS1, localized in the xylem parenchyma cells, is also suggested to mediate Na^+ efflux from xylem vessels under high salinity. Incoming Na^+, in root and shoots, is stored in the large central vacuole maybe by tonoplast-localized NHX exchangers (NHX1-4). Plasma membrane (PM) H^+-ATPase (P-ATPase), PM H^+-PPase (PM-PPase), tonoplast H^+-ATPase (V-ATPase) and tonoplast H^+-PPase (V-PPase) generate electrochemical potential gradient for secondary active transport.

I.1.2. Salt stress tolerance mechanism

The sessile nature of plants has obliged them to develop mechanisms to overcome the detrimental effects of high salt concentration in soil. The mechanisms of salinity tolerance consist of 3 main processes: osmotic stress tolerance, Na^+ exclusion of the cell and Na^+ compartmentalization in the vacuole. The first one, involves biosynthesis and accumulation of compatible organic solutes to maintain water uptake (Munns and Tester 2008) helping maintain protein structure or increasing scavenging of reactive oxygen species. The other two methods are becoming more important since maintaining a balanced cytosolic K^+ /Na^+ ratio has come to be a key point in salinity tolerance mechanism, attributing salt stress sensitivity almost exclusively to K^+ deficiency (Véry and Sentenac 2003).

Na^+ exclusion from roots is mainly achieved by transporters that controls Na^+ extrusion out of at epidermis and cortex at the root level, and load of the ion into the xylem or retrieval from the xylem to the parenchyma cells before reaching the photosynthetic tissues in the shoot (Figure 1). Two main proteins have been described to be involved in this process: SOS1/AtNHX7 and HKT1(Shi et al. 2002; Shi and Zhu 2002; Sunarpi et al. 2005; Pardo 2010; Kronzucker and Britto 2011; Conde et al. 2011). The High Affinity Potassium Transporter family (HKT) (Munns and Tester 2008; Roy et al. 2014) is divided in two distinct classes (Platten et al. 2006). In Arabidopsis, class I HKTs are localized mainly to the xylem/symplast boundary of roots and shoots, where they unload Na^+ from the xylem to the xylem parenchyma cells in both roots and shoots, reducing Na^+ transport from root to shoot and avoid excessive Na^+ accumulation in the shoots (Mäser et al. 2002; Berthomieu et al. 2003; Sunarpi et al. 2005; DAVENPORT et al. 2007). Disruption of AtHKT1;1 causes a higher accumulation of Na^+ in the shoots but reduced concentration in roots, with little effect on the net Na^+ uptake (Pardo 2010; Kronzucker and Britto 2011). It is also true for rice OsHKT1;5 (Horie et al. 2012; Cotsaftis et al. 2012) and wheat TmHKT1;5D (Munns et al. 2012).

SOS1/AtNHX7 is a plasma membrane protein member of the CPA1 family (discussed later). This antiporter uses the proton motif energy generated by the plasma membrane P-type H^+-ATPase (P-type H^+ ATPases) to extrude one Na^+ ion to the apoplast, introducing a H^+ to the cytosol. Different orthologues have been identified in several plants including Arabidopsis , rice, wheat, barley and tomato (Wu et al. 1996; Martínez-Atienza et al. 2007; Xu et al. 2008). The significance of SOS1/AtNHX7 arise for it implication in the SOS pathway, which is one of the most important pathway involved in Na^+ homeostasis and salt tolerance (Shi and Zhu 2002; Shi et al. 2003; Oh et al. 2009, 2010; GAO et al. 2012; Ji et al. 2013). It consists of three

components: a calcineurin-B like protein (CBL) which binds calcium, located in the plasma membrane (SOS3/CBL4); CBL-interacting protein (CIPK) that is a serine/threonine protein kinase (SOS2/CIPK24); and a Na+/H+ antiporter (SOS1/AtNHX7). The influx of Na^+ under salinity stress is sensed by the plant, triggering Ca^{2+} release from the sink organelles. Upon sensing the variation in cytosolic calcium concentration, SOS3/CBL4 recruits SOS2/CIPK24 to the plasma membrane and binds to its regulatory domain to activate it. Then, SOS2/CIPK24 is able to phosphorylates SOS1/ AtNHX7, stimulating it to extrude Na^+ in exchange for H^+ into the apoplast of root cortex and epidermis (Halfter et al. 2000; Shi et al. 2002; Quintero et al. 2011). The membrane depolarization induced by salt stress, enhances P-type H^+ -ATPase activity, and it hyperpolarizes the membrane. The proton motive force generated across maintain SOS1 activity. The SOS pathway takes place in both shoot and root with a difference in the Ca^{2+} sensor protein. While CBL4 has only been described to be expressed in the roots of Arabidopsis thaliana, in the shoot it is replaced by another the orthologue SOS3-like Ca^{2+} binding protein, SCaBP/CBL10, AtNHX7 activity needs to be activated by the complex CBL/CIPK24 in order to extrude Na^+ (Ji et al. 2013)(Figure 1).

Finally, Na^+ is compartmentalized at intracellular level (especially in the vacuole) reducing the deleterious effect of Na^+ in the cytosol and driving water uptake to cells (Munns and Tester 2008). Vacuolar Na^+/H^+ antiport activity was shown for the first time in tonoplast vesicles from red beet storage tissue (Blumwald and Poole 1985). The Na^+/H^+ antiport was described as dependent of the electrochemical – gradient of protons generated by the vacuolar H^+ ATPase and (V-ATPase) and the vacuolar H^+ pyrophosphatase (V-PPase) (Blumwald 1987). But the identification of AtNHX1 as the responsible of this transport, and the existence of other NHX in Arabidopsis genome, was possible with the *Arabidopsis* genome-sequencing project. This was based in the conservation and similarity of the AtNHX protein with the previously described Na+/H+ antiporter in yeast (Nhx1). Later it was demonstrated that the expression of AtNHX1 in yeast suppresses some of the salt sensitivity phenotypes of the of the *Δnhx1* mutant, suggesting a similar functioning (Gaxiola et al. 1999; Aharon et al. 2003). Moreover, the first assays overexpressing AtNHX1 in Arabidopsis, showed an increased salt tolerance respect to the wild type plant, sustained growth and increased vacuolar antiport of Na^+, activity consistent with increased vacuolar compartmentation of Na^+. This made the AtNHX proteins of high interest for agricultural application. Constitutive overexpression of *AtNHX1* also increased salt stress tolerance in tomato (Zhang and Blumwald 2001) and cotton (He et al. 2005).

However, Venema et al. (2002) showed that AtNHX1 can transport Na^+ and K^+ with equal affinity, suggesting not only a function on Na^+ detoxification upon saline stress, but also K^+ transport would imply a function in endosomal osmoregulation and/or pH control. Later studies with Arabidopsis *nhx1 nhx2* double mutant made evident that the AtNHX proteins are essential mediating K^+/H^+ exchange rather than Na^+/H^+ (Bassil et al. 2011b; Barragán et al. 2012; Andres et al. 2014), and it was proposed that Na^+/H^+ exchange would take place in situations in which the Na^+ concentrations in the cytosol is higher than K^+ concentrations (Jiang et al. 2010; Maathuis 2014). For these reason, it is more likely that the contribution of NHX-like protein to plant salt stress tolerance is the maintenance of K^+ homeostasis rather than sequestration of Na^+ into the vacuole (Maathuis 2014)

I.2. Arabidopsis thaliana NHX family.

AtNHXs are integral membrane proteins encoded by a multigene family formed by AtNHX1 through NHX6, residing in the intracellular membranes, and two additional proteins, AtNHX7/SOS1 and AtNHX8, which are found in the plasma membrane (Apse et al. 1999; Shi et al. 2000; Pardo et al. 2006; An et al. 2007; Apse and Blumwald 2007). They belong to the highly conserved monovalent cation/proton antiporter superfamily (Brett et al. 2005a; Pardo et al. 2006; Chanroj et al. 2012) , were they are classified into different subgroups depending on their localization.

The monovalent cation proton antiporter (CPA) superfamily is a highly conserved group of transmembrane proteins that exchange cation for H^+ in the opposite direction to modulate locally pH, electrical and cation balance. This highly conserved family is ubiquitous in organisms across all phyla and kingdoms, and underlies fundamental homeostatic mechanisms to control monovalent ions (Na^+, H^+ and K^+). The superfamily of monovalent CPAs can be classified into two families: CPA1 and CPA2 (Brett et al. 2005a; Chanroj et al. 2012, 2013).

AtNHX proteins belong to the CPA1-type transporters (Brett et al. 2005a). This family arose from archea NhaP genes and are known to transport Na^+, K^+ or Li^+ ion exchange for H^+ in an electroneutral and pH-dependent manner (Chanroj et al. 2012). This is the best characterize family and can be divided into three subfamilies according to their location in the cell: intracellular NHE like proteins (IC-NHE), plasma membrane NHE like proteins (PM-NHE) and third group named SOS1/NhaP-like, which is restricted to bacteria, protozoa, and plants proteins, and shows similarity to both PM-NHE and IC-NHE CPA1 subfamilies (Brett et

al. 2005a; Rodríguez-Rosales et al. 2009; Chanroj et al. 2012) (Figure 2). In this latter one can be found AtNHX7 and AtNHX8. The IC-NHE can be subdivided in classes according to the location in the intracellular membrane the protein is localized:

AtNHX1 to AtNHX4, which localize to the vacuole, are included in the IC-NHE class I, which is exclusively presented in plants. It also includes at least two proteins in *Oryza sativa* (rice; OsNHX1 and OsNX2; (Fukuda et al. 1999), one in tomato (LeNHX1;(Venema et al. 2003), one in *Brassica napus* (Wang et al. 2003), one in Japanese morning glory (*Ipomoea nil*; InNHX (Yoshida et al. 2005), among others.

AtNHX5 and AtNHX6, localize in the endosomal system, so they are included in IC-NHE class II with yeast ScNHX1, at least one LeNHX2 from tomato (*Lycopersicon esculentum*) and other mammalian proteins.

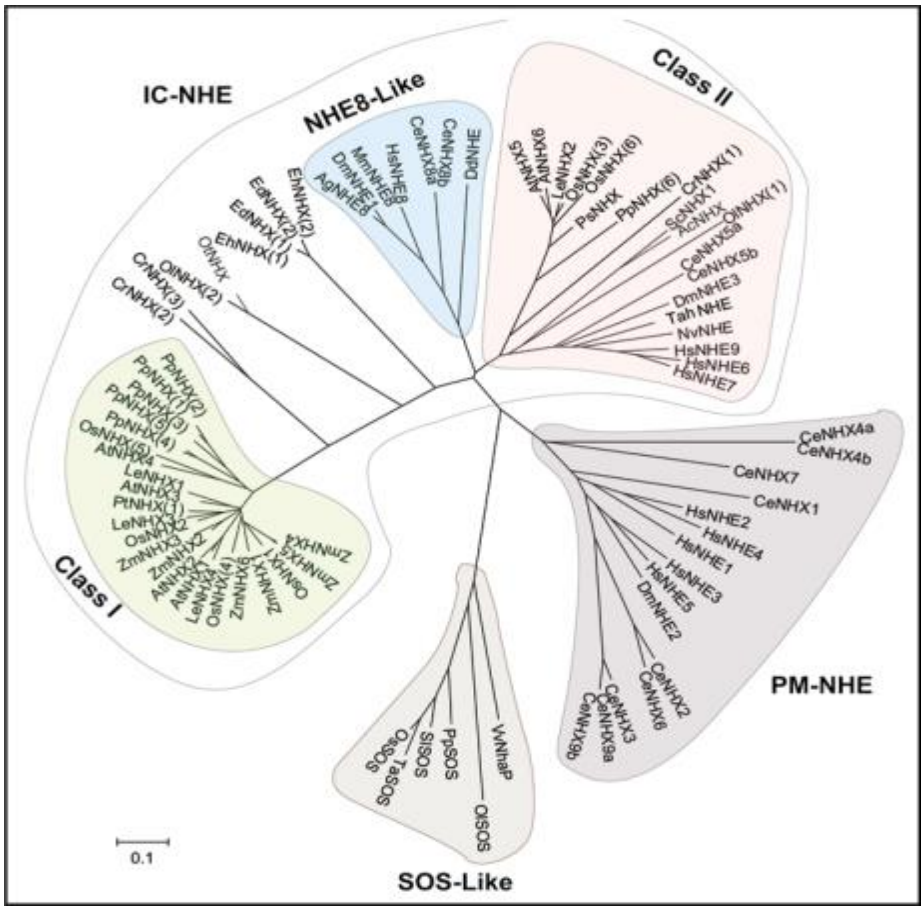

Figure 2. Phylogenetic Tree of Several Members of the Monovalent Cation Proton Antiporter CPA1 Family. AtNHX1-4 belong to the class I of intracellular NHE (IC-NHE) while AtNHX5 and AtNHX6 belong to the class II. Figure taken

Ectopic expression of many of the plant NHX genes in yeast *nhx1Δ*mutants partially complements the salt- and hygromycin-sensitive phenotypes of the latter (Yokoi et al. 2002; Xia et al. 2002; Fukuda et al. 2004, 2011; Wu et al. 2009; Ye et al. 2009).

Biochemical characterization of representative members has shown that they are able to transport both K^+ and Na^+. However certain selectivity for ion substrate can be distinguish between the exchangers. While the vacuolar members show similar Na+/H+ and K+/H+ exchange affinity (Venema et al., 2002; Apse et al., 2003; Barragán et al., 2012) the endosomal class-II proteins present a preference for K+ over Na+ as substrate (Venema et al., 2003). The NHX proteins couple their activity to the H^+ electrochemical gradient maintained by the V-type H^+-ATPase (V-ATPase) and Vacuolar pyrphosphatases (V-PPase), They serve as proton leaks to counter acidification promoted by the activity of V-ATPases and V-PPase in the intracellular compartments, making them excellent regulators of intracellular pH (Andres et al. 2014; Bassil and Blumwald 2014; Reguera et al. 2015).

The CPA2 family comes from a common ancestral bacterial proteins; CHX and KEA proteins from Arabidopsis belong to this family, and the only two mammals' proteins are found: the HsNHA1 and HsNHA2 (Brett et al. 2005a; Schushan et al. 2010). They have a common archaeal bacterial protein, *Escherichia coli* NhaA (EcNhaA), which was the first protein of this superfamily which crystal structure was obtained (Hunte et al. 2005a; Padan et al. 2009; Lee et al. 2014). The knowledge of the structure of this protein has allowed a better understanding of its functionality and regulation, and has shed light on the knowledge of more evolved proteins of the superfamily. CPA2 members are electrogenic proteins. It was believed that this property was due to the active center formed by two essential aspartic acids located in transmembrane 5 of the protein. Nonetheless, recent studies in *Thermus thermophilus* NapA (TtNapA) has put this hypothesis in in jeopardy (Uzdavinys et al. 2017). Uzdavinys et al (2017) postulated showed that the mutation of a conserved lysine in the transmembrane fragment number 11 into arginine turned the electrogenic protein in electroneutral. This conserved residue in CPA1 family is exchanged for an arginine. CPA1 proteins are electroneutral, and they all have an active center formed by an asparagine and an aspartic acid (ND-motif) which, according to the literature gives them the electroneutral properties (Hunte et al. 2005a).

I.2.1. AtNHX expression pattern

The intracellular location of AtNHX has been widely studied and documented either the vacuolar AtNHX1-4 (Hamada et al. 2001; Yokoi et al. 2002; Fukuda et al. 2004; Ohnishi et al. 2005; Yoshida et al. 2005; Jin et al. 2016) and the endosomal AtNHX5-6 (Pardo et al. 2006; Rodriguez-Rosales et al. 2008; Bassil et al. 2011a). Less has been reported about the tissues or cells specific expression.

Yokoi et al. (2002) reported that the six AtNHX (1-6) genes are transcriptionally active seedlings. In these study, using total RNA from 21-day-old Col-0 seedlings they showed that AtNHX1 and 2 are the most abundant AtNHX mRNA products in shoots and roots, and AtNHX5 was found in the same locations but in lower abundance. The AtNHX3 transcript was apparent only in roots, and AtNHX4 and AtNHX6 were only detected by RT-PCR in shoots and roots using. These results establish that all six AtNHX genes are transcriptionally active in seedlings, and indicate that their function is not restricted to a later developmental stage. Moreover, they demonstrated that AtNHX1 and 2 are inducible by NaCl in a ABA dependent manner, while AtNHX5 was induced by NaCl, but independently of ABA. Although in Yokoi et al. (2002) AtNHX3 transcript remained constant under hyper-osmotic stress or exogenous ABA treatment, the transcripts level of AtNHX3 after ABA and NaCl treatments of 8-day-old seedlings showed transient upregulation in other analysis (Li et al. 2009). In the latter study they also demonstrated that AtNHX3 mRNA was present in seedlings and various tissues of mature plants including roots, rosette leaves, cauline leaves, stems, flowers, and siliques. On the other hand, AtNHX4 mRNA was only detected in germinating seeds, flowers and siliques.

Further promoter:: GUS expression analyses were also performed. In the case of AtNHX1, it is expressed at all developmental stages and throughout the Arabidopsis plant (Yokoi et al. 2002). In 2- day-old seedlings AtNHX1 is expressed in the root tip, with a strong expression in the emerging radicle and lateral roots, and relatively weaker in the hypocotyl. From 3-day-old seedlings on, the expression can be detected throughout the plants except the root tip. Strong expression has been observed in the root hair of young seedlings, guard cells and inflorescence stem, with strong staining in parenchyma cells of the cortex and vascular strands. In flowers, it can be found in sepals, in pollens within anthers and in the base and tips of siliques (Shi et al. 2002; Apse et al. 2003). AtNHX2, is also expressed in most tissues of Arabidopsis seedlings. High expression was observed in the vasculature, root tip and at the points of emergence of secondary roots; also guard cells, filament of the stamens, the ovarian stigma, mature pollen grains within the anthers, and the pollen tube. In immature siliques,

septum and to the silique tip and base (Wang et al. 2007; Barragán et al. 2012) *AtNHX3* promoter activity was observed in transgenic plants transformed with a 2 kb fragment of the putative promoter of *AtNHX3*. Analyses of the plants showed high expression in 10- day-old seedlings and in stems (Li et al. 2009). GUS activity was also detected in stigma and calyces, but not in petals and stamens. However, previous studies with a similar promoter length and the same expression vector demonstrated a different pattern (Wang et al. 2007). They showed strong pAtNHX3::GUS staining in germinating seeds and peduncles, with the expression disappearing in mature plants. Wang et al. (2007) reported GUS expression in petals, anthers and top of siliques. Something similar occurred with the expression of AtNHX4. Wang et al. (2007) showed that in transgenic arabidopsis expressing pAtNHX4::GUS fusion, the GUS reporter was expressed at all developmental stages, detected in 1-day-old germinating seed, with stronger GUS staining in cotyledons and the vascular bundle in seedlings with true leaves and in mature plants. However, Liu et al (2010) reported that the expression of GUS under AtNHX4 promoter was limited to germinating seeds, disappearing in 3-day-old seedlings and rosette leaves. A strong GUS activity was also detected in pollen grains and siliques. The expression of NHX5 *and* NHX6 has been less studied. In different organs it was analyzed by in different organs and developmental stages. Both *NHX5* and *NHX6* were expressed in flowers, flower buds, stems, rosette leaves, and roots, as well as flowers, flower buds and siliques (Yokoi et al. 2002; Bassil et al. 2011a). The overall level of expression *NHX5* was slightly higher than that of *NHX6* except in siliques and seeds.

I.2.2. AtNHX Topology

To date no X-ray structure has been determined for any eukaryotic NHE/NHX. The most closely related proteins for which structural determination has been completed are the NhaA from *Escherichia coli*, which was solved by high resolution X-ray chromatography (3.45Å; (Hunte et al. 2005a; Lee et al. 2014), and the CPA2 protein TtNapA (Lee et al. 2013c); or the more closely related to AtNHX NhaP1 from *Methanococcus jannaschii* (Goswami et al. 2011) and the *Pyrococcus abyssi* NhaP (PaNhaP1) (Wöhlert et al. 2014). This analysis revealed 12 (CPA1 proteins) or 13 (CPA2 proteins) transmembrane helices at the N-terminus, with a hydrophilic, cytosolic short C-terminal extreme, and arranged in an antiparallel manner. Multiple sequence alignment comparing CPA members from all phyla indicated that the N-terminus transmembrane domains were highly conserved, suggesting that the structure and

orientation are conserved as well (Landau et al. 2007; Schushan et al. 2010; Wang et al. 2014). The tridimensional structure of other eukaryotic proteins have been modeled using these crystalized structures: HsNHE and HsNHA2 (Landau et al. 2007; Schushan et al. 2010), PeNHX3 (Wang et al. 2014), AtNHX6 (Ashnest et al. 2015). All these proteins have a common transmembrane organization. Most eukaryotic members also have a C-terminal tail with an important function in activity regulation (Brett et al. 2005a; Slepkov et al. 2007; Wang et al. 2014; Ashnest et al. 2015).

Different approaches have been used to determine the AtNHX protein topology. One of these approaches was developed using yeast for heterologous expression, and applying an epitope tagging and protease protection assays to full length expressed AtNHX1 (Yamaguchi et al. 2003) According to their results, AtNHX1 has nine transmembrane segments, with an additional three "buried" domains that do not entirely span the membrane. According to this study the N-terminal cytosolic, the C-terminal tail was placed in the vacuolar lumen (Yamaguchi et al. 2003; Bassil et al. 2011a). This differs from the common proposed cytosolic C-terminus orientation of CPA proteins (Hunte et al. 2005a; Landau et al. 2007; Wang et al. 2014). However, another study performed by Sato and Sakaguchi (2005), showed that AtNHX1 contains eleven transmembrane domains and a cytosolic C-terminus. The C-terminus orientation was finally showed to be cytosolic by Hamaji et al. (2009) in a protease protection assay applied to isolated vacuoles expressing ATNHX1 fused to GFP.

I.2.3. AtNHX regulation.

Little is known about the signaling pathways that regulate the expression and function of AtNHX antiporters to regulate their activity.

I.2.3.1. Phosphorylation dependent regulation.

Phosphoproteomic studies in Arabidopsis and rice suggested that NHX antiporters are regulated by phosphorylation (Whiteman et al. 2008b, a). Andrés (2013, thesis dissertation) showed that both AtNHX1 and AtNHX2 are phosphorylated in their C-terminal tail in Ser526 and Ser532 residues respectively. Later it was demonstrated that this phosphorylation was due the Mitogen Activated Protein Kinase 6 (MAPK6) activity (FJ Quinter and JM Pardo, unpublished). The MPK6 had already been described to activate AtSOS1. So far, the biological role of such post-translational modifications has not yet been functionally characterized.

MPK6 is activated by a phosphatidic acid produced under salt stress by Phospholipase Dα1 (PLDα1). As this PLD isoform contains a Ca^{2+}-binding C2 domain for its activation it is feasible that salt-induced $[Ca^{2+}]_{cyt}$ increase could activate SOS1 through this lipid-mediated pathway via MPK6 (Yu et al. 2010a, 2015). In yeast, Hog1 MAPK mediates the rapid activation of a Na+ ⁄H+ antiporter (Nha1), which precedes the transcriptional response (Proft and Struhl 2004).

The hyperosmotic component of the salt stress generates rearrangements in the cytoskeletons. PDL activation is related mainly with hyperosmotic stress, and it has been reported to interact with both actin and tubulin regulating cytoskeleton reorganization. (Kusner *et al.* 2003 (Huang *et al.* 2006). Moreover, MPK6 and MPK4 in Arabidopsis thaliana are related in cytoskeletal organization and remodelation (Takáč et al. 2016; Zhang et al. 2016). CPA proteins have also been related to cytoskeleton remodelation::HsNHE C-terminal tail interacts with the cytoskeleton (Donowitz et al. 2009), and the quadruple mutant *nhx1 nhx2 nhx3 nhx4* under high K+ showed pronounced root skewing, suggesting that the organization of the cytoskeleton might be perturbed (McCubbin et al. 2014). Whole. Taking all these together, the phosphorylation of AtNHX dependent on MPK6 could be related to possible cytoskeleton interaction and reorganization under stress.

The distal region of the C-terminal tail of NHE1, is also target of different kinases which moves the set point to alkaline pH values. Among these kinases ERK1/2 (extracellular- signal-regulated kinase 1/2), via the MAPK (mitogen-activated protein kinase) cascade; p90rsk (p90 ribosomal S6 kinase) and CaMKII (Ca2+/calmodulin-dependent kinase II) are found. NHE1 is also directly phosphorylated by p38 MAPK which inhibits NHE1 (Slepkov et al. 2007)

I.2.3.2. Ca^{2+} dependent regulation.

Calcium is a well-known secondary messenger in all cells. An early detectable response to NaCl stress is an increment in the cytosolic free calcium concentration. This increment is sensed by cytosolic EF-hand containing Ca2+ binding protein (Kudla et al. 2018) that activate different signaling pathways in order yo to improve the K+/Na+ ratio in favor of K+ at the expense of Na+ (Shabala et al. 2006). In plant cells the most important Ca^{2+} sensors are the Calmodulin (CaM), CaM-like proteins (CML) and Calcineurin B-like proteins (CBL). Qiu et al. (2004) reported that NHX activity in Arabidopsis is regulated by SOS2 (CIPK24) in a SOS3 (CBL4) independent and phosphorylation free manner. It was demonstrated that SOS2 is able to stimulate the tonoplast ion exchange activity without in vitro protein

phosphorylation through direct protein-protein interaction as is the case of CAX1 (Cheng et al. 2004) and the V-ATPase (Batelli et al. 2007). In addition, Andrés (2013, thesis dissertation) demonstrated strong interaction of AtNHX1 with CIPK23, and AtNHX2 with CIPK23, CIP24 and CIPK26. However, direct phosphorylation of AtNHX1 by them has not been reported yet. According to BIFCs results, CIPK23 interacts with AtNHX1 and AtNHX2 in the tonoplast. CIPK23 has been described to be involved in the control of K+ homeostasis at the plasma membrane under low-K+ stress by regulating AKT1 K^+ uptake activity in roots, and guard cell turgor regulation in aerial tissue (Xu et al. 2006; Li et al. 2006; Cheong et al. 2007; Nieves-Cordones et al. 2012). In addition, CIPK23 is involved in the stomatal function as a negative regulator of the ABA signaling in guard cells and in fact, *cipk23* mutants showed a more efficient stomatal closure in response to ABA than the wild type (Cheong et al., 2007; Nieves-Cordones et al., 2012). CIPK24 protein has been reported to interact with CBL10. In this location interaction with AtNHX1 and V-ATPases has been described (Batelli et al. 2007). H^+ transport activity of tonoplast vesicles isolated from sos2-2 plants was reduced by 30% compared to the wild type (Batelli et al. 2007), and vacuolar Na^+/H^+ antiporter activity found in cipk24 mutant plants was lower than wild type (Qiu et al. 2004). It has been hypothesized that the role of CIPK24 in Na^+ sequestration to the vacuole is to increase the transmembrane H+ gradient generated by V-ATPases, that in turn will activate cation/H^+ exchangers. However, the double mutant *vha-a2 vha-a3* does not show differences in Na^+ accumulation and salt tolerance compared to the wild type (Krebs et al. 2010). In other plants, only the AtNHX7 orthologue has been shown to interact with CIPK, NHX interact with CIPK proteins, indicating their main function involved in involved in CBL-CIPK pathway during salt stress responses, such as *Populus trichocarpa* NHX7 (PtNHX7, (Tian et al. 2017) or *Sorghum bicolor* NHX7 (SbNHX7, (Hima Kumari et al. 2018). In tomato, LeNHX2 (endosomal) and LeNHX4 (vacuolar) can interact with SlSOS2 (Belver et al. 2012)

The involvement of Ca2+ sensor proteins in salinity tolerance mechanisms is becoming more clear. CML9 (a member of the Calmodulin-like (CML) gene family) was found to be upregulated during salt stress and *cml9* loss of function mutants displayed hypersensitivity in germination assays on medium containing either NaCl or ABA, whereas adult *cml9* plants show enhanced tolerance towards irrigation with salt water (Magnan et al., 2008). AtNHX1 interacts with CaM15/CML18 in a Ca^{2+} and pH dependent manner (Yamaguchi et al. 2005). According to the authors, the interaction takes place in the vacuolar lumen and regulate the affinity of the transporter so that at physiological conditions (i.e., high, vacuolar, free Ca^{2+} concentrations and acidic vacuolar pH). According to this publication, under control

physiological conditions, when the vacuole pH is acidic (pH 5.5) and the Ca^{2+} concentration is high, AtCML18 is bound to the AtNHX1 C-terminal tail, resulting in a higher K^+/H^+ exchange activity over Na^+/H^+ activity. However, the vacuolar alcalinization produced by salt stress would reduce AtCML18binding to AtNHX1, leading to an increase in Na^+/H^+ exchange activity.

Mammalian members of the family CPA1, HsNHE however have also shown to be regulated by Ca^{2+} fluxes inside the cell. The C-terminal domain of the NHE is the location by which these proteins interact with a myriad of proteins (Landau et al. 2007; Snabaitis et al. 2008b; Donowitz et al. 2009). Among them, there are specific domains for Calcium interacting proteins: Calcineurin homologous protein (CHP), Calmoudlin (CaM) CaM KinaseII (CaMKII) (Donowitz et al. 2009; Köster et al. 2011a). The structure of the binding domains of CHP (Ammar et al. 2006; Mishima et al. 2007) and CaM (Köster et al. 2011a) have been crystalized. In the latter case, elevated Ca^{2+} concentrations CaM binds to NHE1 C-terminal domain and stimulate sodium-proton exchange. Moreover, in the absence of bound CaM and low Ca^{2+} concentration, NHE1 CaMBD autoinhibits HsNHE1 through by binding to a H^+ modifier site located in a TM segment of the protein (Aronson et al. 1982; Snabaitis et al. 2008b). CaM binding to HsNHE1-CaMBD weakens the interaction of the autoinhibitory region with the proton modifier site. Protons have then unhindered access to this site to up-regulate the transport activity of NHE1. Mutations in the CAM-BD of HsNHE1 however shift the set up to a more alkaline pH (Ikeda et al. 1997; Shigeo Wakabayashi et al. 1997). CHP-BD in the C-terminal tail of HsNHE1 is essential for the protein activity. Deletion of the binding region inhibited the HsNHE1 activity by inducing the acidic shift of intracellular pH dependence. The same effect was observed in single mutation of essential residues (I534D, I534K and Ile537) (Ammar et al. 2006). These findings suggest that CHP is required both for supporting the basic activity and regulating the pH-sensing of HsNHE1.

I.2.3.3. Regulation by pH

The pronounced pH dependence of the CPA members' activity has always been explained by the presence of specific domains in the protein named pH sensors, which were able to sense the medium pH and according to it activate or inhibit the protein (Hunte et al. 2005a; Călinescu et al. 2014). For prokaryotic CPA proteins a model to explain the mechanism of action has been proposed (Mager et al. 2011; Călinescu et al. 2014) according to which the pH sensor is in the active site of the protein. Electrophysiological studies of MjNhaP1 showed that at least in prokaryotic CPA proteins, the pH dependence is an inherent property of their transport mechanism (Călinescu et al. 2014). This property had already been proposed (Mager et al. 2011; Lee et al. 2014), and can be applied to both CPA1 and CPA2 proteins. According to this transport mechanism, at extreme pH the protein activity is down-regulated preventing excessive cytoplasmic acidification (CPA2 transporters) or alkalinization (CPA1). Due to the high conservation observed, Calinescu et al (2014) proposed that this model can explain the eukaryotic proteins mechanistic principles of pH regulation, but further mechanisms modulating their pH dependence mediated by the cytoplasmic regulatory domain should be analyzed.

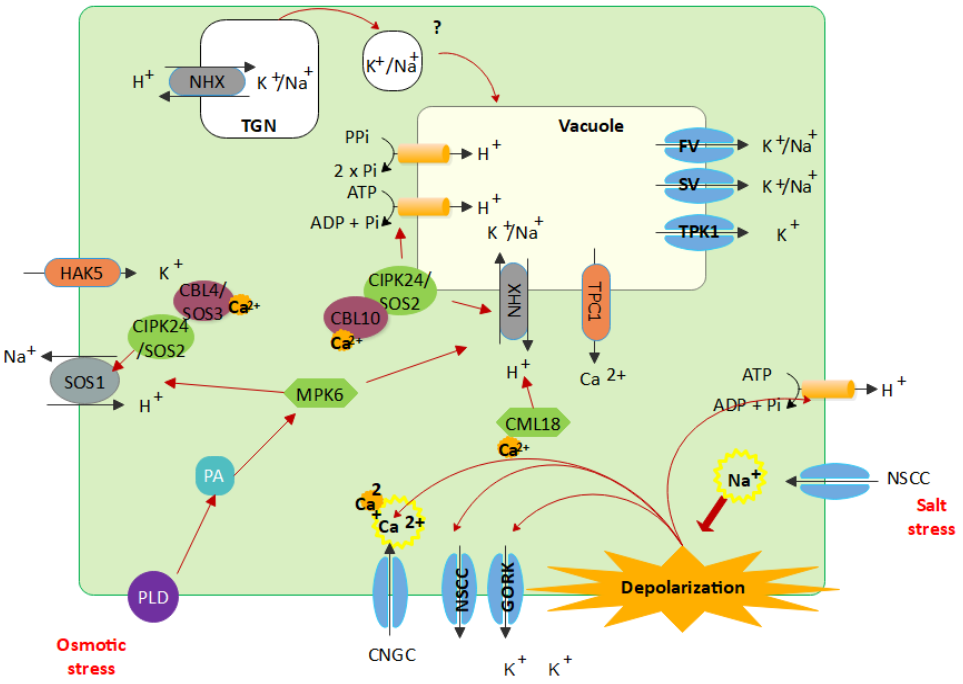

Figure 3. Schematic representation of cell signaling under salt stress. (adapted from Almeida et al., 2017. The enctrance of Na+ induces depolarization of the membrane activatingthe extrusion of K+ and influx of Ca2+. P-type ATPase is activated repolarizaing the membrane. The influx of Ca2+ activates different signaling routes dependent on calcium binding proteins (CBL and CML).

No pH sensors have been identifying for most of the eukaryotic CPA proteins. The most likely candidates to form these pH sensors are amino-acids able to change their protonated conditions in the physiological pH range are the most likely candidates. Histidines have a pK value near 6.5. reason why they change their protonated state can be physiological pH 6.5–7. There is experimental evidence that histidine functions in the pH-dependent modulation of a number of ion transporters, including GLT-1, AE2, ROMK1, PEPT (Zhang et al. 1994; Sekler et al. 1996; Chanchevalap et al. 2000; Rajan et al. 2000; Vahisalu et al. 2008) and in Na^+/H^+ exchangers (Aronson et al. 1982; Wakabayashi et al. 1992; Gerchman et al. 1993; Wang et al. 1995; Rimon et al. 1995; Ikeda et al. 1997). Marshansky (2007) proposed that histidine residues in the a2-subunit of V-ATPase could also be involved in the function of the V-ATPase as a pH-sensor.

For HsNHE3 a pH sensor consisting of two histidine residues (H479-H499) in the C-terminal tail was reported. This region presents a highly a-helical structure and overlaps with the CHP binding domain (Cha et al. 2003), and disruption of CHP binding drastically reduces Na+/H+ exchange activity (Pang et al. 2001). However, no studies on how the mutations generated affected the CHP binding to the protein at different pH. Moreover, the HsNHE1 CAMBD also interacts with the proton modifier site, integrating the pH sensing and CaM regulation too. In HsNHE1 a HsNHE1 contains a non-transporting H^+-binding site, known as a 'proton-modifier site', which is involved in the regulatory mechanism to increase in NHE activity depending on pH (Slepkov et al. 2007).

I.2.4. AtNHX function

The Na+(K+)/H+ exchange activity of the AtNHX antiporter family have come to be regarded as a key player in intracellular Na+/K+ and pH homeostasis, growth and development, stomatal functions, protein and vesicle trafficking, and tolerance to abiotic stress (Jiang et al. 2010; Andres et al. 2014; Reguera et al. 2015; Ashnest et al. 2015; Dragwidge et al. 2018).

I.2.4.1. . Salt tolerance

As previously discussed, AtNHX protein have a role in tolerance to salt stress. Although AtNHX7 is essential to extrude Na^+ from shoot and roots from leaves (AtNHX7), the activity of AtNHX1 to 6 is not mainly related to compartmentalization of Na^+ as it was believed. Vacuolar

AtNHX show the same affinity to transport Na^+ and K^+ across membrane (Venema et al. 2003). Tomato LeNHX2 reconstituted in proteoliposomes transported K^+ with a low affinity but strong selectivity over other cations (Venema et al. 2003). Based on functional expression in yeast, also AtNHX5 is thought to prefer K^+ to Na^+ (Yokoi et al. 2002)

Although constitutive overexpression of *AtNHX1* appears to increase salt stress tolerance in yeast (Aharon et al. 2003), Arabidopsis (Apse et al. 1999), tomato (Zhang and Blumwald 2001) and cotton (He et al. 2005), most of the role of NHX antiporters in ion accumulation and salt tolerance have been studied by overexpression or deletion of the genes, or by comparison of NHX gene expression and ion accumulation in closely related species that differ in salt tolerance (Rodríguez-Rosales et al. 2009; Katschnig et al. 2015), which may lead to erroneous conclusions. As an example of the latter case are, *Salicornia dolichostachya* and the taxonomically related glycophytic *Spinacia oleracea*. While growth in *S. oleracea* is negatively affected by low increases in salinity, growth in *S. dolichostachya* increased from 10 mM NaCl to moderate salinity (50 and 100 mM NaCl). In these species the NHX1 expression at 10 mM salinity was approximately 2-fold higher in *S. dolichostachya* shoots than it was in *S. oleracea* leaves; but at the same time SOS1 is constituvely expressed in *S. dolichostachya*, while in in *S. oleracea* is upregulated with increasing salinity. In addition, the salt tolerance reports by overexpression of AtNHX these reports of salt tolerance is not always associated to the expected increment in vacuolar Na+ accumulation, and all the combinations of changes in Na+ and/or K+ concentrations can be found when the ion profiles were measured (e.g. higher Na+ and lower K+ (Apse et al. 1999); higher Na+ and K+ (Brini et al. 2007); higher K+ and lower Na+ (Rodriguez-Rosales et al. 2008; Leidi et al. 2010).

Yeast have only one NHX isoform that belongs to the IC-NHXE clade II. The disruption of ScNHX1 affects intracellular Na+ and K+ concentrations (Gaxiola et al., 1999; Quintero et al., 2000; Venema et al., 2003). Yeast cells which have the two Na^+ efflux systems at the plasma membrane, the NHA1 exchanger and Na^+-ATPases ENA disrupted, show decreased salt tolerance. This phenotype is increased when ScNhx1 is mutated, decreasing the intracellular Na+ content and, notably, by producing a great diminution of internal K+ (Quintero et al. 2000; Venema et al. 2003). Overexpression of AtNHX1 and AtNHX2 isoforms in an *ena1-4 nha1 nhx1* mutant yeast strain strongly increases intracellular K^+ and Na^+ while the overexpression of endosomal AtNHX5 and LeNHX2 increases intracellular K^+ while reducing Na^+ content (Yokoi et al. 2002; Venema et al. 2003)

These results seem to indicate that it is likely that the contribution of NHX-like protein to plant salt stress tolerance is the maintenance of K^+ homeostasis rather than sequestration of Na^+ into the vacuole (Maathuis et al. 2014). The Na^+/H^+ exchange would be only take place in situations in which the Na^+ concentrations in the cytosol are higher than K^+ concentrations (Jiang et al. 2010; Maathuis 2014).

In order to explain the high compartmentalization into the vacuoles of Na^+ observed under salt-stress, different hypothesis have been proposed to explain Na^+ sequestration Hamaji et al. (2009) reported that AtNHX1 is present in vesicles in the cytoplasm of salt-treated cells mediating Na^+ influx into the vesicles, which move, fuse and deliver their load to the vacuole. In halophytes, direct uptake of Na^+ from the apoplast into the vacuole through pinocytosis (not requiring an Na^+/H^+ exchange activity) has been reported (Shabala and Mackay 2011). In a similar line, Krebs and colleagues (2010) postulated that the TGN/EE could be con contributing to vacuolar pH homeostasis in V-ATPase mutants. However, no evidence in glycophytes has been reported.

I.2.4.2. . K+ nutrition and homeostasis.

Potassium (K^+) is the most abundant inorganic cation in plants, comprising up to 10% of a plant's dry weight (Amtmann et al. 2018). Besides, it is a macronutrient for plant, with functions in metabolism, growth and stress adaptation, enzyme activation, stabilization of protein synthesis, neutralization of negative charges on proteins and maintenance of cytoplasmic pH homeostasis. On the other hand, potassium movement is the driving force for osmotic changes in stomatal movement, light-driven and seismonastic movements of organs, or phloem transport; also provides charge-balancing counter-flux, essential for sustaining the movement of other ions, sugars, amino acids and nitrate. Finally, accumulation of K^+ (together with anions) in plant vacuoles creates the necessary osmotic potential for cell extension. Rapid cell extension relies on high mobility of the used osmotic and therefore only few other inorganic ions (e.g. Na^+) can replace potassium in this role. Once cell growth has come to a halt, maintenance of osmotic potentials can be carried out by less mobile sugars and potassium ions can partly be recovered from vacuoles.

Because of the vital role that potassium plays in plant growth and metabolism, potassium-deficient plants show a very general phenotype, which is characterized by reduced growth especially of aerial parts and lateral roots. The various physiological components of potassium deficiency, such as limited cell extension, reduced photosynthesis and impaired regulation of

transpiration, can easily be linked to known functions of potassium. As before mentioned, salt stress often induces perturbations in the cellular K^+ homeostatic balance, with a consequential alteration in all these physiological processes. Maintaining a high cytosolic K^+/Na^+ ratio would constitute a stress tolerance strategy (Himabindu et al. 2016). To that end root K^+ uptake, xylem loading for translocation to the shoot and cellular influx are enhanced, while cytosolic K^+ efflux is restricted at the same time.

K^+ uptake from soil is performed by a well-organized system of transport proteins each operating on a determined range of K^+ concentrations (Aleman et al. 2011). The main K^+ uptake systems in *Arabidopsis* roots have been described to be the *Shaker*-like K^+ channel AKT1 and the K^+ transporter AtHAK5 (Hirsch et al. 1998; Gierth et al. 2005; Rubio et al. 2008) At external K^+ concentrations between 0.01 mM and 0.05 mM both AtHAK5 and AKT1 contribute to K^+ uptake. At higher external K^+ concentrations, AKT1 together with other unknown low affinity K^+ uptake systems are responsible (Rubio et al. 2010; Pyo et al. 2010; Caballero et al. 2012). Finally, the outward rectifying *Shaker*-like channel *SKOR* is expressed in the pericycle and the xylem parenchyma in roots and is responsible for loading K^+ to the xylem that will transport the K+ along the plant.

Cytosolic K+ concentrations are tightly regulated and is thought to decline only when the vacuolar K+ reserve has been depleted below the thermodynamical equilibrium with the cytosolic pool (Walker et al., 1996). Conversely, surplus K+ is placed into the vacuole to maintain cytosolic K+ within narrow limits independently of K+ abundance in the growth medium.

The overexpression of the Arabidopsis AtNHX1 in tomato was found to enhance tolerance to salinity by mediating vacuolar K^+ sequestration, and enhanced intracellular K^+ retention (Leidi et al. 2010). The transgenic plants showed stress symptoms only under K^+-limiting conditions as a result of an enhanced K^+ compartmentation at the expense of the cytosolic K^+ pool. Arabidopsis transgenic plants overexpressing the tomato LeNHX2 exhibited earlier physiological and molecular symptoms of K^+ deficiency under K^+ deprivation and took up K^+ more avidly than control lines. (Rodriguez-Rosales et al. 2008). Moreover, Arabidopsis nhx1/nhx2 double null mutants have impaired vacuolar K^+ accumulation, enhanced vacuolar Na^+ uptake, and a salt (NaCl) insensitive phenotype, compared to wild-type (Barragán et al. 2012).

nhx1nhx2 double mutants of Arabidopsis cannot create vacuolar K^+ pools resulting in compromised turgor generation for cell expansion (Barragán et al. 2012). These plants grow

only within a narrow range of K^+ concentrations, and plants suffer of reduced growth rate, delayed flowering, lesser and smaller siliques, and reduced seed viability (Bassil et al. 2011b; Barragán et al. 2012). These symptoms are linked to the role of K^+ as osmoticum. The incapability to accumulate K^+ of *nhx1nhx2* double mutants, leads to the impairment for to regulate the osmotic pressure and consequently the capacity to control stomatal movement adequately when induced in a KCl buffer. The dynamic movement of these cells nonetheless is recovered in a NaCl buffer. This make evident the existence of transporters other than AtNHX1 and AtNHX2 for Na^+ (Andres et al. 2014). As a result of the impaired stomatal movement, these plants have an impaired hydric relation with the environment.

All these data demonstrate the vacuolar AtNHX are responsible for the accrual of K+ into the vacuole where it fulfils osmotic roles involved in physiological processes such as cell expansion and stomatal movements.

I.2.4.3. pH homeostasis regulation.

The homeostatic regulation of pH and ion concentrations in plant cells is crucial for their viability. Maintaining stringent pH conditions in the cytosol and endomembrane system is required for efficient metabolism, membrane trafficking, protein stability and sorting, proteolytic processing of proteins, cell elongation. Proton gradients across the cellular membranes are required for active transport processes. Moreover, localized and transient H^+ fluxes have been observed in response to different stress conditions, suggesting that pH could act as a signaling element (Pittman 2012) (Pittman, 2012).

The NHXs serve as proton leaks to counter acidification promoted by the activity of V-ATPases and V-PPases in the intracellular compartments, making them excellent regulators of intracellular pH (Andres et al. 2014; Bassil and Blumwald 2014; Reguera et al. 2015).

A clear example of tonoplast NHX involvement in pH regulation is best illustrated by studies of Japanese morning glory (*Ipomoea nil* or *Ipomoea tricolor*) flower petal coloration. During flower development, anthocyanins are accumulated in *Ipomoea*'s vacuole, which has a low pH (6.6), giving the petals a redish color. Upon flowering, an increase in *InNHX1* transcripts 12 h before flower opening, is concomitant with an increased vacuolar pH to values of 7.7, and a shift in the petals color to blue (Ohnishi et al. 2005; Yoshida et al. 2005, 2009). The purple (*pr*) mutation of *Ipomoea nil,* abolishes the activity of *InNHX1*, partially hampers vacuole alkalinization and prevents the full color shift from red to blue in opening flowers (Yamaguchi

et al. 2001). The partial pH change and color in *pr* mutant has been suggested to rely on the activity of another abundantly expressed vacuolar NHX-type member, *InNHX2* (Ohnishi et al. 2005). A concomitant increased activation of the V- ATPase and vacuolar H+-PPase was shown to occur (Yoshida et al. 2005) so that a balance between H^+ pump and cation/H^+ exchange activities are necessary to regulate vacuolar pH. These authors also suggested that this increased vacuolar accumulation of K^+ may contribute to the increase in vacuolar osmoticum for cell expansion growth and thus drive flower opening in a manner that is directly coordinated with color change.

This concept of vacuolar NHX transporters as mediators of K^+ homeostasis and vacuolar pH has been also seen in other plant development stages. In Arabidopsis thaliana *nhx1 nhx2* double mutant vacuolar pH of mature root cells was reduced from pH 6.3 in wild type to pH 5.8, and reduced from pH 5.5 to 5.2 in hypocotyl cells (Bassil et al. 2011b). Vacuolar pH regulations by AtNHX1 and AtNHX2 are essential in the regulation of stomatal movement (Andres et al. 2014). In guard cells AtNHX proteins couple two simultaneous processes: the alkalinization of the endosomal compartments that induces vacuolar fusion to increase vacuolar surface area and volume, and the accumulation of osmotically active K+ with the subsequent entry of water and increase of cell turgor. Moreover, the alcalinization of the vacuole is necessary to activate TPC1.

The heterologous expression of AtNHX proteins in yeasts mutant lacking all the Na^+/H^+ antiporters, which presented a more acidic vacuole pH in comparison to the wild type, were also able to restore the pH (Plant et al. 1999; Ali et al. 2004; Brett et al. 2005b)

In the case of endosomal ICII-NHE proteins something similar has been described. In yeasts, *nhx1* mutant have a more acidic cytoplasm and vacuole, which blocks vesicular trafficking out from the Golgi/Prevacuolar compartment, growth sensitivity to acidic media and deleterious processing and mis-sorting protein (Bowers et al. 2000; Ali et al. 2004; Brett et al. 2005b). The Arabidopsis endosomal AtNHX5 and AtNHX6 co-localize with known Golgi and TGN markers, and with the secretory pathway V-ATPase (VHA-a1). In the *nhx5 nhx6* double mutant endomembrane these compartments are hyper-acidified (Dettmer et al. 2006; Viotti et al. 2013; Reguera et al. 2015; Luo et al. 2015), AtNHX5 and AtNHX6 regulate endosomal pH by preventing acidification through leakage of H^+ out of the compartments, and regulate protein transport by controlling three distinct stages: the binding of vacuolar sorting receptor (VSR), recycling of VSRs and the subcellular localization of the SNARE complex (Reguera et al. 2015; Qiu 2016a, b)with negative effects in processing of seed storage

proteins, vacuolar trafficking and protein secretion and recycling in (Reguera et al. 2015; Ashnest et al. 2015). The endosomal pH and ion regulation by AtNHXs in endosomes has been shown to be important for functional Golgi and TGN/EE motility and the endosome-cytoskeleton association, protein recycling at the TGN/EE, and regulation of endomembrane ion balance (Dragwidge et al. 2018). In plants, pH is also critical for maintaining vesicular identity (through receptor association) (Martinière et al. 2013a)

In yeasts the function of ScNHX1 in pH homeostasis is well established. This protein is localized in several endomembrane compartments such as vacuoles (Qiu and Fratti, 2010), trans-Golgi/TGN compartments, early and late endosomes in the biosynthetic, endocytic, and recycling pathways (Kojima et al., 2012) and also in the multivesicular bodies (MVBs) (Mitsui et al., 2011). All these organelles pH are regulated by this ScNhx1. Deletion of ScNHX1 renders the yeast cells sensitive to low pH, and they show more acidic cytoplasmic and vacuolar pH (Brett et al. 2005b). Moreover, the Δnhx1 mutants show characteristic phenotypes like protein missorting (vacuolar carboxypeptidase Y (CPY)) and accumulation in endosomes of the G protein coupled receptor Ste3, which in wild type is delivered to the vacuole in (Bowers et al. 2000; Brett et al. 2005b). In addition, a strong sensitivity to the drug hygromycin B, that is detoxified at the vacuole is developed, suggesting that the VPS phenotype is dependent on defective vacuolar biogenesis (Gaxiola et al. 1999; Bowers et al. 2000)

AtNHX proteins complement the NaCl, KCl and hygromycin sensitivity exhibited by the yeast *Δnhx1* disruption mutant (Quintero et al. 2000; Yokoi et al. 2002; Rodriguez-Rosales et al. 2008). Which is in accordance to the role for plant NHX proteins in endosomal and vacuolar pH regulation.

It is less clear whether plant NHX-type exchangers are involved in cytosolic pH regulation. However, in poppy, the product (lysophosphatidylcholine) of microbial elicitor-activator phospholipase A2 induces a cytosolic acidification via activation of a vacuolar Na+/H+ exchanger, giving rise to an estimated cytosolic pH shift from pH 7.3 to 6.7 (Viehweger et al. 2002). This study implicates a vacuolar ion/H+ exchanger not only in the modulation of cytosolic pH, but in the generation of a pH signal.

OBJECTIVES

Salt stress, in the form of high salt soils or by irrigation, is one of the most important causes of crop failure causing average yield losses of more than 60% for major crops worldwide. Under these conditions, plants activate physiological and molecular responses that allow minimize the detrimental effect in their fitness and growth of toxic ions. Among the adaptations to saline stress, the preservation of the K^+/Na^+ ratio in the cytosol is critical for the maintenance metabolic functions since Na+ cytotoxicity is largely due to competition with K+ for binding sites in enzymes. Adaptation Saline stress, as well as plant nutrition, depends on the activity of membrane transporters that translocate minerals from the soil into the plant and mediate their intra- and intercellular distribution.

The NHX proteins of *Arabidopsis thaliana* have important roles in salinity stress tolerance, K^+ nutrition and compartmentation, osmotic adjustments, turgor generation and stomata movements. Recently, they have been shown to regulate luminal pH en endosomes (NHX5 and NHX6) and vacuoles (NHX1 and NHX2). However, very little is known regarding how these proteins are regulated at the biochemical level or how the may sense the pH in endomembranes and/or the cytosol that they help regulating. Moreover, two other members of the *NHX* gene family of Arabidopsis, NHX3 and NHX4, have been largely overlooked and their function remains uncertain.

Based on these premises, the main aims of this thesis were:

1. Analyze the structural-function relationship of AtNHX1 protein based in the highly conservation nature of the CPA superfamily.

2. Improve our understanding on the mechanisms underlying the cis- and trans-regulation of the AtNHX1 protein by pH and the interaction with calmodulin-like proteins.

3. Investigate the dynamics of cytosolic pH generated by saline stress in the root cells of *Arabidopsis thaliana*.

4. Study the function of AtNHX3 and AtNHX4 in *Arabidopsis thalian*

MATERIALS AND METHODS

M.1. Biological Material

M.1.1. Bacteria

M.1.1.1. Strains

Eschericha coli

The following *E. coli* strains were used for plasmid propagation:

Strain	Genotype	Reference
One Shot® TOP10	*F-, mcrA, (mrr-hsdRMS-mcrBC),80lacZM15, lacX74, recA1, ara139, (araleu)7697, galU, galK, rpsL, (Str$_R$), endA1,nupG>*	Invitrogen™ Life Technologies.
Rosetta™ 2(DE3)pLysS	*BL21: F- ompT hsdSB(rB- mB-)gal dcm (DE3) pLysSRARE2 (CamR)*	Novagen 71403
NEB® 5-alpha F'*Iq* Competent *E. coli* (High Efficiency)	*F´ proA+B+ lacIq Δ(lacZ)M15 zzf::Tn10 (TetR) / fhuA2Δ(argF-lacZ)U169 phoA glnV44 Φ80Δ(lacZ)M15 gyrA96 recA1 relA1 endA1 thi-1 hsdR17*	New England Biolabs

Agrobacterium tumefaciens

Agrobacterium tumefaciens was used for transient expression in *Nicotiana benthamiana* and for transformation of *Arabidopsis thaliana*.

Strain	Genotype	Reference
GV3101	*Rif$_R$, pMP90 (pTiC58DTDNA)*	(Koncz and Schell 1986)
p19	*pBin61-p35S:p19*	(Voinnet et al. 2003)

M.1.1.2. Bacterial culture media and growth conditions

Eschericha coli

Escherichia coli strains were cultivated in Luria-Bertani medium (LB). When needed, ampicillin at 100 mg/L, kanamycin at 50 mg/L or streptomycin at 25 mg/L were added into the cultures. Unless otherwise stated, *E. coli* strains were grown at 37°C.

Bacto™ yeast extract (Difco)	0.5% (w/v)
Bacto™ tryptone (Difco)	1 % (w/v)
KCl	1% (w/v)

For preparing solid LB medium 1.5% (w/v) of Bacto™ Agar (Difco) was added.

2xTY medium was used for recombinant protein expression in the strain Rossetta 2.

Tryptone	1.6%
Yeast Extract	0.5%
NaCl	10mM
Glucose	2%

Super Optimal Broth medium (SOB) and Super Optimal broth with Catabolite repression medium (SOC) were used for growth and preparation of *E. coli* competent cells.

SOB medium:

Bacto™ tryptone (Difco)	2% (w/v)
Bacto™ yeast extract (Difco)	0.5% (w/v)
NaCl	10 mM
KCl	2.5 mM

SOC medium:

Bacto™ tryptone (Difco)	2% (w/v)
Bacto™ yeast extract (Difco)	0.5% (w/v)
NaCl	10 mM
KCl	2.5 mM
$MgCl_2$	10 mM
$MgSO_4$	10 mM
Glucose	20 mM

Agrobacterium tumefaciens

Yeast Extract Peptone medium (YEP) was used for *Agrobacterium* growth. When needed, rifampicin at 50 mg/L, gentamicin at 20 mg/L or kanamycin at 50 mg/L were added into the cultures. Unless otherwise stated, *A. tumefaciens* strains were grown at 30°C.

YEP medium:

Bacto™ yeast extract (Difco)	1% (w/v)
Bacto™ peptone (Difco)	1% (w/v)
KCl	0.5% (w/v)

For preparing solid YEP medium 1.5% (w/v) of Bacto™ Agar (Difco) was added.

M.1.2. *Saccharomyces cerevisiae*

M.1.2.1 S. cerevisiae strains

Strain	Genotype	Use	Reference
AXT3K	*MATα, ena1::HIS3::ena4,nha1::LEU2, nhx1::KanMX,ura3-1, trp1, ade2-1, can1-100*	Functional studies of AtNHX proteins	(Quintero et al. 2002)
AH109	*MATa, trp1-901, leu2-3,112, ura3-52, his3-200,gal4Δ, gal80Δ, LYS2::GAL1$_{UAS}$GAL1$_{TATA}$HIS3, GAL2$_{UAS}$-GAL2$_{TATA}$ADE2,URA3::MEL1$_{UAS}$MEL1$_{TATA}$-lacZ*	Yeast two-hybrid assays.	(ClontechLaboratories ,Mountain View,California, USA)

M.1.2.2. Yeast culture media and growth conditions

Yeast manipulation techniques and growth conditions were performed as described in (Guthrie and Fink 1991; Ausubel et al. 1996). Unless otherwise stated, yeast cultures were grown at 28°C.

For routine growth and propagation of yeast cells YPD medium was used.

YPD medium:

Bacto™ yeast extract (Difco)	1 % (w/v)
Bacto™ peptone (Difco)	2 % (w/v)
Glucose	2 % (w/v)

For preparing solid YPD medium 2% (w/v) of Bacto™ Agar (Difco) was added.

YNB medium:

The minimal YNB medium media lacking the appropriate aminoacids, according to the strain genotype, was used as selective medium

Yeast nitrogen base w/o aminoacids	0.17% (w/v)
(NH4)2SO4	0,5% (w/v)
Glucose	2% (w/v)

For preparing solid YNB medium 2% (w/v) of bactoagar (Difco) was added, and pH was adjusted at 6.5 with NaOH.

For yeast two-hybrid assays, YNB medium was supplemented with an amino acid dropout solution.

Modified 10X Dropout solution:

L-Isoleucine	300 mg/L
L-Valine	1500 mg/L
L-Adenine hemisulfate salt	200 mg/L
L-Arginine HCl	200 mg/L
L-Histidine HCl monohydrate	200 mg/L
L-Leucine	1000 mg/L
L-Lysine HCl	300 mg/L
L-Methionine	200 mg/L
L-Phenylalanine	500 mg/L
L-Threonine	2000 mg/L
L-Tryptophan	200 mg/L
L-Tyrosine	300 mg/L
L-Uracil	200 mg/L

AP medium:

For complementation studies in yeasts (section M.8.2) and vacuolar pH measurements in yeasts, the alkali cation-free AP medium was used (Rodríguez-Navarro and Ramos 1984)

Yeast nitrogen base w/o aminoacids	0.17% (w/v)
$(NH_4)_2SO_4$	0,5% (w/v)
Glucose	2% (w/v)
H_3PO_4	8 mM
L-arginine	10 mM

$MgSO_4$	2 mM
$CaCl_2$	0.2 mM
KCl	1 mM
Glucose	2 % (w/v)
Trace elements (100X stock)	1 % (v/v)
Vitamins	1% (v/v)

pH was brought to 6.5 with L-arginine. LiCl was added as required.

Trace elements 100X stock:

H3BO3	**50 mg/L**
CuSO4	4 mg/L
KI	10 mg/L
Fe3Cl	20 mg/L
Na2MoO4.2H2O	20 mg/L
ZnSO4 .7H2O	4 mg/L
MnSO4.H2O	40 mg/L

To avoid contamination, several chloroform drops were added.

Vitamins 100x stock:

Biotin	1mL (0.2 mg/mL in ethanol)/100 mL
Nicotinic acid	4 mg/100 mL
Pyridoxine	4 mg/100 mL
Thiamine	4 mg/100 mL
Panthotenic acid	4 mg/100 mL

Vitamins solution was sterilized by filtration, and added to the autoclaved medium.

M.1.3. Plant material

M.1.3.1. Plant species

Arabidopsis thaliana

For the experiments where insertional T-DNA mutants *in AtNHX3* (*At3g06370*) and *AtNHX4* (*At5G55479*) genes were studied the following Arabidopsis lines were used:

Line	Source
***Arabidopsis thaliana* Col-0**	Arabidopsis Biological Resource Center (ABRC, Ohio State University, Ohio, EE.UU).
SAIL_827_D04 (*At_nhx3*)	Arabidopsis Biological Resource Center (ABRC, Ohio State University, Ohio, EE.UU).
SALK-082277 (*At_nhx4*)	SALK Institute, San Diego, California
***Arabidopsis thaliana* KO**	*Atnhx3 Atnhx4* (this project)
***Arabidopsis thaliana* Col-0 pHGFP-VTI11**	From Prof. Karin Schumacher laboratory
***Arabidopsis thaliana* Col-0 pHGFP-LTI6b**	From Prof. Karin Schumacher laboratory
***Arabidopsis thaliana* Col-0 pHGFP**	From Prof. Karin Schumacher laboratory
***Arabidopsis thaliana sos3* mutant pHGFP-LTI6b**	From Prof. JM Pardo laboratory

Nicotiana benthamiana

Nicotiana benthamina was used for *Agrobacterium*-mediated transient protein expression.

M.1.3.2. Arabidopsis thaliana growth conditions

Plant media

Murashige & Skoog medium (MS) (Murashige and Skoog, 1962).

Macronutrients (mM)		Micronutrients (µM)	
NH_4NO_3	20.6	**H_3BO_3**	100
KNO_3	18.5	**$FeSO_4.7H_2O$**	100
$CaCl_2.2H_2O$	3.0	**$MnSO_4.H_2O$**	100
$MgSO_4.7H_2O$	1.5	**EDTA- Na_2**	100
KH_2PO_4	1.2	**$ZnSO_4.7H_2O$**	30
		KI	5
		$Na_2MoO_4.2H_2O$	1
		$CoCl_2.6H_2O$	0.1
		$CuSO_4.5H_2O$	0.1

The medium solution was supplemented with 30 g/L of sucrose and buffered with MES 2.5 mM, pH was brougth at 5.7 with KOH. MS solid plates were prepared by adding 0.8-1% (w/v) of bactoagar (Difco).

LAK medium (Barragán et al., 2012):

Macronutrients (mM)		**Micronutrients (µM)**	
KH_2PO_4	1	**H_3BO_3**	30
$Ca(NO_3)_2$	2	**$MnSO_4$**	10
$MgSO_4$	1	**$ZnSO_4$**	1
		$CuSO_4$	1
		$(NH_4)_6Mo_7O_{24}$	0.03
		Fe^{2+} as Sequestrene 138-Fe	100

Solution was prepared with deionized water and pH was adjusted to 5.8 with KOH. For low (<1 mM) K medium, KH_2PO_4 was replaced by NaH_2PO_4 and K^+ was added as K_2SO_4.

In vitro plant growth conditions

Unless otherwise indicated, plant materials were handled in a Telstar A-H laminar flow cabinet, to guarantee sterility. Mediums and solutions were sterilized by autoclaving at 120°C and 2 atm for 20 minutes. Scalpels, tweezers and needles were ethanol/flame sterilized.

Seeds were surface sterilized, first they were soaked in 70% ethanol with rotation for 10 minutes, followed by a 5-minute incubation in absolute 96% ethanol. Finally, seeds were dried in sterile paper. To synchronize germination, seeds were stratified at 4°C in the dark for 2-4 days prior to sowing.

Unless otherwise stated, seeds were sawn in 12x12 mm dishes wirh LAK 1 mM K^+ pH 5.6 10 mM MES for phenotyping assays

Plant growth conditions in soil

Seeds of *Arabidopsis thaliana* were sowed on pots with Compo® Sana Universal substrate in a Sanyo MLR-351 plant growth chamber under long day regime: 16h day/8h night, 23/19ºC, 60-70% relative humidity, and 250µmol m^{-2} s^{-1} photosynthetically active radiation (PAR). For routine plant propagation, the same soil substrate was used and plants were grown in a greenhouse under ambient light conditions supplemented with 16 hours per day illumitation with a sodium lamp light.

Seeds harvesting and conservation.

Plants were kept separated by adequate space and attached to wood sticks to avoid cross-contamination. When the inflorescence started to turn brown, they were covered with plastic bags. Only after the whole inflorescence was brown and dry, harvesting was carried out, by cutting the entire plant off at its base and shaking the seeds into a paper bag; in addittion inflorescences were gently handpressed from the outside. After threshing, seeds were kept in Eppendorf tubes inside hermetic containers with Chameleon silica gel (VWRInternational) at room temperature.

M.1.3.3. Nicothiana benthamiana growth conditions

Nicotiana benthamiana plants were grown in Compo® Sana Universal substrate at 25°C and 70% humidity under a 16-h photoperiod and an 8-h dark period in environmentally controlled growth chambers.

M.2. DNA analysis and purification

M.2.1. DNA purification

M.2.1.1. Bacteria

Plasmid mini-preparations (“Minipreps”).

Small scale isolation of plasmid DNA from *E. coli* and *A. tumefaciens* was performed according to (Sambrook et al. 1989). One single colony was inoculated in 3 mL of LB liquid medium containing the appropriate antibiotic and was incubated overnight al 37°C with continous shaking. Eppendorf tubes containing 1.5 mL culture aliquot were centrifuged at 13,000 rpm for 1 min. The supernatant was discarded and cells were resuspended in 200 µL of Solution I. Then, 200 µL of Solution II was added and the mixture was inverted gently 6-8 times. 200 µL of Solution III were added and mixed by inversion. The mixture was centrifuged at 13,000 rpm for 10 min, the supernatant was transferred into a new Eppendorf tube and 500 µL of isopropanol were added. It was mixed by inversion and centrifuged at 13,000 rpm for 10 minutes. The pellet was washed with 1 ml absolute etanol and centrifuged at 13,000

rpm for 5 minutes. Pellets were dried and resuspended in 50 µL of Tris-HCl 10 mM, EDTA 1mM, pH 8.0..

Solution I/GTE: 25 mM Tris, 10 mM EDTA pH 8.0
Solution II: 0.2 N NaOH, 1% SDS
Solution III: 3M AcK pH 5.5

For sequencing reactions (Section) and electroporation (Section.) the GenElute™ Plasmid Kit from Sigma Aldrich (Darmstat, Germany) was used to purify the plasmid DNA, following the manufacturer's specifications.

M.2.1.2. Yeast.

Plasmid DNA.

To extract plasmid DNA from yeast, one colony was inoculated in 10 mL of YNB selective medium and incubated at 30°C o/n with shaking. The culture was centrifuged at 5,000 rpm for 5 minutes. Cells were resuspended in 0.5 mL of sorbitol 1 M, EDTA 0.1 M pH 7.5 and placed in a 2 mL Eppendorf tube and 20 µl of lyticase (5 mg/mL in KH_2PO_4 pH 7.5) were added. The mixture was incubated at 37°C for 1 h.

Afterwards the mixture was centrifuged at 13,000 rpm and the pellet was resuspended in 0.5 mL of Tris 50 mM pH 7.4, EDTA 20 mM. 0.2 mL of AcK 5 M were added before incubating for 1h in ice. The supernatant was placed in a new tube after centrifugation at 13000 rpm for 5 minutes. To precipitate the DNA, 1 volume of isopropanol was mixed with the supernatant and it was incubated 5 minutes at room temperature. After centrifugation at 13,000 rpm for 1 minute the pellet was dried and resuspended in TE buffer (10:1).

M.2.1.3. Arabidopsis thaliana.

Isolation of *Arabidopsis* genomic DNA was performed according to Edwards et al. 1991 with modifications. Around 100 mg of fresh tissue, previously frozen with liquid nitrogen, were grinded with a plastic pestle. 400 µl of extraction buffer (140 mM sorbitol, 220 mM Tris-HCl pH 8, 22 mM EDTA-Na_2 pH 8, 800 mM NaCl, 0.8% (w/v) CTAB, 1% (w/v) n-Lauroylsarcosine) heated to 65°C and 400 µl of chloroform were added to the sample that was vortexed and heated at 65°C for 5 minutes. The celular debris was removed by

centrifugation at 13,000 rpm for 10 minutes and the supernatant transferred to a fresh Eppendorf tube. This supernatant was mixed with 1 volume of isopropanol and left at room temperature for 20 minutes, then centrifuged at 13,000 rpm for 15 minutes. The pellet was washed with ethanol 70% (v/v), air dried and dissolved in 50 µl of milliQ sterile water.

M.2.2. DNA quantification.

DNA concentration was quantified using a NanoDrop® ND-1000 Spectrophotometer (Thermo Fisher Scientific Inc.).

M.2.3. DNA electrophoresis in agarose gels.

Agarose gels for electrophoresis of DNA contained 0.7-1% (w/v) agarose in 1x TAE buffer (40 mM Tris-acetate, 20 mM sodium acetate, 2 mM EDTA. pH 8.2). Electrophoresis was performed in 1x TAE buffer, supplemented with 0.5 µg/mL ethidium bromide, between 70-120 V. After electrophoresis the gel was photographed with a ChemiDocTM XRS Gel documentation system (Bio-Rad). The software Quantity One (Bio-Rad) was used for band densiometry analysis.

M.2.4. Extraction of DNA fragments from agarose gels.

DNA extraction from agarose gels was performed with ISOLATE II Gel and PCR kit from Bioline (London, UK) following the manufacturer's instructions.

M.3. Enzymatic reactions.

M.3.1. Amplification of DNA fragments by PCR with *Taq* DNA polymerase.

Each reaction mix contained ~ 100 ng of DNA, 0.4 µM of both forward and reverse primers, 0.2 mM dNTPs (dATP+dCTP+dGTP+dTTP, Deoxynucleotides Set, 5prime, Hamburg, Germany), 2.5-5 µL of *Taq* buffer 10x (Sambrook et al. 1989) and 1 U of *Taq* polymerase in a volume of 20 µL. Standard conditions were: 95°C for 5 minutes followed by 35 cycles of: 95°C for 30 s; 55°C for 30 s (around 5°C below the lower primer Tm); 72°C for 90 s (1 minute for each kb to

amplify) and a final 5-minutes elongation step at 72°C. Samples were used immediately or stored at –20°C.

Taq polymerase 10X buffer:

KCl	500 mM
Tris-HCl pH 8.3	100 mM
MgCl2	15 mM
Gelatin	0.1% (w/v)

For plant genotyping and difficult reactions, My*Taq* ™ polymerase from Bioline was used. Each reaction mix contained 0.4 µM of both forward and reverse primers, 4 µL of 5x My*Taq* buffer (5mM dNTPs and 15 mM $MgCl_2$) and 1 U of My*Taq* polymerase in a volume of 20 µL. Standard conditions were: 95°C for 3 minutes followed by 35 cycles of: 95°C for 15 s; 55°C for 15 s; 72°C for 40 s (10 s for amplicons under 1 kb or 30 s/kb for amplification of fragments over 1 kb from high complexity template) and a final 5-minutes elongation step at 72°C.

M.3.2. High-fidelity PCR

PCR reactions were performed with the Velocity DNA polymerase kit (Bioline, London, UK) according to the manufacturer's instructions.

M.3.2.1. Point mutation PCR

To generate point mutation alleles two different strategies were followed. In both cases the pBluescript (KS)-NHX1 plasmid was used as template. For the first set of mutants, the NewEnglands Biolabs' Q5® Site-Directed Mutagenesis Kit was used, following the manufacturer's specifications (https://www.neb.com, protocol E0554). Primers for this protocol were designed using the online tool supplied by NEB (http://nebasechanger.neb.com) (Table 1)

The second set was obtained using a high-fidelity polymerase and the following protocol (Wang and Malcolm 1999) (Figure ***2***). Primers for these reactions were designed such that they had the desired mutation flanked by 10 bp 5' and 3' fitting the template (Table 2); and the reverse primer was the reverse complementary sequence of the forward primer. As both primer fit to each other better than to the template, two reactions were set, each one with

only one of the primers, for 5 cycles. Afterwards, 10 µl of each reaction were mixed and, after addition of the polymerase, the combined reaction was allowed to proceed for 13 cycles. The elongation time was chosen to allow the whole template plasmid to be amplified.

After the PCR reaction, 10 µl of the product was treated with 0,5 µl of *Dpn*I, wich cuts only the methylated GATC sites, in the PCR buffer for 1 h 37°C. *E. coli* cells were transformed with 5 µl of the digestion.

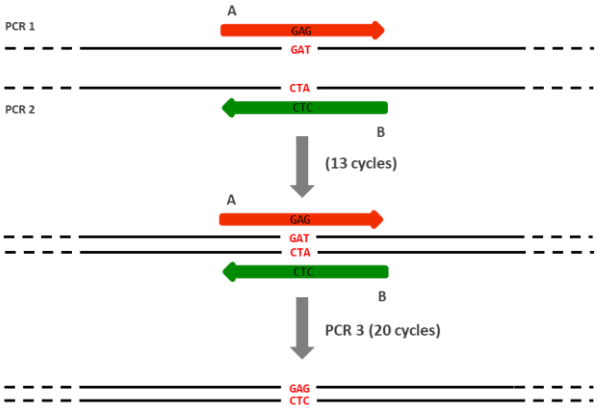

Figure 2. Point mutation PCR scheme.

M.3.2.2. Deletion PCR

In order to generate a *nhx1* allele with a deletion of the CML18 binding domain, mutagenesis by overlapping extension was performed (Ho et al. 1989). This process involves two independent PCRs (Figure ***3***). In the first PCR two fragments that correspond to the flanking regions of the sequence to be deleted are generated. To that end, two pair of oligos are used: each fragment is amplified using one chimeric (primer B and C) and one nonchimeric primer (primer A and D). Chimeric primers are designed so that their 3' ends hybridize to template sequence on one side of the deletion, and the 5' ends are complementary to the template sequence on the other side of the deletion. The AB and CD products generated from the PCR reaction using these primers are therefore overlapping at the deletion point. The resulting two PCR fragments from the first step are gel-purified and used as the template for the second step of PCR. During this second overlapping extension PCR, the purified fragments are mixed and subjected to PCR amplification using the external oligo primers ('A' and 'D') The resulting ligated PCR fragments are gel-purified and used for cloning following the appropriate restriction enzyme digestion.

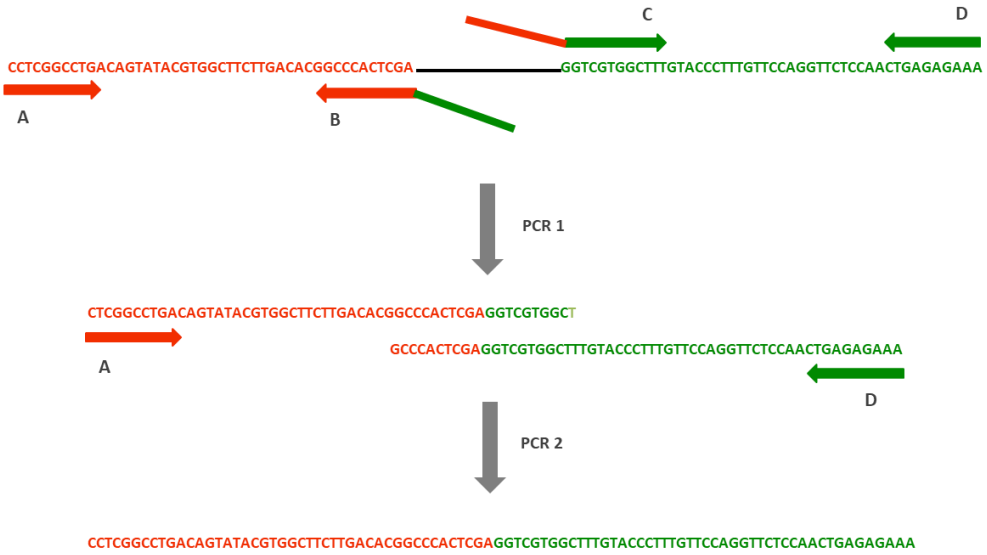

***Figure 3. Scheme of the two-step PCR deletion protocol*.**

M.3.4. PCR DNA fragments subcloning

DNA fragments obtained by PCR reaction, were subcloned into the pSpark® vectorI (Canvax) following the manufacturer's indications.

M.3.5. Ligation of DNA fragments.

For ligation of DNA fragments a ratio of insert to vector 5:1 was used. Each 10 µL ligation mix contained insert DNA, vector, 1U of T4 DNA ligase (Invitrogen™, Karlsruhe, Germany) and 1 µL of the 10X ligation buffer supplied by the manufacturer. Ligations were incubated at 4°C o/n; 5 µL of the ligation mix were used for bacterial transformation

.

M.3.6. DNA digestions with restriction enzymes.

Restriction enzyme digestion of DNA was performed using the buffers and conditions recommended by the manufacturer (New England Biolabs). One µg of DNA was treated with at least 1 U of restriction enzyme. For subsequent manipulations, DNA products digestion were separated by electrophoresis in agarose gels (Section M.2.3.) and the DNA fragment of interest was isolated using the method described in the Section M.2.4.

M.3.7. DNA Sequencing.

DNA samples were sent for sequencing by StabVida (Lisboa, Portugal). Each sequencing reation contained 10 µL of 100 ng/µL plasmid DNA samples and 3 µl of the specific primer at a concentration of 5 µM.

M.4. Protein

M.4.1. Expression and isolation of heterologous protein from bacteria

The complex AtNHX1-BD/CML18 was expressed in bacteria. The cDNA encoding the CML18 protein was cloned as a *Nco*I/*Not*I fragment in the pCDFDuet-1™ expression vector (Novagen, EMD Chemicals, San Diego, CA), with a N-terminal 6xHistidine tag. The cDNA fragment encoding the NHX1-BD (from H445 to G516) was cloned between the *Eco*RI/*Not*I cloning sites of the pGEX-T4 expression vector (GE Healthcare), fused to GST in N-terminal position. The choice of these vectors was based on the compatibilities of their replication origin and antibiotic resistance, as well as their high expression in the host strain used.

	Replicon	**Antibiotic resistance**	**Copy number**	**Tag**
pCDFDuet-1™	CloDF13	Streptomycin/spectinomycin	20-40	N-terminal His-tag
pGEX-T4	pBR322	Ampicilin	20-40	N-terminal GST

The recombinant plasmids were verified by polymerase chain reaction (PCR) and restriction enzyme digestion. *E coli* strain Rosetta™ 2 (DE3) pLysS (Novagen, EMD Chemicals, San Diego, CA), was co-transformed with the recombinant pCDF-HisTag-CML18 and pGEX-T4-GST-NHX1f vectors. The co-transformed cells were selected on LB medium plates supplemented with 50 µg/ml1 kanamycin and 30 µg/ml spectinomycin.

M.4.1.1. Induction of protein expression

Pre-cultures, 5 ml of LB medium, were inoculated using a single colony picked directly from agar plates, and then cultivated at 37°C overnight with shaking at 150 rpm. For protein expression, flasks containing 200 ml culture of 2xTY medium were inoculated with 1 ml of the

pre-culture, and incubated at 37°C with shaking at 150 rpm. At OD_{600} 0,4-0.6, expression of the recombinant proteins was induced by the addition of 0.2 mM IPTG (Sigma, USA). Cultures were incubated overnight at 16°C and 130 rpm. Cells were harvested by centrifugation at 5,000 rpm for 5 min, and washed twice with TBS buffer. The bacterial pellet was resuspended in 10 ml of ice-cold lysis buffer (TBS, 1 mM PMSF).

M.4.1.2. Protein purification

Cells were lysed using a Branson Digital Sonifier at 20% power output, 3×30 sec continuous applications with 30 second cooling intermission. The lysate was centrifuged for 5 min at 10,000rpm at 4°C to remove cell debris. The supernatant containing the recombinant proteins was divided in two fresh tubes to be purified by affinity chomatography.

Sepharose 4B beads

One of the protein extract solution containing the soluble recombinant complex was incubated with 50 µl glutathione immobilized Sepharose 4B resin, that had previously been equilibrated with 1xTBS, for one hour at room temperature with gentle rotation. Non-specifically bound proteins were washed under mild, non-denaturing conditions using 5 ml TBS. The target protein was eluted using 50 mM Tris-HCl, 25 mM gluthatione, pH 8.0, 5 fractions of 200 µl each were collected.

Ni_2^+NTA beads

The second sample containing the complex was incubated with 50µl Ni_2^+NTA affinity resin (Qiagen, Germany), that had been equilibrated with 1xTBS, for one hour at room temperature with rotation. Non-specifically bound proteins were washed under mild, non-denaturing conditions using 5 ml wash buffer (TBS 25 mM imidazole). The target protein was eluted in TBS containing 300 mM imidazole, 5 fractions of 200 µl each were collected.

M.4.3. SDS-PAGE.

Protein electrophoresis was performed using the Mighty Small SE 250 system (GE Healthcare). PAGE gels were prepared following the instructions of Sambrook et al. 1989. Electrophoresis was performed at 20 mA/gel for approximately 1 hour.

Acrylamide gel mix:

Reagents	Running gel 10% (10 mL)	Stacking gel 5% (6 mL)
Milli-Q water	4 mL	4.1 mL
30% Bisacrylamide/Acrylamide	3.3 mL	1 mL
1.5 M Tris pH 8.8	2.5 mL	
1 M Tris pH 6.8		0.75 mL
10% SDS	0.1 mL	0.06 mL
10% APS	0.1 mL	0.06 mL
TEMED	0.004 mL	0.006 mL

Electrophoresis buffer 10X

Tris Base	250 mM
Glycine	1.94 M
SDS	1% (w/v)

The pH of the 1x electrophoresis buffer must be 8.3.

1X Urea sample buffer

Tris-HCl pH 6.8	200 mM
SDS	5% (w/v)
DTT	100 mM
Urea	8M
Bromophenol blue	0,1 % (w/v)

M.4.4. Coomassie blue staining of SDS-PAGE gels.

Proteins in acrylamide gels were stained in two steps (Bradford 1976). First the gel was incubated in Coomassie staining solution with gentle shaking at room temperature for at least 1 h. After removal of the staining solution, the gel was incubated in destaining solution until the protein bands appeared without background stain of the gel.

Staining solution

Glacial acetic acid	50 % (v/v)
Methanol	10 % (v/v)
Coomassie brilliant blue R-250	0.25 % (w/v)

Destaining solution

Glacial acetic acid	10 (v/v)
Methanol	10 % (v/v)

M.5. Genetic transformation.

M.5.1. Bacterial transformation.

M.5.1.1. Preparation of competent cells.

Escherichia coli.

To prepare *E. coli* One Shot® TOP10 chemically competent cells a 1 mL vial of seed stock was inoculated in 250 mL of SOB medium and grown at 20°C to an $O.D._{600}$ of 0.3. Culture was centrifuged at 3,000 g at 4°C for 10 min in a flat bottom centrifuge bottle. The pellet was gently resuspended in 40 mL of ice-cold CCMB80 buffer and incubated on ice for 20 min. Cells were centrifuged at 3,000 g at 4°C for 10 min and resuspended in 5 mL of ice-cold CCMB80 buffer. The $O.D._{600}$ of a mixture composed of 200 µL of SOC medium and 50 µL of the resuspended cells was measured. Chilled CCMB80 buffer was added until reaching an $O.D._{600}$ of 1.0-1.5. Then, the suspensión was incubated 20 minutes on ice. Aliquots of 100 µL in 1.5 mL Eppendorf tubes were immediately frozen in liquid nitrogen and stored at -80°C.

CCMB80 buffer:

KOAc pH 7.0	10 mM
$CaCl_2.2H_2O$	80 mM
$MnCl_2.4H_2O$	20 mM
$MgCl_2.6H_2O$	10 mM
Glycerol	10% (v/v)

Agrobacterium tumefaciens.

In order to prepare electrocompetent *Agrobacterium tumefaci*ens cells, single colonies of strain GV3101 were inoculated in 3 mL of YEP medium supplemented with rifampicin (50 µg/mL) and gentamicin (20 µg/mL) and incubated at 30°C over night with vigorous shaking.

100 mL of YEP medium were inoculated with 0.5 mL of this preinoculum. Cells were incubated to an $O.D._{600}$ of 0.5-1, spun at 3,000 g for 5 minutes and washed with 1/2 volume of cold sterile 10% (v/v) glycerol. Centrifugation was repeated and cells were resuspended in 4 mL of sterile 10% (v/v) glycerol. Cells were centrifuged and finally resuspended in 1.5 mL of ice-cold 10% (v/v) glycerol. Cells were dispensed in 50 µL aliquots into 1.5 mL Eppendorf tubes and immediately frozen by adding liquid nitrogen. Aliquots were stored at -80°C.

M.5.1.2. Bacterial competent cells transformation.

Escherichia coli.

For transformation, 10-100 ng of plasmid DNA, in a maximum volume of 10 µL, were added to 100-200 µL *E. coli* competent cell aliquots. The mix was incubated for 30 minutes in ice before subjecting them to a heat shock of 42°C for 30 seconds and letting to recover for 4 minutes in ice. Then, cells were incubated in 1 ml of LB medium for 1 hour at 37°C. Cells were collected by centrifugation at 13,000 rpm for 1 minute and plated in LB medium supplemented with the appropriate antibiotic using sterile glass beads of 4 mm ø.

Agrobacterium tumefaciens.

50 ng of plasmid DNA were added to 50-100 µl of *Agrobacterium* competent cells and the mix was incubated for 3 minutes in ice. The mixture was placed in a Gene Pulser®/MicroPulser™ electroporation cuvette (Bio-Rad, Richmond, California, EE.UU.) and electroporation was performed with the MicroPulser™ Electroporator (Bio-Rad, Richmond, California, EE.UU.). Cells were collected from the cuvettes and incubated in 2 mL of YEP medium for 2-3 hours at 30°C. Then 100 µl of the culture were plated in YEP medium supplemented with the appropriate antibiotics using sterile glass beads of 4 mm ø.

M.5.2. Yeast transformation.

Yeast transformations were performed using the lithium acetate/PEG method, as described by Elble R, (1992). Yeast celles were inoculated in 10 mL of YPD medium and incubated over night at 30°C. ~ 1 x 10^8 cells (an $O.D._{600}$ of 0.5 is equivalent to ~ 5 x 10^6 cells/mL) were harvested by centrifugation. 1-2 µg of plasmid DNA, 500 µl of PLATE solution and single-stranded carrier DNA were added to the cell pellet that was throughly resuspended by vigorous vortexing. Cells were incubated for 40 minutes at 42°C or over night at 25°C.

Afterwards they were recovered by centrifugation 5' at 5,000rpm, washed once with sterilized water, and plated on YNB selective médium lacking the appropriate aminoacids, using sterile glass beads of 4 mm ø.

PLATE solution:

PEG (WM 3350) 45%	40.5% (v/v)
Lithium acetate	100 mM
Tris-HCl pH 7.5	10 mM
EDTA pH 8	1 mM

M.5.3. Plant transformation.

M.5.3.1. Agrobacterium-mediated infiltration of Nicotiana benthamiana.

Nicotiana benthamina agroinfiltration was performed according to Waadt and Kudla 2008. A colony of *A. tumefaciens* carrying the construct of interest (Section M.6.2.) was inoculated in 5 mL of YEP medium with antibiotics and incubated over night at 30°C. OD_{600} was measured and the volume needed to get a final OD_{600} of 0.5 was calculated according to the formula V= (V_{final} x 0.5)/$O.D._{600}$. For the p19 strain the final OD_{600} was 0.3. The calculated culture volumes of both *Agrobacterium* strains were put together in a Falcon tube and centrifuged at 5,000 rpm for 15 minutes. The supernatant was removed and the pellet resuspended in the final volume of activation buffer, where cells were incubated at least 2 h at room temperature. 5-6-week old well-irrigated *N. Benthamiana* plants were infiltrated with the mixed cultures in the abaxial side of the leaves using a 2 mL syringe without a needle.

Activation buffer

MES	10 mM
$MgCl_2$	10 mM
Acetosyringone	150 µM

M. 6. Obtention of *nhx3 nhx4* null double mutant.

Homozygous plants of single mutants SALK_082277 (*Atnhx4*; *At5g55470*) and SAIL_827_D04 (*Atnhx3*; *At3g06370*) were crossed to obtain the null double mutant. Plants

were grown in soil (Section M.1.3.2.) in individual pots. Both genotypes were used as female and male parentals. For the parental female a single inflorescence per bolt was chosen, opened and immature flowers were eliminated. The chosen immature flower was carefully emasculated under the stereomicroscope SteREO Discovery.V8 (Zeiss). A stamen of the male parental was taken and rubbed over the stigma of the parental female. Once fertilized, the immature flower was closed and covered with plastic film to maintain the humidity until the silique was developed. The mature silique was harvested and placed in an Eppendorf tube until it was completely dry. F1 plants were sown on soil and F2 was obtained by self-pollination of F1 plants. Because the probability of appereance of double null mutants in the F2 is 1/16, F2 plants with the genotype *nhx3/nhx3 NHX4/nhx4* were selected by PCR to obtain a F3 enriched in double homozygous mutants (1/4 instead of 1/16). Therefore, double mutant plants carrying the null alleles *nhx3* and *nhx4* were produced by self-pollination of a plant of genotype *nhx3/nhx3 NHX4/nhx4* and null homozygous *nhx3 nhx4* plants were selected by diagnostic PCR. . .B illustrates the position of the primers used and the PCR bands obtained from the wild type and mutated *loci*

M.6.1. Null double mutant selection by PCR genotyping.

Insertion mutant information was obtained from the SIGnAL website (http://signal.salk.edu) and confirmed experimentally. Mutant *nhx3* has a T-DNA insertion at nucleotide +1559 relative to the start codon, whereas in the mutant *nhx4* the insertion TDNA lies within the UTR 5', To confirm the obtention of the *nhx3nhx4* knockout double mutant line, diagnostic PCR screening with allele-specific primers designed to amplify wild-type or mutant *loci* were performed. For the PCR reaction of the *AtNHX3 locus*, two combinations of primers were used: nhx3-5'/nhx3-3' to identify the wild type allele, and nhx3-3'/Lba1.3 to identify the mutant allele (Annex 3). In a similar way, for the PCR of the *AtNHX4 locus*, nhx4-5'/nhx4-3' and nhx4-3'/LB3a primers were used to identify the wild type and the mutant allele, respectively. .

M.6.2. Physiological characterization of *A. thaliana* mutant lines

M.6.2.1. In vitro assays.

Arabidopsis thaliana seeds were sterilized, sawn and stratified (darkness and 4°C) for two days, and then transferred to a CONVIRON chamber in long day conditions (Section M.1.3.2.).

Sensitivity to salt stress

Germination rate and survival quantification.

Seeds were sawn in square 12x12 cm Petri dishes (36 seeds per genome) containing solid LAK 1 mM K pH 5.6 10 mM MES medium, supplemented with increasing concentrations of NaCl (0, 50, 100, 150). The germination rate was measured after 4 days as the number of seeds with visible radicule, and the survival rate was measured after 21 days as seedlings with visible green parts.

Root growth rate.

Root growth was measured in 12x12 cm Petri dishes with solid LAK medium, supplemented with increasing concentrations of Na (0, 50, 100, 150 mM).

For the root growth assay with increasing concentrations of Na^+, 5 seeds were sown in LAK during four days and then transferred to new plates with LAK 1 mM K pH 5.6 10 mM MES with increasing concentrations of Na^+.

In the case of root growth in different concentrations of K, seeds were sawn in with LAK supplemented with 1 mM Na^+ during four days, and then transferred to new plates with LAK 1 mM Na pH 5.6 10 mM MES with increasing concentrations of K^+.

The length of the root was measured after 21 days (17 days on the treatement dishes).

Sensitivity to K^+

Seeds were sawn and germinated in 12x12 cm Petri dishes with LAK 1 mM NaCl pH 5.6 media 10 mM MES. After four days seedlings were transferred to new plates with LAK 1 mM Na pH 5.6 10 mM MES, supplemented with increasing concentrations of KCl (0, 0.1, 1, 10, 100 mM). 16 days after the fresh and dry weight was measured.

Fresh weight measurements were determined with seeds sawn in 12x12 petri dishes with LAK medium and supplemented with increasing concentrations of KCl (0,0.1, 1, 10, 100 mM NaCl). After two days of cold-stratification, seeds were transferred to a growing chamber for 21 days. On day 21, 3 seedlings per genotype were introduced in an Eppendorf and weighted. Eppenddorfs with seedlings were put open in an oven at 60°C for 24 hours and dry weight was measured.

M.6.2.2. Growth in standard conditions.

Phenotypical characterization.

Plants were grown as described in Section M.1.3.2. To characterize the phenotype of the mutants different parameters were measured: rosette diameter, flowering time, petal size.

To determine the rosette diameter of Arabidopsis wild-type Col-0 and mutant lines, pictures of 3-week-old plants were taken with a Canon EOS D700 camera. To calculate petal area, petals from completely opened flowers were harvested and pasted to a black paper using transparent tape (14-16 petals per genotype). The paper with the petals was scanned with high resolution. In both cases the pictures obtained were analyzed using FIJI software (Schindelin et al. 2012).

To calculate flower opening time, the number of rosette leaves were determined (Reeves and Coupland 2001; Jeong et al. 2015; Sharma et al. 2016). This parameter was measured two times for each plant: when the first flower bud was visible (flowering time) and when the first flower opened (flower opening time). For each experiment 6-8 plants per genotype were used.

M.7. Study of AtNHX1 interacting proteins.

Two different approaches have been used to demonstrate NHXs interactions with other proteins: yeast two-hybrid assays (Y2H) and bimolecular fluorescence complementation (BiFC). Both will be described in detail below.

M.7.1. Yeast two-hybrid assays.

Yeast two-hybrid (Y2H) is a technique used to show physical interactions between two proteins. The two proteins of interest are fused in frame to two separate fragments of the GAL4 transcription factor: the binding domain (BD) that is able to interact with its target DNA and the activation domain (AD) that activates the transcription. Thus, if two proteins interact physically, both fragments of the transcription factor come together and activate a downstream reporter gene.

To test the interaction between AtNHX1ct and AtNHX2ct with CML18, as well as the lack of interaction of AtNHX1ct without the CML18 binding domain (BD) a *Eco*RI/*Bam*HI cDNA fragment encoding the AtNHX c-terminal was subcloned in pGBKT7-BD vector (Clontech) and the *AtCML18* cDNA was subcloned in the pGADT7-AD vector (Clontech) as an *Eco*RI/*Bam*HI fragment, creating the plasmid pGADT7-CML18.

Yeast strain AH109 was cotransformed with all combinations of pGADT7-AD and pGBKT7-BD vectors:

	pGBKT7-BD	**pGBKT7-NHX1ct**	**pGBKT7-NHX2ct**	**pGBKT7-nhx1ΔBDct**	**pGBKT7-NHX1_H499Lct**	**pGBKT7-NHX1_D506Nct**
pGADT7-AD	X					
pGADT7-CML18		X	X	X	X	X

Tansformant colonies carrying the vectors were selected in YNB/-Trp/-Leu plates. Yeast transformants were inoculated in 2 mL of YNB/-Trp/-Leu media and grown at 28°C until saturation (O.D.600 ~ 2). From the saturated cultures, 1:10 serial dilutions were made and 5 µL-drop of each dilution was inoculated on YNB/-Trp/-Leu; YNB/-His/-Trp/-Leu and YNB/-Ade/-Trp/-Leu plates. Plates were incubated at 28°C for 3-4 days.

M.7.2. Bimolecular fluorescence complementation (BiFC).

This technique allows the detection of protein-protein interactions *in planta*. This approach is based on the molecular complementation between two nonfluorescent halves of the YFP fluorescent protein when they are brought together by interaction between two proteins fused to each fragment of the YFP (Hu et al. 2002).

M.7.2.1. BiFC plasmids.

All vectors used have been described in Waadt et al., 2008 (Annex 2) and DNA manipulations were performed as described in Section M.3. *AtNHX* wild-type and mutant cDNAs were subcloned in frame with the carboxi terminal of the eYFP as *Spe*I/*Xho*I fragments

in plasmid pSPYCE(M), and *AtCML18* was subcloned as KpnI-NotI in the vector pSPYNE(R)173 fused to the amino terminal segment of the eYFP protein.

M.7.2.2. Agroinfiltration in N. benthamiana leaves.

Agrobacterium tumefaciens strain GV3101 was transformed with BiFC constructs as described in Section M.5.3.1. The bacterial transformants were infiltrated together with the p19 transformed *Agrobacterium* strain in 5-6-week-old *N. benthamiana* leaves as indicated in Section M.5.3.2.

M.7.2.3. BiFC microscopy.

Microscopy analyses were performed as in Waadt et al., 2008. *N. Benthamiana* leaf discs were cut 3 days after infiltration. To make comparison of different samples and fluorescence intensity quantification, the lower epidermis was analyzed in an inverted fluorescence microscope FluoView FV1000 Confocal Microscope (Olympus) using a 515-nm laser and a 60X objective. Images were analyzed with Fiji software (Schindelin et al. 2012). Images were obtained using constant imaging conditions: exposure time of 1ms for bright field and 1.2 s for U.V. light, gain of 100, without offset and 1 of binning. eYFPC/eYFPN complexes were visualized using a YFP filter.

M.8. Functional study of *NHX* mutant alleles in *Saccharomyces cerevisiae*.

M.8.1. Plasmid constructs and yeast strains generation.

The mutant alleles of *AtNHX1* listed in Table 1 and Table 2 were generated by point mutation PCR as described in Section M.3.2.2, using the vectors pBluescriptII (KS)- NHX1 as template and specific primers. The generated alleles were subcloned in plasmid pDR195 as *Xho*I/*Not*I fragments.

Table 1. NHX1 single mutant alleles. Set I.

Final vector	Original aa	Mutated aa	Primer
pDR-D157N	Asp157 GAT	Asn157 AAT	157mut: 5'TTGCTGCAACAaATTCAGTGTGTAC 157rev 5'ATATGGCACCAATAGCAAGATAATC
pDR- R353L	Arg353 AGA	Leu353 CTA	353mut: 5'CATGGTTGGActAGCAGCGTTCGTC 353rev: 5'ACCAGACCCATTAGGATTGAGC
pDR-N184D	Asn184 AAT	Asp184 GAT	184mut: 5'GGGTGTTGTGgATGATGCAAC 184rev: 5' TCTCCGAATACAAGACTG
pDR-D185N	Asp185 GAT	Asn185 AAT	185mut: 5'GTGTTGTGAATaATGCAACGTCAGTTG 185 rev: 5'CTCTCCGAATACAAGACTGTAAAGC
pDR-H479L	His479 CAC	Leu479 CTC	479mut: 5'CCTTCAGGGAACCtCAATGTGCCTCG 479rev: 5'CTCAATGAACGAGTCTTGGTCCAAC
pDR-H499L	His499 CAT	Leu499 CTT	499mut: 5'CACTCGAACCGTGCtTTACTACTGGAGAC 499rev: 5'GGCCGTGTCAAGAAGCCACGTATAC
pDR-D506N	Asp506 GAT	Asn506 AAT	506mut: 5'GAGACAATTTaATGACTCTTTCATGC 506rev: 5' CAGTAGTAAtGCACGGTTCGAGTG

Table 2. NHX1 Single and double mutant alleles. Set 2.

Final vector	Original aa	Mutated aa	Primer
pDR-R353K	Arg353 AGA	Lys353 AAA	353Kfw: CATGGTTGGAAaAGCAGCGTTCGTC 353Krev: GACGAACGCTGCTtTTCCAACCATG
pDR- R390K	Arg390 AGA	Lys390 AAA	390KFw: CTGGTCTCATGAaAGGTGCTGTATC 390KRv: GATACAGCACCTtTCATGAGACCAG
pDR- N184D-R→K	Asn184 AAT	Asp184 GAT	184mut: 5'GGGTGTTGTGgATGATGCAAC 184rev: 5' TCTCCGAATACAAGACTG
pDR- H499L	His499 CAT	Leu499 CTT	499LFw: CACTCGAACCGTGCtTTACTACTGGAGAC 499LRv: GTCTCCAGTAGTAAaGCACGGTTCGAGTG
pDR- H479L-H499L	His479 CAC	Leu479 CTC	479Lfw: CCTTCAGGGAACCtCAATGTGCCTCG 479LRv: CGAGGCACATTGaGGTTCCCTGAAGG
pDR-H499L D506N	Asp506 GAT	Asn506 AAT	506NFw: GAGACAATTTaATGACTCCTTCATGCG 506NRv: CGCATGAAGGAGTCATtAAATTGTCTC

Yeast cells were transformed with the obtained mutant alleles (Section M.5.2) and selected in YNB –H-U plates. Positive transformants were used in growth assays (Section M.8.2), and vacuole pH measurement (Section M.9.4

M.8.2. Yeast growth assay.

M.8.2.1. Drops in solid media.

Yeast growth assays were used to determine the tolerance of AXT3K yeast transformants to different NaCl or LiCl concentrations in AP medium, and different hygromycin B concentrations in YPD medium. Yeast were transformed with the pDR-NHX1 alleles and selected in YNB without histidine and uracil (Section M.5.2). Yeast transformants were inoculated in 2 mL of YNB media supplemented with the corresponding amino acids and grown at 30°C overnight. The cells were then harvested and resuspended to a final OD_{600} of 0,5. The cells were then serially diluted 10-fold in water, and 5 µl of each dilution were spotted onto the selective media: AP with different NaCl or LiCl concentrations, or YPD plates supplemented with different concentrations of hygromycin B. Plates were incubated at 30°C during 3-5 days.

Pictures of the plates were taken using a Canon EOS D700 camera.

M.8.2.2. Growth assays in liquid media.

Yeast growth assays were used to determine the tolerance of AXT3K yeast transformants to different NaCl and LiCl, concentrations in AP medium or hygromycin B in YPD medium. Transformant yeast cells expressing the different pDR-NHX1 alleles were inoculated in 2 mL of YNB media supplemented with the corresponding amino acids and grown at 30ºC overnight. The cells were then harvested and resuspended to a final OD_{600} of 0,5. 20 µl of this dilution was used to inoculate a 96-well plate containing 200 µl of liquid media per well. From the first well, 10-fold serial dilutions were made.

Plates were incubated at 30°C. The OD_{600} of the culture was measured 24 and 48 days after the inoculationwith the Varioskan LUX Multimode Microplate Reader (ThermoFisher Scientific)

Three independent AXT3K transformant colonies were used in each assay., The mean and standard error (SE) of the growth of each transformant was calculated using Microsoft Office Excel software.

M.9. Microscopy

M.9.1. Root imaging pH measurements

The method described in (Waadt et al. 2017) was used, with modifications. *Arabidopsis thaliana* Col-0 plants expressing the pHGFP fluorescent reporter were grown vertically in solid LAK 1 mM K pH 5.6 10 mM MES-Tris medium in a growth chamber (Conviron CMP 6010, Berlin, Germany). Three-day-old seedlings were transferred to microscope dishes (MatTek, Ashland, MA, USA) supplemented with LAK 1 mM K pH 5.6 10 mM MES-Tris and 0,7% low melting point agarose (Roth), and incubated vertically overnight in the growth chamber. Before imaging, seedlings were placed horizontally and 90 µl of liquid LAK media 1 mM K pH 5.6 10 mM MES-Tris was added. Seedlings were gently pressed back into their agarose bed and incubated for 40–60 min for recovery. Imaging was performed with a Leica SP5II using a ×10 objective (HC PL Fluotar ×10/0.3 DRY). The wavelengths for reporter excitation were 405 and 488 nm, and emission was detected in a 500-550 range by HyD2 detector. Frames were acquired every 6 seconds during 40 minutes. After 4 minutes of imaging (stack 40) roots were treated with different treatments adding 10µl of the desire solution on the side of the root.

For image processing the following steps were conducted using Fiji (Schindelin et al. 2012): background subtraction, gaussian blur, 32-bit conversion, threshold, ratio calculation and royal look up table. Image data were obtained from processed 32-bit images using Fiji. Entire images were quantified for presentations of global responses. Heat maps were generated by analyses of 64 adjacent regions of 16 × 178 pixels (24.2 × 268.2 µm). Normalized datasets ($\Delta R : R$) were calculated as $(R - R0)/R0$, where $R0$ represent mean 4 min baseline values. Normalized heat maps were obtained from registered movies and each region was normalized to its respective baseline. Graphs and heat maps were generated using OriginPro.

M.9.2. Seedlings pH measurements

Plants expressing the pHGFP fluorescent reporter were grown on LAK medium (pH 5.6 10 mM MES-KOH) as described in Section M.1.3.2. Three-day-old seedlings grown vertically in the growth chamber were transferred to new plate with the same media and supplemented with either KCl, NaCl or LiCl (in different concentrations) or no treatment (control plate), and grown for an additional 24 h. Microscopy analyses were performed using a Leica TCS LSI microscope equipped with a PLAN APO ×5.0 macro objective (Leica Microsystems, Wetzlar, Germany). pHGFP reporter was sequentially imaged with excitation wavelength of 405 nm

and 488 nm, and emission wavelength of 500–550 nm. Seedlings were directly imaged from the plate without any manipulation. To image entire seedlings in x, y and z, z-stacks at multiple positions were acquired. Image processing and analysis was performed using Fiji (Schindelin et al., 2012). Fluorescence intensity values of z-stacks were summed up and individual tiles were stitched together using the Grid/collection stitching tool (Preibisch et al. 2009). After background subtractions, ratiometric image calculations proceeded as described by (Kardash et al. 2011).

M.9.3. BCECF to measure petals vacuolar pH

Vacuolar pH of *Arabidopsis thaliana* opened-flower petals was determined using the fluorescent cell-permeant dye BCECF AM (Molecular Probes). BCECF 2',7'-Bis-(2-Carboxyethyl)-5-(and-6-)-Carboxyfluorescein Acetoxymethyl Ester is a pH sensitive dual-ratiometric dye that has been used to measure intracellular pH. The protocol used was based in Bassil et al. 2013 with modifications.

M.9.3.1. Loading of the dye.

Plants were grown as described in section M.3.2. At least 4 independent plants per genotype. When all plants presented completely opened flowers, petals were harvested and placed in a 96-well micro-plate: 8 petals per well, 6 wells per genotype. Loading of the dye was performed in liquid media containing 1/10 MS medium, 0.5% sucrose, and 10 mM Mes-KOH (pH 5.8) in the presence of 10 µM BCECF AM. First, petals were subjected to 15 minutes vacuum, and afterwards they were incubated 1 h at 22 °C in darkness. After that, the petals were washed two times for 10 min in the medium mentioned above. BCECF fluorescence was detected using a microplate reader.

M.9.3.2. In situ calibration

To obtain the calibration curve, dye loaded petals were incubated in each of the pH calibration buffers for no longer than 15-20 min. Then the solution was replaced by liquid medium containing 1/10 MS medium. The ratios for each pH incubation were plotted against pH to obtain the calibration curve. A sigmoidal regression (Boltzmann function) was fitted to

describe the calibration curve and to calculate subsequent pH values from the equation describing the curve.

Calibration buffer

Ammonium acetate	50 mM
Mes-BTP (pH 5.2-6.4) or 50 mM-HEPES-BTP (pH 6.8-7.6)	50mM

M.9.3.3. pH measurement

Fluorescence intensity and absorbance values were acquired using (aquí falta lo que quieras que usaras para medir). Settings for calibration and measurement should be identical. Samples were sequentially excited by two wavelengths: 440 nm and 495 nm, fluorescence emition was detected at 525 nm for each of the two excitation wavelengths. Three reads per well and weavelenght were done.

The data obtained was analysed in a Microsoft Excel sheet. First, after blank subtraction (petals without BCECF treatment), the Ratio 495/440 was calculated for the calibration wells dividing emission values excited with 495 nm by the emission values excited with 440 nm. Means and standard deviations of technical replicates were calculated.

The calibration curve was created plotting pH values of the buffers used in the calibration against the respective values of Ratio 495/440 calculated. Using OriginPro, a sigmoidal regression fit (Boltzamn fit) was performed with the calibration data. The obtained equation was used to calculate the pH of the problem samples. To that end, the Ratio 495/440 values of the problem samples were calculated after blank subtraction as before mentioned obtained s directl, and by interpolating these values in the equation, the pH was obtained.

M.9.4. BCECF to measure yeasts vacuolar pH

M.9.3.1. Loading of the dye.

To measure vacuolar pH in yeast, the protocol described by Ali et al., 2004 was used, with the proper modifications to make the pH measurements in a microplate reader (Brett et al. 2005b). Yeasts were grown overnight in AP pH 6.0 medium without histidine and uracil. Culture in exponential phase of growth (OD_{600} 0.5-0.6) were harvested, washed two times and finally resuspended in AP medium without aminoacids, to a final OD_{600} of 0.2-0.3. Three independent colonies per mutant allele and control were used. Each smaple was incubated

with 50 µm de 2',7'-bis-(2-carboxietil)-5-(y-6)-carboxifuoresceein acetoximetil ester (BCECF-AM; Molecular Probes, Eugene, OR) at 28ºC, with gentle shaking.

After 20 minutes, the culture was centrifugated 10' at 5,000 rpm and washed three times with AP medium without aminoacids and without BCECF (incubating during 10 min with the new medium after each centrifugation). Finally, yeast cells were resuspended in 100 µl of AP medium without aminoacids and without BCECF end immediately the fluorescence was measured.

Fluorescence measurements were performed using a Varioskan LUX Multimode Microplate Reader (ThermoFisher Scientific) at 20 ºC, that were shaked before each measurement.

M.9.3.2. pH measurement

Fluorescent intensity and absorbance values were recorded using a Varioskan LUX Multimode Microplate Reader (ThermoFisher Scientific). Settings for calibration and measurement were identical. Samples were sequentially excited by two wavelengths: 450 nm and 490 nm; emition fluorescence was detected at 535 nm for each of the two excitation wavelengths. Absorbance was also measured with 600 nm weavlength. Three reads per well and weavelenght were done. Measurements were repeated three times for each culture, washing the cells in between with AP medium without aminoacids and without BCECF.

M.9.3.3. In situ calibration

At the end of each experiment, a calibration curve of fluorescence intensity versus pH was obtained. Each of the 200 µl culture used were treated with the following experimental medium:

MES	50 mM
HEPES	50 mM
KCl	50 mM
NaCl	50 mM
Ammonium acetate	200 mM
NaN_3	10 mM
2-deoxyglucose	10 mM
Cyanide m.chlorophenylhydrazone	50 µM

Buffers were titrated to eight different pH values (5.2, 5.6, 6.0, 6.4, 6.8, 7.2, 7.6, 8.0) using 1 M NaOH.

To estimate accurately acid pH values below 5.0, the James-Kracke (1992) approximation was performed. According to this, in a pH close to neutrality, BCECF fluorescence measured as H^+ activity, or hwat is the same, H^+ concentrations using the formula:

$$H^+ = K_a x \frac{(R_{max}-R)}{(R-R_{min})} \; x \; \frac{F_{base\ 450}}{F_{acid\ 450}} \quad (1)$$

Being: K_a the acid dissociation constant, R the ratio of the emited fluorescence by BCECF excited at 490 and 440 (Ratio 490/450), R_{max} is the maximun Ratio 490/450 value, obtained in alkaline conditions, R_{min} is the minimum Ratio 490/440, in acid conditions. $F_{base450}/F_{acid450}$ is the ratio of the fluoreacence at 450nm in acid and basic conditions (James-Kracke 1992)

The logarithmic transformation of the ecuation is:

$$pH = pK_a - log\left(\frac{F_{base\ 440}}{F_{acid\ 440}}\right) - \log\left(\frac{(R_{max}-R)}{(R-R_{min})}\right) \quad (2)$$

In the isosbestic point $F_{base450}/F_{acid450}$ is 1, reason why:

$$pH = pK_a - \log\left(\frac{(R_{max}-R)}{(R-R_{min})}\right) \quad (3)$$

Where R_{max} and R_{min} are obtained from the most alkaline and most acid pH buffers measured.

Th values obtained for each culture treated with different buffers were background subtracted and normalized to cell density. The pH calibration curve was obtained by plotting $\log\left(\frac{(R_{max}-R)}{(R-R_{min})}\right)$ against pH. The resulting equation was used to obtain the pKa.

M.9.3.4. Data analysis.

The data obtained was analysed in a Microsoft Excel sheet. After blank subtraction (yeast without BCECF tratment) and cell density normalization. To obtain pH values, the ratio 490/440 was calculated in each case, and the values obtained were extrapolated from the calibration curve.

M.10. Bioinformatics

A BLAST search against the SwissModel database (Bienert et al. 2017; Waterhouse et al. 2018) using the AtNHX1 protein sequence was conducted to find templates that allow us generate a topological and 3D structural model of AtNHX1. The protein sequences of the proteins with better scores identified were obtained from the UniProt database. All pairwise alignments and multiple alignments of proteins sequences performed in this project were conducted using the default parameters of the MUSCLE software. (Edgar 2004). 3D model structures were generated using the FIJI software (Schindelin et al. 2012).

The evolutionary conservation for AtNHX1 was calculated using the ConSurf server (http://consurf.tau.ac.il/)(Landau et al. 2005). The HMM was generated using the HMMblits tool from the Bioinformatics department of the Max Planck Institute for Developmental Biology, Tübingen (https://toolkit.tuebingen.mpg.de/#/tools/hhblits).

M.11. Statistical analysis

Unless otherwise stated, statistical analysis was performed using the OriginPro 2017 program.

RESULTS

R.1. AtNHX1 topological model.

To date, no crystallographic structure has been determined for any eukaryotic NHE/NHX protein. Nonetheless, different topological models have been described for the Arabidopsis NHX1, with contradictory results (Yamaguchi et al. 2003; Sato and Sakaguchi 2005). On the one hand, Yamaguchi et al (2003) proposed a model in which the N-terminus of the protein is cytosolic while the C-terminus is facing the vacuolar lumen; according to this model, the hydrophobic domain of AtNHX1 presents nine transmembrane domains and three hydrophobic regions that appear to be membrane-associated. On the other hand, Sato and Sakaguyi (2005) proposed a model in which both N- and C-termini are cytosolic, and the pore domain is arranged as 12 transmembrane segments with an intramembrane loop, i.e. not crossing the membrane entirely. Although the latter model is more consistent with previous studies with other proteins of the CPA superfamily, the study of Sato and Sakaguyi (2005) may be questioned by the use of fragments of AtNHX1 rather than the full-length protein. The main controversy in these descriptions is the orientation of the C-terminal tail. However, the presence of phosphorylated residues within the C-terminal tail of the mammalian and the fungal proteins has been described in HsNHE1 and ScNHX1 (Gruhler et al. 2005; Albuquerque et al. 2008) as well as in Arabidosis NHX1/2 (Whiteman et al. 2008a) implying that their C-termini must be cytosolic as no intravacuolar protein phosphorylation has been described so far.

Using prediction tools and in silico modeling, the topology and 3D models of plant proteins of the CPA family have been generated based on known atomic structures of prokaryotic Na^+/H^+ antiporters that are phylogenetically related. Tridimensional structures have been generated for the tree halophyte *Populus euphratica* PeNHX3 using as template the structure of EcNhaA from *E. coli* (PDB ID 1ZCD) (Wang et al. 2014) and for CHX17 using the TtNapA structure of *Thermus thermophilus* as the template (PDB ID 4bwzA) (Czerny et al. 2016). Moreover, the Arabidosis AtNHX6 structure was modeled using the MjNhaP of *Methanococcus jannaschii* as the template (Ashnest et al. 2015). However, the confidence of these structures was not assessed by experimental approaches to corroborate the structures proposed.

In this study, a model structure for AtNHX1 was generated to better understand the structure-function relationships of the protein. To generate a final model, five steps were followed: (i) identification of suitable structural template(s) phylogenetically related to AtNHX1, (ii) alignment of target sequence and template secondary structure(s), (iii)

refinement and adjustment of the secondary structure, (iv) generation the 3D structure with appropriate software, and (v) *in silico* and *in vivo* validation of the model.

R.1.1. Identification of AtNHX1 template structures.

The AtNHX1 sequence was used as the query sequence in the SwissModel web-server dedicated to homology modeling of protein structures (Bienert et al. 2017; Waterhouse et al. 2018). As a result, this software generated a list of proteins with known structure that were the best fits in terms of sequence conservation with the target sequence. When using AtNHX1 as the target, the SwissModel results pointed to bacterial and archaea proteins previously used in the modelization of eukaryotic proteins: *E. coli* NhaA (Lee et al. 2014), *Methanocaldococcus jannichii* NhaP1 (Goswami et al. 2011), *Pyrococcus abysinnia* NhaP (Wöhlert et al. 2014) and *Thermus thermophilus* NapA (Lee et al. 2013c) (**Table 3)** It should be noted that the AtNHX1 sequence in these first alignments included mainly the N-terminal domain of the protein, with a coverage ranging 58-71% of the AtNHX1 length **¡Error! La autoreferencia al marcador no es válida.**), while the C-terminal was not aligned in any case due to the lack of sequence similarities between the eukaryotic protein and the prokaryotic proteins used as templates. In order to refine the results, the protein alignment was repeated using as the query only amino acids 1-435, previously reported to be in the pore domain of the protein. The results obtained, although with better scores, did not depart from the previous ones. (Table 4)

Table 3. SwissModel best-fitting 3D structures (from PDB database) for AtNHX1. Top matches with known Na^+/H^+ exchanger structures (templates) are shown with their PDB code. Sequence Identity refers to the percentage of amino acid identity between the query and the template; GMQE (Global Model Quality Estimation) is a quality estimation reflecting the expected accuracy of a model built with that alignment of the template and the coverage of the target; Sequence Similarity is calculated from a normalized BLOSUM62 substitution matrix; Coverage is the proportion of the full-length target protein that is aligned to the template.

Template	**Protein.**	**Seq Identity**	**GMQE**	**Method**	**Resolution**	**Seq Similarity**	**Coverage**
4cza.1.A/B	PaNhaP	22.11	0.45	X-ray	3.20Å	0.30	0.71
4cz8.1.A/B	PaNhaP,	21.99	0.45	X-ray	3.15Å	0.30	0.71
4cz9.1.A/B	PaNhaP (pH 4)	21.99	0.45	X-ray	3.50Å	0.30	0.71
4czb.2.B/A	MjNhaP1 (pH 8)	18.49	0.44	X-ray	3.50Å	0.28	0.71
4d0a.1.A	MjNhaP1	18.49	0.44	2DX	6.00Å	0.28	0.71
4czb.1.A/B	MjNhaP1	18.49	0.44	X-ray	3.50Å	0.28	0.71
4bwz.1.A	TtNapA	14.68	0.40	X-ray	2.98Å	0.28	0.67
5bz3.1.A	TtNapA (outward - facing)	14.64	0.40	X-ray	2.30Å	0.28	0.67
5bz2.1.A	TtNapA (inward - facing)	15.34	0.40	X-ray	3.70Å	0.28	0.68
4au5.1.A	EcNhaA (low pH)	14.84	0.31	X-ray	3.70Å	0.27	0.58

Table 4. SwissModel best fitting 3D structure (from PDB database) for AtNHX1 protein using amino acids 1-435 as query. Top matches with known Na^+/H^+ exchanger structures (templates) are shown with their PDB code. Sequence Identity refers to the amino acid percentage identity between the query and the template; GMQE (Global Model Quality Estimation) is a quality estimation that reflects reflecting the expected accuracy of a model built with that alignment and template and the coverage of the target; Sequence Similarity is calculated from a normalized BLOSUM62 substitution matrix.; Coverage is the proportion of the full-length target protein that is aligned to the template.

Template	**Protein.**	**Seq Identity**	**GMQE**	**Method**	**Resolution**	**Seq Similarity**	**Coverage**
4cza.1.A/B	PaNhaP	22.49	0.57	X-ray	3.20Å	0.30	0.85
4cz8.1.A/B	PaNhaP, (pH 8)	22.10	0.57	X-ray	3.15Å	0.30	0.85
4cz9.1.B/A	PaNhaP (pH 4)	22.10	0.57	X-ray	3.50Å	0.30	0.85
4czb.2.B/A	MjNhaP1 (pH 8)	18.21	0.54	X-ray	3.50Å	0.28	0.85
4czb.1.A/B	MjNhaP1	18.21	0.54	X-ray	3.50Å	0.28	0.85
4d0a.1.A	MjNhaP1	18.21	0.54	2DX	6.00Å	0.28	0.85
5bz2.1.A	TtNapA (inward - facing)	14.97	0.49	X-ray	3.70Å	0.28	0.81
4bwz.1.A	TtNapA	15.38	0.48	X-ray	2.98Å	0.28	0.81
5bz3.1.A	TtNapA (outward - facing)	15.10	0.48	X-ray	2.30Å	0.28	0.81
4atv.1.A	EcNhaA (low pH)	15.07	0.34	X-ray	3.50Å	0.27	0.63
4au5.1.A	EcNhaA (low pH)	14.71	0.34	X-ray	3.70Å	0.27	0.63

To decide which template to select for further analyses, the following basic parameters were established: the structure should had been obtained by X-ray, the resolution should at least be 3.0 Å, and in case of duplication of proteins the one with the highest score would be chosen. The list was then reduced to four templates for further analyses: 4cza.1 (PaNhaP from *Pyrococcus abyssii*), 4czb.1 (MjNhaP1 from *Methanocaldococcus jannaschii*), 4bwz.1.A (TtNapA from *Thermos Thermophillus*); and Aau5.1.A (EcNhaA, from *Escherichia coli*).

R.1.2. Topological model of AtNHX1

To obtain a consensus topological model for the pore domain of AtNHX1, the template protein sequences selected above where aligned pairwise with AtNHX1 using ClustalW software (Annex 4). Each of these alignments was used to assign the boundaries of the transmembranes of AtNHX1 based in the secondary structure described in the crystal structure of the templates. Finally, the sequences of AtNHX1 with the assigned secondary structures of each alignment were compared (Figure 4). From these alignments it was concluded that the EcNhaA template was not appropriate to model AtNHX1. In the first place, a large segment in the N-terminal portion of the sequence was not covered by the alignment, while it was present in the alignment of the phylogenetically closer structures of PaNhaP and MjNhaP1. Of note is that the structure of the NhaP-type proteins comprised thirteen complete TM segments instead of the twelve in the case of EcNhaA. Something similar occurred in the C-terminal portion of the pore domain, in which there is a large portion of the known hydrophobic core AtNHX1 that was not covered by the EcNhaA template. As a result, the alignment of AtNHX1 with the EcNhaA did not allow the location of the complete

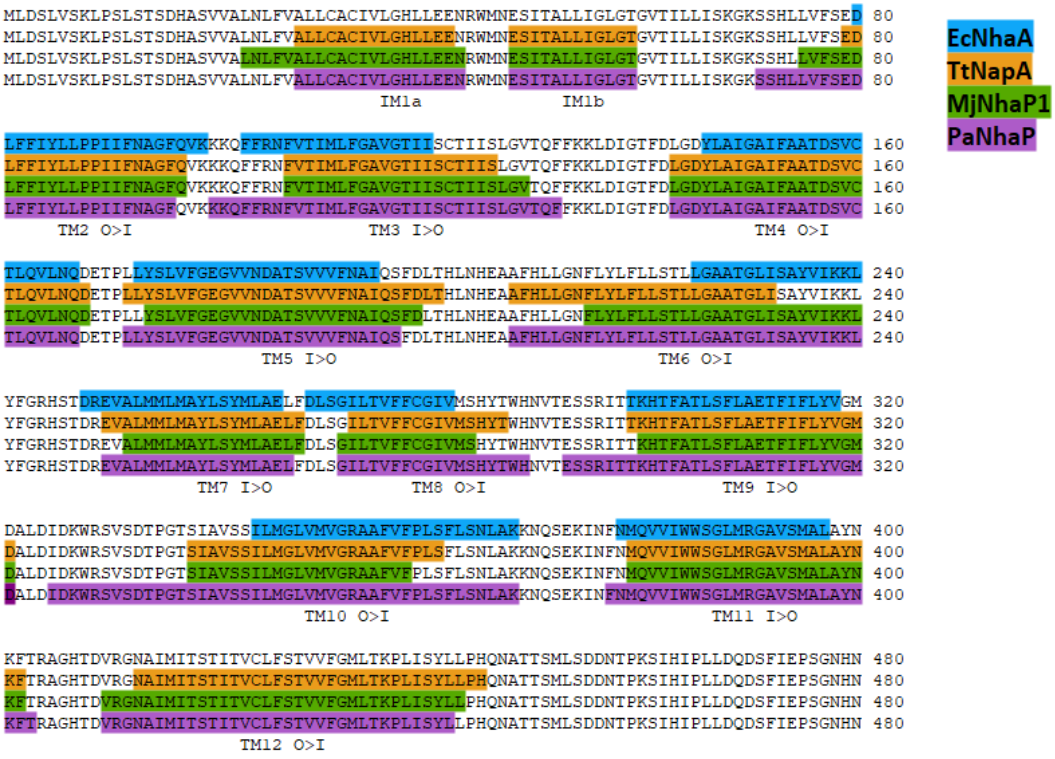

Figure 4. Predicted TM segments in AtNHX1 according to the alignment with amino acid sequences of crystallized homologous proteins from bacteria and archaea. The sequence, repeated four times, corresponds to the AtNHX1 protein on which the corresponding TM segments confirmed in the ternary structure of EcNhaA (blue), TtNapA (orange), MjNhaP1 (green), and (purple) is marked to derive a consensus topology for AtNHX1. The orientation of the twelve TMs predicted in AtNHX1 is marked as outside-to-inside (O>I) or inside-to-outside (I>O).

hydrophobic domain of the protein. However, the other three templates not only allowed the alignment of the complete sequence, but also the predicted segments in each case had a similar arrangement of transmembranes regardless the template used.

Consequently, the final proposed topological was generated based in the alignment of AtNHX1 with PaNhaP, MjNhaP1 and TtNapA templates (**¡Error! No se encuentra el origen de la referencia.**A).

Based in previous experimental data from AtNHX1 topological studies (Yamaguchi et al. 2003; Sato and Sakaguchi 2005) and the results of aligning the AtNHX1 protein sequence with other CPA1 family proteins of known structure, the proposed topological model for AtNHX1 consist of two well defined domains: an hydrophobic core that includes the largest portion of the protein (from residues A28 to T434~~)~~ that corresponds to the pore domain involved in ion transport, and a hydrophilic and cytosolic C-terminal tail (from amino acids K435 to A538). The C-terminal tail is the most variable region among plant NHX proteins and may integrate the signals for the protein regulation, such as protein phosphorylation. In our model both N- and C-termini are cytosolic and, moreover, the complete C-terminal domain downstream the pore domain is in the cytosol (**¡Error! No se encuentra el origen de la referencia.**). The N-terminal portion of the pore domain consist of two intramembrane (IM) semihelices (IM1.a and IM1.b) followed by eleven TM segments with an antiparallel topology, so that the odd TM segments (TM3, TM5, TM7, TM9 and TM11) are oriented from inside (cytosol) to outside (vacuole), while the even TM segments (TM2, TM4, TM6, TM8, TM10 and TM12) from outside to inside. These TM segments are connected by short loops of varied length, being the shorter of 4 amino acids (between TM4 and TM5), and the longest of 18 (between IM1.b and TM2).

A

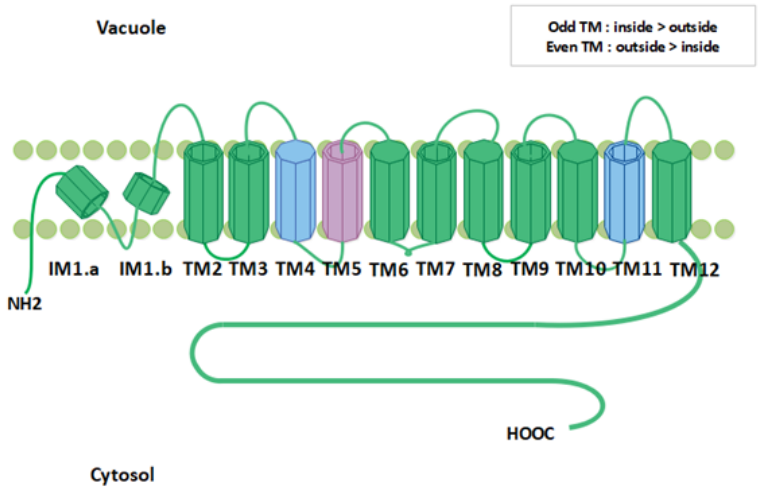

B

```
EcNhaA   DPITREGW---AIPAATD-IAFA-------------LGVLALLGSRVPLALKIFLMALAIIDDLGAIIIIALFYTNDLSM---- 184
TtNapA   LP-FLGGYLYGLEIGFETLPALFLGTALVATSVGITARVLQELGV-LSRPYSRIILGAAVIDDVLGLIVLACVNGVA-ET---- 173
HsNHA2   LP-WQWGFILGFVLGAVS-PAVVVPSMLLLQGGGY--------G--VEKGVPTLLMAAGSFDDILAITGFNTCLGIAFST---- 292
PaNhaP   F---LLGFLFGAIIGATD-PATL-------------IPLFRQYR--VKQDIETVIVTESIFNDPLGIVLTLIAISMLVPGYGGG 180
MjNhaP1  YT-SPVGYLFGAITAATD-PATL-------------IPVFSRVR--TNPEVAITLEAESIFNDPLGIVSTSVILGLF------G 176
HsNHE1   IG-LLDNLLFGSIISAVD-PVAV-------------LAVFEEIH--INELLHILVFGESLLNDAVTVVLYHLFEEFANYE---- 284
AtNHX5   LP-FVECLMFGALISATD-PVTV-------------LSIFQDVG--TDVNLYALVFGESVLNDAMAISLYRTMSLVNRQS---- 210
AtNHX6   LP-FVECLMFGSLISATD-PVTV-------------LSIFQELG--SDVNLYALVFGESVLNDAMAISLYRTMSLVRS-H---- 210
AtNHX4   LS-ARDYLAIGTIFSSTD-TVCT-------------LQILHQDE---TPLLYSLVFGEGVVNDATSVVLFNAVQKIQFES---- 202
AtNHX3   LT-IADYLAIGAIFSATD-SVCT-------------LQVLNQDE---TPLLYSLVFGEGVVNDATSVVLFNAIQRFDLTN---- 205
PeNHX3   LD-IGDYLAIGAIFAATD-SVCT-------------LQVLSQDD---TPLLYSLVFGEGVVNDATSVVLFNAIQSFDLTN---- 205
AtNHX1   FD-LGDYLAIGAIFAATD-SVCT-------------LQVLNQDE---TPLLYSLVFGEGVVNDATSVVVFNAIQSFDLTH---- 202
AtNHX2   FD-LGDFLAIGAIFAATD-SVCT-------------LQVLNQDE---TPLLYSLVFGEGVVNDATSVVLFNAIQSFDLTH---- 204
```

TM 4 TM 5

```
EcNhaA   DGLTS------ILPLGIIAGLLIGKPLGISLFCWLALRLKL------------------AHLPEGTTYQQIMV----------- 330
TtNapA   PVVLV-A------GTVVTVIAILGKVLGGFLGALT-----------QGV--RSALTVGCGMAPRGEVGLIVAAL----GLKAGA 347
HsNHA2   ETVGL-C------VATV-GIAVLIRILTTFLMVCF-----------AGFNLKEKIFISFAWLPKATVQAAIGSVALDTARSHGE 480
PaNhaP   SNLG--KG-----LLVALGVMILARPLATLPLL-------------KWWNFREYLFIALEGP-RGVVPSALASLPLSLALKYKS 382
MjNhaP1  NYFI--PG-----LLVALGSIFLARPLGVFLGLI-----------GSKHSFKEKLYFALEGP-RGVVPAALAVTVGIEILKNAD 367
HsNHE1   NWTFV---------ISTLLFCLIARVLGVLGLTWFINKFRI-----VKLTPKDQFIIAYGGL-RGAIAFSLGYLLDK----KH- 473
AtNHX5   SHVGF--------ILFSILFIGVARAVNVFGCAYLVNLFRQ---ENQKIPMKHQKALWYSGL-RGAMAFALALQSLHDLP--E- 407
AtNHX6   SHLGF--------IFFSILFIVIARAANVFGCGYLVNLARP---AHRKIPMTHQKALWYSGL-RGAMAFALALQSVHDLP--E- 407
AtNHX4   KTSSLSFGGTLGVSGVITALVLLGRAAFVFPLSVLTNFMNRHTERNESITFKHQVIIWWAGLMRGAVSIALAFKQFTYSGVTL- 411
AtNHX3   DVVRNSPGQSIGVSSILLGLILLGRAAFVFPLSFLSNLTKS--SPDEKIDLKKQVTIWWAGLMRGAVSMALAYNQFTTSGHTK- 412
PeNHX3   RFVSDSPGTSVAVSSILLGLVMVGRAAFVFPLSFVSNLSKK--SPHEKIGFRQQFIIWWAGLMRGAVSMALAYNKFTSAGHTN- 412
AtNHX1   RSVSDTPGTSIAVSSILMGLVMVGRAAFVFPLSFLSNLAKK--NQSEKINFNMQVVIWWSGLMRGAVSMALAYNKFTRAGHTD- 420
AtNHX2   RFVSDSPGTSVAVSSILMGLVMLGRAAFVFPLSFLSNLAKK--HQSEKISIKQQVVIWWAGLMRGAVSMALAYNKFTRSGHTE- 411
```

Figure 5. Topological model of AtNHX1 based in the alignment of AtNHX1 sequence with prokaryotic templates. (**A)** Schematic representation of AtNHX1 topology based on sequence aligments to templates PaNhaP, MjPhaP1, TtNapA (see Figure 6). AtNHX1 consist of two domains: a hydrophobic catalytic core and a C-terminus hydrophilic tail. The catalytic core is formed by two intramembrane (IM) semi-helices followed by eleven TM segments with antiparallel orientation. Both the N- and C-termini are cytosolic. (**B)** Sequence alignment of CPA1 and CPA2 proteins described in this thesis. The most important conserved amino acids in the hydrophobic core and the TM segments where they are located are highlighted. TM numeration is according to the toplogical model of AtNHX1 shown in panel A.

R.1.3. Tertiary structure model of AtNHX1

Although a 3D computer-generated model is not a substitute for an experimentally determined structure, the quality of the 3D models has proven to be sufficiently high to identify critical domains and residues for protein function (Landau et al. 2007; Schushan et al. 2010; Kondapalli et al. 2013; Wang et al. 2014; Czerny et al. 2016).

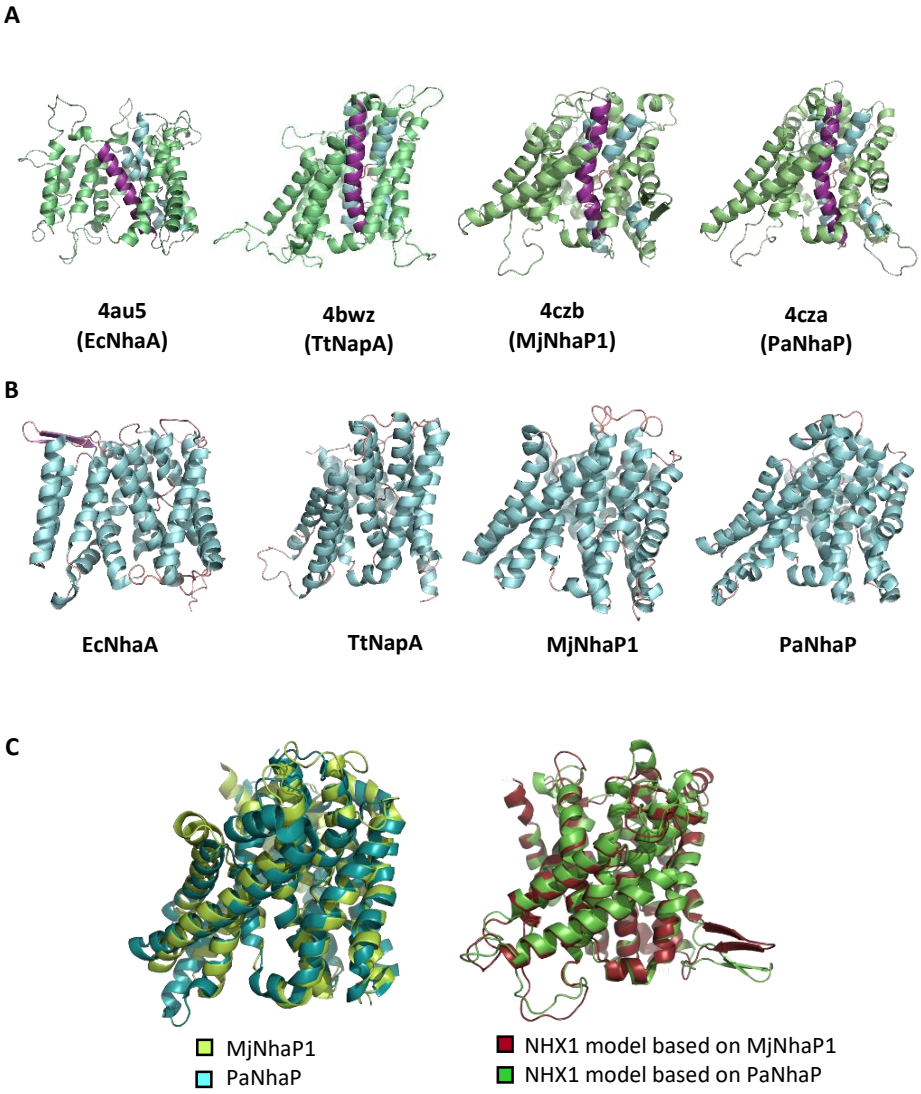

Figure 6. Modelization of AtNHX1 structure based in crystalized prokaryotic templates. (A) Tridimensional structure representation of AtNHX1 based in the modelization made by SwissModel using the indicated structural templates. TM5 is highlighted in purple, TM4 and TM11, in blue. **(B)** Crystal structure of the prokaryotic template proteins. (C) Structure ovelay with Pymol software of the archea proteins

Using the modeling data retrieved from the SwissModel server and visualized with the Pymol software (The PyMOL Molecular Graphics System, Version 2.0 Schrödinger, LLC), the 3D structure model of the complete pore domain of AtNHX1 was generated (**¡Error! No se encuentra el origen de la referencia.**A). From these figures, the similarity between the different AtNHX1 models generated based on the prokaryiotic proteins was evident (displayed in (**¡Error! No se encuentra el origen de la referencia.**A)). As mentioned before, the AtNHX1 structure modeled with the EcNhaA template was the less robust because of the limited coverage of the template protein and the lack of important structures, such as the beta sheet between TM1 and TM2 indicated by the model produced with other templates.

Among the SwissModel results, the two templates with the highest scores corresponded with two phylogenetically related archaea proteins: PaNhaP and MjNhaP1 (Table 4) which have been shown to present similar structure and function (Călinescu et al. 2014, 2016). Due to this proximity, the results obtained in the alignments with AtNHX1 (Annex 4), and the similarities observed in the generated AtNHX1 structures, it was concluded that both templates would produce redundant results. To prove that, the real structures of templates PaNhaP and MjNhaP1 were aligned to each other, and the modeled structure of AtNHX1 for each template as well. The differences observed between structures were negligible (**¡Error! No se encuentra el origen de la referencia.**C). For that reason, only one of the templates was used for further analyses and we selected PaNhaP because, unlike MjNhaP1, this protein is able to bind Ti^+ besides Na^+ and Li^+, whose ion radius (1.5 Å) is similar to that of K^+ (1.44Å) and larger than that of Na^+ (1.12 Å) (Padan and Michel 2015). On the other hand, the TtNapA protein, although being an electrogenic exchanger, is structurally more similar to PaNhap and MjNhaP1 than to EcNhaA (Hunte et al. 2005b). For this reason, the AtNHX1 model generated using TtNapA as template was more similar to the ones obtained from PaNhaP and MjNhap1 as models, allowing the coverage of the complete AtNHX1 sequence, but also the location and orientation of the TM segments and conserved amino acids, unlike EcNhaA.

R.1.4. NhaA-fold in the active center of AtNHX1.

The structural assembly in the active center for the EcNhaA protein, the first CPA family member to be crystallized, is known as the Nha-fold (Hunte et al. 2005b; Padan et al. 2009). In this non-canonical conformation of TM helices, the helical secondary structure of TM4 and TM11 of EcNhaA is interrupted by extended chains in the middle of the membrane, leaving

instead two short helices in each TM flanking the centrally located extended chains (Hunte et al. 2005b; Lee et al. 2014). The interrupted helices of TM4 and TM11 comprising the NhaA-fold cross each other at the extended chains in the proximities of the active site, which is located in TM5 (Figure 7). As a result, two short helices oriented either toward the cytoplasm (c) or toward the periplasm (p) create two partial positive (TM4c and TM11p) and two partial negative (TM4p and TM11c) dipoles facing each other (Hunte et al. 2005a; Călinescu et al. 2017). These charges are compensated by Asp133 in TM4 and Lys300 in TM10, respectively (Lee et al. 2014), creating a balanced electrostatic environment in the middle of the membrane at the ion binding site. This fold it has been confirmed for all the crystallized CPA superfamily members (Hunte et al. 2005b; Lee et al. 2013c, 2014; Paulino et al. 2014; Wöhlert et al. 2014) and incorporated into the modeled structures (Landau et al. 2007; Schushan et al. 2010; Wang et al. 2014).

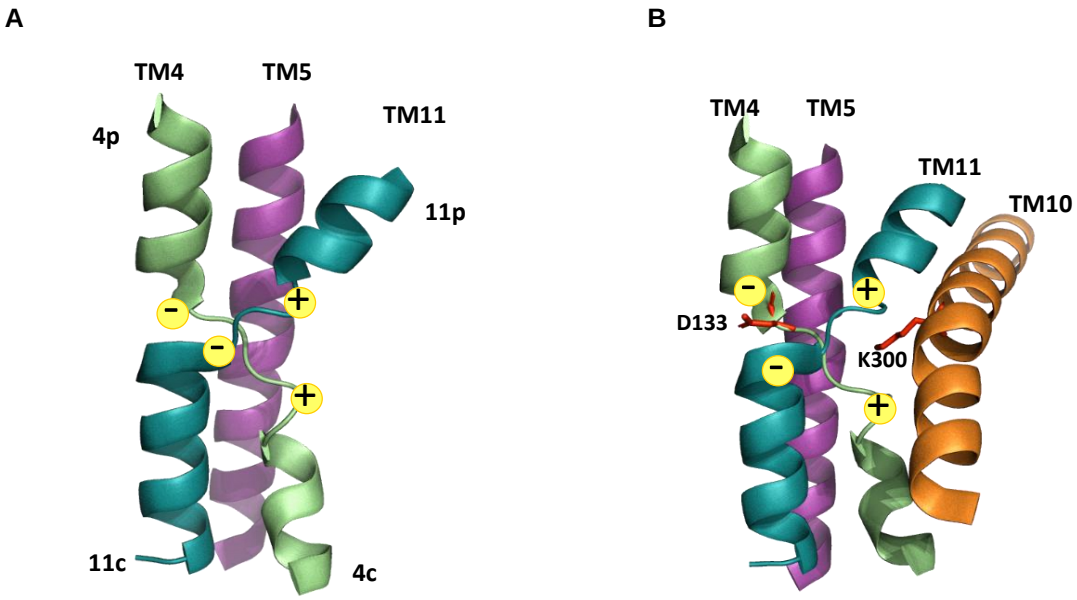

Figure 7. Schematic diagram of the NhaA structure. **(A)** TM4 (green) and TM11 (blue) are discontinuous and cross over in the center of the protein, near TM5. The discontinuous helices generate dipoles of opposite charge. **(B)** Asp133 in TM4 and Lys300 in TM10 neutralize the positively and negatively charged helices. Structure is based in the crystal structure of EcNhaA 4AU5 (Lee et al., 2014)

Highlighting the TM segments homologous to the ones forming the Nha-fold of the prokaryotic proteins (TM5 in magenta, TM4 and TM11 in blue, Figure 6) in the 3D model of AtNHX1, illustrates that they are localized in the center of the protein. When these TM segments are isolated from the rest of the structure, the characteristic Nha-fold becomes apparent (Figure 8A).

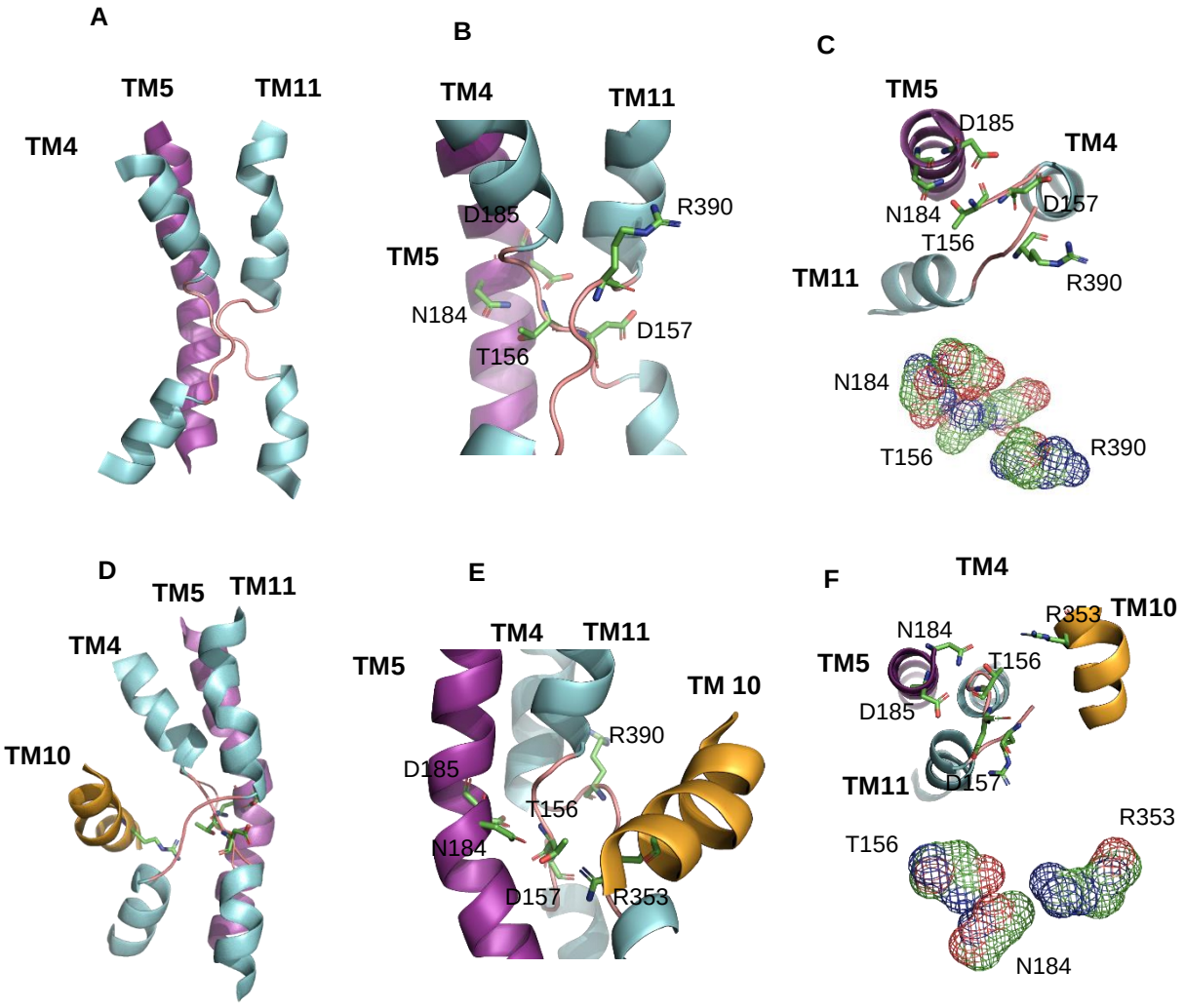

Figure 8. **NhaA-fold in the active center of AtNHX1. NhaA-fold in the active center of AtNHX1.** **(A**) Isolated representation of TM4, 5 and 11 in the AtNHX1 structure based on the TtNapA template showing the NhaA-fold in the active center of the protein**. (B**), Close-up view of the cross-over of the extended chains in TM4 and TM11 indicating the highly conserved residues T156 and D157 in TM4, N184 and D185 in TM5, and R390 in TM11. **(C)** A top-view (inside to outside) to show how D157 and R390 side chains compensate the dipoles generated by the crossing of TM4 and TM11. Nearby, T156 and N184 side chains are close enough to interact. **(D)** Representation of the active center with the NhaA-fold and the TM10. **(E)** Closer view of the NhaA-fold and the localization of R353 in TM10 relative to the active center. **(F)** A top-view (inside to outside) to show the interaction of N184 , R156 and R353 side chains.

R.1.5. Conserved residues in the pore domain

Alignment of the primary structure of representative proteins of the CPA superfamily allowed the identification of highly conserved amino acids (Table 3, Figure 5B). The aspartic acid at position 185 (D185) and an asparagine (N184) in TM5 comprise the active site of the protein. This ND-motif is highly conserved among electroneutral CPA1 family members, as described for MjNhaP1 (N160-D161, (Paulino et al. 2014), PaNhaP (N158-D159(Wöhlert et al. 2014)), HsNHE1 (N266-D267, (Landau et al. 2007) and all members of the plant NHX family described (see the *Arabidopsis thaliana* NHX proteins in**¡Error! No se encuentra el origen de la referencia.**). In the electrogenic members of the CPA2 family, like EcNhaA or TtNapA, this ND-motif is exchanged for a DD-motif (D163-D164 and D200-D201, respectively) (Hunte et al. 2005a; Padan et al. 2009; Maes et al. 2012; Lee et al. 2013b), (**¡Error! No se encuentra el origen de la referencia.**B). These results are consistent with the placement of AtNHX1 in the CPA1 clade, the structure of active center, and the predicted electroneutral exchange activity (Venema et al. 2002).

Two conserved, positively charged amino acids, R353 in TM10 and R390 in TM11, were detected in AtNHX1 (7B;Figure 8). Other electroneutral proteins of the CPA1 family have also been described to present conserved basic residues at equivalent positions, e.g. R425 and R458 in HsNHE1, and R432 and K460 in HsNHA2 (Landau et al. 2007; Schushan et al. 2010) (Table 1). In MjNhaP1 and PaNhaP, the first arginine is conserved in TM11 (equivalent to TM10 of AtNHX1) as residues R320 and R337, respectively. The crystal structures have shown that this conserved arginine interacts with a glutamate in TM6 (E156 in MjNhaP1 and E154 in PaNhaP; equivalent to TM5 of AtNHX1) that is also conserved in the CPA1 antiporters (**¡Error! No se encuentra el origen de la referencia.**). In the models obtained for AtNHX1 based on PaNhaP and MjNhaP1, R353 seems to interact with E180 (Figure 9B and C). Moreover, E180 interacts with N184 in the three AtNHX1 models shown in Figure 9**Figure 9.** The second arginine, R390 in TM11 of AtNHX1, is also conserved (Paulino et al. 2014; Wöhlert et al. 2014), but little is known about the function of this conserved residue. In HsNHA2 this residue is exchanged for a Lys.

.

Table 5. Conserved residues in CPA superfamily members.
Summary of the described conserved summary in crystalized CPA proteins and modelized CPA proteins..

Protein	Residues	TM	Reference
EcNhaA	T132-D133	4	Maes et. al (2012) Padan (2009)
	D163-D164	5	
	K300	10	
MjNhaP1	T131-D132	5	Goswami et al. (2011) Paulino et al. (2014)
	N160-D161	6	
	E156	6	
	R320	11	
	R347	12	
PaNhaP	T129-D130	5	Wöhlert et al. (2014)
	S155	6	
	N158-D159	6	
	E154	6	
	R337	11	
	R362	12	
TtNapA	T126-S127	4	Lee et al. (2013)
	D156-D157	5	
	K305	10	
NHE1	D238	4	Landau et al (2007)
	N266-D267	5	
	E262	5	
	R425	10	
	R458	11	
NHA2	S245	4	Schushan et al. (2010)
	D278-D279	5	
	R432	10	
	K460	11	
PeNHX3	Y149	4	Wang et al. (2014)
	N187-D188	5	
	R356	10	
AtCHX17	T170	4	Czerny et. al (2016)
	D200-D201	5	
	K355	10	
	K383	11	

Conserved threonine and aspartate residues in TM4 form a TD-motif in the unwound chain, which is also conserved in EcNhaA (T132-D133) (Galili et al. 2002; Maes et al. 2012), and in the archea proteins MjNhaP1 and PaNhaP (Table ***5***). In both cases, bacterial and archea proteins, this TD-motif has been described to take part in ion coordination (Paulino et al. 2014; Wöhlert et al. 2014). Moreover, T129 and T131 of PaNhaP and MjNhaP1 interact by their side chain with residues N158 and N160, respectively. These asparagines do not participate in the coordination of the substrate ion, but control the access to the ion-binding site (Paulino et al. 2014; Wöhlert et al. 2014). In the mammalian HsNHE1 and HsNHA2 and in prokaryotic TtNapA this motif is not conserved (Landau et al. 2007; Schushan et al. 2010; Lee et al. 2013c). In the modeled structure of PeNHX3 no conserved TD motif was described, and instead the presence of a non-charged Tyr in position 149 was proposed to be substitute for the Thr residue in the TD-motif (Wang et al. 2014). However, the alignment of the CPA proteins shown in Figure 7 indicates that the TD-motif is conserved in PeNHX3. In AtNHX1 this motif is conserved as well (T156-D157) (Figure 5**¡Error! No se encuentra el origen de la referencia.**B, Figure 8B), and according to all the models obtained for AtNHX1, there seems to be an interaction of T156 with N184, as described previously for the archaea NhaP proteins (Figure 9)

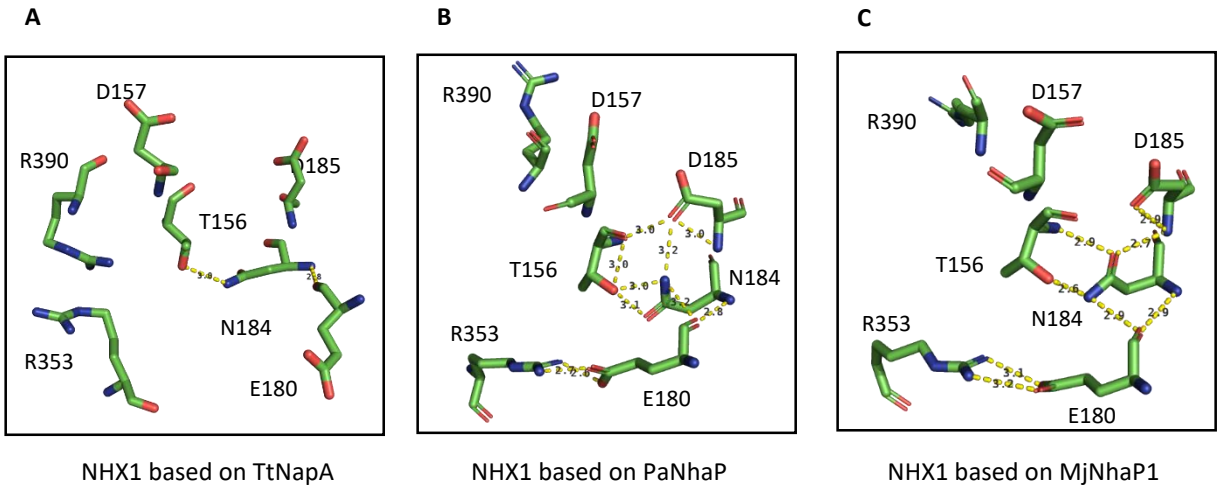

Figure 9. **Predicted amino acid interactions in the active site.** Representation of the side chains of the amino acids proposed to be affecting the activity or structure of the AtNHX1 protein according to the model obtained from the **(A)** TtNapA, **(B)** PaNhaP and **(C)** MjNhaP1 templates. Yellow dashes indicate the possible interactions based in the distance between residues.

The results described so far have shown the high structural conservation among the CPA superfamily in general, and more specifically among the CPA1 family members, making it plausible to translate the knowledge obtained from prokaryotic proteins to better understand the function and structure of eukaryotic proteins. However, it is important to note the need to experimentally confirm the conclusions since even between phylogenetically close proteins structural differences can be observed that in turn could result in different mechanism of transport or protein regulation.

. R.1.6. In silico validation of the AtNHX1 structural model

To evaluate the quality of the structural model generated for AtNHX1, several in silico analyses were used (Landau et al. 2007; Schushan et al. 2010; Kondapalli et al. 2013; Wang et al. 2014). These analyses include generic characteristics commonly displayed in membrane proteins, such as the distribution of positively charged residues (Fleishman and Ben-Tal 2006) and the pattern of evolutionary conservation (Bowie 2005).

R.1.6.1. The 'positive-inside' rule

The topology of most of the intrinsic membrane proteins is such that intracellular positions are enriched with positively charged residues (Arg and Lys) compared to extracellular regions (Wallin and von Heijne 1998). This is known as the "positive-inside rule" and has been used to evaluate the quality of structural models of membrane proteins, including the structures of the antiporters EcNhaA, HsNHE1, HsNHA2 or PeNHX3 (Hunte et al. 2005a; Landau et al. 2007; Schushan et al. 2010; Wang et al. 2014). Analysis of charge distribution in the AtNHX1 three-dimensional structure modeled with templates TtNapA, MjNhaP1 and PaNhaP confirmed this rule (Figure 10A). When the PaNhaP1-derived model was taken into consideration, out of 25 Arg and Lys residues in the AtNHX1 protein, 14 residues are in the cytosolic side of the membrane, 9 in the outside (vacuolar lumen), and 2 are intramembrane (Figure 10A). By contrast, modeling of AtNHX1 with EcNhaA did not follow the rule (Annex 6), presumably due to the incomplete modeling achieved with this template.

R.1.6.2. Hydrophobicity profile

As expected for an intrinsic membrane protein, the predicted AtNHX1 structure showed that the polar residues were clustered either in the inner structures of the protein or at the extramembrane loops, while maximizing the exposure of hydrophobic residues to the membrane lipids (Figure 10B).

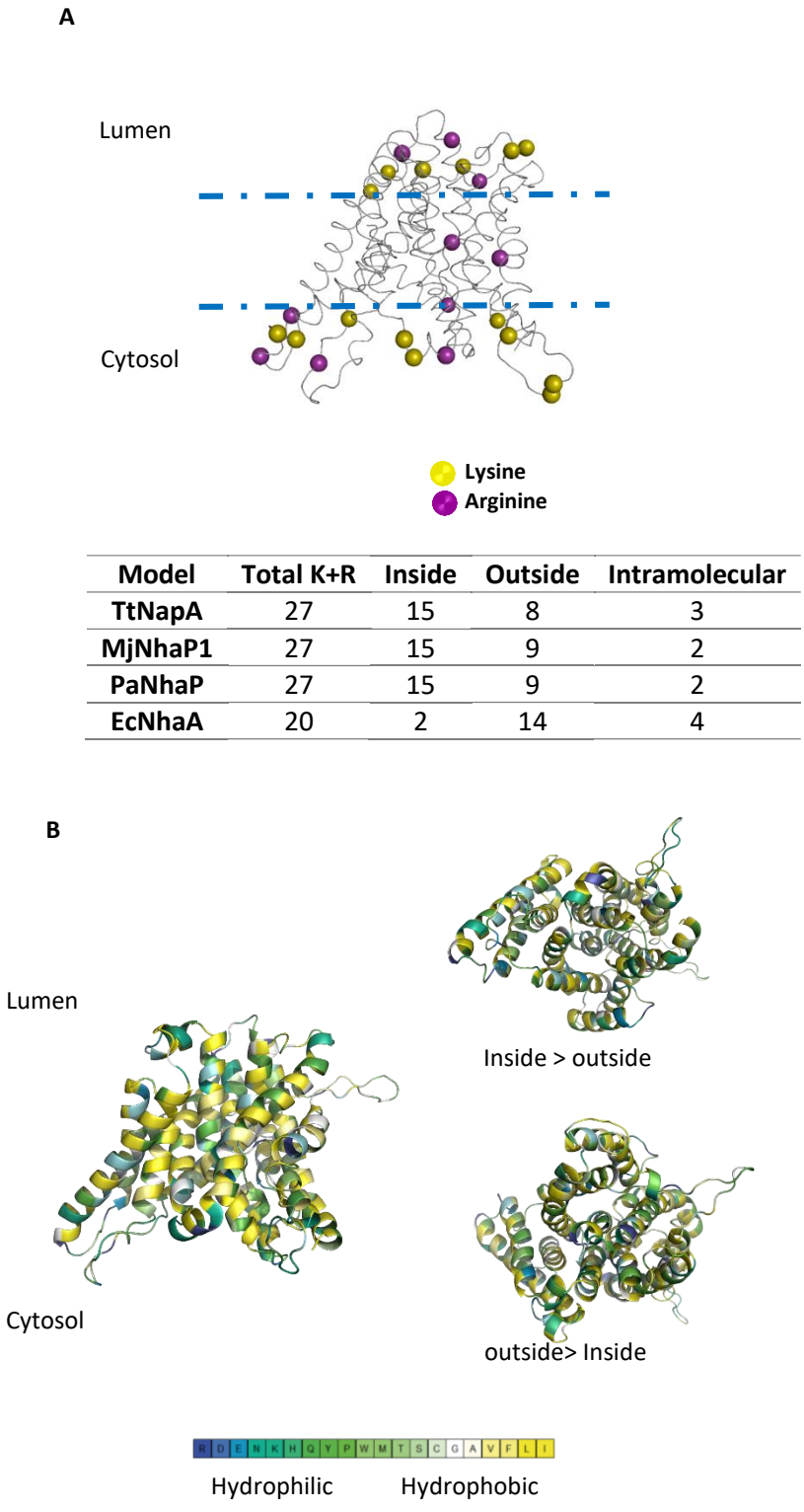

Model	Total K+R	Inside	Outside	Intramolecular
TtNapA	27	15	8	3
MjNhaP1	27	15	9	2
PaNhaP	27	15	9	2
EcNhaA	20	2	14	4

Figure 10. **Validation of the modeled AtNHX1 structure.** The AtNHX1 model represented corresponds to the PaNhaP template**. (A)** The Cα of lysines (yellow) and arginines (purple) are highlighted in the structure to determine their distribution in the protein**.** Except for the model based on EcNhaA, other modeled structures of AtNHX1 are in accordance with the 'positive-inside' rule'. **(B)** Distribution of the amino acids according to their hydrophobicity across the AtNHX1 structure. Aminoacids are colored based on the hydrophobicity scale of Kessel and Ben-Tal (Schushan et al., 2010).

R.1.6.3. Evolutionary conservation

volutionary conservation of amino acids has been previously used to assist structure modeling. Ion transporters are subjected to evolutionary pressure mainly restricting amino acid changes in regions that take part in ion binding or translocation, but also of inter-helical interfaces, crucial for stabilizing the architecture of the helix bundle. For that reason, it is expected that the protein core would be conserved whereas residues that face the lipids or are in the cytosolic and luminal loops were more variable (Fleishman and Ben-Tal 2006).

The evolutionary conservation for AtNHX1 was calculated using the ConSurf server (http://consurf.tau.ac.il/)(Landau et al. 2007; Schushan et al. 2010). To generate a conservation model, three different approaches with increasing levels of stringency were used (Section M.10 and Figure 11A). In brief, AtNHX1 sequence was used as a query in the UNIPROT database (Bairoch et al. 2005) using PSI-BLAST (Altschul et al. 1997) to collect homologous sequences. Redundant (>95% sequence identity) or with low coverage of the protein (< 60% identity) as well as fragmented sequences were discarded. The resulting 216 sequences were aligned using MUSCLE (Edgar 2004) with default parameters, and the final Multi-Sequence Alignment (MSA) was used to generate a Hidden Markov Model (Eddy 1996). The sequences generated were subsequently used to generate a new alignment in the MUSCLE server with default conditions (Figure 11A, arrow (a)), or to collect remote homologous sequences from the UNIPROT database using PSI-BLAST that were aligned using MUSCLE (Figure 11A, arrow (b)). The final alignment including proteins from all kingdoms was exclusive to Na^+/H^+ exchangers related to AtNHX1, and highly reliable to infer position-specific evolutionary information for this transporter. A final step was done using only the AtNHX1 PDB sequence generated by SwissModel and the ConsrufServer (http://consurf.tau.ac.il/) default conditions to generate the MSA for the conservation analysis (Figure 11A , arrow (c)). Based on the MSA obtained in steps (a) and (b) (formed by 352 and 243 sequences respectively), or the MSA defined by the ConsurfServer-sequence, evolutionary conservation scores were calculated using a Bayesian method (Mayrose et al. 2005), and the ConSurf web-server (http://consurf.tau.ac.il/) (Landau et al. 2005). The scores obtained were projected onto the 3D model of AtNHX1.

The results showed that the model structure of AtNHX1 is compatible with the conservation pattern: the protein hydrophobic core is highly conserved while the residues facing the lipid bilayer or located in extramembrane regions are variable (Figure 11B, C and D; Annex6). These results are similar to the previously described for PaNHX3, NHE2, NHE9

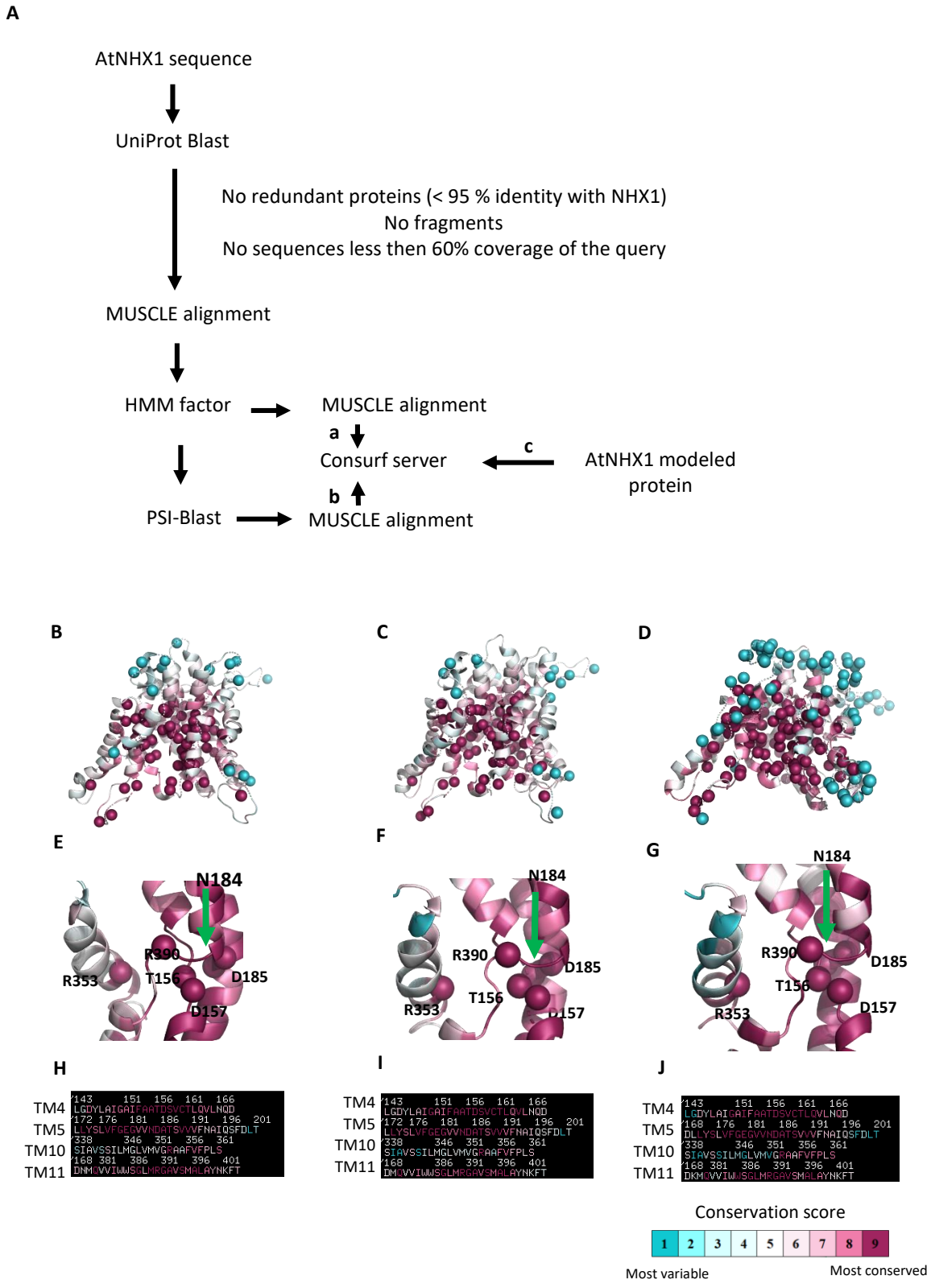

Figure 11. **Evolutionary conservation *of AtNHX1***. **(A)** Flow chart of the methods followed to obtain the evolutionary conservation profile of AtNHX1 calculated via the ConSurf web-server (http://consurf.tau.ac.il). **(B-G)**. The evolutionary conservation profile of AtNHX1 obtained by the previous methods; **(B)** and **(E)** corresponds to the process following arrow *a*; **(C)** and **(F)** with arrow *b*, and **(D)** and **(G)** with arrow *c*. The profiles are colored according to their conservation-grades using the color-coding bar, indicating turquoise the most variable residues and purple the most conserved. variable-through-conserved. The most variable and most conserved positions of each transporter are shown as spheres. In all three cases the pattern was repeated: a highly conserved intramembranous core while intervening loops and lipid-facing residues are variable. **(H-J)** Representation of the sequences in TM4, 5, 10 and 11 for each process following arrows routes *a*,, *b* and *c* respectively. Note the high conservation of the residues in TMs contributing to the NhaA-fold in the active center. TM10 is not so highly conserved, except for the R353 residue. The AtNHX1 model shown is based on PaNhaP template.

(Schushan et al. 2010; Kondapalli et al. 2013; Wang et al. 2014). Of note is the high conservation observed among the residues found in the core of protein near the active center, and more importantly in TM4, TM5 and TM11 (Figure 11 H, I, J)**Figure 10**. These sites are highly occupied by tritable residues, whose presence in the membrane is often associated with function. It is also noteworthy that although the overall conservation of TM10 is mostly low, R353 shows a high conservation score (Figure 11E, F and G). Interestingly, variability of peripheral amino acids seems to be higher at the vacuolar side of the membrane than the cytosolic side.

R.1.7. Validation of the AtNHX1 model *in vivo*

To determine the relevance of the conserved aminoacids described above in AtNHX1 activity, site-directed mutations were done at each residue judged as structurally important (Section M.8.1). The yeast strain AXT3K lacks the plasma membrane Na^+ efflux proteins ENA1-4 and NHA1, and the prevacuolar Na^+/H^+ exchanger ScNHX1, which renders these cells sensitive to NaCl and hygromycin B (hygB) (Quintero et al. 2002). The expression in AXT3K cells of the AtNHX1 and AtNHX2 proteins suppressed the salt- and hygromycin-sensitive phenotype of this strain (Yokoi et al. 2002; Quintero et al. 2002; Barragán et al. 2012). Hence, the wild-type AtNHX1 and the mutant alleles were cloned in the yeast expression vector pDR195 and transformed in the yeast strain AXT3K to test the functionality of the mutant proteins in both solid and liquid media. Plasmid pDR195 uses the strong and mostly constitutive *PMA1* gene promoter to drive the expression of the recombinant protein. Expression of wild-type AtNHX1 improved AXT3K growth in the presence of 50 µg/ml of hygB (Figure 12**¡Error! No se encuentra el origen de la referencia.**). Cells transformed with the mutant alleles showed different phenotypes. The mutation of the D185 residue into a Leu or Asn generated non-functional proteins, as expected since D185 corresponds to the active center residue of CPA1 proteins. Other mutations of residues at the core of the active center of the protein that are part of the NhaA-fold (D157N, R353L) generated equally inactive proteins. These results indicate that the conserved residues of the active core in AtNHX1 have an important functional and/or structural role in the protein, and they are assential for the protein activity in the conditions tested. However, the mutation in which the active center residue N184 was subsitutted by an Asp suppressed the sensititivty to hygB partly. This would imply that the N184 is important but not essential.

Previous reports have shown that the electrogenic antiporters HsNHA2 and EcNhaA lost their transport activities when the DD-motif of CPA2 proteins was substituted for an ND-motif (Schushan et al. 2010; Lee et al. 2013a). Although the mutation N184D to generate a DD-motifslightly abrogate AtNHX1 protein activity, it was still able to overcome the hygB sensitivity. The integrity of the ND-motif is not essential for AtNHX1 activity, but it is important to reach optimal functioning. Recently Uzdavinyz et al (2017) have demonstrated that the electrogenic properties of CPA2 family members is not due to this DD-motif as previously thought, but to the presence of a conserved Lys in TM10, which in CPA1 members is exchanged for an Arg that promotes electroneutral activity (Uzdavinys et al. 2017). This position in AtNHX1 is occupied by R353, which is coherent with the electroneutral exchange of AtNHX1 (Venema et al., 2002). Mutagenic studies of this conserved Arg in TM10 in different CPA1 family members have been performed, and there is no consensus with the results (Hellmer et al. 2003a; Schushan et al. 2010; Wang et al. 2014). To study the relevance of the conserved R353 in TM10 of AtNHX1, and to explore if it was possible to make AtNHX1 electrogenic, a set of allelic variants was generated at the R353 position, so that all possible conditions of ND/DD motifs and R/K residues were studied as indicated below:

DD-Motif + R353/R390

ND-motif + R353K

ND-motif + R390K

DD-motif + R353K

DD-motif + R390K

The R390K mutation was used as control to determine whether the electrogenicity (if changed) was only dependent of the R353 or the active center motif.

Functional assays using the AXT3K yeast strain would not directly allow to determine the su ccessful transformation of AtNHX1 into an electrogenic protein, but at least it would inform whether the new arrangement of catalytic amino acids was compatible with protein activity in vivo. As seen in Figure 13A, any allele bearing an R→K mutation generated an inactive protein in solid media conditions, irrespective of the presence of an ND- or DD- motif in the active center. The only mutant that remained active was the N184D single mutant, although with slightly less activity than wild-type AtNHX1 protein as monitored by yeast growth. These results, as the previous ones, meant that the N184 is not essential for the activity of AtNHX1, but the presence of the conserved arginines in TM10 (R353) and TM11 (R390) was essential

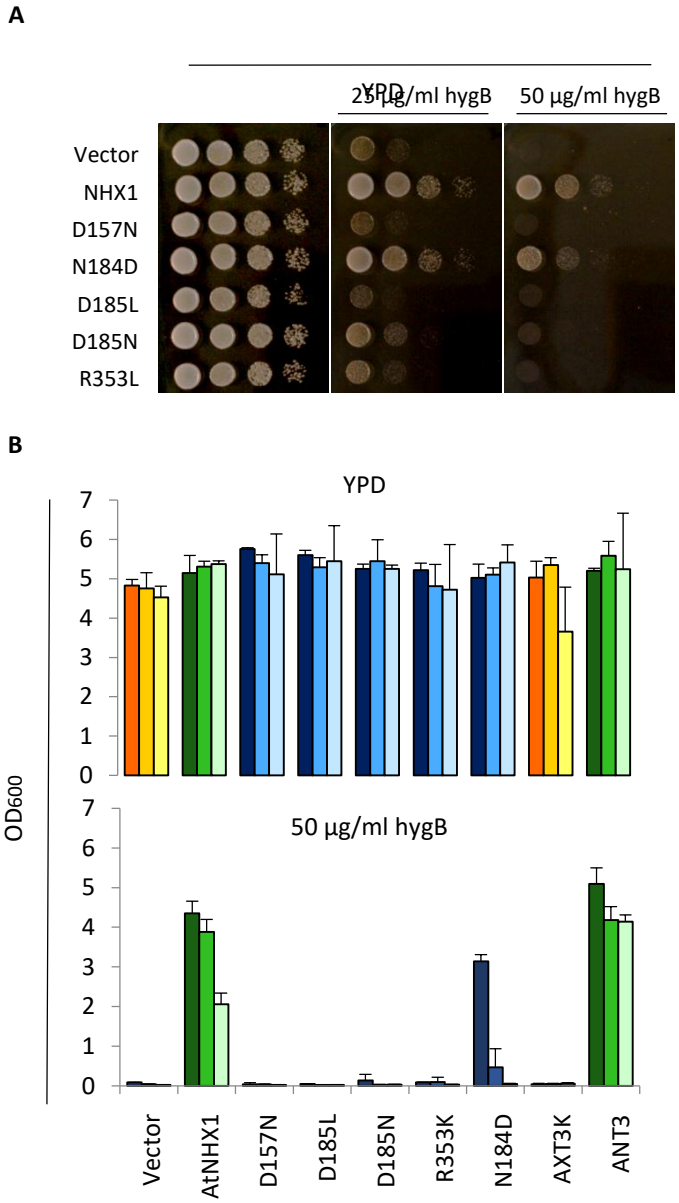

Figure 12. Complementation of the yeast AXT3K mutant with an allelic series of AtNHX1 mutants in conserved residues. The cDNAs of AtNHX1 and of the indicated mutant alleles of conserved residues were cloned into the yeast expression vector pDR195 and transformed into strain AXT3K (Δena1-4 Δnha1 Δnhx1). Overnight cultures were normalized in water to OD600 of 0.5. Aliquots (5 µL) from normalized cultures and 10-fold serial dilutions were spotted onto YPD solid medium plates **(A)** or used to inoculate 200 µL of YPD liquid medium in 96-well plates **(B)** with different concentrations of hygromycin B. Liquid cultures were grown at 30°C overnight before measuring the optical density. Pictures were taken after 2-3 days at 30°C

to maintain protein functionality. Moreover, although a charged amino acid in the active center in TM5 is necessary for the activity, the positively charged N184 is not essential and it can be exchanged for a negatively charged amino acid like an Asp (N184D mutation) with minimal effects.

In the CPA2 protein family there is an interaction between a conserved Lys in TM10 and the Asp residue of TM5 in the active center. This Lys does not participate in ion binding; rather a competition-based transport mechanism has been suggested. The exchange cycle would start with a periplasmic/outer side open conformation of the protein in which D164 (in EcNhaA) or D157 (in TtNapA) is unprotonated, whereas D163 and D156, respectively, are engaged in a salt bridge with K300 or K305, which stabilizes this conformation. At low H^+ concentration, the binding of ions to the DD-motif breaks the salt bridge, the structure becomes less rigid, and a conformational transition takes place releasing the transported ions to the cytosol. Deprotonated D163 and D156 again form a salt bridge with Lys at TM10, inhibiting the reorientation of the unloaded transporter. When Na^+ binds from the cytoplasm, the salt bridge is broken and a conformational transition allows Na^+ release at the periplasmic/outer side of the membrane (Maes et al. 2012; Lee et al. 2014; Călinescu et al. 2017). The same mechanism has been described for PaNhaP and MjNhaaP1 (Călinescu et al. 2016). However, in MjNhaP1 and PaNhaP, the Arg replacing this Lys does not interact with the ND-motif but forms an ion bridge to the neighboring conserved glutamate in TM5 (Paulino et al. 2014) while the conserved Asn in TM5 interacts with the conserved Thr in TM4. The main feature of this competition-based transport mechanism is that it is self-regulatory,nsuring that transport activity is switched off at extreme pH values to prevent excessive acidification or alkalinization of the cytoplasm (Călinescu et al. 2016). This is in accordance to the notion that the K300 in EcNhaA and K305 in TtNapA seem to have more than a functional role in the protein, and that they could be part of the pH activation mechanism, as the pH dependence of both in K300R and K305R mutants were shifted to the alkaline side by one pH unit in comparison to the wild-type proteins (Lena Kozachkov et al. 2007; Maes et al. 2012; Călinescu et al. 2017).

Based in all these considerations, we aimed to determine whether the non-functional mutants of AtNHX1 in medium YPD plus hygB had a different behavior under other growth conditions. To that end, similar assays were performed in liquid YPD media buffered at different pHs, with and without addition of hygB. Of note is that the inhibitory effect of hygB was much higher in the medium buffered at pH 7. Regarding mutant growth, the results were similar in all tests: any of the alleles that included a R→K mutation (either in R353 or R390) failed to recover the hygB-sensitive phenotype of AXT3K (Figure 13B) regardless of the

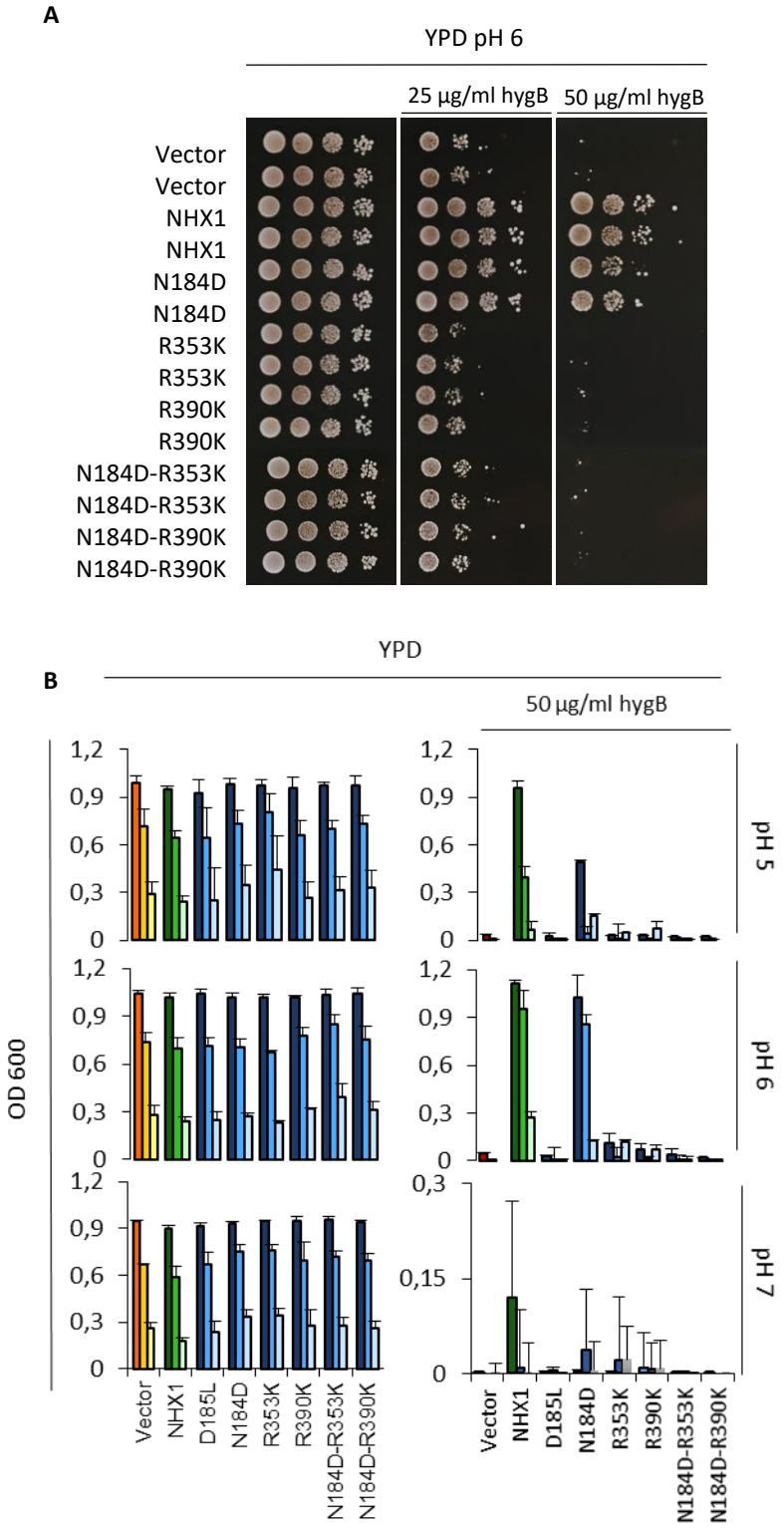

Figure 13. Functional assay of AtNHX1 mutant alleles in amino acids at the ion coordination pocket. The cDNAs of wild-type AtNHX1 and the indicated mutant alleles of the conserved residues were subcloned into the yeast expression vector pDR195 and transformed into the AXT3K (*Δena1-4 Δnha1 Δnhx1*). Overnight cultures were normalized in water to OD_{600} of 0.5. Aliquots (5µL) from normalized cultures and 10-fold serial dilutions were spotted onto YPD solid medium plates **(A)** or used to inoculate 200 µL of YPD liquid medium in 96-well plates with different concentrations of hygromycin B **(B)**. To determine whether the mutated amino acids had a role in pH sensing, the experiment in liquid media was performed at different pH (buffering with 10 mM MES). The liquid cultures were grown at 30°C overnight before measuring the OD. Plates were incubated 2-3 days at 30ºC and pictured

external pH, and there were also no differences in their growth without the antibiotic. Interestingly, the only active allele was again N184D, but it did behave differently in the presence of hygB at acidic pH: the N→D mutation showed to be detrimental for the protein activity at pH 5, as indicated by the reduced ability to suppress the sensitivity to hygB (Figure 13B)

Growth was also tested medium supplemented with Li^+, and the phenotypes were the same as the ones observed in hygB (Figure 14). The N184D allele was able to sustain grow like wild-type AtNHX1, while the R→K mutants could not suppress the ion sensitivity.

Combined, these results of yeast growth in various conditions indicate that N184 in the active center might contribute to pH sensing. This would be in accordance to what have been previously described for EcNhaA and TtNapA (electrogenic proteins with a DD-motif) which are more active at basic pH in comparison to MjNhaP1 and PaNhaP (with the ND-motif), that have been shown to be more active at acidic pHs (Călinescu et al. 2014; Uzdavinys et al. 2017).

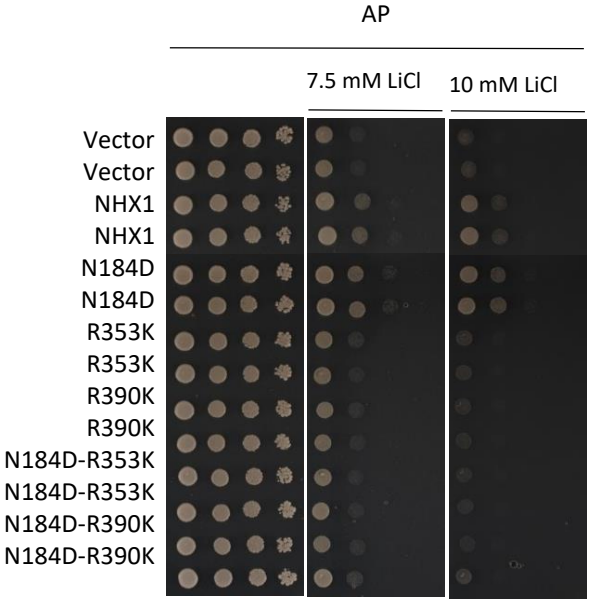

Figure 14.. **Functional assay of AtNHX1 mutant alleles in amino acids at the ion coordination pocket.** The cDNAs of wild-type AtNHX1 and the indicated mutant alleles of the conserved residues were subcloned into the yeast expression vector pDR195 and transformed into the AXT3K (*Δena1-4 Δnha1 Δnhx1*). Overnight cultures were normalized in water to OD_{600} of 0.5. Aliquots (5µL) from normalized cultures and 10-fold serial dilutions were spotted onto AP medium plates- Plates were incubated 2-3 days at 30ºC and pictured.

.

R.1.8. Vacuolar pH with AtNHX1 mutants

The activity of AtNHX1 and AtNHX2 *in planta* constitutes a leak pathway for vacuolar protons that contributes to control the vacuolar pH (Andrés et al., 2014). The results presented herein made us question whether the mutation of the conserved residues could have an effect on the activity of AtNHX1 and the regulation of the pH in the vacuolar lumen (pHv). Most of these mutations could not recover the yeast strain sensibility to HygB or NaCl.

To obtain a better insight on this possibility, the vacuolar pH (pHv) of the AXT3K yeast strain expressing the mutant alleles of AtNHX1 was measured. To assess the roles of AtNHX1 and the different variants in the pH regulation of the yeast, the ratiometric fluorescein-based pH sensitive dye, 2',7'-bis-(2-carboxyethyl)-5-(and-6)-carboxyfluorescein (BCECF) was used (section M.9.4). Ratiometric dyes have the distinct advantage of not being significantly affected by dye loading, cell size, or tissue morphology, unlike other non-ratiometric dyes.

The excitation spectrum of BCECF is sensitive to pH, so it can be used as ratiometric pH indicator. This dye has an isosbestic point so that when it is excited with a 450 nm wavelength, the emission remains constant independently of the media pH. However, after excitation with a 490 nm wavelength the ensuing fluorescence emission increases proportionally to the pH of the solution. The two excitation wavelengths are measured at a single emission wavelength (535 nm), and the ratio of the intensity emitted (I_{490}/I_{450}) provides a measure of pH. However, BCECF has a p*Ka* value near 7.1, and for that reason the I_{490}/I_{450} ratio does not accurately estimate low pH values. Different approaches have been developed to overcome this problem (Brett et al. 2005b; Diakov et al. 2013). The method proposed by James Kracke (1992) was applied in this project. This method allows to convert intensities for BCECF to pH between 4 and 9 by using the formula used to calculate $[Ca^{2+}]_i$ from the fluorescence of Fura2 inverted after using with a set of buffers titrated at different pHs and in the presence of a protonophore (FCCP or CCCP) to generate the calibration curve (section M.9.3). The inversion of the equation is needed because H^+ binding to BCECF causes a decrease in fluorescence, whereas Ca^{2+} binding to Fura2 causes an increase in fluorescence. This type of calibration procedure allows BCECF to be used over a wider range of pH.

BCECF localizes into the vacuole of yeast when introduced in its acetoxymethyl ester form (BCECF-AM) (Ali et al. 2004; Brett et al. 2005b; Diakov et al. 2013). In previous assays, BCECF-AM has been used to measure the pHv of the *S. cerevisiae nhx1* mutant, to monitor responses to changing extracellular condition, to study how V-ATPase mutations affect its activity, and to examine the communication between organelles and extracellular media (Plant et al. 1999;

Martínez-Muñoz and Kane 2008; Diakov and Kane 2010; Tarsio et al. 2011). This ratiometric dye has been used in population-based measurements with a microplate reader (Brett et al. 2005b).

Previous studies have reported pHv values between 5.5 – 5.9 in wild type *S. cerevisiae* strains (Plant et al. 1999; Martínez-Muñoz and Kane 2008; Diakov and Kane 2010; Tarsio et al. 2011; Diakov et al. 2013; Coonrod et al. 2013). Experiments using BCECF in yeast have demonstrated that overexpression of the ScNHX1 protein resulted in the alkalinization of the vacuole and, conversely, the lack of expression in the *nhx1* mutant produced acidification (Ali et al. 2004; Brett et al. 2005b).

It is important to note that *in vivo* pH measurements are sensitive to the growth and metabolic conditions of the yeast cells themselves, which can be a source of variability between measurements (Diakov and Kane 2010; Tarsio et al. 2011; Diakov et al. 2013). Moreover, it has been reported that pHv of wild-type and mutants rapidly change according to the external pH (Plant et al. 1999; Brett et al. 2011). Under acidic pH stress Brett et al. (2011) pHv in wild-type was around 5.28±0.14, and upon alkali stress the pHv jumped to 5.83±0.13. To avoid that experimental noise, pHv measurements in our experiments were taken from yeast cells at the same growth phase (early logarithmic phase) and all media were buffered to 6.0 with arginine. Fluorescence ratios were transformed in pHv values following the protocol described by James Kracke (1992).

Firstly, yeast strains differing in the presence or absence of NHX exchangers were compared, and significant differences were observed. Mutation of the *nhx1* gene produced vacuolar acidification of 0,83 pH units relative to the wild-type strain and expression of AtNHX1 restored wild-type values (Figure 15A). These results validated the experimental approach.

To test whether the AtNHX1 mutants affecting conserved residues at the pore domain had an effect in the pHv, the BCECF experiment was repeated three times, using three independent colonies each time. The results comparing the pHv of yeast cells expressing various AtNHX1 mutants showed a consistent tendency in independent experiments, but experimental variation in absolute pHv values between experiments meant that no statistically significant differences could be demonstrated in most samples. The lack of significance could be due to the dynamic range of the ratiometric dye or the calibration method. Representative data from one of the experiments is shown In Figure 15B. As

expected the mutant D185L had an acid pHv similar to the empty-vector control since the protein is inactive . The N184D mutant had a near wild-type pHv.

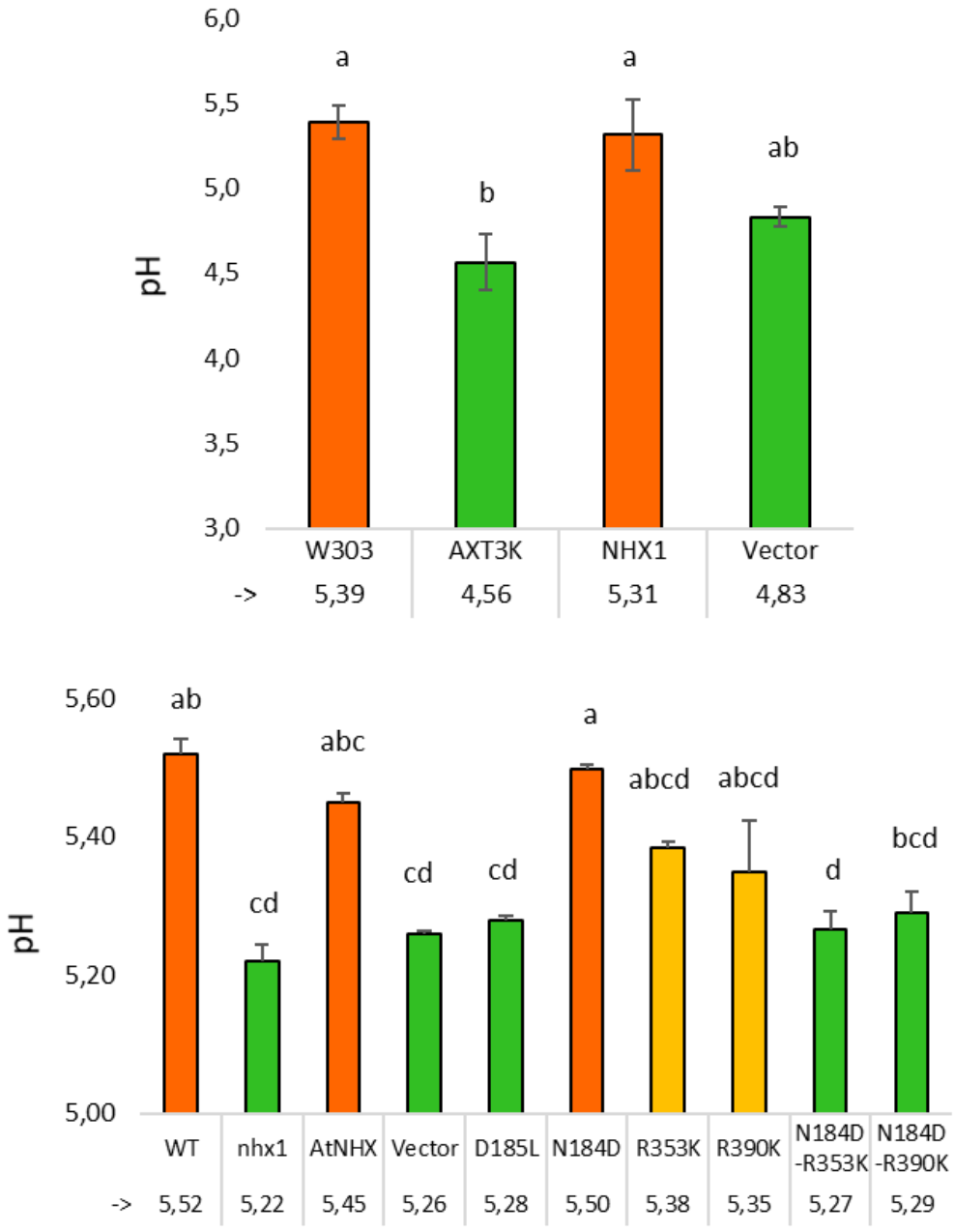

Figure 15. Vacuolar pH measurement in yeast expressing the AtNHX1 mutants of the N-terminal core by BCECF-AM. (A). Vacuolar pH of the wild type (W303) and mutant (AXT3K) strains. AXT3K vacuolar pH was measured in the untrasnformed strain, and two transformed strains: expressing AtNHX1, or with the empty vector (pDR195. B. Vacuolar pH values of the AtNHX1 mutant alleles of the conserved N-cterminal domain. In both graphics the results of one representativve experiment is represented. In each experiment three independent colonies were used to meaure the pH. The pH value obtained in each case is shown. Statistical analysis. Different letters indicate statistically significant different poblations in pairwise comparison by Tukey HSD test. ($p < 0.05$)

Conservative mutations in the conserved arginines R353K and R390K showed intermediate pHv values halfway between the wild-type and the null mutant. However, combining the R353K and R390K mutation with the N184D mutation that had no effect per se, produced more acidic vacuoles similar to loss-of-function mutants, suggesting compromised exchange activity and reduced H^+ leak.

R.2. *Cis*-and *Trans*-regulation of AtNHX1

As previously discussed, the eukaryotic proteins of the CPA superfamily present a hydrophilic C-terminal tail that is absent in the prokaryotic members (Hunte et al. 2005b; Donowitz et al. 2009), allowing a more complex regulation of the eukaryotic ones. The C-terminal domain of the mammalian NHE family has been extensively studied and characterized (Slepkov et al. 2007; Donowitz et al. 2009; Köster et al. 2011b; Amith et al. 2017). It consists of a long tail with different domains that mediate the interaction with multiple regulatory proteins such as calcineurin B homologue (CHP), calmodulin 1 (CaM), Na^+/H^+ exchanger regulatory factor (NHERF), ezrin, phospholipases (PICγ), protein kinase A (PKA), serum and glucocorticoid kinase (SGK), or dipeptidyl peptidase (DPP) (Cha et al. 2003; Alexander and Grinstein 2009), all of which can modify and regulate NHE activity or mediate interaction with the cytoskeleton. Moreover, this tail is thought to contain the pH sensor of the protein (Cha et al. 2003) and an auto inhibitory domain (Köster et al. 2011b).

There is no much knowledge about the structure or function of the cytosolic C-terminal domain of eukaryotic NHX proteins, and how this might be regulating exchange activity. In a proteomic study of vacuolar-localized proteins (Whiteman et al. 2008b), the phosphopeptide GFVPFVPG[pS]PTER corresponding to an identical sequence present at the C-terminal domains of AtNHX1 and AtNHX2 was identified. In addition, interaction of both AtNHX1 and AtNHX2 with different CIPK protein kinases and with MPK6 through their C-termini has been found (Andrés 2013; PhD Dissertation), but how these two transporters are regulated by the Ca^{2+}-dependent phosphorylation by CIPKs or by MPK6 remains unknown. Moreover, AtNHX1 has been shown to interact with the calmodulin-like protein CAM15/CML18 (Yamaguchi et al. 2003) in a pH and Ca^{2+} dependent manner. Last, AtNHX proteins are essential to control pH of endomembrane organelles (Yamaguchi et al. 2001; Bassil et al. 2011b; Barragán et al. 2012; Martinière et al. 2013a; Andres et al. 2014; Reguera et al. 2015; Ashnest et al. 2015; Fan et al.

2018), but there is no knowledge on how pH is sensed by AtNHXs or how pH regulates protein activity.

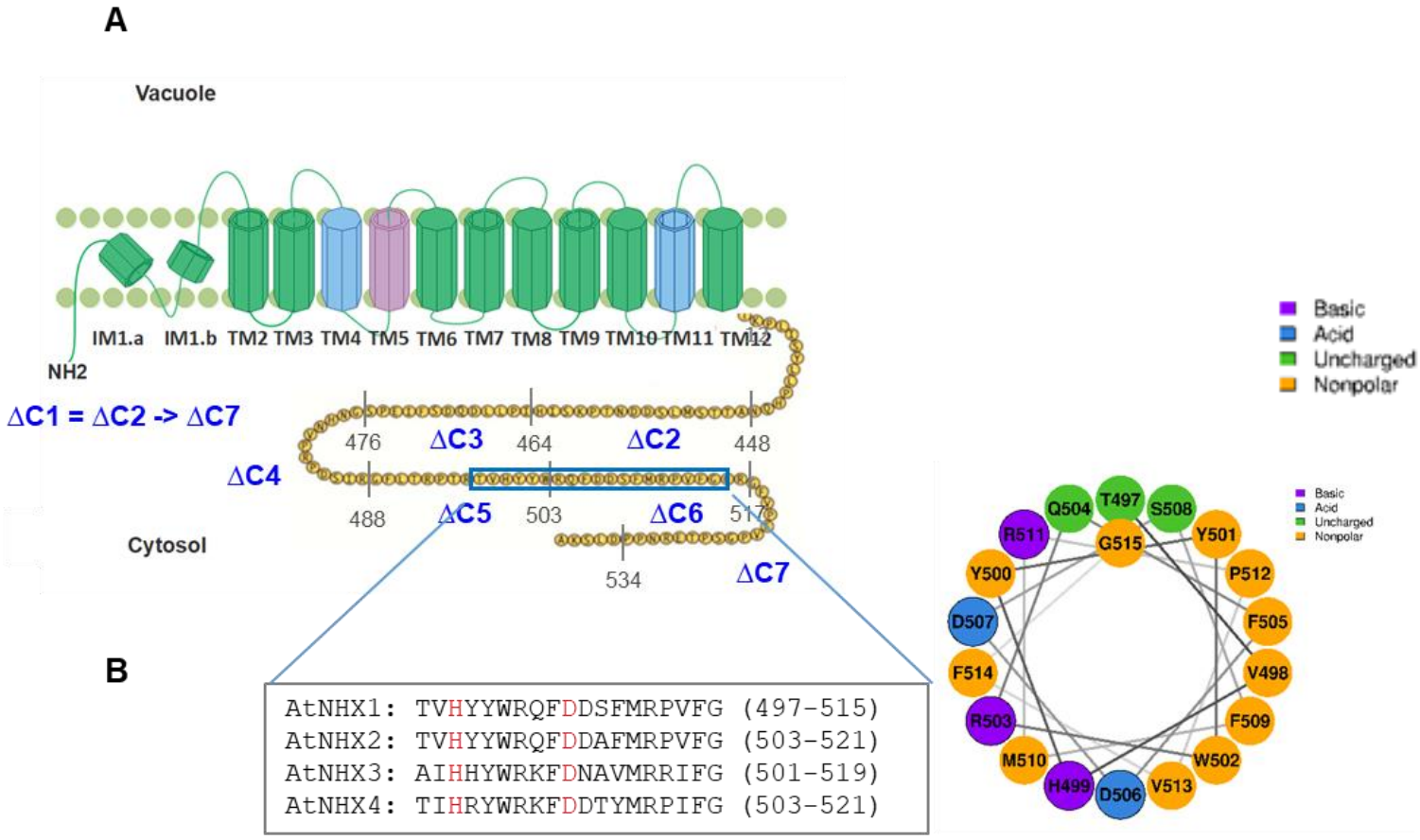

Figure 16. CML18 binding domain at the cytosolic domain of AtNHX1 and scanning deletions. (A) Schematic representation of the CML18 binding domain (CML-BD) in the cytosolic C-terminal portion of AtNHX1 and the scanning deletions marked as consecutive sectors, from ΔC1 to ΔC7; ΔC1 corresponds to the deletion of the complete C-terminal tail. Numbers indicate the amino acid position in which each deletion begins and ends. **(B)** Alignment of the CML-BD of the vacuolar NHX proteins of Arabidopsis thaliana (AtNHX1-4). The conserved His and Asp residues are highlighted in red.

R.2.1 Structure of the C-terminal domain of AtNHX1

According to the proposed topological model in this thesis, AtNHX1 has a hydrophilic cytosolic C-terminal domain comprising amino acids from T435 to A538 (Figure 16. ***CML18 binding domain at the cytosolic domain of AtNHX1 and scanning deletions. (A)*** *Schematic representation of the CML18 binding domain (CML-BD) in the cytosolic C-terminal portion of AtNHX1 and the scanning deletions marked as consecutive sectors, from ΔC1 to ΔC7; ΔC1 corresponds to the deletion of the complete C-terminal tail. Numbers indicate the amino acid position in which each*

deletion begins and ends. ***(B)*** *Alignment of the CML-BD of the vacuolar NHX proteins of Arabidopsis thaliana (AtNHX1-4). The conserved His and Asp residues are highlighted in red.*

And 8A). Computational analyses suggested the presence of a calmodulin-binding domain (CML-BD) at the C-termini of AtNHX1. The physical interaction between this domain of AtNHX1 and the calmodulin-like protein AtCML18 has been experimentally confirmed by Yamaguchi et al (2005). Moreover, the sequence alignment of all family members in Arabidopsis, AtNHX1 to 6, indicates that this domain is highly conserved in sequence and relative position within the vacuolar proteins AtNHX1 to AtNHX4, but not in the endosomal AtNHX5 and AtNHX6 (***Figure 16***B). In AtNHX1 this CML18-binding domain (CML-BD) comprises a fragment of 19 amino acids, from T497 to G515.

A detailed analysis of the CML-BD allowed the detection of putative essential amino acids that are highly conserved. Of special interest are residues H499 and D506 (numbering as of AtNHX1). These residues are not only fully conserved in the putative CML-BD of the vacuolar isoforms (AtNHX1-AtNHX4 (Figure 16) but also they are well at a distance equal to a helix turn, which could allow them to form salt bridges, generating a pH-sensing motif. Salt bridges between histidine and acidic amino acids that become disrupted when His is deprotonated at neutral and basic pH constitute a common pH-sensing module in proteins (Pope et al. 2004; Törnroth-Horsefield et al. 2006; Blundell et al. 2007; Thompson et al. 2008; Fritz et al. 2008).

Histidine has a pKa of 6.5 and relatively small shifts in cellular pH will change its average charge. Consequently, His residues are integral to many pH sensors in proteins (Srivastava et al. 2007; Casey et al. 2010). Histidine residues have been demonstrated to be important for pH-sensing in various Na^+/H^+ exchangers (Aronson et al. 1982; Wakabayashi et al. 1992; Gerchman et al. 1993; Wang et al. 1995; Ikeda et al. 1997). Cha et al (2007) demonstrated that two His in the C-terminal domain of HsNHE3, H479 and H499, are important for determining the pH sensitivity of the protein. Mutation of these amino acids shifted the set point of HsNHE3 to more acidic values. On the other hand, amino acids R440, G455 and G456 of the human NHE1 protein are known to modify the pH dependence of this exchanger (Slepkov et al. 2007). In the case of prokaryotic CPA members, the pH regulation has been proposed to be an intrinsic characteristic of the protein binding site (Mager et al. 2011; Lee et al. 2014; Călinescu et al. 2014; Uzdavinys et al. 2017).

The analysis of the AtNHX1 C-terminal domain evidenced the presence of two conserved histidines at positions 479 and 499, the same positions than H479 and H499 comprising the

pH-sensor of HsNHE3. Thus, these two histidines of AtNHX1 could be important for sensing the cytosolic pH. As previously mentioned, the H499 is localized in the CML-BD, and could form salt bridges with the Asp in position 506, and thus play an important role integrating pH and CML18 regulation of the protein.

R.2.2. Regulation of AtNHX1 protein by pH and CML18

To identify regulatory regions at the C-terminal domain that could be affecting AtNHX1 activity or interaction with other proteins, a deletion-scanning approach was performed. A set of seven AtNHX1 mutants was generated by consecutive deletions of fragments of the cytosolic C-tail; fragments to be deleted were spliced out leaving the remaining C-terminal domain intact (**¡Error! No se encuentra el origen de la referencia.**A). In these mutants the putative CML-BD was divided between two of the mutants, ΔC5 and ΔC6. The new alleles were cloned in the vector pDR195 and expressed in the yeast strain AXT3K sensitive to high salinity and hygromycin. A drop-test complementation assay was done in YPD supplemented with hygB, or AP medium supplemented with LiCl (Figure 17). The deletion of the complete

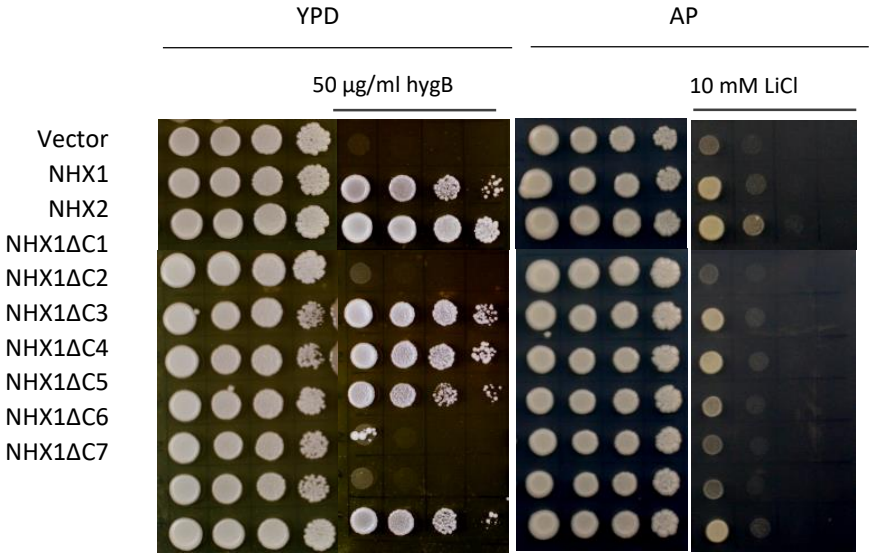

Figure 17. The CML18 binding-domain segments are essential for AtNHX1 activity. The cDNAs of AtNHX1 mutant alleles ΔC1 – ΔC7 were subcloned into the yeast expression vector pDR195 and transformed into the AXT3K (Δ*ena1-4* Δ*nha1* Δ*nhx1*). Yeast cells were normalized in water to OD_{600} of 0.5. Aliquots (5µL) from normalized yeast cultures or 10-fold serial dilutions were spotted onto YPD or AP solid medium plates. In order to test the functionality of the protein, YPD media was supplemented with hygromycin, and different concentrations of LiCl were added to the AP medium. The strains were grown at 30°C for 2-4 days.

tail (mutant ΔC1) generated an inactive protein, making evident that the C-terminal tail is essential for the normal activity of the protein. In addition, the alleles comprising deletion of the CML-BD (ΔC5 and ΔC6) did not complement the sensitive phenotype either, suggesting that is the lack of this domain the reason of the null phenotypes.

R.2.2.1. Interaction of AtNHX1 and AtNHX2 with CML18.

To confirm the previously described interaction between AtNHX1 and AtCML18 (Yamaguchi et al. 2003), and to determine whether the interaction was specific of AtNHX1, or not, different protein-protein interaction assays were performed.

The yeast-two-hybrid assay (Y2H) reports the in vivo interaction of two proteins taking place in the nucleus of the cell by heterologous co-expression of two proteins in yeasts. To use this method in our analysis, the C-terminus of the AtNHX1 protein (amino acids from T435 to A538) and AtNHX2 (amino acids from G434 to P546) were fused to the activation domain of the GAL4 transcription factor (pGBKT vector, Clontech), and the complete cDNA sequence of AtCML18 was fused to the binding domain of the GAL4 transcription factor (pGADT7 vector). These constructs were co-transformed in *S. cerevisiae* strain AH109 (section M.7.1). Co-transformants were grown overnight in YNB-L-W, collected and resuspended to OD_{600} = 0.5. Finally, drops were plated onto selective solid media. Only those cells expressing proteins that interact physically could grow in selective media without Ade or His.

As expected, AtNHX1 and AtCML18 interacted in the Y2H system. Moreover, AtCML18 was able to interact with AtNHX2 as well (**¡Error! No se encuentra el origen de la referencia.**These interactions were confirmed by BiFC assays with transient expression in *Nicotiana benthamiana*. In this case the complete cDNAs of AtNHX1 and AtNHX2 proteins were cloned in the pSPYNE173 vector, with a C-terminal fusion to the N-terminal half (amino acids 1–173) of the eYFP fluorophore, and AtCML18 was cloned into the pSPYCE(M) vector with a C-terminal fusion to the C-terminal half (amino acids 155–239) of the same fluorophore. Transient expression in *N. bentamiana* was performed as described in Section M.7.2 . Small discs of agroinfected leaves were cut and inspected with a confocal microscope after 48 hours of having infiltrated the plants, as described in Waadt et al. (2008).

The results confirmed that both AtNHX1 and AtNHX2 interact with AtCML18 in transient expression in leaves of *N. benthamiana* (Figure 18). The expression of tagged AtNHX1 or AtNHX2 with the empty pSPYCE(M) vector produced no fluorescence, confirming the

specificity of the interaction between these proteins and AtCML18 (Figure 18C). Moreover, the possibility of the cleavage of the N-eGFP from the AtNHX protein was ruled out since no interaction was seen inside organelles like the nucleus, as would be expected from free GFP molecules.

Finally, we aimed to purify the CLM-BD of AtNHX1 in complex with CML18 by co-expressing these proteins in bacteria. To that end, a C-terminal fragment of AtNHX1 comprising the CML-BD domain (amino acids 445 to 516) was cloned in the pGEX expression vector to fuse an N-terminal GST tag. On the other hand, CML18 was cloned in the pCDFDuet vector and fused to an N-terminal Hisx6 tag. Both constructs were co-transformed in the bacterial strain Rossetta 2. Recombinant proteins were induced and extracted as described in Materials and Methods (Section M.7.3). The protein extract was divided in two equal parts: one half was used to purify the NHX1-CML18 complex in a GSH-Sepharose column to pull-down the GST:NHX1 tag; the other half was purified in a Ni^{+} column to pull-down the complex using the CML18:His6x tag. The proteins recovered from affinity columns were separated by SDS-PAGE in denaturing conditions, and the gel was finally stained with Comassie blue. In parallel, GST:CML-BD and CML18:His6x were individually purified from Rossetta2, following the same protocol (Figure 19).

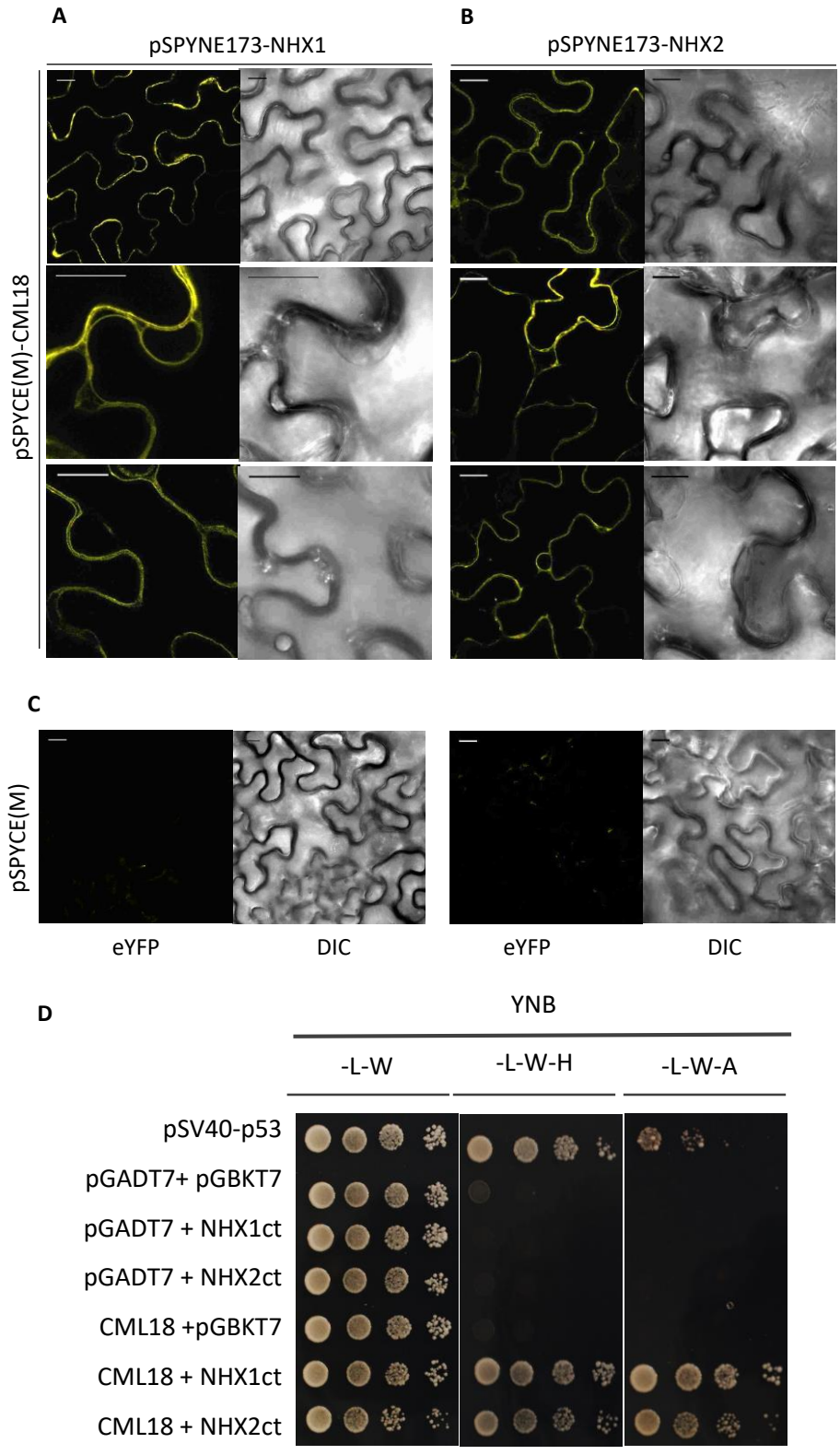

Figure 18. AtNHX1 and AtNHX2 interaction with AtCML18 visualized by BIFC and Y2Y. Confocal images of *Nicotiana benthamiana* leaf sections expressing **(A)** AtNHX1 or **(B)** AtNHX2 fused to the N-terminal fragment of the eYFP in combination with AtCML18, fused to the C-terminal fragment of the eYFP protein. **(C).** Expression of AtNHX1 and AtNHX2 fused to the N-terminal fragment of the eYFP protein in combination with the empty vector expressing the C-terminal fragment of the eYFP.for each genotype. **(D)** 10-fold serial dilutions of AH109 yeast transformed with activation domain (pGADT7) vectors and binding domain (pGBKT7) vectors expressing the indicated coding sequences were spotted on selective YNB media without Leu and Trp (for selection of positive double transformants) or without Leu, Trp and His or Ade (for selection of interaction). Plates were photographed after 2 days at 28°C.

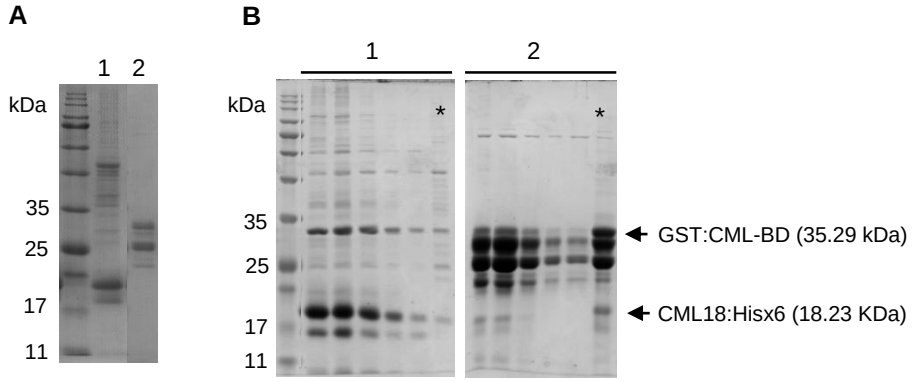

Figure 19. Analysis of the co-precipitation of complexes AtNHX1 CML-BD fragment and CML18. **(A)** Isolation of (1) CML18:Hisx6 expressed in Rossetta 2 bacteria and purified in a Ni^+ column, and (2) GST:CML-BD expressed in Rosetta2 bacteria and purified in a Sepharose column. **(B)** Co-purification of the complex CML-BD and CML18 co-expressed in Rossetta2. Induction and extraction were performed as mentioned in Material and Methods. The extracts were divided in two: one half was purified in a sepharose column (1), and the other half in a Ni^+ column (2). The proteins were eluted in the adequate buffers. Proteins were resolved by SDS-PAGE and stained with Comassie blue. Lanes contain the serial eluates of the Ni^+ (1) and GST (2) columns. Resins was recovered and submitted to the SDS-PAGE to estimate protein retention (*).

The results showed that, when expressed in bacteria, CML-BD and CML18 formed a complex that allowed the co-purification of both peptides (Figure 19B). However, when the GST-tag was used to pull-down the complex most of the GST:CML-BD protein was retained in the resin and the recovery efficiency was quiet low, and the yield of CML18 was much lower compared to the abundance of the GST-fused CML-BD (Figure 19B). Moreover, bands of lower size than the full-length GST:CML-BD were observed. Likely these results were due to the premature termination of translation of the recombinant GST:CML-BD protein. Better results were obtained when the purification was done by pulling-down using the Hisx6 tag. In this case, a full-length GST:CML-BD protein was recovered whose abundance was commensurate to that of CML18:His6x.

R.2.2.2. Requirement of the CML-BD in the interaction between AtNHX1 and CML18

To demonstrate that the AtNHX1-CML18 interaction was taking place through the putative CML-BD, the nhx1ΔBD mutant, lacking this binding domain, was also cloned in the pGBKT7 vector, and the Y2H assay was repeated (Figure 20A). The co-transformants expressing AtCML18 and the nhx1ΔBD peptide were unable to grow in selective media without His or

Ade, indicating that the protein interaction was lost and that the interaction between AtNHX1 and AtCML18 occurs through the proposed CML18-binding domain.

BIFC assays were also performed with the *nhx1ΔBD* allele cloned in pSPYNE173 and transiently co-expressed with CML18 in *N. benthamiana* leaves. As shown in Figure 20B, the interaction between AtNHX1 and AtCML18 was lost when the CML-BD in the C-terminal of AtNHX1 was deleted. Of note is that the interaction of the truncated nhx1ΔBD protein with AtNHX2 remained similar to the fluorescence observed with wild-type proteins AtNHX1 and AtNHX2, and fluorescence labeled the tonoplast membrane. These results demonstrate that the nhx1ΔBD mutant protein was correctly expressed and sorted to the organelle membranes. The lack of the CML-BD was only affecting the interaction with AtCML18, showing both the requirement and sufficiency of that domain to mediate the interaction.

Unexpectedly, if instead of using the complete deletion of the CML-DB (as in the *nhx1ΔBD* allele) in the Y2H assay, the nhx1ΔC5 and nhx1ΔC6 proteins were fused to the GAL4 binding domain and co-expressed with pGADT7-CML18 in the yeast strain AH109, the results were different. Alike the nhx1ΔBD mutant, the nhx1ΔC6 protein was unable to interact with CML18. However, the interaction of nhx1ΔC5 with CML18 remained positive (Figure 21A). Since the expression of the mutant nhx1ΔC5 tested also positive when co-expressed with the empty vector, yeast growth could be considered a false positive. Indeed, when YNB –L-W-H plates were supplemented with increasing concentrations of 3-amino-1,2,4-triazole (3AT), growth of cells carrying the empty vector was suppressed, but not of cells co-expressing CML18 with nhx1ΔC5 whose interaction remained even at high concentrations (20 mM 3AT). Nonetheless, yeast growth was not as robust as of cells co-expressing the wild-type C-terminus of AtNHX1 (Figure 21B). 3AT is a competitive inhibitor of the His3 gene product used as a reporter gene in Y2H assay, and yeasts cells grow in presence of 3AT only if the level of His3 gene product is sufficient to overcome the inhibitory effect of 3AT. To confirm the false positive, the Y2H assay was repeated in selective medium scoring for adenine restoration of adenine auxotrophy, which imposes a greater stringency than selection for histidine auxotrophy (Figure 23A). These results indicate that the nhx1ΔC5 mutant retained some ability to interact with AtCML18, whereas the interaction between nhx1ΔC6 and AtCML18 was completely abrogated.

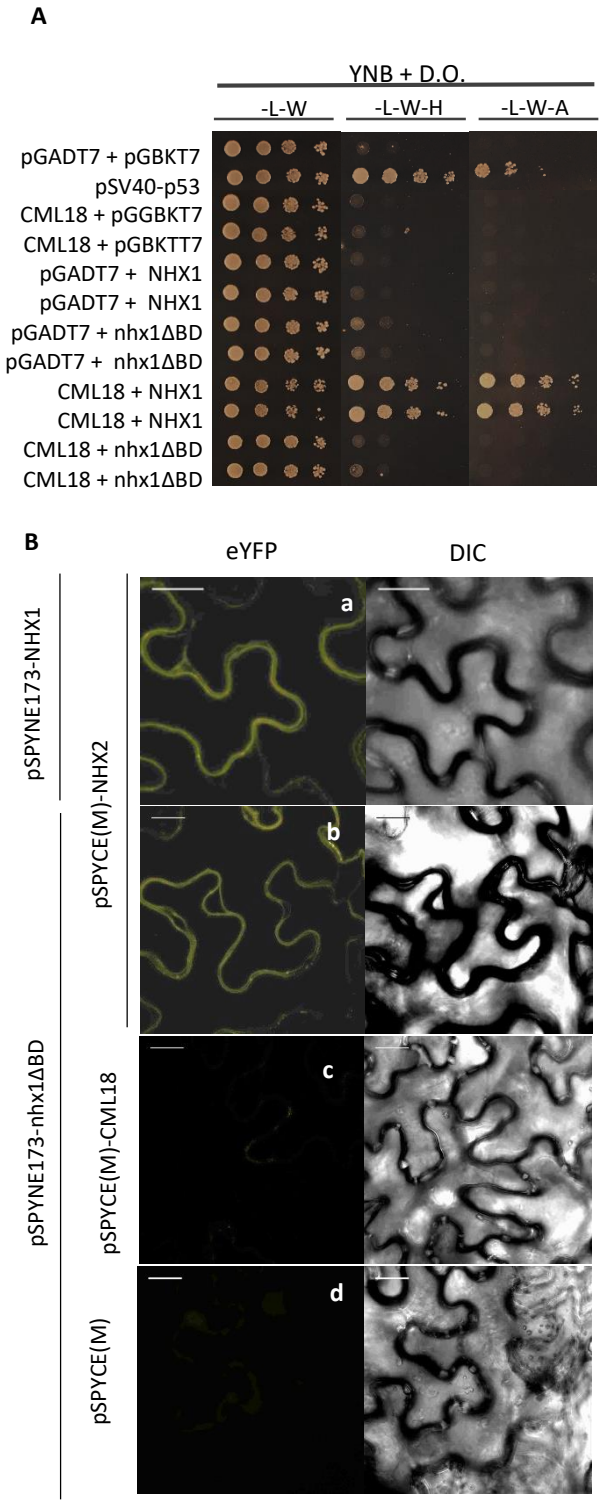

Figure 20. Analysis of the interaction between AtNHX1ct allele mutants nhx1ΔC5 and nhx1ΔC6 with AtCML18 by Y2H. (A) Ten-fold serial dilutions of overnight cultures of yeast AH109 transformed with activation domain (pGADT7) vectors and binding domain (pGBKT7) vectors expressing the indicated coding sequences were spotted on selective YNB media without Leu and Trp (for selection of positive double transformants) or without Leu, Trp and His or Ade (for selection of interaction). Plates were photographed after 2 days at 28°C. Drops were spotted on selective YNB media without Leu and Trp (for selection of positive double transformants) or without Leu, Trp and supplemented with 20 mM 3AT (to eliminate false positive results). Plates were photographed after 2 days at 28°C. **(B)** Confocal images of Nicotiana benthamiana leaf sections expressing (a) AtNHX1 or (b,c, d) nhx1ΔBDct fused to the N-terminal fragment of the eYFP in combination with AtNHX2 (a and b) , AtCML18 (c) or pSPYCE(M) empty vector (d) fused to the C-terminal fragment of the eYFP protein.

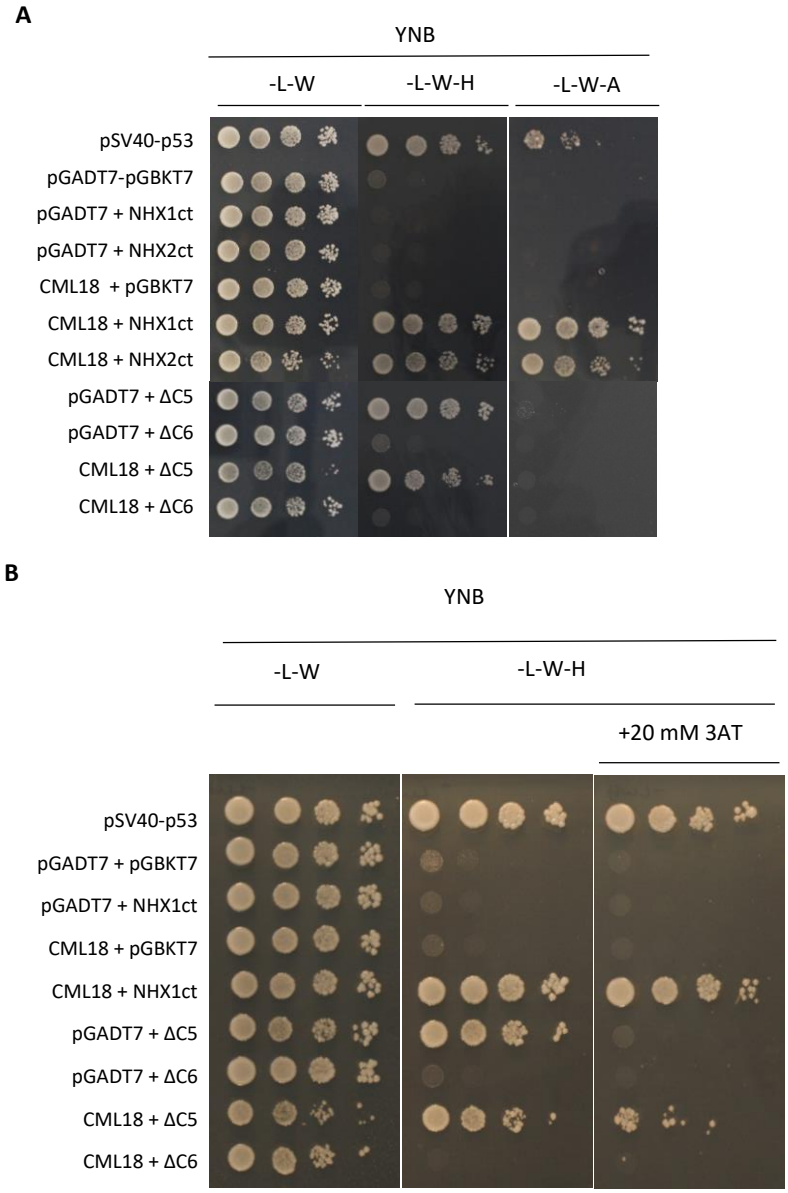

F**igure 21. Analysis of the interaction between AtNHX1ct allele mutants nhx1ΔC6ct and nhx1ΔC5ct with AtCML18 by Y2H.** A. 10-fold serial dilutions of AH109 yeast transformed with activation domain (pGADT7) vectors and binding domain (pGBKT7) vectors expressing the indicated coding sequences were spotted on selective YNB media without Leu and Trp (for selection of positive double transformants) or without Leu, Trp and His or Ade (for selection of interaction). Plates were photographed after 2 days at 28°C. B. Drops were spotted on selective YNB media without Leu and Trp (for selection of positive double transformants) or without Leu, Trp and supplemented wir 20 mM 3AT (to eliminate false positive results). Plates were photographed after 2 days at 28°C

Last, the role of the CML-BD domain in controlling AtNHX1 activity in vivo was determined by complementation of the AXT3K strain. As shown in the AtNHX1 protein in which the CML-DB had been deleted (nhx1ΔBD) was unable to suppress the sensitivity to HygB and to LiCl (Figure 22).

Together, these results indicate that the protein fragment of AtNHX1 bearing the CML-BD is necessary for the normal activity of the protein and for the interaction between AtNHX1 and CML18 to take place. Moreover, the second half of the CML-BD, defined by deletion ΔC6, appears to be essential for this interaction. Even though the loss of the first half of the CML-BD (ΔC5) did not preclude the interaction between AtNHX1 and CML18, the 3AT results indicate that this interaction was weaker than the one observed with the wild type protein (Figure 21).

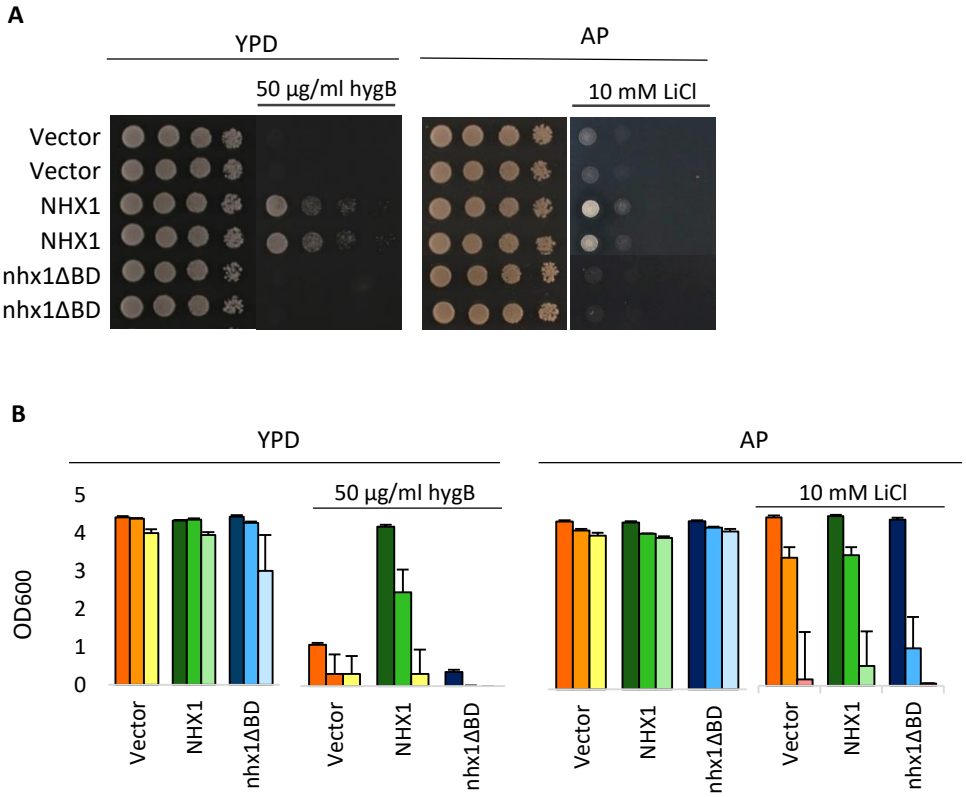

Figure 22. The CML18 binding-domain is essential for AtNHX1 activity. The cDNA of AtNHX1 mutant allele nhx1ΔBD was cloned into the yeast expression vector pDR195 and transformed into the AXT3K (*Δena1-4 Δnha1 Δnhx1*). Overnight cultures were normalized in water to OD*600* of 0.5. Aliquots (5µL) from normalized yeast cultures or 10-fold serial dilutions were spotted onto YPD or AP solid medium plates. To test the functionality of the protein, YPD media was supplemented with hygB **(A)**, and different concentrations of LiCl were added to the AP medium **(B).** The strains were grown at 30°C for 2-4 days. Two independent transformants for each genotype are shown. ***(C)*** Ten-fold serial dilutions of overnight cultures were spotted onto 200 µL YPD or AP liquid medium in 96-well plates. Cells were grown at 30°C and OD*600* was measured after 24h. Results are the media of three independent colonies for each genotype. Shown are the mean and SEM values.

R.2.2.3. Regulation of AtNHX1 by cytosolic pH

The cytosolic domain of AtNHX1 contains two conserved histidines at positions 479 and 499 that could be equivalent the residues H479 and H499 comprising the pH-sensor of human HsNHE3. To verify whether the conserved H479 and H499 residues constitute a pH sensor in the cytosolic domain of AtNHX1, single and double mutant alleles were generated (Section M.8.1), and functional assays were performed by expressing the mutant proteins in the yeast strain AXT3K as previously described (Section M.8.2.2)

AXT3K cells expressing the H479L and H499L mutants of AtNHX1, or the double mutant H479L-H499L, were able to grow in YPD media supplemented with hygB (**Figure 23**A), as well as in AP with LiCl or NaCl (***Figure 26***). The phenotype observed in these conditions was no different of the observed with the yeasts expressing the wild-type AtNHX1 protein, meaning that the residues H479 and H499 are not essential for the normal activity of AtNHX1. However, these results do not rule their possible function as cytosolic pH sensors.

To test whether H479L and/or H499L have a function in sensing the pH and could modulate AtNHX1 activity under conditions that disturbed the cytosolic pH, growth assays were repeated in YPD liquid media with hygB and buffered at different pHs. If these residues were important for sensing the pH, the yeasts expressing the mutant alleles would grow differently from the ones expressing the wild-type AtNHX1 at the pH in which these resides would activate/deactivate the protein. As shown in Figure 23**Figure 23**B, yeast cells were generally more sensitive to hygB at pH 7 (Figure 23). Proteins H499L and H499L-H479L supported reduced growth at pH 5 and 6 relative to the wild-type and H479L proteins (Figure 23B), but not at pH7, suggesting that H499L is a partially active protein. However, no evidence was found that residues H479 and H499 were important regulators of AtNHX1 activity in the yeast system because the greatly reduced growth of yeast cells at pH 7 in the presence of hygB precluded the analysis at non-acidic pH.

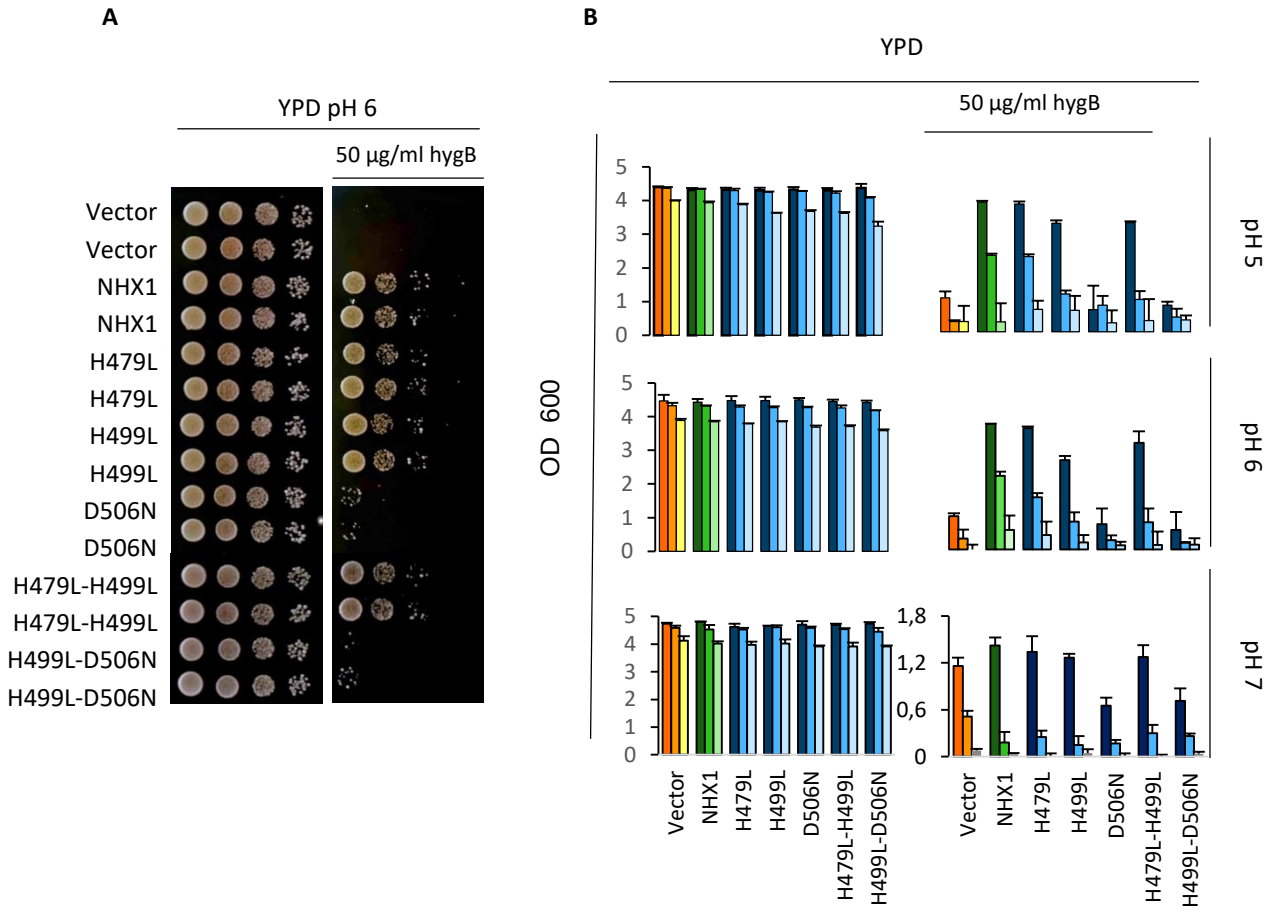

Figure 23. Functional assay of AtNHX1 mutants of conserved amino acids at the C-terminal cytosolic domain. The cDNAs of AtNHX1 and the mutant alleles obtained by point mutation of the indicated residues were cloned into the yeast expression vector pDR195 and transformed into the AXT3K (Δena1-4 Δnha1 Δnhx1). Overnight yeast cultures were normalized in water to OD600 of 0.5. Aliquots (5 µL) from normalized yeast cultures or 10-fold serial dilutions were spotted onto onto AP solid medium plates with different concentrations of LiCl or NaCl. Cells were grown at 30°C for 2-4 days.

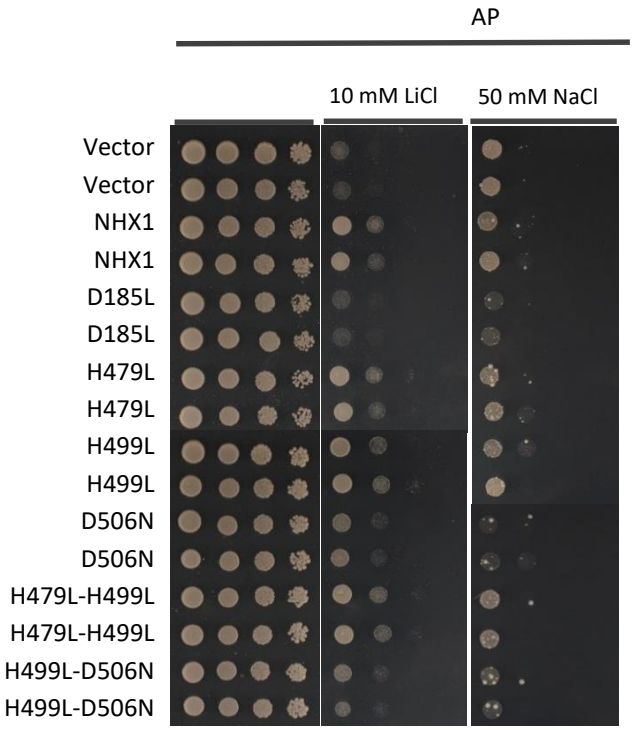

Figure 24. Functional assay of AtNHX1 mutants of conserved amino acids at the C-terminal cytosolic domain. The cDNAs of AtNHX1 and the mutant alleles obtained by point mutation of the indicated residues were cloned into the yeast expression vector pDR195 and transformed into the AXT3K (Δena1-4 Δnha1 Δnhx1). Overnight yeast cultures were normalized in water to OD600 of 0.5. Aliquots (5 µL) from normalized yeast cultures or 10-fold serial dilutions were spotted onto onto AP solid medium plates with different concentrations of LiCl or NaCl. Cells were grown at 30°C for 2-4

R.2.3. Cross-talk of pHcyt and Ca^{2+}/calmodulin binding

The likely structure of the CML-BD of AtNHX1 was modeled using as template the resolved structure of the homologous human exchanger NHE1 bound to the rat CaM1 (Köster et al. 2011b)(Figure 26). According to the HsNHE1-CaM structure, the interaction takes place in an antiparallel or *head-to-tail* manner and the NHE1 domain folds as two semi-helices that are connected by a short and flexible linker flanked by residues H561 and D567 (Figure 25). A similar modeled structure was obtained for the AtNHX1 CML-BD (Figure 26). The two semi-helices of AtNHX1 CML-BD were linked by a short fragment flanked by the conserved residues H499 and D506.

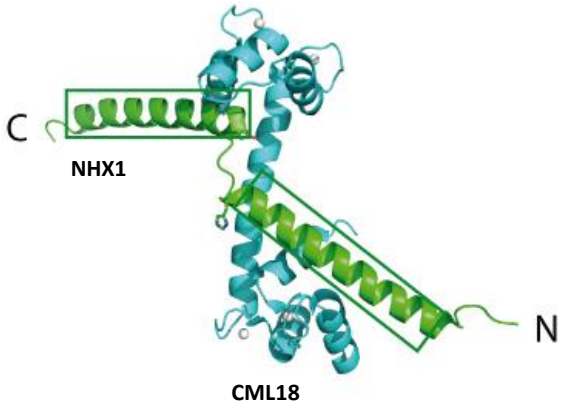

Figure 26. Modelled structure of the NHX1 CML-BD and CML18 complex. NHX1 CML-BD (green) consists of two helices connected by a short loop, in which extremes there are located the residues H499 and D506. CML (blue) contains two lobes connected by a central helix.

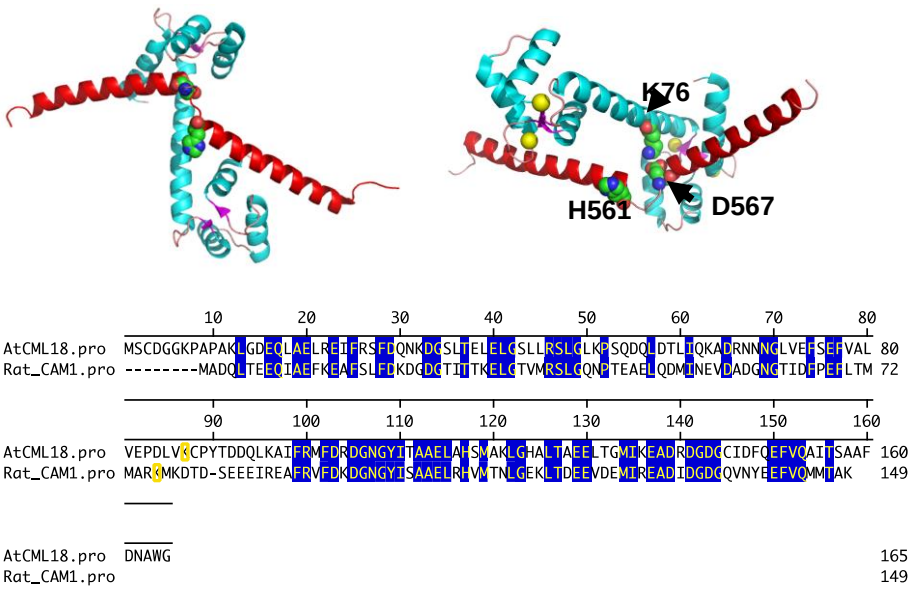

Figure 25. **NHE1-CaM complex structure. (A)** 3D representation of the HsNHE1-CaM complex. Putative important amino acids for the interaction are highlighted. **(B).** AtCML18 and rat Cam1 alignment. K76 in CaM and the putative homologue in CML18 are highlighted.

To test the importance of H499 and D506 for the interaction between AtNHX1 and AtCML18, different approaches were followed. First, mutation H499L compromised the ability of AtNHX1 to fully suppress the sensitivity to hygB at pH5 and 6, although no effect was seen in suppressing the sensitivity to LiCl and NaCl (Figure 23 and Figure 24). Secondly, the Y2H assays with the nhx1ΔC5 and nhx1ΔC6 mutants showed different results. Removing the CML-BD half comprising the H499 residue (ΔC5) supported a weaker interaction of with AtCML18 compared to the wild-type AtNHX1 protein, but no interaction was observed when the half containing the D506 residue (ΔC6) was removed (Figure 21). Thus, we generated the AtNHX1 single mutant D506N and the double mutant H499L-D506N alleles, and complementation assays with the yeast strain AXT3K expressing these AtNHX1 mutants was performed. The result indicated that the D506 residue was essential for AtNHX1 activity since both alleles D506N and H499L-D506N were unable to recover the sensitive phenotype of the yeast in either YPD media supplemented with hygromycin, or AP media supplemented with LiCl or NaCl (Figure 23 and Figure 24). Moreover, changes in the media pH did not affect this phenotype. All these results indicate that the acidic residue D506 is an essential feature of the CML-BD and for the normal activity of the protein.

To prove conclusively the requirement of the D506 for the interaction of the AtNHX1 CML-BD with CML18, Y2H assays using mutants AtNHX1-H499L and AtNHX1-D506N were performed. The results showed that the D506 is essential for the interaction between AtNHX1 and AtCML18 since the AH109 cells co-expressing AtCML18 and the AtNHX1 mutant D506N were unable to grow in YNB-L-W without Ade or His (Figure 27A). By contrast, H499 was not essential for the interaction. However, this interaction is not as strong as with the wild-type AtNHX1. AH109 cells co-expressing AtCML18 and the mutant H499L were able to grow in YNB–L-W-H media but not when the media was supplemented with 3AT (Figure 27B), in contrast to the wild-type CML-binding domains of AtNHX1 and AtNHX2.

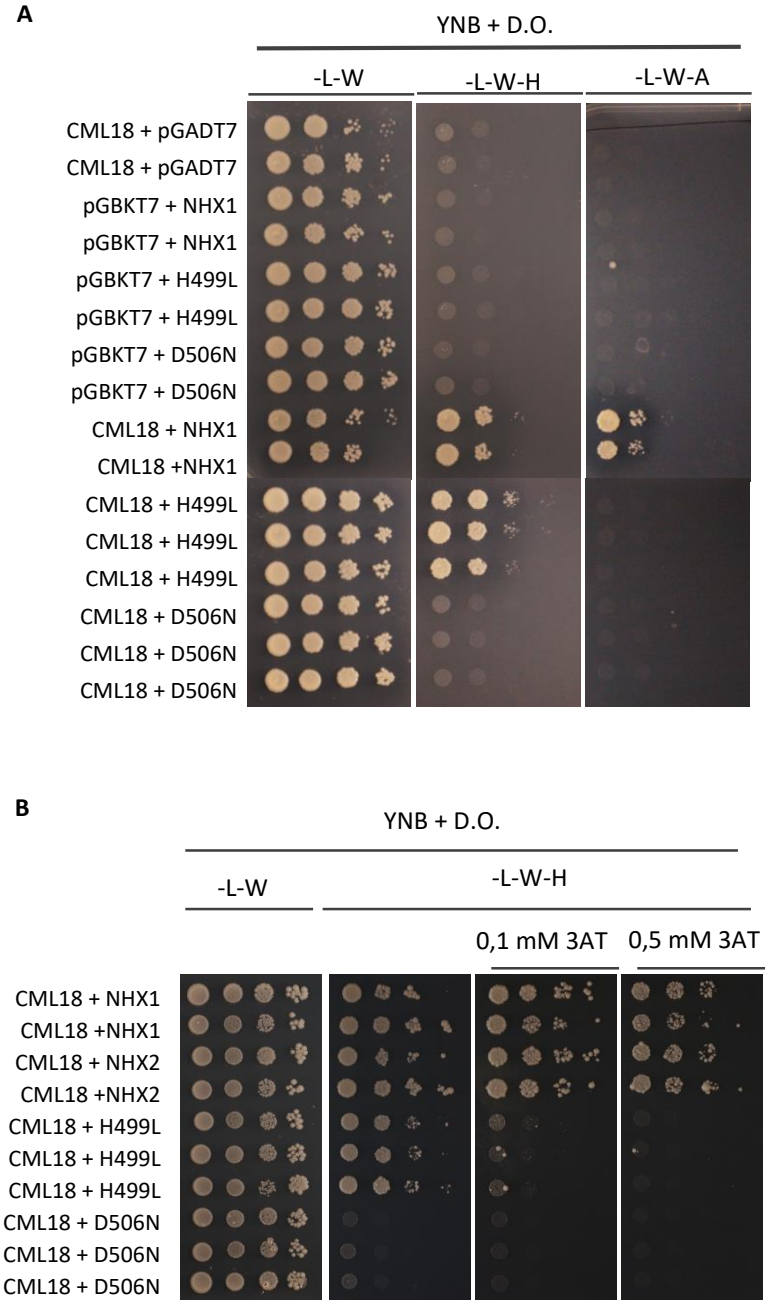

Figure 27. Analysis of the interaction between H499ct and D506Nct mutants alleles with AtCML18 by Y2H. (A) 10-fold serial dilutions of AH109 yeast transformed with activation domain (pGADT7) vectors and binding domain (pGBKT7) vectors expressing the indicated coding sequences were spotted on selective YNB media without Leu and Trp (for selection of positive double transformants) or without Leu, Trp and His or Ade (for selection of interaction). Plates were photographed after 4 days at 28°C. **(B).** Drops were spotted on selective YNB media without Leu and Trp (for selection of positive double transformants) or without Leu, Trp and supplemented with 3AT. Plates were photographed after 4 days at 28°C

R.2.4 Mutation in CMLBD effect in vacuolar pH regulation.

As mentioned earlier, deletion of the CaM binding domain of HsNHE1 shifted the pH set point to a more alkaline value as well (Ikeda et al. 1997). This CaM binding site has been described to inhibit the pH-sensor (Pouysségur 1994; Shigeo Wakabayashi et al. 1997). Moreover, in HsNHE3, the mutation of two histidines in the C-terminal cytosolic domain, H479 and H499, shifted the pH set point of the protein towards a more acidic region.

To obtain a better insight on how the CML-BD mutant alleles could be affecting the role of AtNHX1 in regulating the vacuolar pH (pHv), the same assay as for the pore-domain mutants expressed in AXT3K yeast strain was performed using the the ratiometric fluorescein-based pH sensitive dye BCECF. For the mutants affecting the C-terminal cytosolic tail two different groups are distinguished. On the one hand, a group of mutants of the putative pH-sensor that included H479 and H499 were tested in single and double mutant conformation, and the results have been shown in the previous section. The second group included mutants in the CML18 binding site, H499L and D506N, also in the single and double mutant combination. In addition, the mutant lacking the complete CML18 binding domain (CML18-BD) was also included to confirm the lack of activity of that protein.The experiment was performed as before and results are presented in Figure 28, where the graphics represent the mean of three independent colonies for each genotype of one representative experiment.

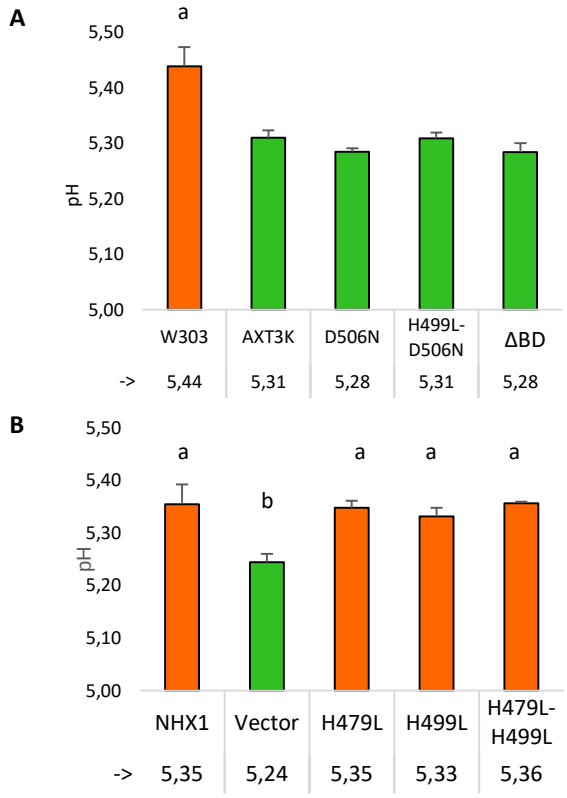

Figure 28. Vacuolar pH measurement in yeast expressing the AtNHX1 mutants of the C-terminal tail by BCECF-AM. (A). Vacuolar pH of the wild type (W303) and untransformed mutant (AXT3K) together with the mutant alleles of the C-terminal domain implicate din the CML18 interaction. **(B).** Vacuolar pH values of the AtNHX1 mutant alleles of the conserved C-cterminal tail implicated in the 'pH-sensing'. In both graphics the results of one representativve experiment is represented. In each experiment three independent colonies were used to meaure the pH. The pH mean value obtained in each case is shown. Different letters indicate statistically significant different poblation (A, $p< 0.05$) (B, $p<0.5$) in pairwise comparison by Tukey HSD test.

Once again, a clear trend was observed but no robust statistical significant differences could be obtained in all experiments. In agreement with the previous demonstration that CML18-BD and D506N mutants could not overcome the sensitivity of the AXT3K strain to HygB or NaCl (Figures 9 and 10), the vacuoles of yeasts expressing these alleles were more acidic, with pHv values similar to that of the AXT3K strain Figure 28A).

On the other hand, the results observed for the residues in the putative pH sensor, comprising the H479L, H499L and H479L-H499L mutants, did not show significant differences with the wild-type control (Figure 28B). The results are in accordance to the previous conclusions that these H to L mutants are active proteins.

R.3. In vivo measurement of cytosolic pH

The activity of AtNHX1 and AtNHX2 has been shown to be important for the regulation of pH of vacuoles (Bassil et al. 2011b; Andres et al. 2014) and TGN (Bassil et al. 2011a; Reguera et al. 2015) with significant impact in different aspects of cell and organ function and development, such as stomatal movements (Andres et al. 2014), vacuolar trafficking (Dragwidge et al. 2018), and protein accumulation in seeds (Ashnest et al. 2015). Moreover, the SOS1 (AtNHX7) exchanger in the plasma membrane extrudes Na^+ from the cytosol to the apoplast, contributing to the load of the ion in the xylem and delivery to shoots (Shi et al. 2002). Since the activity of AtNHX1 and AtNHX2 is able to change pH in a large volume such as the vacuole, we hypothesized that the liberation of H^+ into the cytosol by NHX proteins might also create variations in the cytosolic pH.

The development of genetically encoded pH-sensitive reporters has been a major achievement enabling a better understanding of pH homeostasis in vivo and in real-time. These reporters present several advantages over conventional fluorescent dyes: they do not need a loading protocol, allow non-invasive imaging and can be targeted to almost any organelle compartment. These reporters are based in the fluorophore sensitivity to changes in the media pH due to the protonated state of amino acids placed around the chromophore (Benčina 2013).

Using these reporters, a pH-map of the endomembrane system has been created that allows a better understanding the functioning of these organelles (Shen et al. 2013; Martinière et al. 2013a). The biochemical processes taking place in the luminal space of

endosomes are highly dependent of the cytosolic activity, and the changes on the homeostatic conditions in any of the compartments need to be communicated to the other.

In order to study how the cytosolic pH varies in the proximities of different organelle membranes or the plasma membrane under different environmental conditions that were relevant to the function of NHX proteins, a cytosolic pH-map was obtained for roots of Arabidopsis in collaboration with Prof. Karin Schumacher (Centre for Organismal Studies, University of Heidelberg). These maps would also enable to determine how the activity of different organelles under specific stresses or physiological states modifies cytosolic pH.

We selected the genetically encoded ratiometric pH-sensor pHGFP. This protein is based in the pH-sensitive GFP derivative 'ratiometric pHluorin', which is especially useful for ratio imaging in the pH range between 5.5 and 7.5 (Miesenböck et al. 1998; Moseyko and Feldman 2001). The original pHluorin protein was modified to overcome the technical problems hindering its application for monitoring pH changes in plants, like aberrant splicing or low protein solubility. To that end, the coding sequence upstream the pH-sensitive mutation of pHluorin was exchanged with the corresponding part of the plant-modified smGFP gene (Davis and Vierstra 1998). The resulting pHGFP has been used in Prof. Schumacher's laboratory to generate the Arabidopsis lines used in this work (section M.1.3.1)).

To generate a map of the pH-status of cytosolic compartments, specific markers of different membranes were used to create translational fusions targeting the recombinant protein to specific membranes. In this project, only three of the constructs generated in Prof. Schumacher laboratory were used: the tonoplast marker (pH-GFPVTI11), the plasma membrane marker (pHGFP-LTI6b) and the cytosolic marker (free-pHGFP). These constructs were designed so that the pHGFP localized in the cytosolic side of the membrane. These constructs were transformed independently in *A. thaliana* Col-0 line, and homozygous lines expressing the fusion proteins were obtained.

R.3.1. Analysis of the pHGFP-expressing lines sensitivity to pH variations

The first step in creating pH-maps was to determine whether the lines expressing pHGFP-VTI11 and pHGFP-LTI6b constructs were sensitive to imposed cytosolic pH variations and how reliable the sensing reporters were. To that end, we followed the method reported by (Waadt et al. 2017) (Figure 29A), with modifications regarding the growth medium perfused during the experiment. In brief, *A. thaliana* Col-0 plants expressing the pHGFP fluorescent reporter

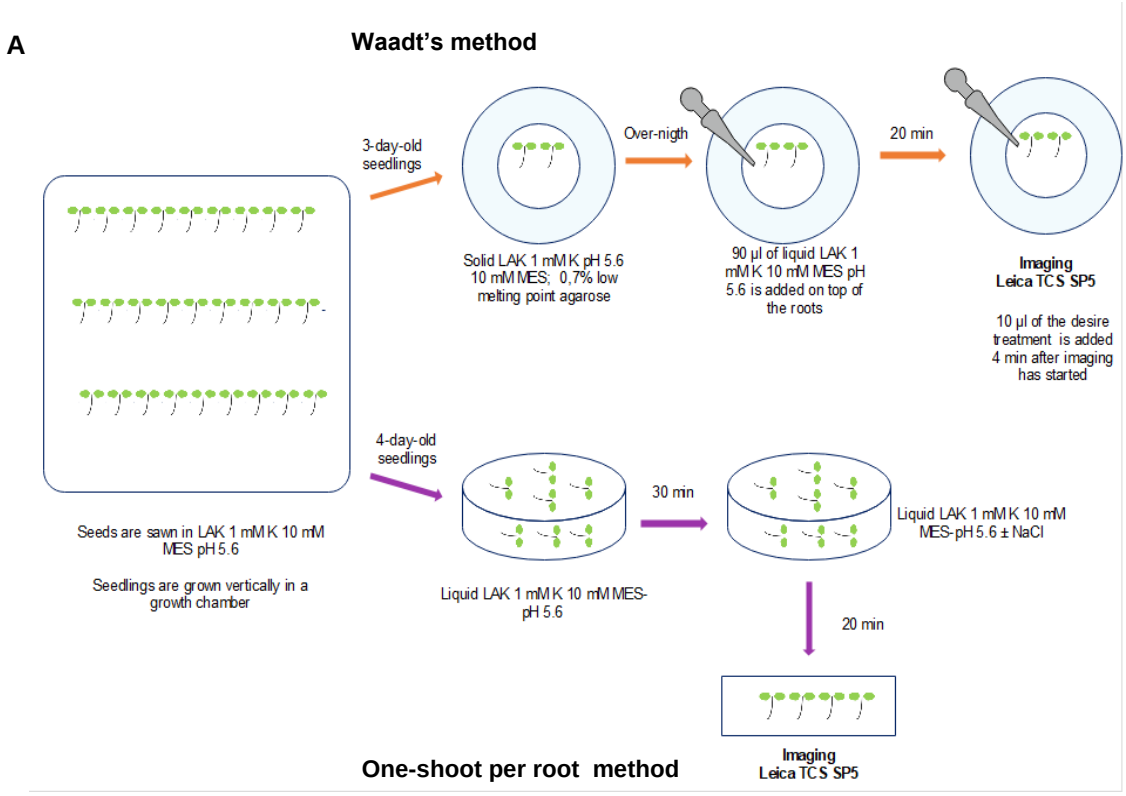

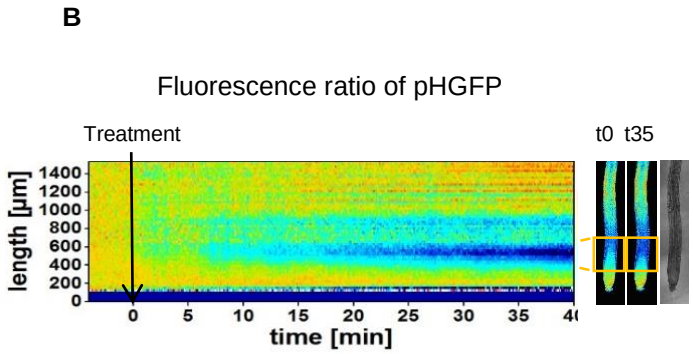

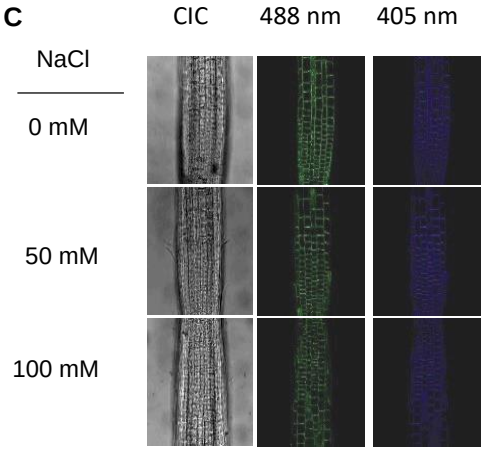

Figure 29. Imaging methods to measure pHcyt in roots and visualization of results. (A) Representation of the steps, times and buffers used in the two methods to measure pHcyt in roots. **(B)** Graphical presentation of results according to the Waadt's method. The heat-map presents the values of 64 adjacent regions (268.2 x 24.2 µm) that comprises 1400 µm of the root of one single seedling. Values are normalized to the initial 4 min baseline recordings. On the right, images of a root after being processed with the Fiji software. Framed in yellow is the root zone with the highest variations in pHcyt chosen for further data analysis. **(C)** Example of images obtained by the One-shoot per root method. Resolution was improved by using a 63x objective. The example show pictures of Col-0 expressing free pHGFP under different salt conditions. Left, transmitted light; center, fluorescence image at 405 nm; rigth, fluorescence image at 488 nm.

were grown vertically in LAK 1 mM KCl, 10 mM MES pH 5.6 in a growth chamber. Three-day-old seedlings were transferred to microscope dishes (MatTek, Ashland, MA, USA) with the same medium and 0,7% low melting point agarose (Roth). Seedlings were incubated vertically overnight in the growth chamber. Before imaging, seedlings were placed horizontally and 90 µl of liquid LAK medium was added. Seedlings were gently pressed back into their agarose bed and incubated for 40 -60 min for recovery. Imaging was performed with a Leica SP5 using a ×10 objective. The pHGFP reporter was excited with 405 and 488 nm light wavelengths, and emission was detected in a 500-550 range by a HyD2 detector. Frames were acquired every 6 seconds during 40 minutes. After 4 minutes of imaging (stack 40) 10 µl of the desired solution imposing different treatments were added on the side of the root and imaging acquisition continued.

The fluorescence images were treated with Fiji software, and the data was analyzed with OriginLab software. The final data obtained correspond to the ratio I_{405}/I_{488} (intensity of the light after the excitation with the 405nm and 488nm wavelength, respectively), corrected according to Waadt et al (2017) and presented graphically as a heat-map Figure 29B depicts a typical result. The heat-map represents the pH variation along the root with time. A region between the maturation and elongation zones of the roots is where the pH variations were detected more clearly. This behavior was observed in almost all the roots analyzed, independently of the treatment used. For that reason, even though the experiments were done imaging the complete roots, the numerical data analyzed was taken from this selected zone comprising the meristematic and elongation zones (MEZ segment; 750 µM upwards from the root tip) to avoid the possible masking of cytosolic variations by less responsive zones of the root.

To verify the sensitivity of the pHGFP-VTI11 to detect changes induced by the pH of the medium, seedlings were treated with 10 mM BTP-MES/HEPES buffers adjusted to different pH (5.2, 6.8, 7.6 and 8.4). The results indicated that the pHGFP-VTI11 construct was sensitive to cytosolic pH (pHcyt) variations, at least in the range of the buffers used (5.2 to 8.4) (Figure 30) . The variation in pHcyt was immediately detected when the buffers with more extreme values were applied (pH 8.4 and 5.2)(Figure 30B and Figure 30E). When the buffer applied had a pH near neutrality (pH 7.6 and 6.8), the detection of pHcyt variations was delayed in time (Figure 30A; 33C and 33D). The results, as expected, showed that the addition of acidic buffer (pH 5.2) decreased the ratio emission ratio (Figure 30A and 33E), indicating an acidification of the cytosol. The opposite occurred when a basic buffer was added and the ratio increased, indicating an alkalization of the cytosol (Figure 30A and 33B).

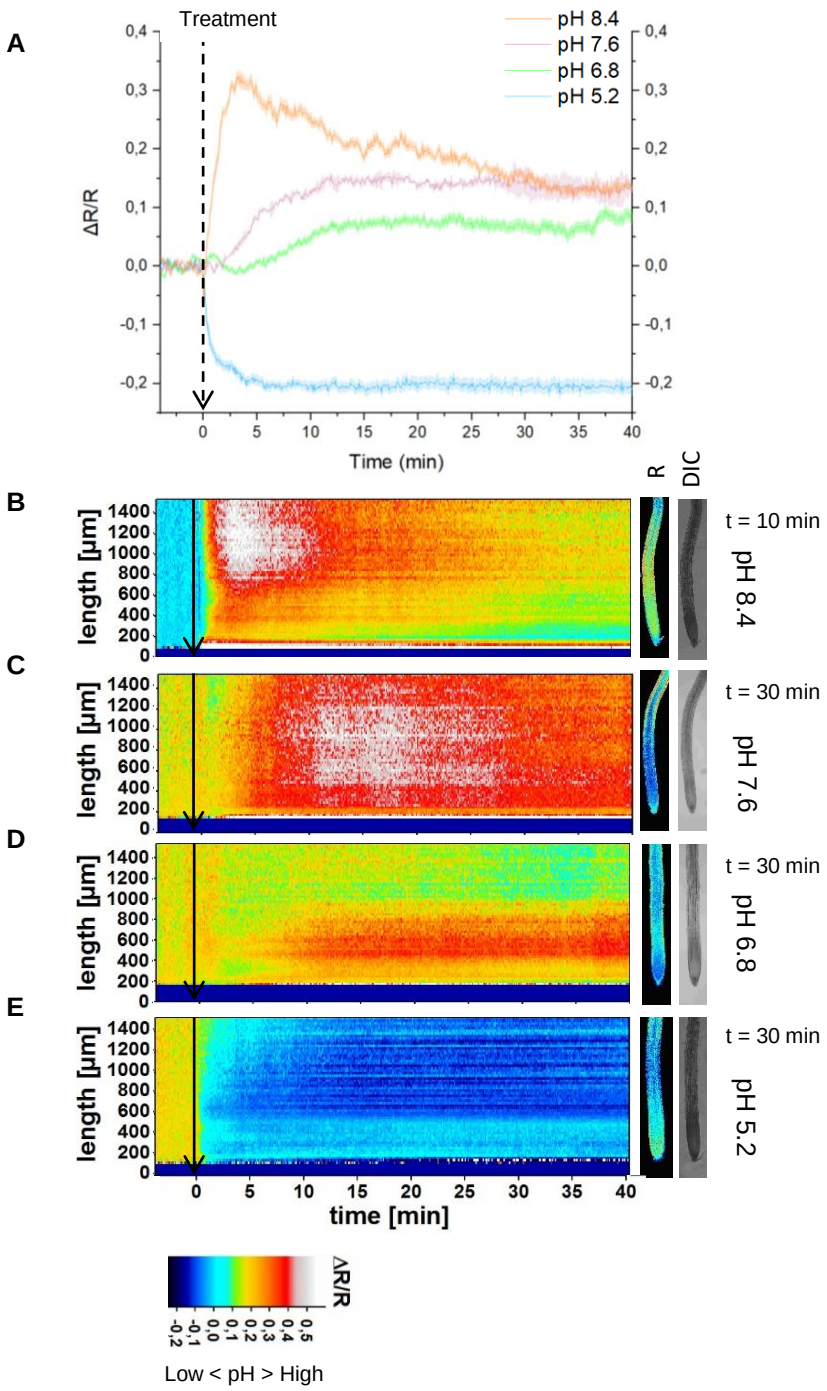

Figure 30. Response of reporter pHGFP-VTI11 to external pH. Measurement of variations in pHcyt sensed by the pHGFP-VTI11 reporter in *Arabidopsis thaliana* Col-0 seedlings. **(A)** Normalized emission ratio (ΔR/R) changes, presented as means ± SEM. Values derive from the quantifications of ΔR/R in the MEZ zone of at least two independent experiments per treatment. (B-D) Heat-maps of normalized data derived from 64 adjacent regions (268.2 x 24.2 µm) according to the scale depicted on the left. Arrows indicate the time the treatment started (t=0). Small panels on the right show bright field (DIC) and emission ratio (R) images of representative roots used in the experiment at the end of the measurements, frames with calibration bars of the heat map. Heat-maps and root pictures are representative of at least 2 independent experiments for each treatment.

Unexpectedly, the addition of pH 6.4 buffer increased the ΔR:R value, which corresponds with sensing an increase in pH (Figure 30A and 33BD). A possible explanation to this is that the medium in which the plants were grown before treatments was buffered to pH 5.6 and thus the transfer to pH 6.8 could elicit the increase in pH detected by the reporter. This explanation would also apply to the steep increase in pHcyt detected after transfer to pH 7.2 (Figure 30C).

Another point to note is the capability of the reporter to detect how the cells in the root, when treated with basic buffers, tried to recover homeostatic values by decreasing the pHcyt (Figure 30A and 33B) All the roots treated with basic pH buffers tended to a common point in the ΔR:R values, maybe because this point is the neutral common pHcyt in these cells. On the other hand, the root treated with the acidic buffer at pH5.2 did not show signs of recovering, at least in the time lapse analyzed.

In a second tier of experiments, it was important to determine whether the new constructs were sensitive to cytosolic pH variations in the physiological range. To assess this, the different approaches followed intended modifying the activity of membrane proteins. To that end, the line expressing the tonoplast construct pHGFP-VTI11, reporting pHcyt changes in the proximities of the vacuolar membrane, were treated with the V-ATPase specific inhibitor concanamycinA (ConcA) to a final concentration of 5 µM (Huss et al. 2002; Dettmer et al. 2006; Krebs et al. 2010). Since V-ATPase activity implies the acidification of the vacuolar lumen by the translocation of H^+ from the cytosol, the inhibition of this enzyme would increase the concentration of H^+ in the cytosolic side of the tonoplast, thus decreasing pHcyt. When the pHGFP-VTI11 Arabidopsis lines were treated with ConcA, cytosolic acidification was detected (Figure 31A). However, the same acidification was detected after the mock treatment with the ConcA solvent DMSO (Figure 31A). From these results, it was not possible to determine whether the acidification detected by pHGFP-VTI11 was due to the V-ATPase inhibition or a secondary effect of the DMSO.

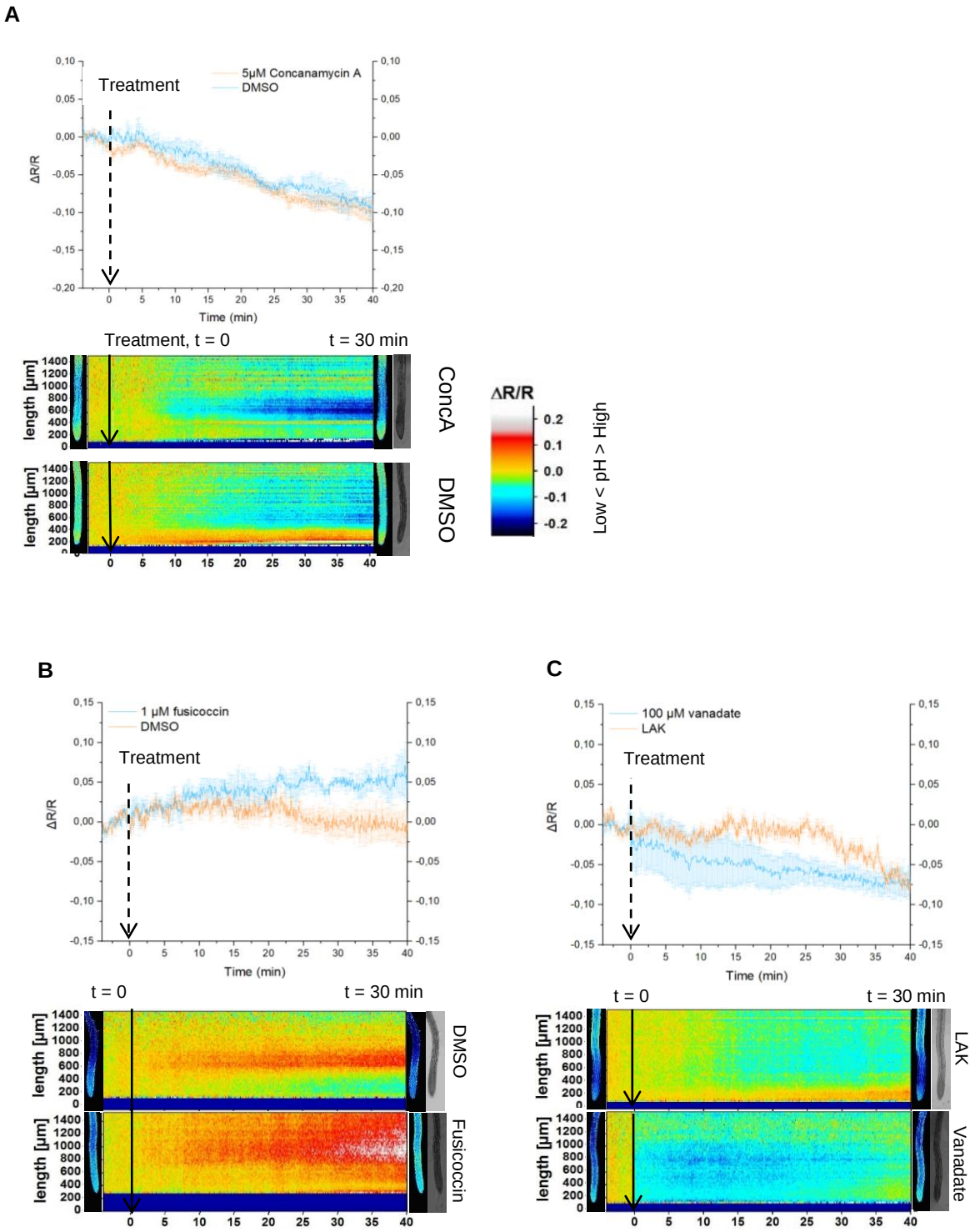

Figure 31. Sensitivity of pHcyt reporters pHGFP-VTI11 and pHGFP-LTI6b to altered activity of H^+-pumps. (A) pHGFP-VTI11 sensitivity to V-ATPase inhibition by concanamycin A. The diagram represents the mean of 3 independent experiments ± SEM. **(B)** pHGFP-LTI6b sensitivity to activation of the plasma membrane H^+-ATPase by fusicoccin. The diagram represents the mean of 2 independent experiments ± SEM. **(C)** pHGFP-LTI6b sensitivity to inhibition of the effect of the plasma membrane H^+-ATPase by vanadate. The diagram represents the mean of 2 independent experiments ± SEM. Arrows in the three panels indicate the time the treatment started (t=0). Heat-maps are representative experiments.

To study if the plasma membrane reporter pHGFP-LTI6b was sensitive to pHcyt variations due to physiological altered conditions, two assays were performed. As a first treatment, the fungal toxin Fusicoccin (FC) was used. This compound binds to the complex formed by the plasma membrane H^+-ATPase and the 14-3-3 proteins, stabilizing the interaction. As a result, the proton pump is permanently activated and generates a hyperpolarization of the membrane. The enhanced extrusion of protons from the cytosol should be reported by pHGFP-LTI6B as an pHcyt increase (Würtele et al. 2003; Ottmann et al. 2007; Duby and Boutry 2009; Saponaro et al. 2017). As in the case of ConcA, FC was dissolved in DMSO and a control mock treatment using this solvent was also done. The pHGFP-LTI6b reporter detected the increased pHcyt due to the treatment with FC (Figure 31B). However, this increase was not as high as it would be expected. Moreover, the DMSO treatment once again generated a decrease in pHcyt. Together, these results suggest that the DMSO effect could be masking the alkalization produced by the hyper-activation of the H^+-ATPase.

Finally, we analyzed if the pHGFP-LTI6b reporter was sensitive to the acidification of the cytosolic pH promoted by the plasma membrane H^+-ATPase inhibitor vanadate (Lew 1991; Qiu et al. 2002; Sondergaard et al. 2004). Since this reactive inhibits the translocation of H^+ mediated by the H^+-ATPase, proton accumulation in the cytosol should be sensed as an acidification. In Figure 31C the acidification detected by the reporter pHGFP-LTI6b is compared to the control with the solvent, in this case LAK medium without DMSO. Although in both conditions the cytosolic pH decreased, significant differences in time and intensity were observed (Figure 31C).

From these results, we concluded that the Arabidopsis lines expressing the constructs pHGFP-VTI11 and pHGFP-LTI6b are reliable biological tools to study how the cytosolic pH changes under pH variations in the physiological range of plant cells, although care should be taken with the experimental conditions to avoid artifacts.

R.3.2. Cytosolic pH variation at the plasma membrane under salt stress

The salt stress response in *A. thaliana* roots modifies the activity of various ion transporters, that include P-type H^+-ATPases, K^+ transporters and channels, and the Na^+/H^+ exchanger SOS1 that is critically important for salt tolerance (Assaha et al. 2017). These altered ion fluxes could translate into pHcyt variations along the induced adaptive response. To determine how cytosolic pH varies in the process, seedlings of the Arabidopsis line with

the pHGFP-LTI6b reporter were treated with 50 mM NaCl, and the root imaging protocol previously described was performed.

The inclusion of NaCl in the media produced an alkalization of pHcyt in root cells in comparison to the roots treated with the control medium. As previously detected, the main sensitivity was observed at the MEZ segment (Figure 32A). The increase in pHcyt was detected 2-3 minutes after the application of the NaCl treatment. Surprisingly, no tendency to recover to the former resting state during the time lapse of the experiment was observed in any of the experiments. (Figure 32A and 35B)(Annex 7).

From these results, it was concluded that salt stress produced an increase in the cytosolic pH of the root cells, at least next to the cytosolic side of the plasma membrane. However, no much information about pH variation in different tissues could be obtained besides the MEZ root segment. To have an idea of how the pH of whole seedlings varied under salt stress, pH-maps of complete seedling were generated. In this case, the protocol was also according to Waadt et al (2017).

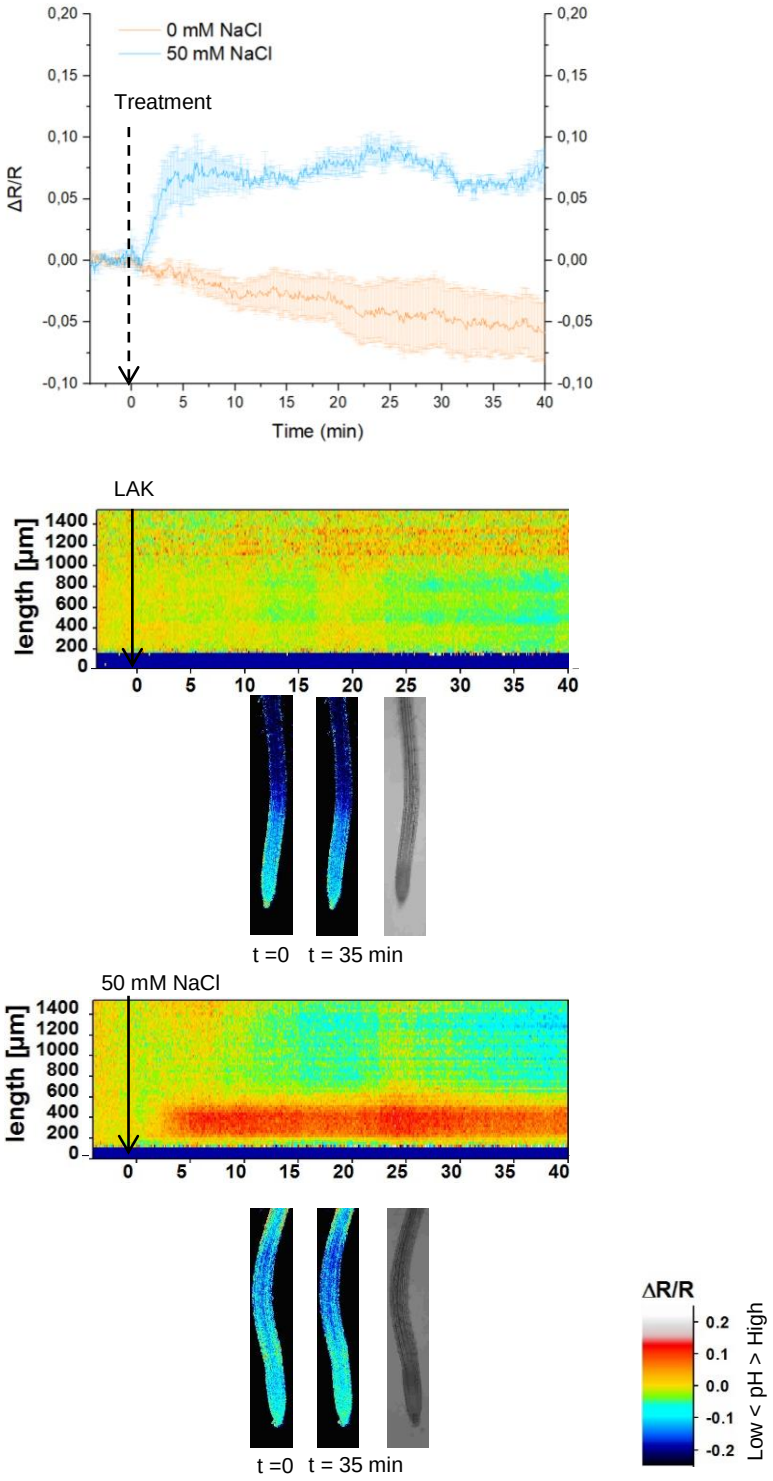

Figure 32. **Cytosolic pH variations under salt stress next to the plasma membrane.** Seedlings of the Arabidopsis line expressing the pH sensor pHGFP-LTI6b were treated with either LAK 1mM K liquid medium **(B)** or LAK supplemented with 50 mM NaCl **(C)** and the variations of pHcyt were measured. **(A)** Normalized emission ratio (ΔR/R) changes of pHGFP-LTI6b with and without salt treatment; lines indicate the mean of emission ratio of the MEZ segment ± SEM. **(B,C)** Heat-maps of normalized data derived from 64 adjacent regions (268.2 x 24.2 µm) Arrows in the three panels indicate the time the treatment started (t=0) according to the scale on the left. Heat-maps and roots pictures correspond to a representative experiment from 5-6 independent experiments.

Three-day-old seedlings expressing the pHGFP-LTI6b construct and grown vertically in plates placed in growth chambers in LAK 1 mM K, 10 mM MES pH 5.6, were transferred to new dishes supplemented with the same medium with or without NaCl, and left overnight in the growth chamber. The day after, seedlings were imaged directly in the dish using a LEICA LSI microscope. The images obtained from these measurements were processed with FIJI software to obtain quantitative pH data. To that end, the emission ratio was measured in separate segments corresponding to four different phenological zones of the root. A transition zone (S2), in which the vascular bundle and root hair primordia were starting to differentiate, was also distinguished between the more cannonical elongation and differentiation zones (S1 and S3) (Figure 33). Data was analyzed using OriginPro software.

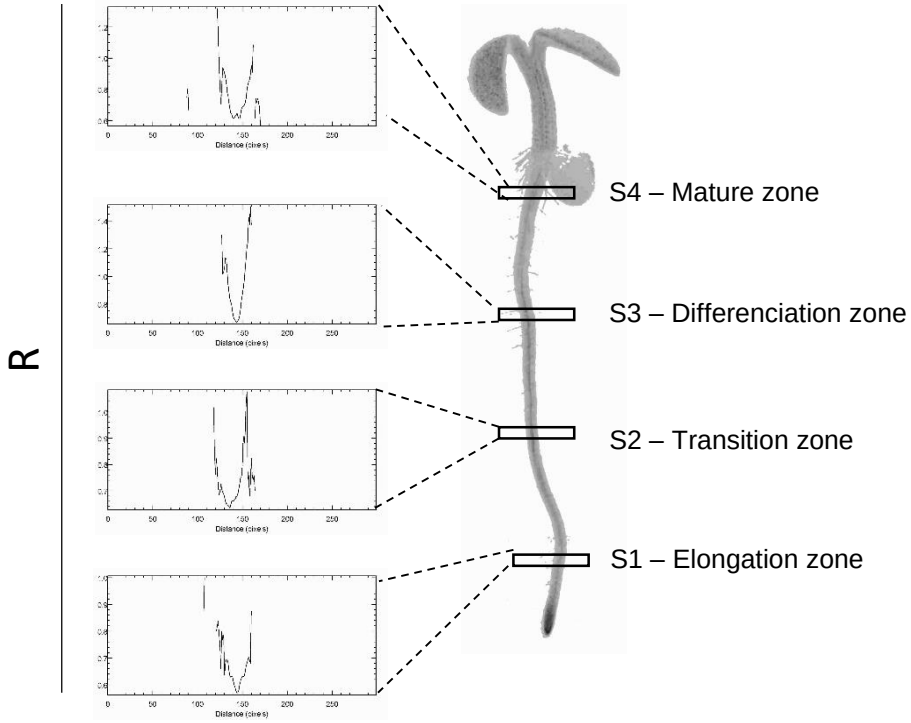

Figure 33. . Schematic diagram of the root the sectors used to analize the pHcyt variations along the complete root of *Arabidopsis thaliana* lines expresing the pHGFP reporters. Sectors were named S1-S4 according to the the develpmental stage and position from the root tip. R is the fluorescence ratio at 405 and 488 nm.

The results showed substantial differences between seedlings in the saline medium and the mock treatment with regular LAK medium (Figure 34A and 37B, Annex 8). From the seedling pH-maps obtained it was clear that seedlings grown in normal conditions had cells with a more basic pHcyt in epidermis and cortex relative to the stele. On the other hand, seedlings treated with NaCl showed an increased pHcyt in cells of the vasculature in comparison with the external layers of the root. Although the whole root seemed to be reacting to this stress in the same way, the data from the segments defined in Figure 33 were measured in at least 6-8 seedlings per treatment, and a profile for each of these segments was created (Figure 34B and 37D). The cross-section graphics showed not only the differential alkalization of the vasculature and the epidermis in both environmental conditions, but also that the reaction to the treatment was not homogeneous along the longitudinal root axis. In the case of the seedlings grown in control LAK medium, the transversal profile did not differ between the five segments. However, in response to salt, even though there was some alkalization in the elongation zone, the most important cytosolic pH increase took place in the transition zone S2.

To determine whether the differences of cytosolic pH between tissues were significant, the plotted data was analyzed statistically by a pairwise comparison of means with the Tukey HSD test ($p<0.05$). The results indicated that the differences of variation observed between the vasculature (V) and the epidermis and cortex (EC) of seedlings under salt treatment were significant. On the other hand, the cellular acidification in the vasculature of non-treated seedlings was also significantly different from the cytosolic pH measured in the external tissues (Figure 34E and 37F).

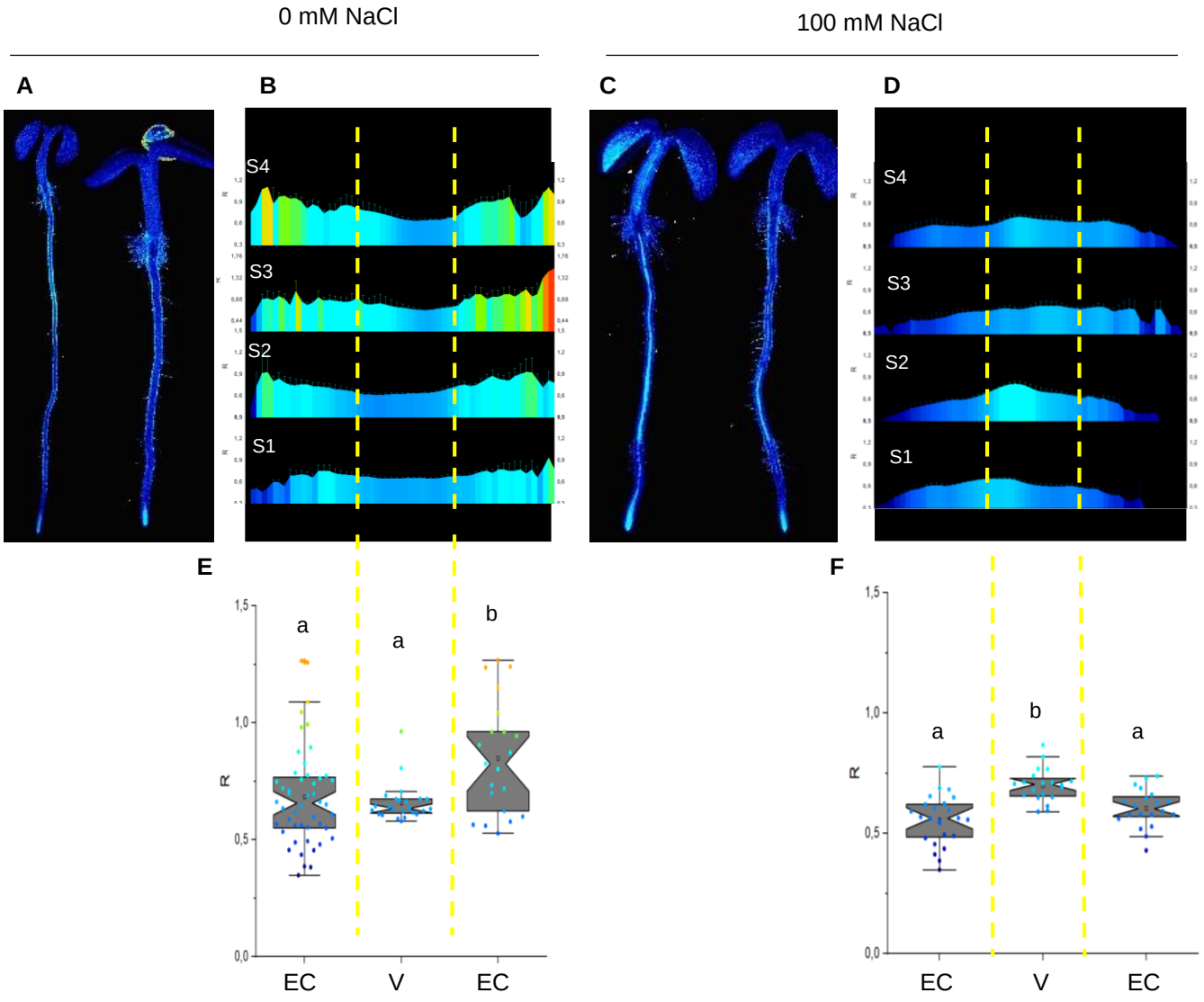

Figure 34. Whole seedling pHcyt maps of *Arabidopsis thaliana* lines expressing the pH sensor pHGFP-LTI6b under salt stress. Emission ratios (R) of pHGFP in 4-d-old seedlings 16 h after being transferred to LAK 1mM K media supplemented (C,D,F) or not (A,B,E) with 100 mM NaCl. **(A,C)** Representative seedlings grown in LAK medium (A) or LAK supplemented with NaCl (C). **(B,D)** Profile of root sectors showing average emision ratios (R) from at least 6-8 seedlings per treatment; the root zones S1 to S4 are named as in Figure 5. **(E,F)** Box plots indicating the mean of the emission ratios (R) in different tissues for each condition. The mean was obtained from the sectors shown above. EC: Epidermis and cortex; V: vasculature. Different letters indicate groups with significantly different values by Tukey HSD test at $p<0.05$.

R.3.3. Cytosolic pH variation at the vacuolar membrane under salt stress.

Ion fluxes at the tonoplast are thought to preserve and help restoring the cytosolic pH and ion homeostasis of the cell. The main physiological activity under salinity stress is Na^+ compartmentalization into the vacuole, which reduces cytosolic toxic concentrations of this ion and maintains turgor pressure of the vacuole. Numerous reports have implicated the NHX protein in this process (reviewed by Jiang et al. 2010). However, it is now accepted that NHX exchangers mainly mediate K^+/H^+ exchange (Barragán et al., 2012; Andrés et al., 2014; Maathuis et al. 2014). The double mutant *nhx1 nhx2* is unable to accumulate K^+ in the vacuole but capable of enhancing vacuolar Na^+ uptake compared to wild-type (Barragán et al. 2012). These and other results indicate that the contribution of the vacuolar NHXs to the salt tolerance of Arabidopsis is the maintenance of K^+ homeostasis rather than the compartmentalization of Na^+ (Maathuis et al. 2014; Almeida et al. 2017). We reasoned that vacuolar NHX proteins could also serve to restore pHcyt after salinity stress. On the other hand, mutants in the endosomal family members AtNHX5 and 6 exhibit severe sensitivity to salt stress (Bassil et al. 2011a). Julkowska and Testerink (2015) suggested that Na^+ is loaded into endosomes by AtNHX5 and AtNHX6 and subsequently these endosomes are fused to the vacuole, but no experimental proof for this trafficking has been provided.

The Arabidopsis line expressing the reporter construct pHGFP-VTI11 was treated with different concentrations of NaCl to determine how the salt stress affected cytosolic pH in the vicinity of the vacuolar membrane and if the activity of transport proteins in this organelle sustained a different pHcyt dynamics compared to the plasma membrane.

Figure 34A shows the changes in pHcyt detected by the reporter pHGFP-VTI11 after treatment with two different NaCl concentrations, 50 mM and 100 mM. In both treatments, the pHcyt near the vacuolar membrane increased around 4 minutes after the saline solution was administrated. At 50 mM NaCl, the alkalization measured at the vacuolar membrane was of lower intensity compared to the plasma membrane (Figure 34A and 37C). The 100 mM NaCl treatment induced an increased pH along the whole root, but again more intense in the MEZ zone (Figure 34D).

It should be noted that the time between the administration of NaCl and the time at which the pH variation was reported by the pHGFP sensor in both plasma membrane and vacuolar membrane were similar. This could mean that the induced response to salt stress could be simultaneously activated in both membranes to overcome the detrimental effects of salinity,

at least within the time frame in which the signals of pH sensors in both membranes could be resolved.

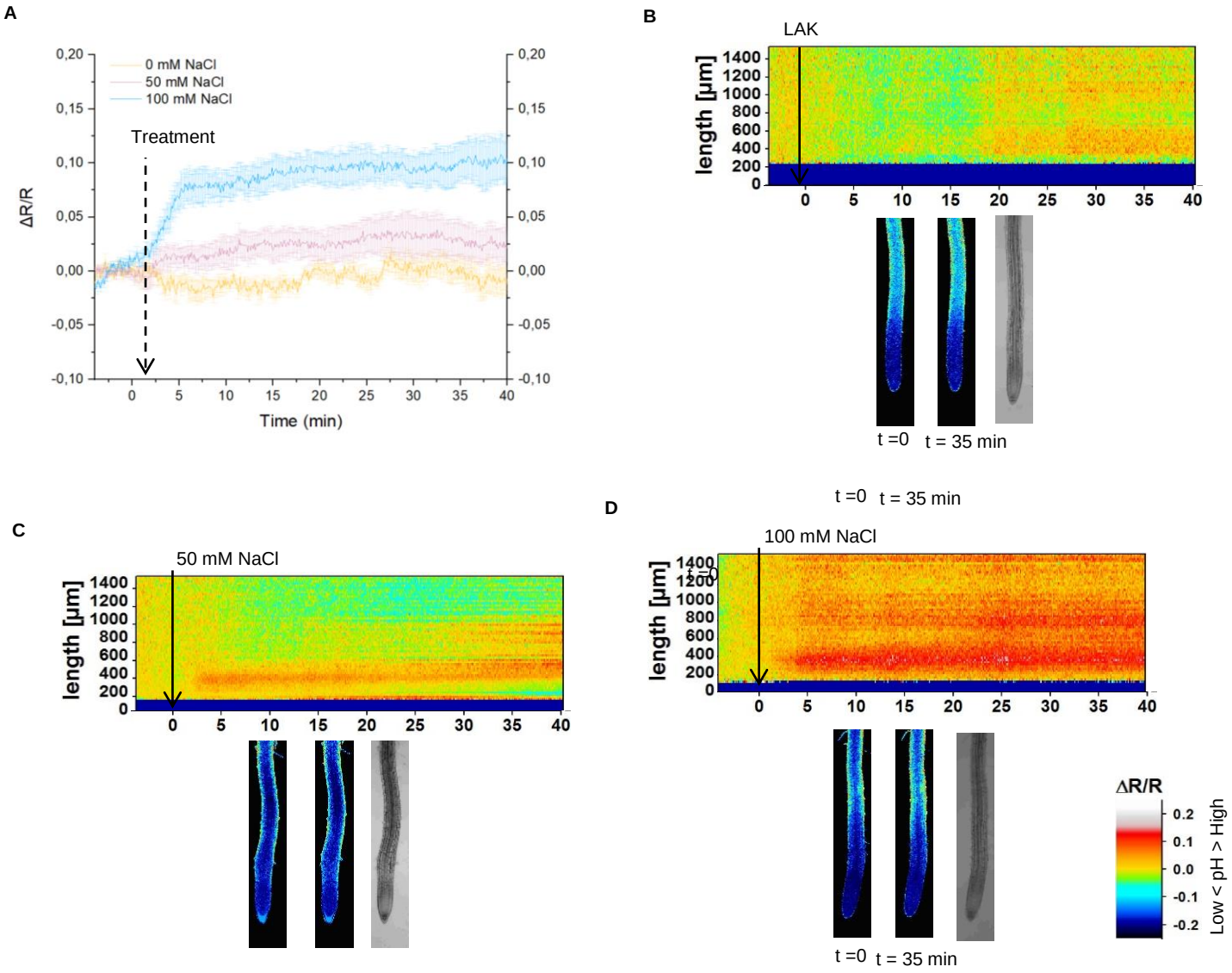

Figure 35. Cytosolic pH variations under salt stress at the cytosolic side of the vacuolar membrane. Seedlings of the Arabidopsis line expressing the pH sensor pHGFP-VTI11 were treated with either LAK 1mM K liquid medium **(B)** or the same medium supplemented with 50 mM NaCl **(C)** or 100 mM NaCl **(D)** and the variations of pHcyt were measured. **(A)** Normalized emission ratio (ΔR:R) changes of pHGFP-VTI11 with or without treatment; lines indicate the mean of emission ratio of the MEZ sector ± SEM from 5-6 seedlings. **(B,C)** Heat-maps of normalized data derived from 64 adjacent regions (268.2 x 24.2 µm) according to the scale on the left. Arrows indicate the time the treatment started (t=0). Heat-maps and root pictures correspond to representative experiments.

As previously done with the plasma membrane reporter pHGFP-LTI6b, whole-seedling maps of the pHGFP-VTI11 reporter lines were obtained to determine whether there were pH differences between root tissues, as previously shown with the plasma membrane reporter. After one night in plates with two NaCl treatments, 50 and 100 mM NaCl, the fluorescence maps were similar to the ones seen for the plasma membrane: seedlings in the control LAK medium had higher pHcyt in the epidermis and cortex and lower in the vasculature, but seedlings in LAK medium supplemented with 100 mM NaCl showed the opposite (Figure 36A and 39C). Notably, seedling treated with 50 mM showed no differences with the untreated seedlings, suggesting that a more severe stress might be needed to elicit a measurable response at the vacuolar vicinity than next to the plasma membrane. The profile of the root segments (Figure 36B and 39D) and the statistical analyses (Figure 36E and 39F) of at least 6-8 seedlings per treatment confirmed these results. The pH differences observed among the root tissues in the NaCl treated seedlings were significantly different, as well as the ones in the control LAK medium.

In the elongation (S1) and transition (S2) zones these differences were not as important as in the differentiation (S3) and mature (S4) zones. Some roots showed in S1 and S2 segments an aberrant morphology with what appeared to be enlarged cells, maybe as a consequence of the high NaCl concentration used during seedling incubation. If cells in these segments were damaged because of the osmotic or saline shock, this could explain the lack of sensitivity in these areas.

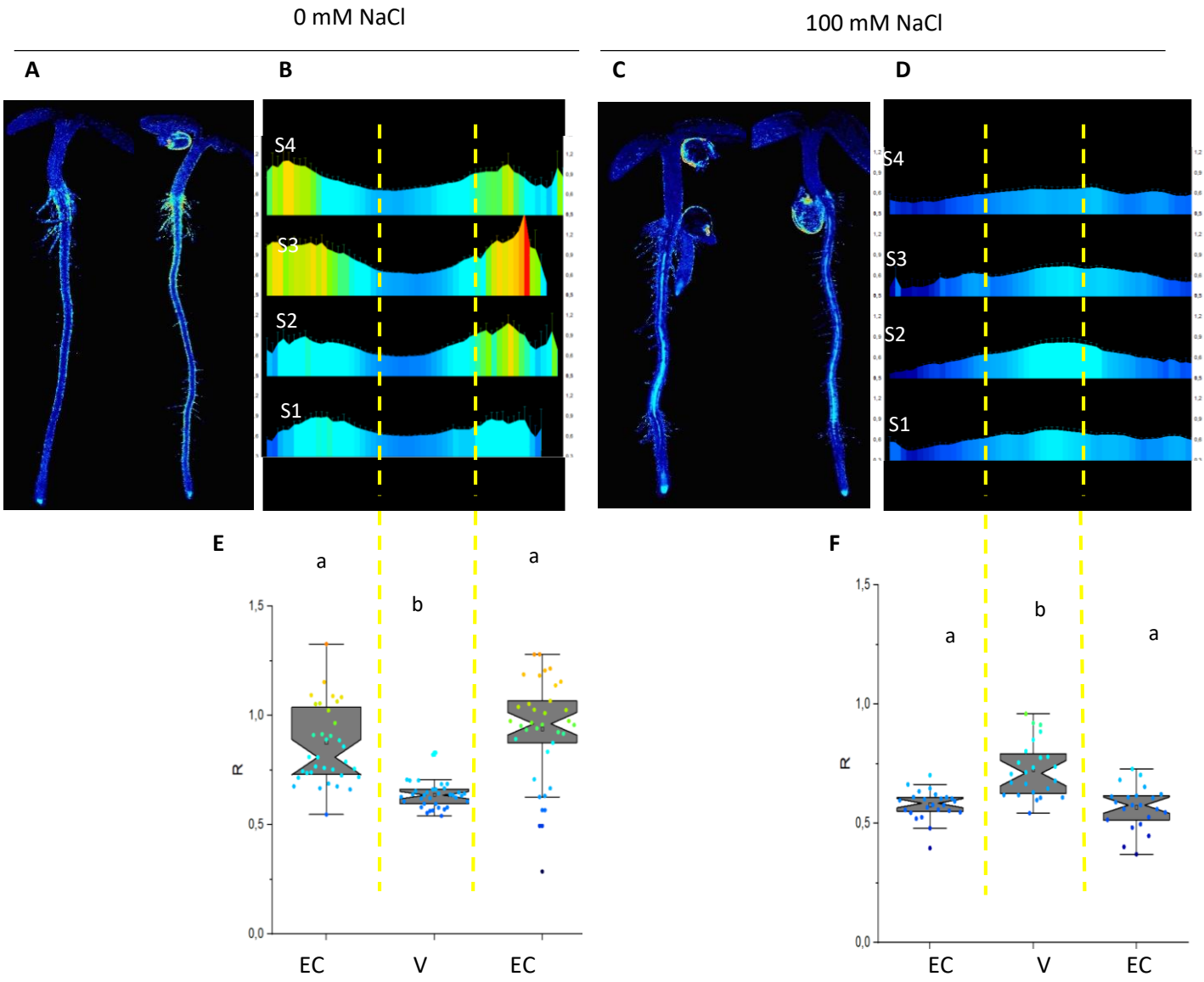

Figure 36. Whole seedling pHcyt maps of Arabidopsis thaliana line expressing the pH sensor pHGFP-VTI11 under salt stress. Emission ratios (R) of pHGFP in 4-d-old seedlings 16 h after being transferred to LAK 1mM K medium supplemented (C,D,F) or not (A,B,E) with 100 mM NaCl. **(A,C)** Representative seedlings grown in LAK medium (A) or LAK supplemented with NaCl (C). **(B,D)** Profile of the roots sectors showing average emision ratios (R) from 6-8 seedlings per treatment; the root zones S1 to S4 are named as in Figure 5. **(E,F)** Box plots showing the mean of emission ratios (R) in different tissues for each condition. EC: epidermis and cortex; V: vasculature. Different letters indicate groups with significantly different values by Tukey HSD test at $p< 0.05$.

R.3.4. Cytosolic pH under compromised salt-stress sensing.

As previously mentioned, the SOS pathway is one of the main and best described processes that plant cells activate under salt stress conditions in order to extrude Na^+ from the cytosol, which is linked to the re-entry of extracellular H^+. This pathway is dependent on the activity of SOS3/CBL4, which is activated by stress-induced increases in cytosolic Ca^{2+}.

To confirm the significance of this sensor protein in the adaptive response to salt stress, pHcyt variation under salt stress conditions were measured in the *sos3* mutant in comparison with the Col-0 wild-type. For that, both lines were transformed with a construct expressing free-pHGFP, which is a soluble protein mainly found in the cytosol. A first approach was aimed to compare the most salt-responsive root zone, the MEZ segment, of the *sos3* mutant and wild-type seedlings. As shown in Figure 37, no differences in pHcyt were observed when the *sos3* mutant expressing the free-pHGFP was treated with either 50 or 100 mM NaCl solution relative to non-treated seedlings, in contrast to previous observations with wild-type seedlings expressing the reporters pHGFP-LTI6b and pHGFP-VTI11 (Figures 35 and 38). These results indicate that the meristem and elongation zone (MEZ) of *sos3* roots is not responsive to salinity stress. However, inspection of whole seedlings evidenced that other root sectors of wild-type and sos3 seedlings had also differential responses to NaCl.

To quantitate these differences a new protocol was designed to overcome the technical limitations of the Waad's method used to measure the pHcyt of roots (small number of samples, long processing time, and limited repetitiveness between individual seedlings). This approach, named as the One-Shot per Root method (Ragel, P and Andres, Z; un-published), still collects fluorescence data resolved in space and time, but allows the manipulation of more samples in the same time frame, thereby improving the statistical analyses while minimizing sample-to-sample experimental noise (Figure 29A). In brief, *A. thaliana* lines plants expressing the cytosolic pHGFP fluorescent reporter were grown vertically in plates with LAK medium in a growth chamber. Four-day-old seedlings were transferred to small dishes with fresh liquid LAK medium (approximately 8-9 seedlings per genotype and treatment), and incubated in the bench for 30 min to allow seedlings stabilization. Next, seedlings were transferred to new dishes with liquid LAK medium supplemented or not with different concentrations of NaCl, and left with the treatment for 20 minutes. Once the 20 minutes had passed and before imaging, seedlings were placed horizontally in a microscope dish and the roots were covered with the same media as the one they were incubated with. One picture per root was acquired with a 63x objective, comprising the most responsive zone

between the meristematic and elongation zone of the root. The reporter pHGFP was excited with 405 and 488 nm light wavelengths, and emission was detected in the 500-550 nm range by the HyD2 detector. Next, images of each root were processed with Fiji and the fluorescence data with the OriginLab software. In **¡Error! No se encuentra el origen de la referencia.**32C is shown an example of the results obtained for roots under different treatments.

The wild-type Col-0 and mutant *sos3* lines expressing the pHGFP protein were treated with increasing concentrations of NaCl (25, 50, 75 and 100 mM NaCl), imaged using the One-Shot per Root method, and the imaging data was statistically analyzed. The histogram representing the results from these analyses (**¡Error! No se encuentra el origen de la referencia.**) showed that, although both genotypes showed the same tendency towards an alkaline shift in pHcyt in response to increasing NaCl concentrations, differences between whole roots of the Col-0 line and *sos3* mutant were observed. Firstly, *sos3* seedlings had a more alkaline pHcyt than Col-0 under control non-saline conditions. Secondly, the pHcyt values were more alkaline in Col-0 at 75 mM NaCl than in *sos3* seedlings. Together, these differences signified that the dynamic range of the pHcyt response was greater in Col-0 than in the *sos3* mutant. At the highest concentration used, 100 mM NaCl, both genotypes showed less alkalinization than at 75 mM NaCl. Because the decline was more pronounced in the salt-sensitive *sos3* seedlings, this could reflect salt-induced toxicity and impaired physiological response. Together, these data imply that whole roots of *sos3* mutant seedlings are less responsive to salt-induced pH-shifts than the wild-type.

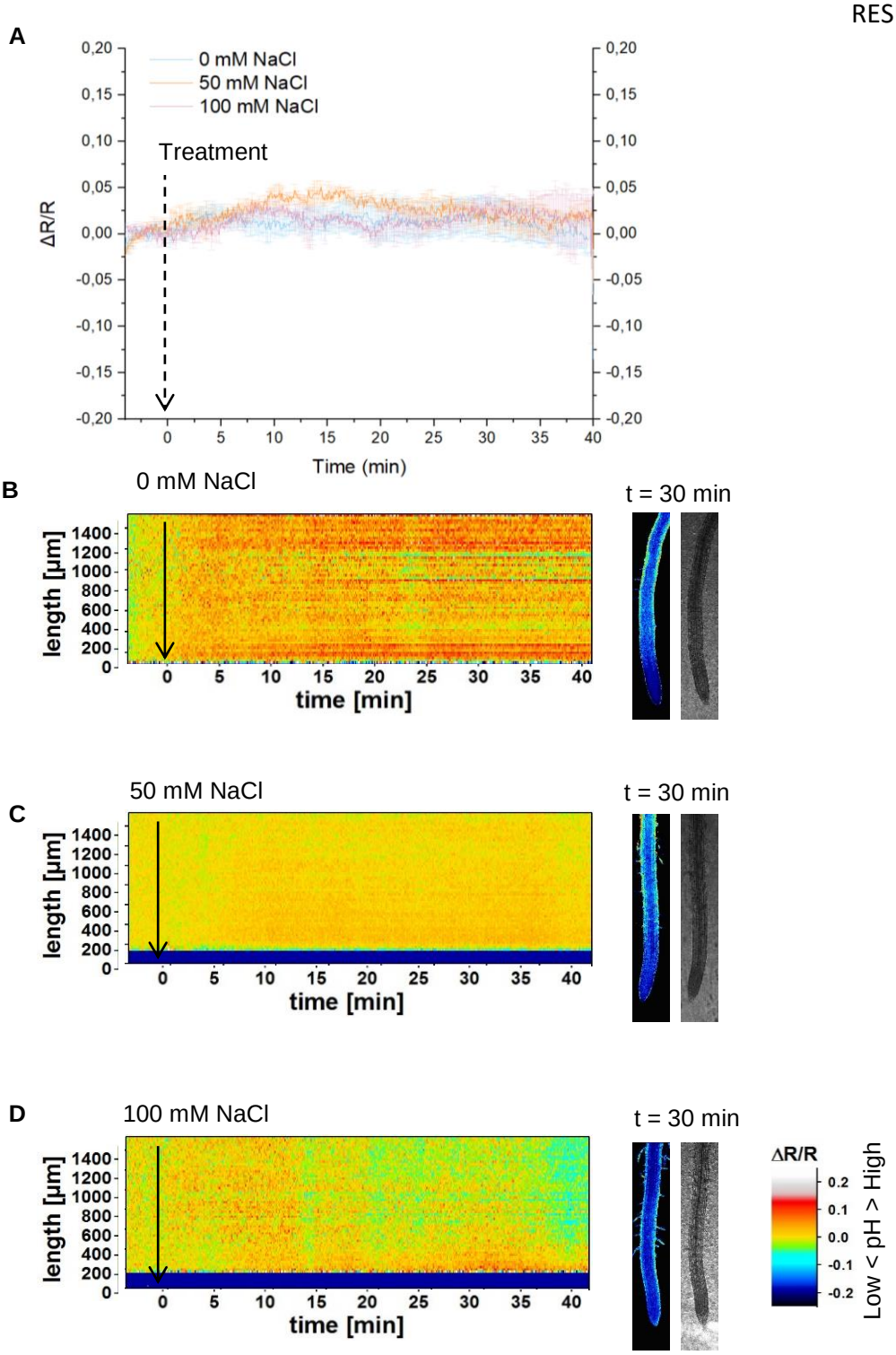

Figure 37. Cytosolic pH variations under salt stress reported by free-pHGFP in *sos3* mutant. Seedlings of a *sos3* mutant line expressing the pH-sensor pHGFP were treated with either LAK 1mM K liquid medium (B) or the same medium supplemented with 50 mM NaCl (C) or 100 mM NaCl (D) and the variations of pHcyt were measured. (A) Normalized emission ratio (ΔR/R) of pHGFP with or without treatment; lines indicate the mean of emission ratio of the MEZ sector ± SEM from 5-6 seedlings. **(B,C,D)** Heat-maps of normalized data derived from 64 adjacent sections (268.2 x 24.2 µm) according to the scale on the left. Arrows indicate the time the treatment started (t=0). Heat-maps and root pictures correspond to representative experiments.

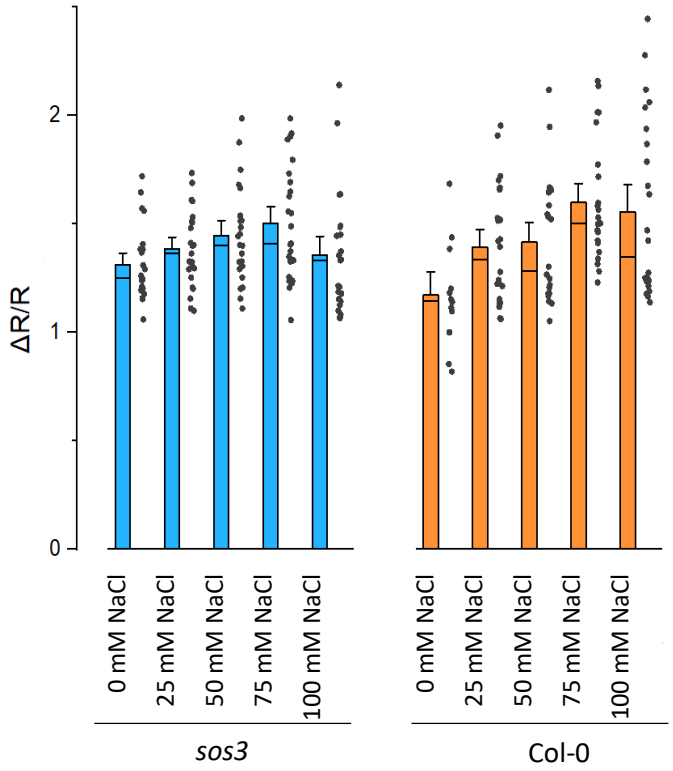

Figure 38. Cytosolic pH variations under salt stress reported by free-pHGFP in wild-type Col-0 and *sos3* mutant seedlings. Seedlings expressing the pH sensor free-pHGFP were treated with either LAK 1mM K liquid medium (B) or the same medium supplemented with increasing concentrations of NaCl and the variations of pHcyt were measured. Handling and measurements followed the One-Shot per Root method. Normalized emission ratio (ΔR/R) changes of pHGFP with or without treatment are represented. Bars indicate the mean emission ratio of the whole root imaged ± SEM.

To test if different root tissues showed a differential response to NaCl depending on the genotype, pH-maps of whole seedlings were generated (Figure 39, Annex 9). The free-pHGFP reporter in wild-type Col-0 seedlings registered the same pHcyt variations previously described for the tonoplast and plasma membrane reporters (**¡Error! No se encuentra el origen de la referencia.**A an 11B). However, the vasculature of the *sos3* mutant did not show the characteristic alkalinization of pHcyt observed in the wild type, independently of the salt concentration applied (Figure 38**¡Error! No se encuentra el origen de la referencia.**D and 41E, Figure 39). The epidermis and cortex of *sos3* seedlings in control conditions and under low NaCl concentration (50mM NaCl) appeared to have a more alkaline pHcyt than the wild type. The emission ratio (R) data obtained for each seedling was aggregated and compared according to the different root tissues as described in Figure 37, i.e. vascular bundle (V), and epidermis plus cortex at both sides of the vasculature (EC1 and EC2). The mean of the emission ratio for each tissue was calculated and plotted (Figure 40). Results showed that at

50 mM NaCl the difference in pHcyt between the vasculature (V) and the surrounding tissues (EC) was more statistically significant in *sos3*, in contrast to the wild type, because the EC tissues were more alkaline in the mutant. Strikingly, the inverted pattern typical in wild-type seedlings at 100 and 150 mM NaCl in which the vasculature became more alkaline that the surrounding tissues was not observed in the *sos3* mutant (**Figure 40**). Again, these results point to SOS3 as an important signaling intermediary in the salt stress response affecting the alterations in pHcyt of root cells resulting from salinity.

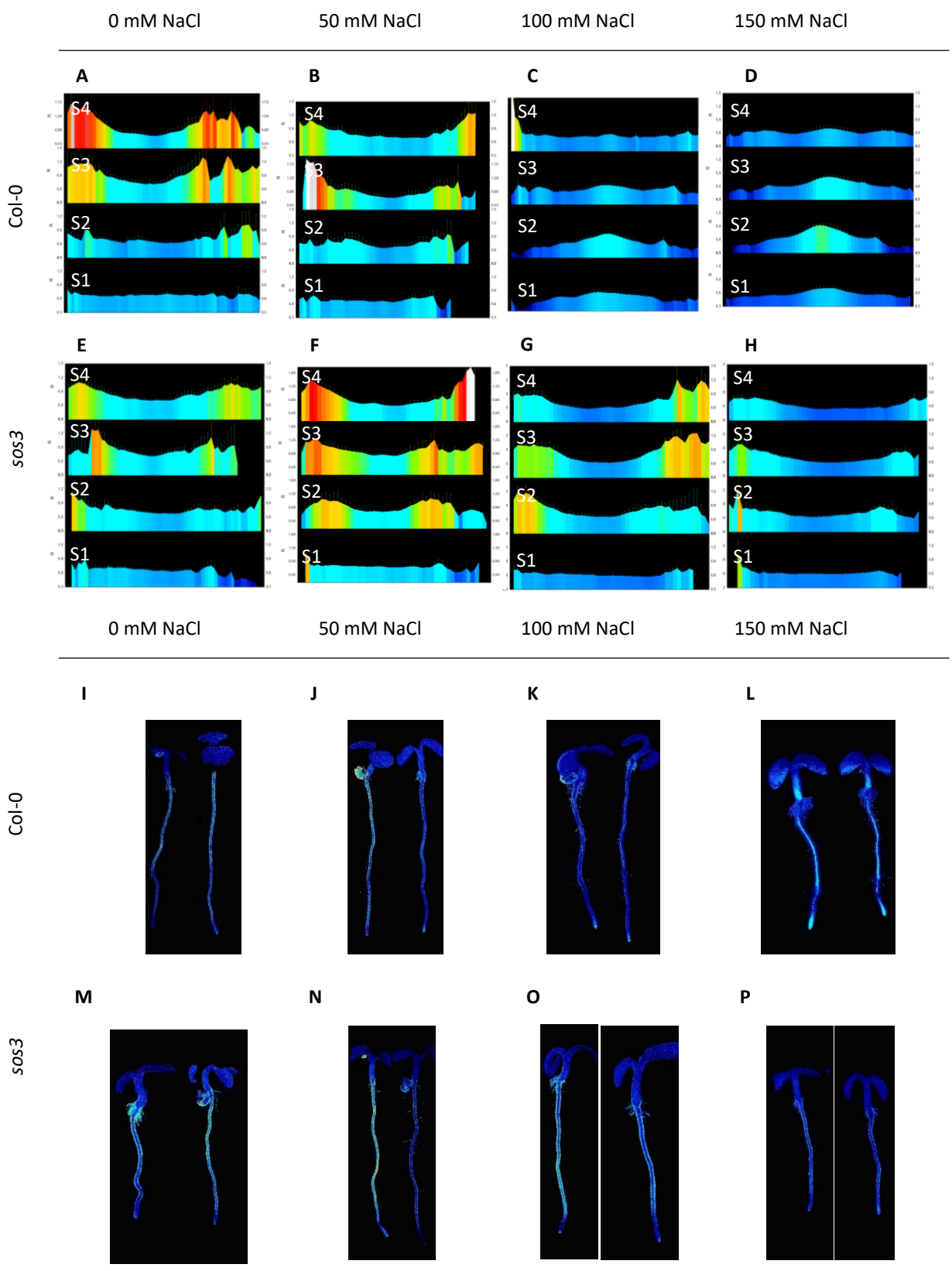

Figure 39. Whole seedling pH-maps under salt stress of wild-type Col-0 and *sos3* lines expressing pHGFP. Emission ratios (R) of pHGFP in 4-d-old seedlings 24 h after being transferred to LAK 1mM K medium supplemented **(B-D, F-H, J-L, N-O)** or not **(A,D,I,M)** with NaCl. **(A-H)** Panels present the emission ratios (R) of cross-sections of the root zones defined in Figure 5. The profiles represent the mean of the ratio (R) of 5-6 seedlings for each segment ± SEM. **(I-P)**, representative whole seedlings grown in LAK medium **(I,M)** or LAK supplemented with increasing concentrations of NaCl **(J-L, N-P)**.

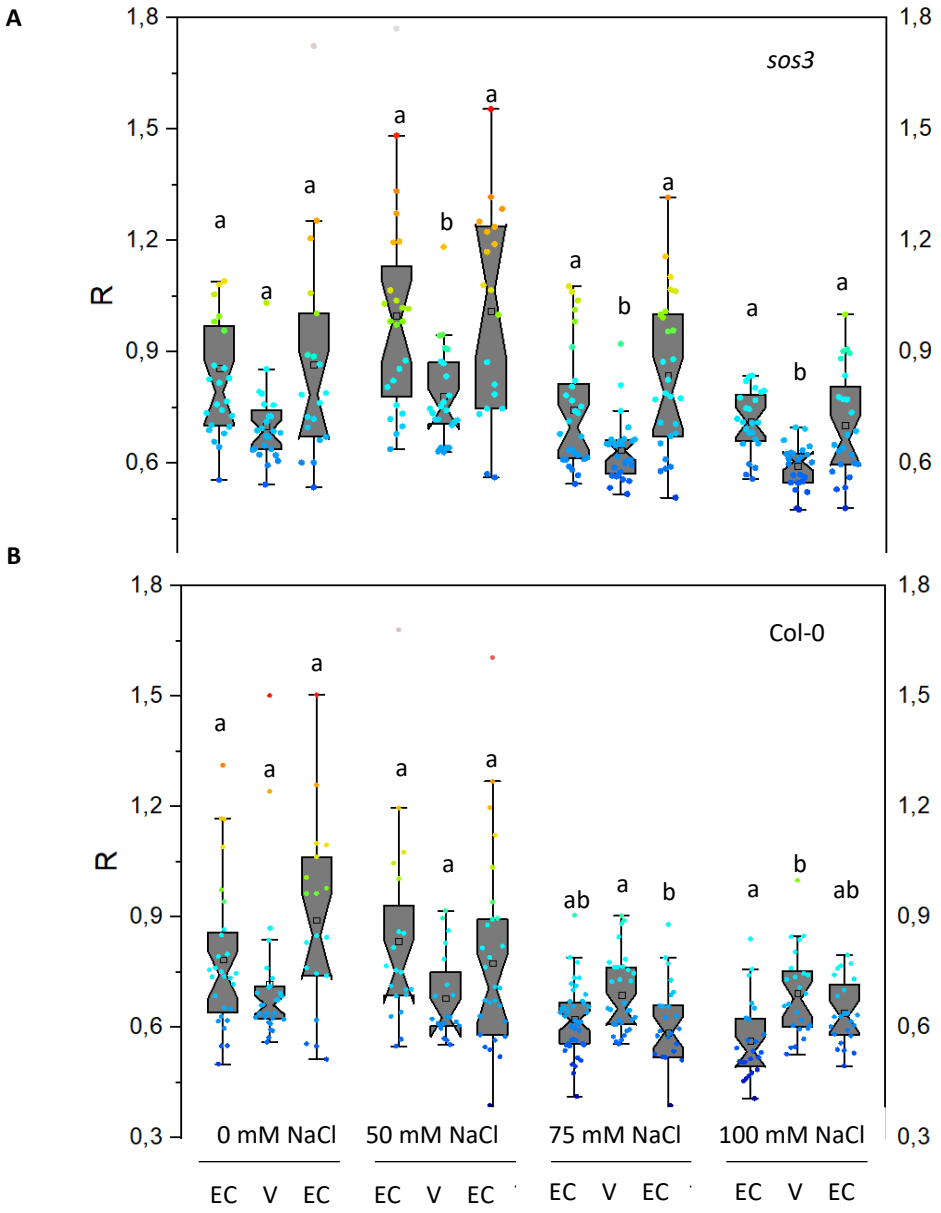

Figure 40. Cytosolic pH variation across root sections in wild-type and the sos3 mutant. Box plots represent the mean emission ratios (R) of pHGFP in different tissues for each condition and genotype. The mean was obtained from the root segments S1 to S4 as defined in Figure 36. EC, epidermis and cortex; V, vasculature. Different letters indicate groups with significantly different means by the Tukey HSD test at p<0,05

R.4. Roles of AtNHX3 and AtNHX4 salt stress resistance and regulation of cellular pH.

The genome of *Arabidopsis thaliana* contains eight *NHX* genes, of which *AtNHX1* to *AtNHX4* encode proteins that localize to the tonoplast. There is a considerable amount of information regarding the function and expression of AtNHX1 and AtNHX2. However, the roles of the AtNHX3 (At3G06370) and AtNHX4 (At5G55470) are not well understood yet. These two NHX proteins have been demonstrated to localize in the vacuolar membrane and to have different gene expression patterns (Li et al. 2009; LIU et al. 2010; McCubbin et al. 2014). McCubbin et al. (2014) suggested that AtNHX3 and AtNHX4 share certain functional redundancy with AtNHX1 and AtNHX2 in K^+ homeostasis and cell expansion. In other reports hand, a *nhx3* knock-out showed enhanced salt tolerance (Li et al. 2009), and AtNHX4 was found to be important for accumulation of K^+ in the vacuole under low K^+ conditions (Liu et al., 2009).

To better understand the functional importance of AtNHX3 and AtNHX4, we decided to analyze of single mutants *nhx3* and *nhx4* and also generate the double mutant *nhx3 nhx4*.

R.4.1. Generation of nhx3 and nhx4 mutants.

To dissect the biological function of AtNHX3 and AtNHX4 of *Arabidopsis thaliana*, a mutant line for each gene was isolated. For the *nhx3* mutant, the T-DNA insertion allele from the SAIL collection Sail_827_D04 was used. Analysis of the sequence indicated that the mutant harbored a T-DNA insertion at exon 10. The mutant chosen to study AtNHX4 belongs to the Salk Collection (SALK_082277 line), and harbors a T-DNA insertion within the UTR 5' of the gene (Figure 41A).

The homozygous T-DNA insertions lines SAIL_827_D04 (*nhx3*) and SALK_082277.0 (*nhx4*) were crossed as described in (section M.6). Diagnostic PCR was performed with allele-specific primers annealing to the chromosomal flanking regions of the T-DNA insertions (which would amply the wild-type locus only) and a specific primer for the left border of the T-DNA (to amplify mutated loci) (Annex 3). . illustrates the position of the primers used and the PCR bands obtained from the wild-type and mutated loci.

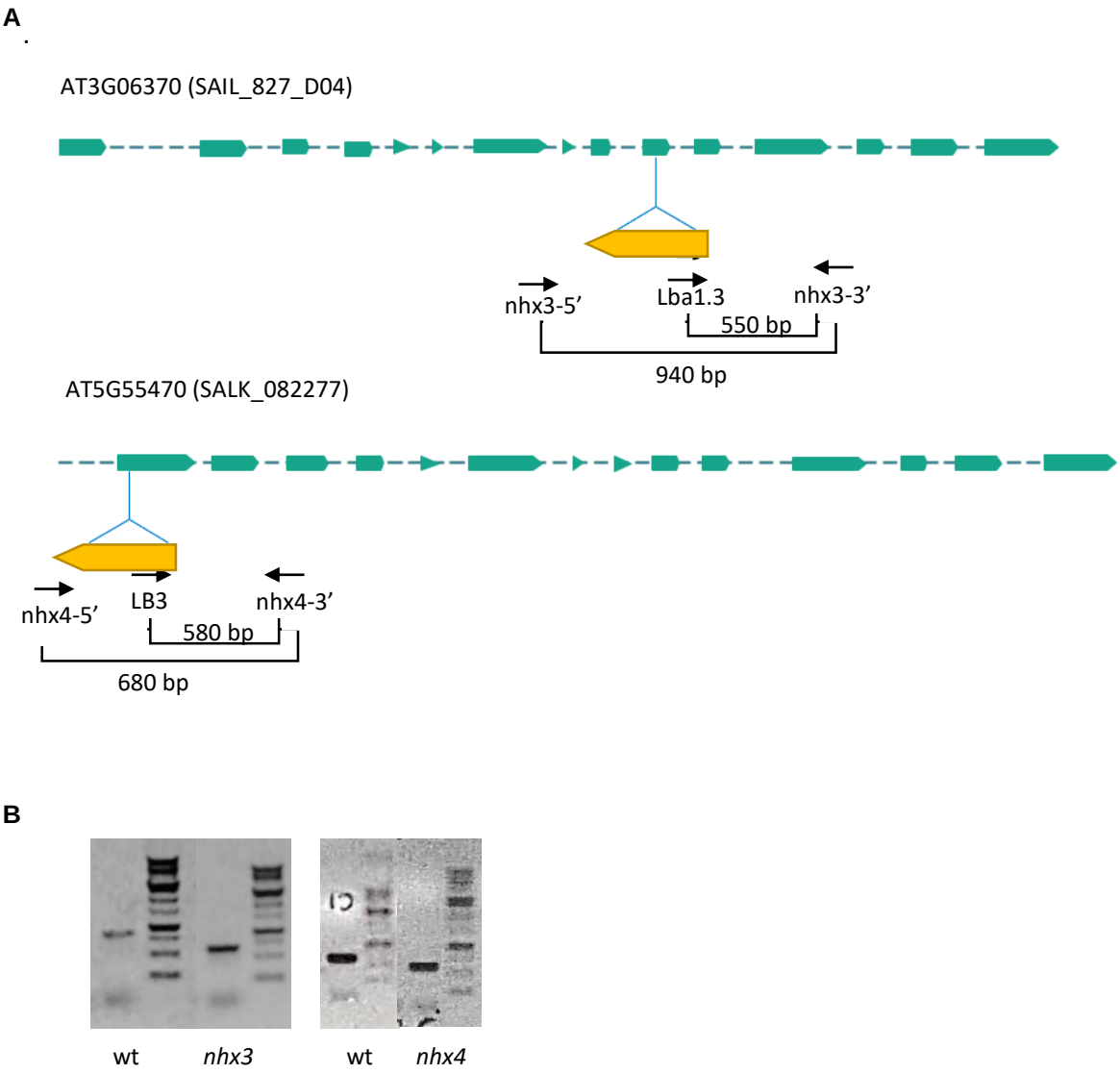

Figure 41. Genotyping of the null double mutant *nhx3 nhx4*. (A) Schematic representation of the genes *AtNHX3* and *AtNHX4*, the T-DNA insertions, and the annealing sites of primers used to genotype the mutants. **(B)** Example of the results obtained by diagnostic PCR using DNA from the wild type (WT) and the *nhx3 nhx4* lines as templates

Double mutant plants *nhx3 nhx4* did not display any noticeable phenotype compared to the wild-type Col-0 under regular growth conditions in soil. Foliar area of plants grown in long-day conditions did not show significant differences between genotypes (**Figure 42**B).

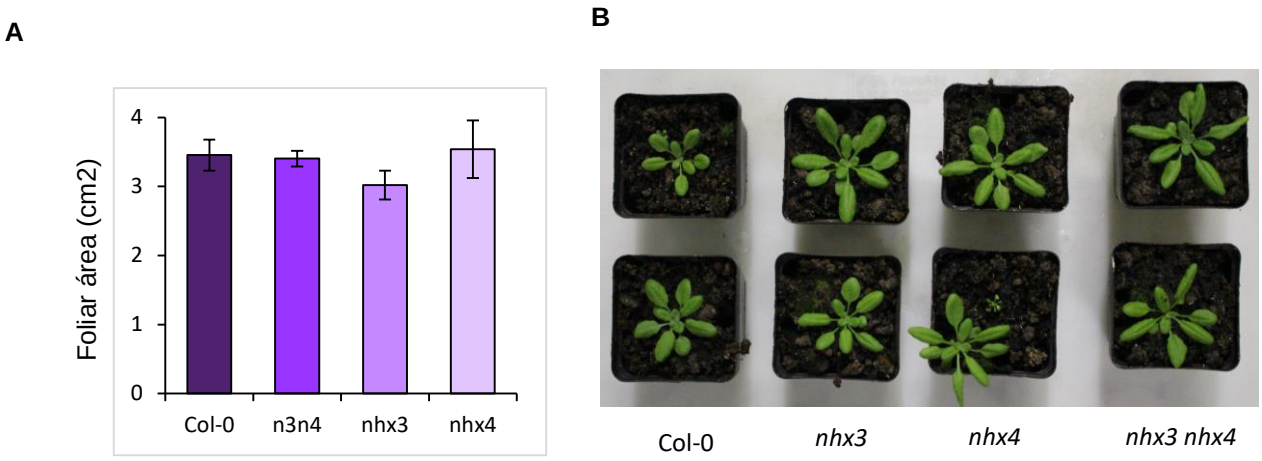

Figure 42. Growth of *nhx3* and *nhx4* single mutants and double mutant. **(A)** Representative 3-week old plants germinated in MS/2 plates and transferred to soil after one week. **(B)** Rosette area of 3-week old plants grown in long-day conditions of genotypes wild-type Col-0, *nhx3* single mutant, *nhx4* single mutant, and *nhx3 nhx4* double mutant (n3n4). Data is the media of 8 plants per genotype. Statistical

To compare the growth and development of the single mutants *nhx3* and *nhx4* and of the double mutant *nhx3 nhx4* to the wild-type under stress conditions, plants of the four genotypes were subjected to saline stress. The carried out *in vitro* test with seedlings in petri dishes since it is feasible to perform a statistically satisfactory number of repetitions using a large number of different conditions in different tests.

R.4.1. Germination and survival.

To determine the salinity tolerance of the different genotypes, the germination and survival percentages were quantified. To that end, seedlings were sown and grown in solid LAK media supplemented with different concentrations of NaCl (50, 100 and 150 mM NaCl) as described in Materials and Methods (section M.6.2.1). After two days of cold stratification, plates were transferred to a Conviron chamber with long-day photoperiod. Germinated seeds were counted after 4 days, and survival was quantified after 21 days of growth. Those seedlings with green aerial organs were considered as survivors. Both parameters were used because the levels of sensitivity to salt during germination is not always the same as at later growing stages (Verslues et al. 2006).

No statistically significant differences were observed in the germination rate or survival to the salt stress (Figure 43). The percentage of germinated seeds was high, even at 150 mM NaCl (Figure 43A and 46D). To calculate the survival percentage, the number of germinated seedlings was used as the reference and not the total number of seeds sown. In this case, the increase of salt concentrations was followed by a diminution in the number of survival seedlings (Figure 43B and 46E). Although statistics analyses showed no significant differences in this parameter between genotypes, as shown in Figure 43B the single mutant *nhx3* as well as the double mutant *nhx3 nhx4* appeared to have difficulties overcoming the high salinity in plates with 100 and 150 mM NaCl. The single mutant *nhx4* had a phenotype similar to Col-0 in all concentrations tested. Previously it had been shown that the germination and survival of the single mutants *nhx1* and *nhx2* was lower than the wild-type Col-0 at concentractions of 150 – 170 mM NaCl (Barragán et al. 2012). The fact that the double mutant *nhx3 nhx4* presents a phenotype similar to *nhx3* but not to *nhx4* mutants implies that the function of AtNHX3 contributes positively to salt tolerance in these early development stages, which is opposite to t he report by Lee et al. (2009).

The germination and survival results were complemented with root elongation measurements. Seedling of the single and double mutants were grown vertically in plates with solid LAK media supplemented with NaCl (0, 50, 100 and 150 mM). This method allows to measure, in a non-destructive way, the root growth over time (Verslues et al. 2006). Seeds were germinated in LAK plates (with 1 mM K) and after 4 days, roots were measured and seedlings were transferred to either control medium (LAK, 1mM K) or LAK medium supplemented with NaCl (Figure 44A and C). After 21 days, root length was measured, and the size increment experienced by each root was calculated (Figure 44B)

.

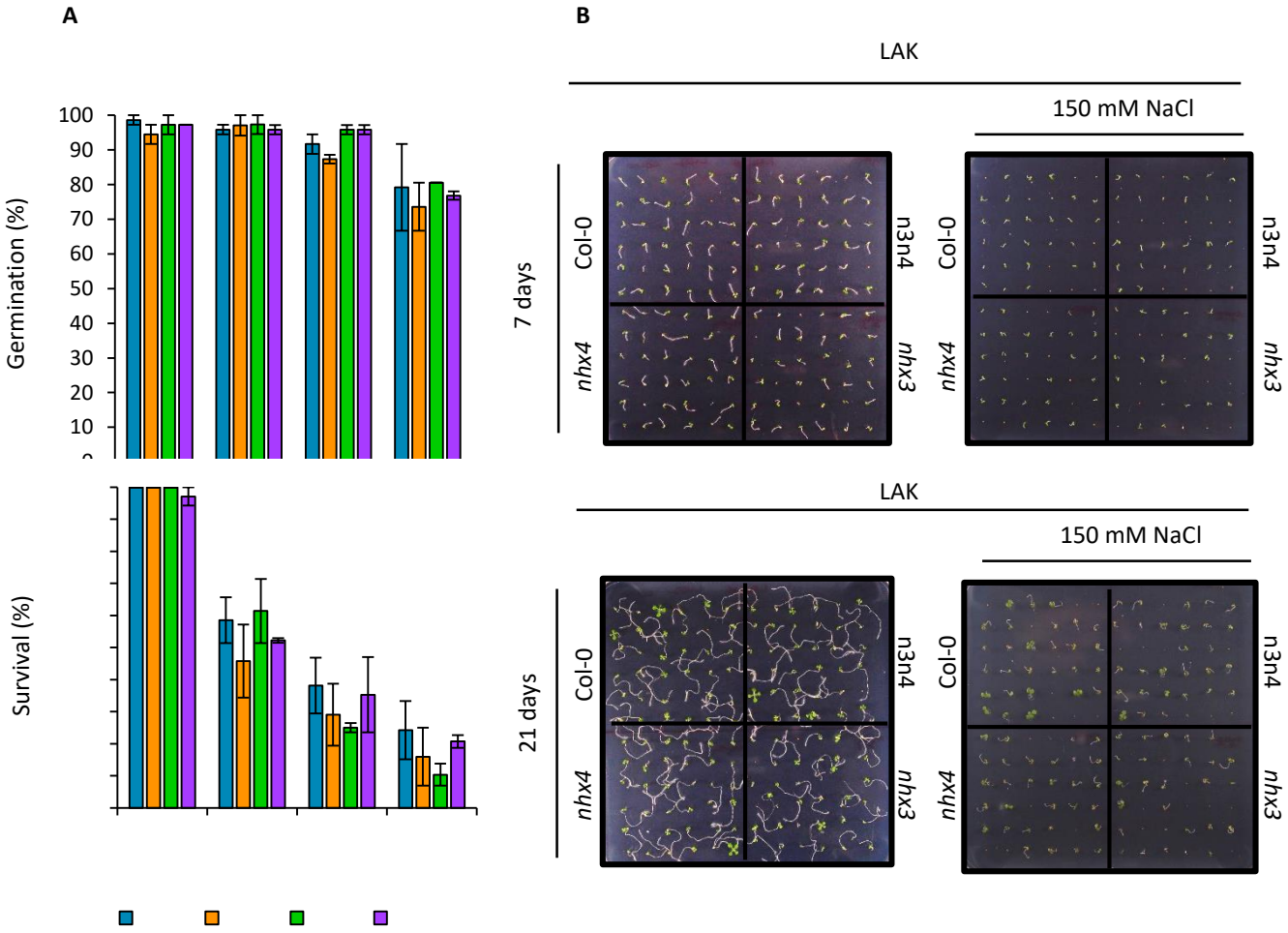

Figure 43. Germination and seedling survival under salt stress. Seeds of wild-type (Col-0), single mutants *nhx3* and *nhx4*, and of the double mutant *nhx3 nhx4* (n3n4) were germinated in control media (LAK with 1 mM KCl) or supplemented with increasing concentrations of NaCl (50, 10 and 150 mM NaCl). **(A)** Germination percentage was quantified 7 days after sowing, scored as radicle emergence. Survival was quantified 21 days later as the number of plants that presented green aerial organs. Data represents the average and SEM (n=36) Statistics was done by Tukey HSD test. **(B)** Representative pictures of germinated seedlings at day 7 and 21.

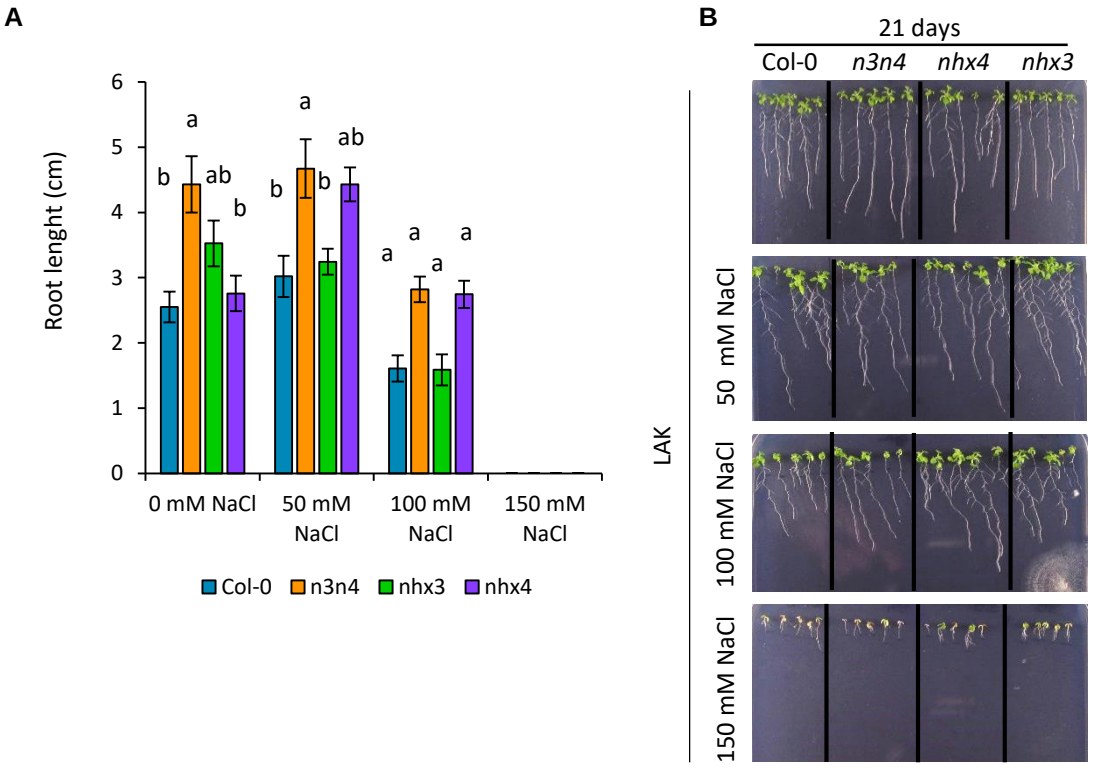

Figure 44. Root growth under salinity stress. Four-day-old seedlings of the the wild type line (Col-0), single mutants *nhx3*, *nhx4* and double mutant *nhx3 nhx4* (n3n4) grown in LAK medium, were transferred to new plates with LAK ,supplemented with 50, 100 and 150 mM NaCl. **(A)** The increment of root length after 17 days of growth under salinity treatment. Data represents average lenght and SEM of two independent experiments (n= 9). Asterisks indicate statistically significant differences by a Tukey HSD test. **(B**) Representative pictures of seedlings at the end of the salinity treatment.

After 21 days growing vertically, some differences were noticed. In the first place, no increment in length was seen in any of the lines in the media supplemented with 150 mM NaCl. In the control medium, mutants *nhx3* and *nhx3 nhx4* showed statistically significant better performance than the wild-type Col-0 and the single mutant *nhx4*. However, with increasing concentrations of NaCl, this growth advantage was cancelled and the single mutant *nhx4* and the double mutant *nhx3 nhx4* showed better salt resistance than that of Col-0 and *nhx3*. (Figure 44B and D). Together, these results suggest that AtNHX3 plays a slightly positive role in the salt tolerance of Arabidopsis at early stages of development, whereas removal of AtNHX4 has the opposite effect and increases root growth under salt stress.

R.4.2. Growth in different concentrations of KCl.

Root growth measurements were also done after supplementing the solid media with increasing amounts of KCl. Seeds were sown in solid LAK medium supplemented with different concen trations of KCl (0, 0.1, 10, and 100 mM) and seedling were grown in long-day conditions, but no differences among genotypes were observed (Figure 46) . To measure fresh and dry weight, 6-7 seedlings per genotype were collected after 21-day growth and weighted together, and three samples per genotype (technical replicas) were collected. In agreement with (LIU et al. 2010), the *nhx4* single mutant showed reduced growth at low-K supply (**¡Error! No se encuentra el origen de la referencia.**). The double mutant *nhx3 nhx4* had a similar phenotpype and the *nhx3* single mutant behaved as the wild-type Col-0 .

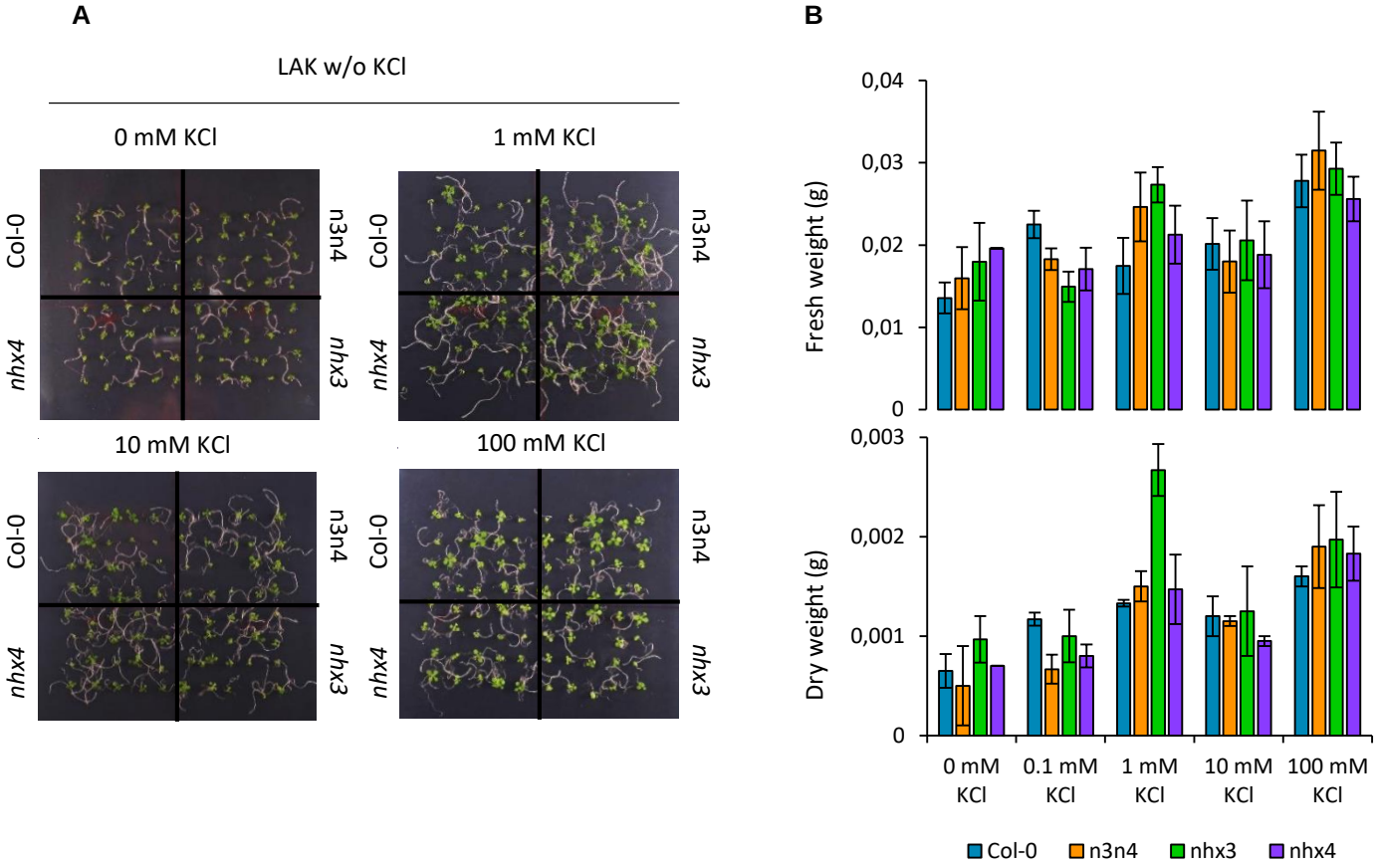

Figure 45. Seedling growth under different K regimes. Seeds of wild-type (Col-0), single mutants *nhx3* and *nhx4*, and of the double mutant *nhx3 nhx4* (n3n4) were germinated in dishes supplemented with increasing concentrations of KCl (0, 0.1, 1, 10 and 100 mM KCl). **(A)** Pictures of seedlings after 21 days of growth. 20 seeds per genotype and treatment were analyzed. **(B)** Fresh weight after 21 days growth in each treatment. **(C)** Dry weight of samples after dessication at 70ºC for 48h. Data represents the mean and SEM; n=18-20 seedlings per genotype and treatment. Statistic analyses were done with Tukey HSD test.

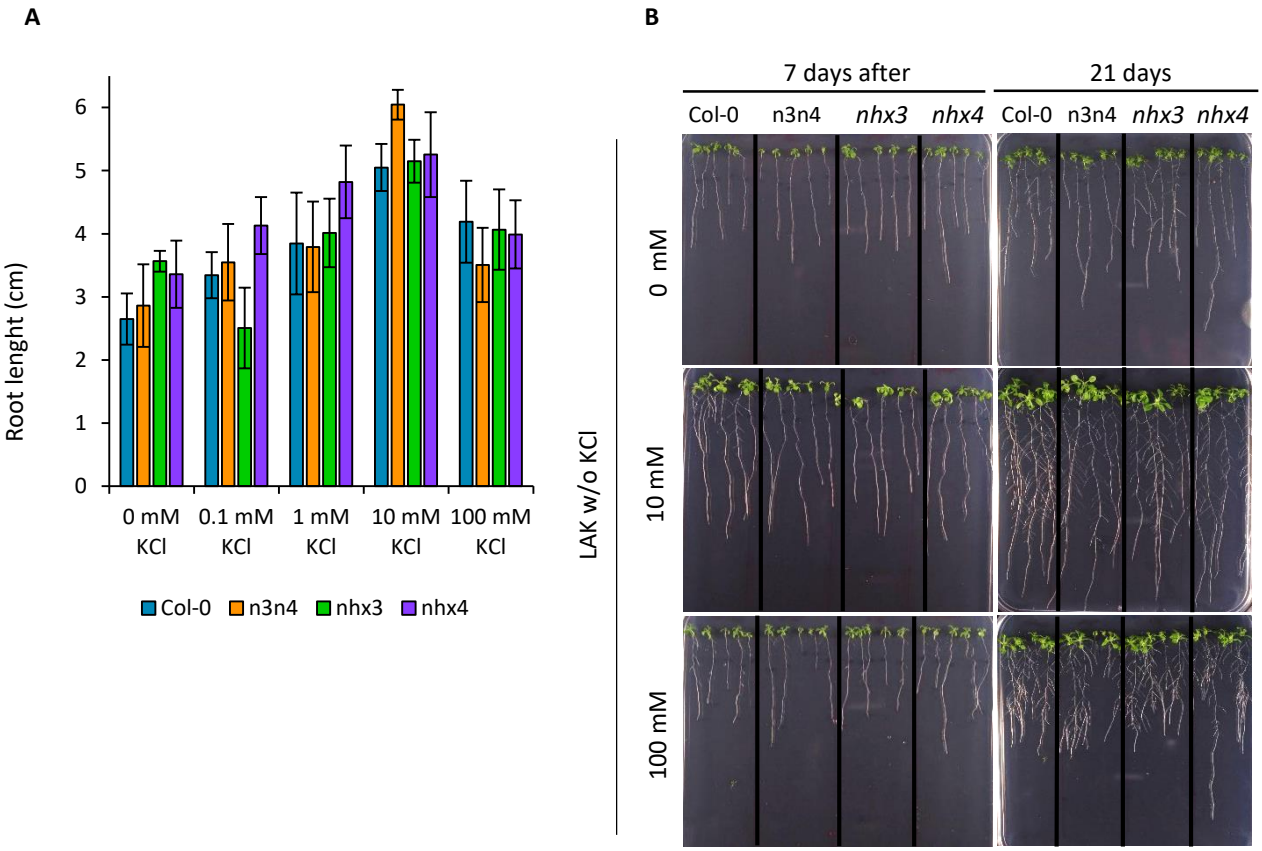

Figure 46. **Root growth in media supplemented with KCl.** Seeds of wild-type (Col-0), single mutants *nhx3* and *nhx4*, and of the double mutant *nhx3 nhx4* (n3n4) were germinated in dishes of LAK medium without KCl and supplemented with increasing concentrations of KCl (0.1, 1, 10 and 100 mM KCl) and grown vertically in Conviron chamber. Five seedlings per genotype were placed in the same plate. (**A)** Root length of 4-day-old seedlings at the time of transfer. **(B)** The length increment after 17 days of growth in various KCl concentrations. Data show the mean and SEM of two independent experiments (n= 10). Statistical analyses were done using the Tukey HSD test. **(C)** Representative picture of seedlings on days 7 and 21 of growth.

R.4.3. NHX3 implication in flowering time and flower opening.

There is evidence that members of the CPA1 protein family regulate the luminal pH of different organelles (Bowers et al. 2000; Casey et al. 2010; Ohgaki et al. 2011). In Arabidopsis, AtNHX5 and AtNHX6 regulate the luminal pH of endosomes (Bassil et al. 2011a; Martinière et al. 2013a; Reguera et al. 2015), whereas the activity of AtNHX1 and AtNHX2 regulates the vacuolar pH (Bassil et al. 2011b; Barragán et al. 2012; Andres et al. 2014). The direct measurements of vacuolar pH in *A. thaliana nhx1 nhx2* double mutant demonstrated that these antiporters are essential for vacuolar pH regulation by importing K^+ into the lumen coupled to H^+ efflux. This function of tonoplast-localized NHX proteins regulating vacuolar pH was first demonstrated in morning glory (*Ipomea*) flower petals (Yoshida et al. 1995). The change of petal color in *Petunia* and *Ipomea* species during flower blooming is due to a change of vacuolar pH. In petunia, flower buds have a purple color and a vacuolar pH of petals cells of 6.3. During flower opening, the pH decreases to a value of 5.3, turning the opened flower color into reddish. (Quattrocchio et al. 2006). The vacuolar acidification is due to the activity of two vacuolar P-type H^+-ATPases, PH1 and PH5 (Faraco et al. 2014; Morita and Hoshino 2018). In *Ipomea* species the contrary occurs. Flower buds have a vacuolar pH of 6.6 and petal cells are red colored. This color turns into blue in opened flowers due to an increase of the vacuolar pH of petals cells to values of 7.7 - 8 (Yoshida et al. 1995; Yamaguchi et al. 2001). In *I. nil*, the *Purple* gene encoding the InNHX1 protein is the only known H^+ transporter gene controlling vacuolar pH in petals and flower color (Fukada-Tanaka et al. 2000). The InNHX1 mutant (purple, *pr*) shows fully expanded purple flowers with a vacuolar pH more acidic than the wild-type line,(Yamaguchi et al. 2001; Ohnishi et al. 2005). However, petal expansion is not affected in the *pr* mutant, indicating the existence of other proteins implicated in the cell expansion and that InNHX1 is not essential for this processes (Fukada-Tanaka et al. 2000; Yamaguchi et al. 2001; Pittman 2012). Yoshida et. al (2005) showed that the NHX homologue in *I. tricolor* (ItNHX1), is temporally expressed in petal cells before blooming. Together with the induction of the *ItNHX1* mRNA there was also an increasing K^+ content in these cell (Yoshida et al. 2009), suggesting that *Ipomoea* NHXs increase vacuolar osmotic pressure by accumulating K^+ for cell expansion and flower opening. As mentioned before, the vacuolar pH in fully open flowers is 7.7 - 8, which seems to be higher than the homeostatic pH (around 7.2) of plant cytosol. Based on the data, it has been proposed that ItNHX1 and InNHX1 use the K^+ gradient rather than H^+ gradient to exchange K^+ and H^+ to control vacuolar pH during flower opening (Morita and Hoshino 2018).

There is no evidence of NHX proteins affecting vacuolar pH of Arabidopsis petals. However, *AtNHX3* transcripts were almost exclusively detected in flower and root tissues (Yokoi et al., 2002; (Aharon et al. 2003). Moreover, there is circumstantial evidence that this protein may have a differential activity compared to the other vacuolar AtNHX. It is unable to recover the AXT3K sensitivity to salt or HygB, and all attempts to express it heterologously in model organisms or tissues (bacteria, onion cells, arabidopsis) have been in vein (Pardo and Cubero, unpublished**).** Although the nhx3 mutant showed a slightly reduced seedling survival in high NaCl that was not statistically significant (Figure 43). the *nhx4* single mutant had a more robust root growth under high NaCl (Figure 44).

We postulated that *AtNHX3* could have a distinctive functional activity in Arabidopsis flowers compared to the other vacuolar AtNHX. By analogy with *Ipomoea*, the H^+/K^+ antiporter activity of AtNHX3 would contribute to the alkalinization of the vacuole and K^+ accumulation to generate turgor and cell expansion for the flower opening. Considering the peculiar characteristics of the *Ipomea* NHX activity (enabling an alkalyne shift in vacuolar pH), the unusual behavior of AtNHX3 could be caused by an extra-alkalinization of the vacuole. Based in this rationale we inspected whether AtNHX3 could have a role in petals cell pH regulation and flower opening. Hence, the influence of AtNHX3 in flowering time and flower opening were evaluated, as well as the contribution to vacuolar pH of petal cells.

R.4..3.1. Flowering time and flower opening quantification.

Flowering time and flower opening time were measured in *nhx3* and *nhx4* mutants. The stages of flower development have been widely studied (Smyth et al. 1990; Bowman et al. 1994; Ferrándiz et al. 1999; Long and Barton 2000; Reddy et al. 2004; Kwiatkowska 2006, 2008; Hepworth et al. 2006). The expansion of petals takes place between stages 8 (beginning of petal expansion), and 12 (petals are visible between sepals) to 13 (complete opened flower). If our hypothesis were right, *AtNHX3* should be expressed along these stages, or even before as observed for ItNHX1 (Yoshida et al. 2005). Based in the classification made by Boyes et al. (2001) on Arabidopsis growth stages, petal expansion takes place between stage 5.10, defined by the emergence of flower buds in the rosette, and stage 6, in which the first flower is open and petals are at 90-degree angle to the pistil.

Regarding flowering time, the usual method is counting the number of leaves in the rosette when flower buds first appear (Reeves and Coupland 2001; Jeong et al. 2015; Sharma et al. 2016) . The number of leaves was counted when the first flower bud was visible and when

the first flower was opened (**¡Error! No se encuentra el origen de la referencia.**B). Results showed that mutation of neither *AtNHX4* nor *AtNHX3* had any effect in flowering time since the apparition of the floral bud in all genotypes occurred at similar developmental stages (12-13 rosette leaves). Flower opening did not show any difference as well.

As previously described for *Ipomea nil*, the lack of expression of the vacuolar NHX1 did not completely inhibit cell expansion and flower opening, meaning that AtNHX3 may contribute to this process but other mechanisms could also be involved. Something similar has been described in the double mutant *nhx1 nhx2*. The absence of AtNHX1 and AtNHX2 in vacuoles of guard cells was detrimental for the opening and closing of the stomata. However, there was still a small and delayed movement, which was proposed to be promoted by the influx of osmotically active solute such as sugars in the late stages of the movement (Andrés et al., 2014). If *AtNHX3* was expressed in the vacuolar membrane of petals contributing to the pH homeostasis and turgor generation for cell expansion, the flowers could present a distinctive phenotype in their form or size. To assess the contribution of this protein in such traits, pictures of the petals were taken and the area measured using the Fiji software. The area of 16 petals (4 flowers) of 2 different plants per genotype were measured. The results demonstrated that the petal size of the single mutants *nhx3* and *nhx4* did not significantly differ from the wild-type Col-0 (Figure 47C). In Figure 47B representative flowers of each phenotype are presented. The results indicated that the only significant difference observed was that the *nhx3 nhx4* double mutant presented a larger petal area than other genotypes (Figure 47C).

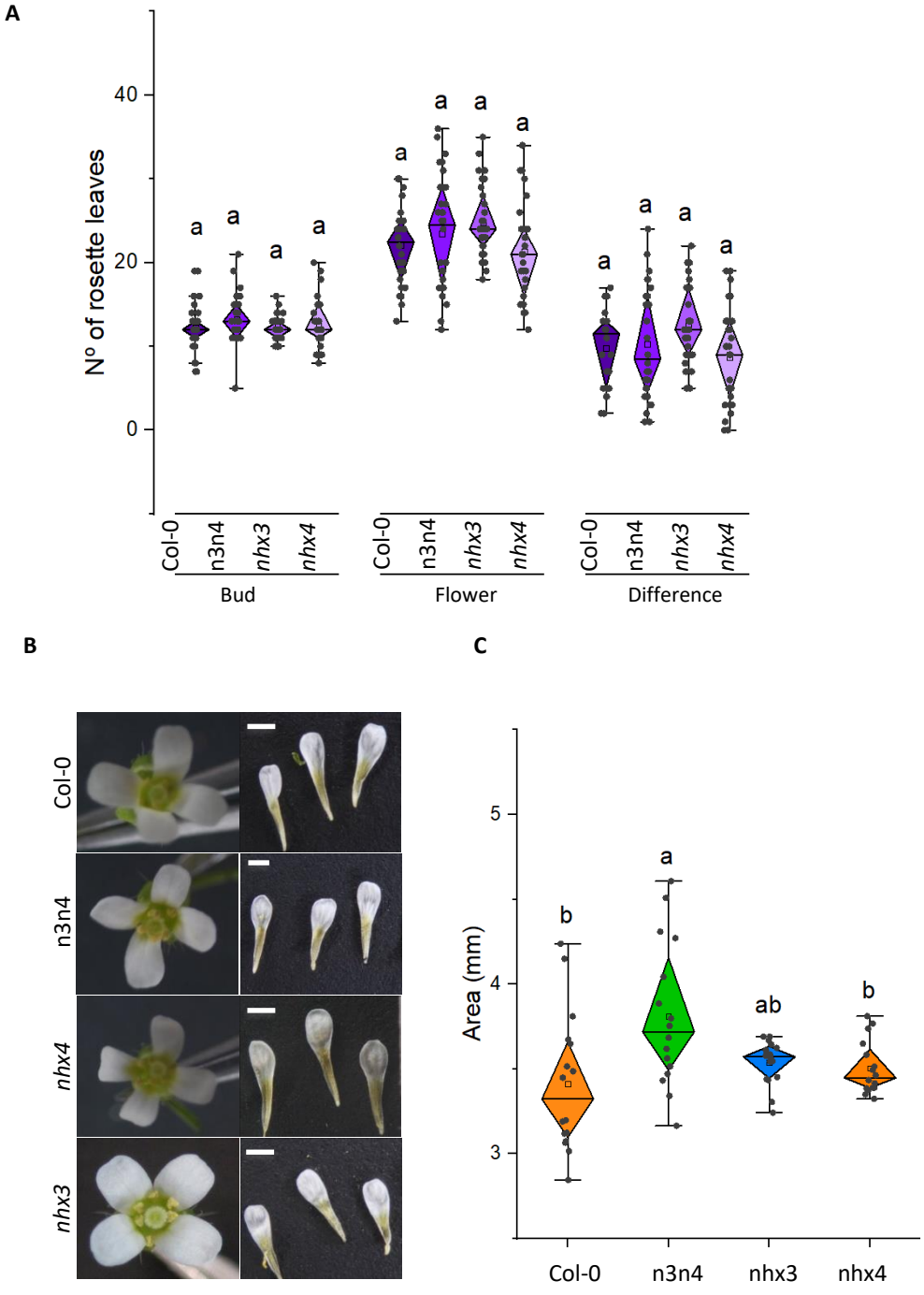

Figure 47. Flowering time and flower opening measurements. **(A)** Represented is the number of rosette leaves at the time the first floral bud appeared, (Bud) and when the first flower opened, (Flower). The difference in rosette leaves between these two events is also represented (Difference). The graphic represents the media and SEM of three independent experiments in which 6-8 plants per genotype were analyzed. **(B)** Picture of representative flowers from each genotype. **(C)** Surface area of 16 petals per genotype. Letters in (A) and (C) indicate statistically significant differences between genotypes by a Tukey HSD test.

R.4.3.2. Vacuolar pH in petals.

Finally, to determine the contribution of AtNHX3 activity to pH regulation in vacuoles of petals, the ratiometric fluorescein-based pH-sensitive dye 29,79-bis-(2-carboxyethyl)-5-(and-6)-carboxyfluorescein (BCECF) was used. Because of the ratiometric nature of this dye, fluorescence values are not affected by dye loading, cell size, or tissue morphology. The membrane-permeant BCECF-acetoxymethyl (AM) derivative readily loads into vacuoles of intact root cells (Swanson et al. 1996; Krebs et al. 2010; Bassil et al. 2011b) , as well as stomata (Andres et al. 2014) or yeasts and animal endomembrane compartments (Ali et al. 2004; Brett et al. 2005b). Since to our knowledge there are no prior reports of measuring the vacuolar pH of Arabidopsis petals cells using the ratiometric dye BCECF, the correct load of the dye to the vacuole of petals cells was confirmed by inspecting the BCECF-loaded petals in a confocal microscope. As seen in Figure 48A, the dye was correctly loaded in vacuoles of both Col-0 and *nhx3* single mutant. Further assays were performed in 96-well plates,. In each well 6-8 petals of 2 independent plants per genotypes were placed and six wells per genotype were measured. The loading protocol was perfomerd as described in the Materials and Methods section M.9.3.1.. Fluorescence was measured using a plate reader. Petals were sequentially excited by two wavelengths: 440 nm and 495 nm, and fluorescence emission was detected at 525 nm for each of the two excitation wavelengths.

Results plotted in Figure 48B indicate that mutants *nhx4* and the double mutant *nhx1 nhx2* had only slightly more acidic vacuoles than the wild-type, but both the single mutant *nhx3* and the double mutant *nhx3 nhx4* presented a significantly more acidic pH than the other genotypes. These results indicate that AtNHX3 is the most relevant protein responsible for this difference.

From these results we concluded that AtNHX3 contributes to the pH regulation of the vacuoles in the petals of *Arabidopsis thaliana*. The fact that no phenotypes in petal area or flowering time are not significantly different from the wild type may be due to the presence of other mechanisms implicated in the same process that overcome the lack of this protein as previously show in other cases (Fukada-Tanaka et al. 2000; Yamaguchi et al. 2001; Pittman 2012)

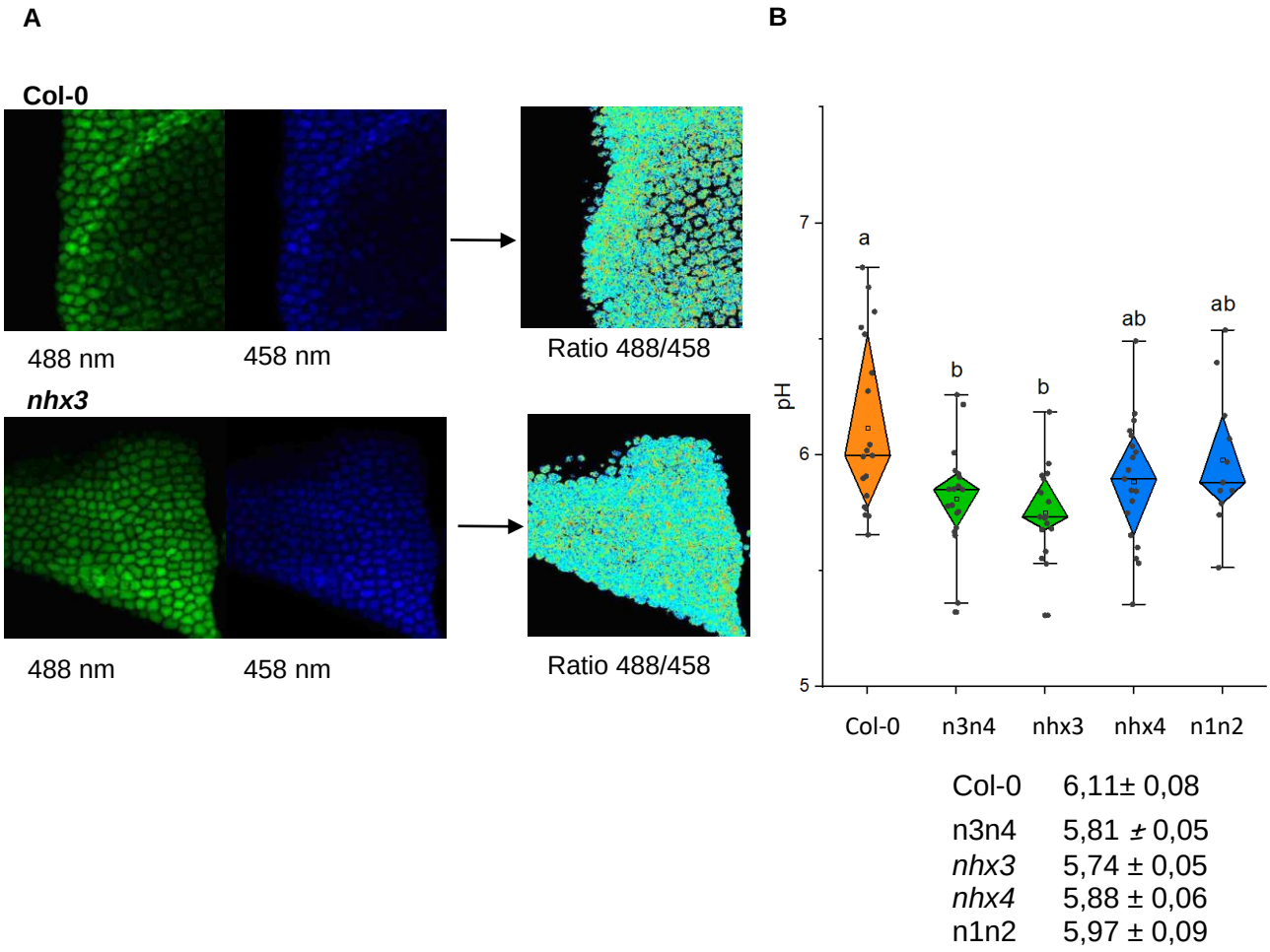

Figure 48. Regulation of vacuolar pH by AtNHX3. (A) Microscopy pictures of petal of Col-0 (upper panel) and single mutant *nhx3* (lower panel) loaded with the BCECF ratiometric dye. Pictures of the same cell layers excited with 435 and 490 nm laser beams, and detected at 535 nm are shown. The ratiometic image obtained after the analysis with Fiji software is shown at the right. **(B)** pH values obtained for wild type Col-0, double mutant *nhx3 nhx4* (n3n4) and single mutants *nhx3* and *nhx4* with BCECF. Double mutant *nhx1 nhx2* was used as reference. The media of 12 independent experiments are shown. Each experiment was conducted with 3-4 flowers of two different plants per genotype.

DISCUSSION

D.1. Structural – function relationship of AtNHX1

D.1.1. Generation of topological and tridimensional models based on phylogenetic relatedness

NHX proteins are essential secondary transporters of the cation-proton antiporter (CPA) family (Brett et al. 2005a; Rodríguez-Rosales et al. 2009). CPA antiporters are conserved across all biological kingdoms and have essential roles in pH, ion homeostasis and volume control. CPA1 antiporters are electroneutral and exchange one cation (K^+ /Na^+) against one H^+ (Călinescu et al. 2014; Wöhlert et al. 2014). Among these proteins, in which plant NHX are included, are also found proteins PaNhaP, MjNhaP1 and HsNHE1. CPA2 antiporters, including EcNhaA from *E. coli* and TtNapA from *Thermus thermophilus* are electrogenic, exchanging one Na^+ against two H^+ (Hunte et al. 2005a; Lee et al. 2013c; Paulino et al. 2014). This family also contains eukaryotic proteins, e.g. HsNHA2 and the plant CHX clade (Brett et al. 2005a; Schushan et al. 2010; Sze and Chanroj 2018).

The first atomic structure of a cation-proton antiporter (CPA family) was the Na^+/H^+ exchanger of *E. coli* NhaA (EcNhaA). The 6 Å structural map of EcNhaA resolved 12 transmembrane helices (TMs) with a characteristic folding of the active center, named the Nha-fold, consisting in two unwound transmembrane stretches that cross each other in the middle of the membrane near the ion binding site by their unwound region creating an X-shaped structure. Later, the structures of two CPA1 members, MjNhaP1 and PaNhaP, were also obtained. Although they have some functional and structural differences with EcNhaA, the overall structure is quite conserved, including the Nha-fold of the active center. The information gained from these structures allowed the *in silico* modeling and a better understanding of the architecture of the more complex eukaryotic CPA proteins, such as eukaryotic human HsNHE1 and HsNHA2 (Schushan et al. 2010; Lee et al. 2013b), *Populus euphratica* PeNHX3 (Wang et al. 2014), and *A. thaliana* AtCHX17 (Czerny et al. 2016) and AtNHX6 (Ashnest et al. 2015). Most modeled structures were based in the first structure available, that of EcNhaA, even if it was not the most adequate model since these CPA1 proteins have been modeled using as template a CPA2 protein (Lee et al. 2013b; Wang et al. 2014). In our work with AtNHX1 four structures available at the SwissModel database were selected as templates because they fitted best to the AtNHX1 protein sequence. These four templates were *Methanococcus jannichii* NhaP1 (MjNHP1)(Paulino et al. 2014), *Pyrococcus abysii* NhaP (PaNhaP) (Wöhlert et al. 2014), *Thermus thermophilus* NapA (TtNapA) (Lee et al. 2013c), and *E.coli* NhaA (Padan 2014). We used these proteins as the reference structures to

generate our own model of a NHX protein, that was also compared to previous modeling reports. The alignment of the primary sequence of AtNHX1 with each of these four proteins individually and the alignment of all proteins together made evident the high conservation of the core structure of the family. Even though EcNhaA showed the lowest sequence conservation at the N- and C- termini among the template proteins compared, the main core in the pore domain of the proteins remained highly conserved, as it had been noticed before in the modeling of HsNHE1 and PeNHX3 proteins (Schushan et al. 2010)(Wang et al. 2014).

The 3D structure obtained for AtNHX1 with each of the model templates were highly similar, with the main differences being in a more lax or tight structure of the protein, which in turn was reflected in the possible interactions that were predicted to take place among residues in the active site of the protein. However, the general structure was the same in all cases, and the predicted transmembrane segments based in individual alignments or in the overall alignment overlapped in most cases. This allowed to generate a topological model that was similar to the previously described for the eukaryotic HsNHE1 or PeNHX3, with 12 TM segments in the hydrophobic N-terminal part, o pore domain, and a long hydrophilic C-terminal tail, with both protein ends being cytosolic. Previous models to explain AtNHX1 topology were inconsistent. Yamaguchi et al. (2003) proposed a model according to which AtNHX1 topology comprised nine transmembrane domains, three hydrophobic regions not spanning the tonoplast membrane, and with the hydrophilic C-terminal domain in the vacuolar lumen. However, this topology was later refuted by Hamaji et al. (2009) who showed by a protease protection assay that the C-terminal tail of AtNHX1 was cytosolic. Also, Sato and Sakaguchi (2005) proposed another topology according to which AtNHX1 and HsNHE1 share the same topology, with 11 TM segments since the first N-terminal TM segment of HsNHE1 is a signal peptide missing in AtNHX1. The major disadvantage of the approach followed by Sato and Sakaguchi (2005) is that the method used to obtain the topological model dealt with fragments of the protein instead of the entire protein. Based in a sequence and structure conservation approach, the model herein proposed yields a topology more similar to the Sato and Sakaguchi's model, and is consistent with the common topology model proposed for the human NHE family and CPA superfamily: 12 TM antiparallel segments with a hydrophilic cytosolic C-terminal tail. An important corollary of this topology is that the interaction of AtNHX1 (and AtNHX2) with CML18 cannot take place in the vacuolar lumen as reported by Yamaguchi et al. (2005).

D.1.1.1. Validation of the models

The best-scored tridimensional models of AtNHX1 using the SwissModel structural database and modeling tools were MjNhaP1 and PaNhaP. This is not surprising since the common ancestors of the CPA1 family are conserved membrane NhaP-like proteins from thermophilic bacteria and archaea (Brett et al. 2005a; Chanroj et al. 2012). Quality checks of the modeled structures based in different conventional analysis are essential to validate the model generated *in silico*. These analyses include the distribution of positively charged and hydrophobic residues (Fleishman and Ben-Tal 2006) and the pattern of evolutionary conservation (Bowie 2005). In the AtNHX1 models generated by MjNhaP1, PaNhaP and TtNapA, as most of the integral membrane proteins, AtNHX1 presents a higher number of positively charged residues (Arg and Lys) in intracellular positions compared with extracellular regions (Wallin and von Heijne 1998), while the polar residues are preferentially located in the intra-membrane core structures or in extra-membrane loops, and away from transmembranes at the periphery of the protein. Finally, the core residues are more conserved than those facing the lipids or those that are cytosolic or luminal (Fleishman and Ben-Tal 2006). These analysis have also been used to validate the predicted structure in other CPA modeling approaches (Schushan et al. 2010; Lee et al. 2013b; Wang et al. 2014; Ashnest et al. 2015). The AtNHX1 models generated using the MjNhaP1 and PaNhaP templates fitted perfectly the expected outcomes of these validation assays, and even the prokaryotic TtNapA, which belongs to the CPA2 family and has been used to model other CPA2 structures (AtCHX17 (Czerny et al. 2016)) produced satisfactory results. However, the EcNhaA not only did not fit with the quality checks, but also one transmembrane segment was missing in the generated 3D-structure.

D.1.2. Identification of conserved residues with functional roles

Integrating the primary sequence comparisons and the topological and ternary models, several residues with probable structural and functional significance were detected (Table 5). The graphical representation of the TM segments in which these residues are located made evident that AtNHX1 present the NhaA-fold on the active center as previously demonstrated for crystalized proteins of the CPA superfamily (Lee et al. 2013c; Padan 2014; Paulino et al. 2014; Wöhlert et al. 2014), and those modeled using a sequence-conservation approach

(Schushan et al. 2010; Lee et al. 2013b; Wang et al. 2014). The active center N184-D185 motif of the CPA1 electroneutral proteins is located in TM5 of AtNHX1. In the vicinity of the ND motif the expanded sectors of TM4 and TM11 cross each other, and in these sectors the conserved T156-D157 motif of TM4, and R390 of TM11 are located. Moreover, TM10 is in the surroundings of the Nha-fold and the conserved R353 in this TM can be found interacting with conserved residues in TM4 and TM11 (Figure 10).

For a long time it was believed that the presence of the DD- or ND-motif in the active center of the protein determined the electrogenicity of the antiporter (Hunte et al. 2005b). The additional negatively charged Asp residue in the DD-motif of CPA2 proteins was proposed to be responsible for the extra H^+ that is transported by these exchangers compared with CPA1 members carrying the ND-motif (Hunte et al. 2005b; Călinescu et al. 2014). For both EcNhaA and TtNapA the DD-motif is essential for the protein activity, and an Asn in this position renders the protein inactive (Inoue et al. 1995; Lee et al. 2013c). In CPA1 protein members, the substitution of the Asp residue in the ND motif showed that it is essential for the protein activity. However, the Asn residue was not. Replacing N160 in MjNhaP1 for an Ala generates an inactive protein, but the N160D substitution mutant of this protein (Hellmer et al. 2003), as well as the N187D substitution in PeNHX3 generated active proteins (Wang et al. 2014). Similar results were obtained for AtNHX1 since the N184D mutation also produced a biologically active protein (Figure 15). Nonetheless, Asn to Asp mutations in the active enter of CPA1 proteins do not render these proteins electrogenic (Hellmer et al. 2003; Wang et al. 2014; Paulino et al. 2014). In the case of AtNHX1 more analyses are required to confirm this. The N184D mutant showed to be detrimental for the yeast growth in the presence of hygromycin, which is indicative of compromised activity, but supported a slightly more robust growth than the wild-type AtNHX1 when grown in 10 mM LiCl (Figure 15 and 16).These results indicate that the highly conserved N184 in the active center is not essential for the activity of AtNHX1, as previously demonstrated for MjNhaP1or PeNHX3 (Wang et al. 2014; Paulino et al. 2014), but could have a role in substrate selectivity by changing the geometry of the active center. In MjNhaP1, it was proposed that the homologuous Asn is necessary to stabilize the proton or substrate-bound state, which can also be fulfilled by an aspartate (Paulino et al. 2014). As for HsNHA2, the mutation of de DD-motif into an ED-motif decreased Li^+ tolerance, which is opposite to what we observed when the ND-motif of AtNHX1 is exchanged for a DD-motif (Figure 16), implying again that the presence of an Asp in the first position of the motif can modify ion affinity and/or selectivity (Schushan et al. 2010).

The R353 in AtNHX1 located in TM10 has counterpart homologues in MjNhaP1 (R320) and PaNhaP (R337), both in TM10. The X-ray structure of these proteins shed light on their function in these proteins. These Arg form ion bridges with a conserved glutamate in TM5: R320 with E156 in MjNhaP1, and R337 with E154 in PaNhaP. This Arg-coordinating Glu is conserved in all CPA1 antiporters, and in AtNHX1 is residue E180. These highly conserved residues essential for activity seem to have a role in stabilizing the protein (Hellmer et al. 2003a; Goswami et al. 2011). Recent studies showed that the electrogenic activity of TtNapA is due to the presence of a Lys in TM10 (K305) but not to the DD-motif in the active center (Uzdavinys et al. 2017). This Lys is the equivalent to residue to R353 of AtNHX1. They also demonstrated that HsNHA2 is an electroneutral protein despite of the DD-motif in the active center and because of the presence of an Arg (R432) in the homologous position to K305 of TtNapA. Later, Călinescu et al. (2017) showed that, although having an important role in protein activity and stability, the homologue Lys in EcNhaA (K300) is not essential for electrogenic transport. Together, these results indicate that the DD-motif is not the basis for electrogenicity and that the K/R dichotomy in TM10 explains only partially this transport mode.

In the CPA2 family proteins there is an interaction between the conserved Lys in TM10 and the Asp residue in the active center, and this interaction regulates the pH sensing and the activity of the protein in a competition-based transport mechanism that ensures transport activity as long as no extreme pH values are reached, in order to prevent excessive acidification or alkalinization of the cytoplasm (Maes et al. 2012; Lee et al. 2014; Călinescu et al. 2016, 2017). In the case of PaNhaP and MjNhaP1 (Călinescu et al. 2016) the Arg replacing the Lys does not interact with the ND motif but forms an ion bridge to the neighboring conserved glutamate in TM6 (Paulino et al. 2014), and the conserved Asn of the ND-motif in TM5 interacts with a conserved Thr in TM4. The essential role of R353 in function or stability has been confirmed by functional analysis in yeasts. In the mammalian CPA1 proteins NHE1 and NHA2, the Arg in TM10 is conserved (**¡Error! No se encuentra el origen de la referencia.**) but, unlike the AtNHX1 mutant R353K, the R→K mutant of NHA2 retained partial activity.

Something similar occurs with the conserved positively charged residue in TM11 (R458 in HsNHE1, K460 in HsNHA2, R390 in AtNHX1). Although the replacement of this residue in HsNHE1 failed to express, the mutant K460A of HsNHA2 exhibited a Li^+ selective phenotype signifying that the mutant protein had gained greater affinity for Li^+ than the wild-type protein (Landau et al. 2007; Schushan et al. 2010). In prokaryots, the functionally important Arg in the unwound TM11 (R285 in MjNhaP1, R362 in PaNhaP, R390 in AtNHX1) might have as well an

stabilizing function by interacting with residues in the active site (Paulino et al. 2014; Wöhlert et al. 2014), but not much is known about them. In this study even the conservative change R390K was unable to recover the AXT3K sensitivity to HygB (Figure 15) indicating that might have as well a functional or structural role in the AtNHX1 protein. The mutation of K305 to arginine in TtNapA rendered the protein inactive (Uzdavinys et al. 2017).

In EcNhaA the conserved residues T132 and D133 (TD-motif) are involved in the ion coordination and translocation, but they are not essential for protein activity (Galili et al. 2002; Maes et al. 2012). Instead, a function in the stabilization of the active site has been proposed (Maes et al. 2012) and recently confirmed (Rimon et al. 2018). In the archea proteins PaNhaP and MjNhaP1 the TD-motif is conserved and is essential for the coordination of the ion (Paulino et al. 2014; Wöhlert et al. 2014). In PaNhaP and MjNhaP1 residues Thr129 and Thr131 have been described to interact by their side chain with N158 and N160, respectively, which do not participate in the ion coordination but control the access to the ion-binding site (Paulino et al. 2014; Wöhlert et al. 2014). In the mammalian NHE1 and NHA2, and in TtNapA this TD-motif is not conserved (Landau et al. 2007; Schushan et al. 2010; Lee et al. 2013c). Although for PeNHX3 only the presence of a non-charged Tyr in position 149 was described (Wang et al. 2014), the alignment of the CPA proteins performed herein indicates that the TD-motif is in fact conserved (Figure 7B). This motif is also conserved in AtNHX1 (T156-D157), and according to all the models obtained for AtNHX1, there seems to be an interaction of T156 with N184, as described for the archeas NhaP. The yeast complementation assays have shown that D157 of the TD-motif is essential for AtNHX1 activity, but a mutant in T156 was not tested.

The AtNHX1 topological and tridimensional structure generated by homology modeling in this study sheds light on its transport mechanism. In addition, the analysis of the most conserved residues demonstrate that AtNHX1 maintain essential properties of the CPA1 family, but also carries unique features in ion binding and translocation. Additional ion transport assays in tonoplast vesicles should be done to confirm the functionality of the described amino acids in the electroneutral nature of AtNHX1 or in the affinity traits.

D.1.3. Regulation of vacuolar pH by AtNHX1.

One of the main functions of NHX proteins is to regulate the luminal pH of organelles (Yamaguchi et al. 2001; Bassil et al. 2011c; Andres et al. 2014; Reguera et al. 2015). This function is highly conserved in eukaryotic organisms, including yeasts in the which *Δnhx1*

mutant has been shown to have a more acidic endosomal pH when subjected to acid stress (Plant et al. 1999; Ali et al. 2004; Brett et al. 2005b; Diakov et al. 2013). The yeast Nhx1 protein resides in late endosomes/pre-vacuolar compartments, and Nhx1 effects on organelle pH seem to be tied to intracellular trafficking. The *nhx1* mutant is also known as *vps44* (vacuolar protein-sorting 44) (Bowers et al. 2000; Bowers and Stevens 2005). The *vps44* mutant secreted 35% of a vacuolar carboxypeptidase Y (CPY) and missorted markers associated with PVC, Golgi, or vacuolar membrane. These results evidence that Na^+,K^+)/H^+ activity is essential for endosomal function and protein sorting in a eukaryotic cells, and that proper pH homeostasis in LE/PVC is critical for the sorting of proteins.

Alkaline pH is stressful to *S. cerevisiae* (Mendoza et al. 1994). When extracellular pH approaches the cytosolic pH, nutrient and ion uptake can be disrupted because the pH gradient across the plasma membrane is lost. The *ENA1* gene, encoding a Na^+-ATPase, is induced by alkaline conditions and encodes a pump capable of exporting toxic Na^+ in the absence of a H^+ gradient (Haro et al. 1991). This protein is mutated in AXT3K, and it may explain why no growth was observed at pH 7.0 in any assay (Kane 2016). Yeast mutants with loss of function in ScNhx1 are sensitive to external pH and/or extreme alkali cation levels. The expression of AtNHX1 confers yeast tolerance to high K^+ or Na^+ at acidic pHext , but on alkaline medium AtNHX1 is ineffective (Sze and Chanroj 2018). Attempts to monitor AtNHX1 in yeast based on resistance to hygromycin instead to Na^+ or Li^+ were also unsuccessful because, for unknown reasons, to toxicity of hygromycin increased greatly at pH 7 (Figure 15)

In this thesis, measurements of pHvac in yeast cells by the pH-sensitive fluorochrome BCECF showed results that could be expected in most cases. The pHvac of the *nhx1* mutant was more acidic than that of the wild type (Figure17A), consistent with the idea that ScNHX1 catalyzes K^+ uptake and H^+ efflux from compartments acidified by the vacuolar H^+-pumping ATPase (Brett et al., 2005). However, although trends in pHvac differences between genotypes were maintained, quantitative estimations of pHvac varied notably from experiment to experiment, complicating the statistical analysis of data. Cytosolic and vacuolar pH can vary significantly under different growth conditions and during different growth phases, which could explain these variation (Orij et al. 2012). Even though all possible measures were taken into consideration, the source of the experimental noise when estimating the pHvac between experiments could not be cancelled. Nonetheless, qualitative differences in pHvac between genotypes marked clear tendencies regarding the contribution of NHX activity to pHvac that were coherent with the complementation test of AXT3K cells.

When the vacuolar pH of strain AXT3K expressing the AtNHX1 mutants affected in the active center was measured, important differences were observed. The vacuole of yeast carrying the AtNHX1 mutant N184D had a more basic pHvac than AXT3K and similar to the wild-type AtNHX1, which correlates with the ability of this mutant to suppress the sensitivity to HygB. In CPA1 proteins, it has been described that the conserved Asn in the active center (ND-motif) interacts with the Thr in the TD-motif in TM4 (Paulino et al. 2014). The exchange of Asn by Asp in the N184D mutant might disrupt this interaction and still maintain the protein active at pH 6, but could be detrimental for growth at pH 5 (Figure 15). The equivalent N187D mutant of PeNHX3 also complemented the yeast *nhx1* mutant, but the vacuolar pH was not measured (Wang et al., 2014). In MjNhaP1 however, the N160D mutant showed lower activity compared to the wild type. It could be hypothesized that the Asp in the place of Asn generates a constitutively opened transporter at acidic pH and that the continuous release of protons into an already acidified cytosol would be detrimental. Our results may also indicate that residue N184 of AtNHX1 has a role in the selectivity and/or affinity of ion binding. In the medium with Li^+, yeast cells expressing the N184D mutant grew better than those with the wild type AtNHX1, perhaps because the new conformation of the active center increased the affinity for this ion. It has been demonstrated for *Vibrio chlorae* that the residue of a Gly for an Ala (G159A) in the active center conferred to the cation/proton antiporter VcNhaP the hability to exchange Li^+ for H^+ (Schubiger et al. 2017). Also, mutation of de DD-motif of into an ED-motif HsNHA2 decreased Li^+ tolerance, implying that the presence of an Asp in the first position of the DD-motif (ND in CAP1 proteins) can modify ion affinity and/or selectivity (Schushan et al. 2010).

Surprisingly, the single mutants in which the two conserved arginines R353 and R390 where exchanged to Lys showed a pHvac only slightly lower than the wild-type. This was an unexpected result since in the growth assays no complementation of the AXT3K sensitivity to HygB or LiCl by R353K and R390K mutants was detected. The double mutants in which the ND-R arrangement was completely changed to the DD-K configuration found in electrogenic CPA2 proteins, showed an acidic pHvac but still higher than the expected from a loss-of-function mutant. There are no reports of other R-to-K mutations in CPA1 proteins in which the protein is inactive (Schushan et al. 2010; Wang et al. 2014). However, most of the R-to-K and K-to-R mutants in CPA proteins showed lower activity (Hellmer et al. 2003; Schushan et al. 2010; Wang et al. 2014; Uzdavinys et al. 2017). The phenotype of yeast expressing the R-to-K variants could be explained by a lower activity of the AtNHX1 protein that was insufficient to suppress the phenotype of the yeast *nhx1* mutant. Although in normal growth conditions

these proteins are able to translocate K^+ into the vacuole in exchange of H^+, the selective conditions applied in the functional assays in yeast could still be inhibiting the yeast growth thereby masking the reduced protein activity. This low activity of R353K and R390K mutants could be explained by a change in ion selectivity or the inability to coordinate properly the substrates due to a new, less than optimal structure. This could also explain the sensitivity of AXT3K cells expressing R353K and R390K mutant proteins in AP media with LiCl. Moreover, in the event that the nature of the mutant AtNHX1 protein changed from electroneutral to electrogenic, it could be deleterious to yeast in selective conditions even though the protein remained active. Nevertheless, all these suppositions are only based on indirect evidence gathered from growth assays and measurements of the vacuolar pH as affected by the AtNHX1 mutants. A direct assay measuring the ion transport of the mutants in tonoplast vesicles is necessary.

In TtNapA, the mutation of the conserved K305 for other basic amino acids, such as Gln or Arg generated alleles only slightly active at high pH 8. Moreover, the new alleles had lost electrogenic properties and their activity became electroneutral. The activity could only be recovered to wild-type levels in a D156N-K305Q mutant. This made evident the need of an interaction of a positive amino acid different from Lys in TM10 with the Asn in the active center for the activity of electroneutral proteins (CPA1). This double mutant was also electroneutral, but the only mutation of K to R was enough for this conversion. Recently, it has been reported that EcNhaA could be converted from electrogenic to electroneutral by mutating the D163 into Asn, and two other amino acids out of the conserved amino acids herein mentioned, but with strategic positions near the active center (A106S and P108E)(Rimon et al. 2018). These results demonstrate that is not only essential the presence of certain conserved amino acids for the activity of the protein, but also the interactions they maintain to keep the conditions in the active site for the kind of transport that takes place. However, their conclusions are different in the fact that according to Uzdavinys and colleagues the conserved Lys in TM10 is essential for the electrogenicity of the protein, while for Rimon and colleagues it is the Asp of the active site. Moreover, in both cases it was possible to mutate the active site of an electrogenic DD-motif into a ND-motif obtaining an active protein, always balanced by mutations of other strategic residues that maintain the right conditions for the translocation of ions, generating electroneutral proteins from a electrogenic one. This would mean that to convert AtNHX1 into electrogenic and keep it active probably more than one mutation should be done. This has also been observed in previous attempts trying to create electrogenic proteins out of CPA1 members (Wang et al. 2014).

Based in published results, the N184D-R353K mutant of AtNHX1 may act already as electrogenic, but to demonstrate this transport assays in yeast vesicle should be done.

D.2. Regulation of AtNHX1 through the cytosolic C-terminal tail

The activity of CPA proteins is highly dependent on the cytosolic pH, which is also an important regulator of these proteins. This pronounced pH dependence has always been explained by the presence of specific domains in the protein named 'pH-sensors', which are able to sense the milieu pH and according to it activate or inhibit the protein (Hunte et al. 2005a; Călinescu et al. 2014). Amino acids able to change their protonated conditions in the physiological pH range are the most likely candidates to form part of these pH-sensors, and histidines often accomplish that requirement. With a pK value near 6.5, histidines can be protonated at physiological pH 6.5–7, resulting in a positive charge at this residue. There is experimental evidence that histidines function in the pH-dependent modulation of a number of ion transporters, including GLT-1, AE2, ROMK1, PEPT (Zhang et al. 1994; Sekler et al. 1996; Chanchevalap et al. 2000; Rajan et al. 2000; Vahisalu et al. 2008) and in Na^+/H^+ exchangers (Aronson et al. 1982; Wakabayashi et al. 1992; Gerchman et al. 1993; Wang et al. 1995; Rimon et al. 1995; Ikeda et al. 1997). Marshansky (2007) proposed that histidine residues in the a2-subunit of V-ATPase could also be involved in the function of the V-ATPase as a pH-sensor.

In the bacterial Na^+/H^+ antiporter EcNhaA, mutation of H226 changed its pH profile (Rimon et al. 1995; Gerchman et al. 1999). However, recent studies using electrophysiological techniques in MjNhaP1 showed that at least in prokaryotic CPA proteins, the pH dependence is an inherent property of their transport mechanism (Călinescu et al. 2014). This property had already been proposed by (Mager et al. 2011; Lee et al. 2014), and can be applied to both CPA1 and CPA2 proteins. According to this transport mechanism, the protein activity is down-regulated at non-physiological pH preventing excessive cytoplasmic acidification (CPA2 transporters) or alkalinization (CPA1). Eukaryotic transporters seem to follow the same mechanistic principles of pH regulation due to the structural similarity of their transmembrane domain, but further mechanisms modulating the pH dependence of their activity mediated by the large cytoplasmic regulatory domain have also been proposed, as discussed below.

No pH-sensor in the AtNHX1 protein has been described before. However, pH regulation of its activity was assumed due to its nature as cation/proton antiporter. In other CPA1 members, such as HsNHE3 and HsNHE1, the presence of pH-sensors has already been described. In the latter case, it consists of a proton modifier site located in the cytoplasmic region at the C-terminal end of the transmembrane domain that regulates the transport site (Shigeo Wakabayashi et al. 1997; Köster et al. 2011a). On the other hand, the pH-sensor of HsNHE3 consists of two histidine residues (H479 and H499) in the C-terminal tail of the protein. The substitution of H479 and H499 shifted the pH profile to a more acidic region. Looking for conserved residues in AtNHX1, two histidines were found in the C-terminal tail that could have a similar role, H479 and H499. The expression of AtNHX1 single (H479L and H499L) and double (H479L-H499L) mutant alleles in yeasts evidenced that the residue H499 might have a role in the pH-sensing in the protein.

Complementation assays in yeast showed that the His-to-Leu mutations rendered the protein as active as the wild-type AtNHX1 in plates containing HygB, which was an expected result since these residues were thought to have a regulatory and not a catalytic role. However, differences were observed when the yeasts were grown in liquid media buffered at different pHs. In these conditions, the H479L mutant activity, monitored a resistance to hygB, did not vary in relation to the wild type, but the H499L mutant did. At pH 5 and 6 both H499L and H479L-H499L mutants showed a slightly decreased growth in comparison with the wild type AtNHX1, but a wild-type phenotype at pH 7. These results indicate that these mutant proteins are mostly active.

The transient changes of intracellular Ca^{2+} concentration triggered by different stimuli differ from each other in terms of amplitude, duration, frequency, and spatial distribution inside the cell. These stimulus-specific Ca^{2+} transients are named 'the Ca2+ signature' (Webb et al. 1996). Stimulus-specific signals are decoded by downstream effector proteins to generate specific or overlapping responses. Adding a new level of regulation specificity is achieved by Ca^{2+} binding proteins that function as signal-sensor proteins (Batistic and Kudla 2004). These proteins decode and relay the information encoded by Ca^{2+} signatures into specific protein–protein interactions, defined phosphorylation cascades, or transcriptional responses (Luan et al. 2002; Sanders et al. 2002). Consequently, a stimulus specific response is generated. Among the effectors, Ca^{2+} sensor proteins are represented by three major types in plants, namely calmodulin (CaM) and CaM-like (CML) proteins, calcium-dependent

protein kinases (CDPKs) and calcineurin B like (CBL) proteins (Luan et al. 2002; Luan 2009; Kudla et al. 2010).

Of great interest in the understanding of AtNHX1 regulation is the CML family because one out of the 32 CaM-like proteins expressed in the Arabidopsis genome has been described to interact with and regulate AtNHX1 activity. Yamaguchi et al (2005) showed that AtNHX1 is capable of interacting specifically with the AtCML18 protein in a Ca^{2+} and pH dependent manner. In a previous publication they had described a different topology as the one adopted here and experimentally demonstrated by Hamaji and colleagues (2009), in which the C-terminal tail was located in the vacuolar lumen (Yamaguchi et al. 2003), where the interaction between AtNHX1 and CML18 would take place.

The topological model generated by the sequence-conservation approach locates the C-terminal tail of AtNHX1 in the cytosol and comprises amino acids from T435 to A538. Using bioinformatics approaches, the presence of a CaM/CML protein was detected in AtNHX1 (Figure 18).The CaM binding domains (CaMBD) generally consist of a stretch of 12–30 amino acids in the target protein not conserved in their primary structure. However, most of the CaMBD domains share a conserved secondary structure consisting in an amphipathic helix with hydrophobic residues arranged on one side and positively charged residues arranged on the other side (Yamniuk and Vogel 2005; Bender and Snedden 2013) (Snedden and Fromm 2001; Du and Poovaiah 2005). CMLs could follow similar models to interact with their targets and, indeed, the helical projection of the AtNHX1-CMLBD showed similar arrangement (Figure 18B).In addition, CaMBDs, or closely juxtaposed regions, often function as autoinhibitory or pseudosubstrate domains, maintaining the target in an inactive state in the absence of a Ca^{2+} signal (Snedden and Fromm 2001).

Herein, we demonstrated that the lack of the CMLBD, either the complete or partial deletions, rendered the protein inactive when expressed in yeast as they were unable to overcome the sensitivity to HygB or salt (Figure 19 and 25).This result made evidence the need of this domain for the AtNHX1 protein to be active. The interaction between AtCML18 and AtNHX1 was confirmed via Y2H and BIFC assays (Figures 20 and 21). When the AtNHX1-CMLBD was deleted the interaction was lost in both approaches, meaning that this is the domain by which the interaction takes place. Moreover, protein interaction was confirmed by co-precipitation of AtCML18 and the CMLBD of AtNHX1 expressed in bacteria. The high conservation of the CMLBD among the vacuolar AtNHX proteins was observed by aligning the C-terminal tail of the six AtNHX proteins. These results indicate that the vacuolar isoforms AtNHX1-4 but not the endosomal ones AtNHX5-6 can be regulated by AtCML or AtCaM

proteins, at least following the model proposed here (Snedden and Fromm 2001; Tidow and Nissen 2013). Due to the high functional and sequence conservation between AtNHX1 and AtNHX2, we reasoned that AtCML18 could interact with this protein as well, and this was confirmed using the same approaches followed with AtNHX1. However, the interaction between AtNHX2 and AtCML18 seem to be weaker. Possibly, AtNHX2 is able to interact with AtCML18 in different conditions, or with other CML different from CML18 but highly similar in sequence. This remains to be studied.

One of the intriguing properties of CaM is its ability to activate numerous target proteins that share very little amino acid sequence similarity in their binding sites. As observed for other signaling proteins like CBL-CIPK, the selectivity of the interaction could be given by the developmental stage, tissue expression, or stress conditions (Batistic and Kudla 2004; Mao et al. 2016). Based on microarray experiments, the expression patterns of individual members of the CaM/CML family often differ spatially, temporally and in magnitude in response to the stimuli, suggesting specificity in their roles in signal transduction (Zhang et al. 2016). This could mean that the AtNHX1/2 interaction with CML18 specificity could be restricted to certain conditions and that either CML18 could have more targets in the cell or AtNHX1/2 could interact with other CMLs in different conditions. More studies on CML18 expression in Arabidopsis should be done to explore these possibilities.

From our results we conclude that AtNHX1 and AtNHX2 interact with AtCML18. Moreover, the CMLBD sequence in AtNHX1 is essential for the protein activity in the studied conditions, as well as for the interaction between AtNHX1 and AtCML18. The physiological conditions for this interaction to take place, or how the interaction *in planta* would affect the protein's activity still remind to be determined. Moreover, in planta determination of AtCML18 expression should be done, to understand the physiological significance of the interaction, mainly under salt stress (Ranty et al. 2006). According to the BAR eFP Browser (http://bar.utoronto.ca/), *AtCML18* is highly expressed in hypocotyl and roots of seedlings, mature and senescent leaves and in the first and second internode, which highly co-localize with *AtNHX1* and *AtNHX2* expression. As observed in the alignment of C-termini the AtNHX proteins, AtNHX3 and AtNHX4 CMLBD are quiet conserved and they could interact with AtCML18 as well, but since the expression pattern of these proteins is different (Wang et al. 2007) this might not occur in planta.

Interestingly, looking for AtCML18 most similar proteins in *Arabidopsis thaliana* genome, three sequences got the highest scores: AT1G32250, AT3G25600.1 (CML16) and AT1G18530.1 (CML15). The first one is only recognized as a Ca-binding protein, and the Bar-Toronto eFP Browser shows a specific expression in the stamens and mature pollen. More interesting were the paralogs CML16 and CML15. These protein have a 74% identity to each other (Ogunrinde et al. 2017). The expression pattern however are quiet different, according to the promoter::GUS analyses, *CML15pro::GUS* was observed exclusively in mature anthers and developing pollen grains, but C*ML16pro::GUS* activity was detected in floral tissues (although excluded from anthers); in guard cells in seedlings but not in mature plants, suggesting a role for CML16 in early guard cell development; and in vascular tissues. These results are in accordance with the public transcriptome databases (bar.utoronto.ca). Moreover, in the databases, AtCML16 is highly expressed in floral tissue, especially in sepals and petals. The differential expression pattern together with the high similarity with AtCML18 makes CML16 a good candidate to interact with AtNHX in floral development, probably in a specific manner with AtNHX3. These evidences should be empirically demonstrated.

D.2. 1. Integration of the pH and CML regulation by the CMLBD.

The AtNHX1-AtCML18 interaction is not the first report of a CPA1 family member being regulated by a CaM/CML protein since HsNHE1 had previously been described to interact with calmodulin. The interaction between HsNHE1 and CaM takes place in the cytosol, in a Ca^{2+} dependent manner, but no pH dependent (Shigeo Wakabayashi et al. 1997; Köster et al. 2011a). Both binding sites seem to be the integration point of several regulation pathway, but their mechanism of action is different. In the first place, the HsNHE1-CaM interaction is inhibited by the phosphorylation of the Ser648, located in the center of the CaM-BD (Snabaitis et al. 2008a). Secondly, this binding domain acts at the same time as an autoinhibitory domain. In normal condition the CaM-BD binds to a proton modifier site in the cytosolic side of the protein, which has to be protonated in order to have an active protein, making more difficult for protons to access this site. Elevated Ca^{2+} concentrations cause CaM to bind to HsNHE1. CaM binding weakens the interaction of the autoinhibitory region with the proton modifier site. Protons would then gain access to this site to up-regulate the transport activity of NHE1 and stimulate sodium-proton exchange.

The structure CaM-BD of HsNHE1 bound to CaM was obtained by crystallization (Köster et al. 2011a). The results showed that the CaM-BD structure consists of two α-helices (α1 and

α2) connected by a short loop, in which extremes there are a histidine and an aspartic acid. The same arrangement was observed when, using the 3D-structure of the NHE1-CAMBD, the CMLBD of AtNHX1 was modelled. The CMLBD, which comprises the fragment between T497 and G515 generate two α-helices linked by a loop in which extremes there are a histidine (H499) and an aspartic acid (D506), at an appropriate distance to establish a salt bridge when H499 is protonated.

We have developed a model positing that H499 and D506 of NHX1 comprise a pH-sensing module that controls the binding of CAM (Figure 50). According to our hypothesis, at neutral or acidic pH the H499 is protonated and occludes D506 by creating a salt bridge with it. This would render the CML18-binding domain in a "closed" folding, preventing the entry of CML18 and the interaction of residue D506 with a positively charged amino acid of CML18. As a result, the protein would be inactive and no cation/H^+ exchange would take place. When the cytosolic pH reaches values over 6.5-7, H499 would be deprotonated, leaving the D506 residue free to interact with AtCML18 which, in a Ca-dependent manner, would bind to the CML-BD via this residue. This interaction would activate the AtNHX1 and cation/H^+ exchange would take place at the tonoplast until a cytosolic pH near to the physiological set point is reached, or the Ca^{2+} present in the cytosol diminishes. Having this hypothesis in mind, now it is possible to understand the phenotype observed in the functional assays in AXT3K yeast strain. Although H479 seems not to be affecting pH sensing, when H499 is mutated to Leu it is not able to form salt bridges with the D506, and this residue is then continuously able to interact with CML18, even in acidic media. This would render the protein constitutively active (provided that that the yeast calmodulin is bound to Ca2+ and thus able to interact with AtNHX1) and thus AtNHX1-H499L will acidify the cytosol even more,. This model explains in molecular terms the observation that yeast cells expressing the AtNHX1-H499L mutant became specifically sensitive to pH 5 (**¡Error! No se encuentra el origen de la referencia.**Figure 26). As for the D506N mutant, since the protein would never be able to be activated by CML18 (or the yeast CAM), the transport in the vacuoles would be null. In this way, the CML-BD of AtNHX1 would integrate the regulation by pH and CML18/Ca2+.

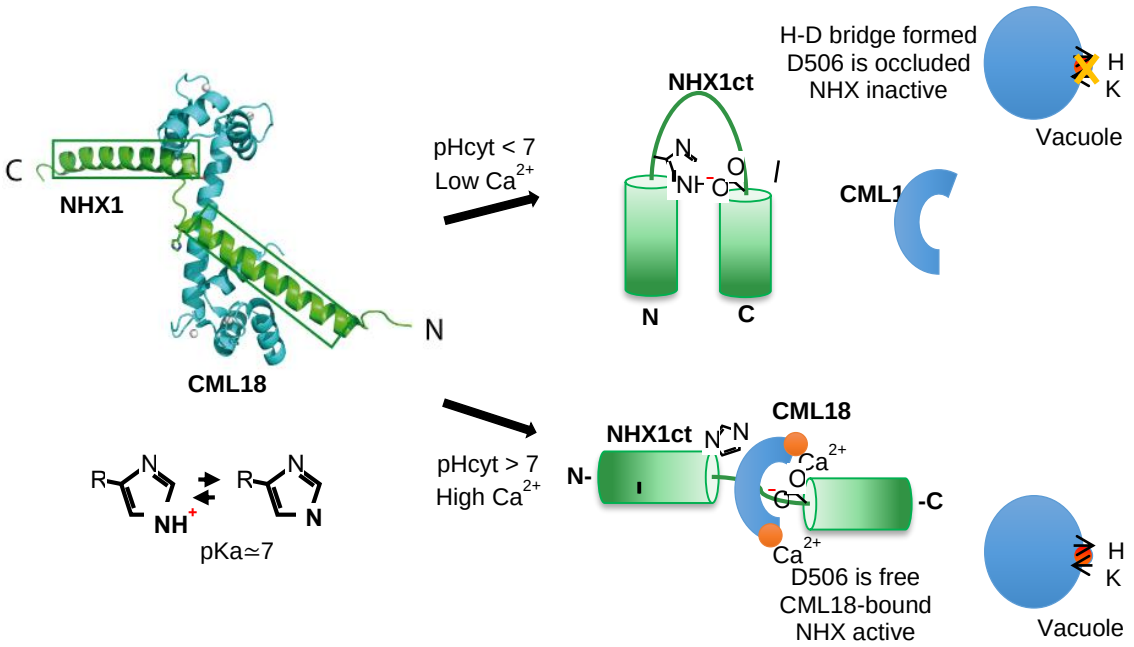

Figure 49. Proposed model for the regulation of AtNHX1 by the integration of the pH sensing and CML18 interaction via the C-terminal domain of the protein.

According to the model proposed in this project the interaction of AtCML18 and AtNHX1-CMLBD is both Ca^{2+} and pH dependent, as previously described by Yamaguchi et al (2005). Moreover, not only the location of the C-tail proposed by them is located in the vacuolar lumen and the one proposed herein is in the cytosol, but also the conditions for the interaction to take place would be the opposite. Yamaguchi et al. (2005) showed that AtCML18 binds AtNHX1-CMLBD at acidic pH of the vacuolar lumen, enhancing the protein activity and the Na^+ translocation into the vacuole. However, at leas acidic or neutral vacuolar pH, CML18 could not bind CMLBD of AtNHX1, reason why the protein activity was lower, and the selectivity for K^+ increased. In our model, AtCML18 binds AtNHX1-CMLBD in the cytosol and the interaction takes place at neutral or basic pH, when the H499 is de-protonated making the D506 free to interact with AtCML18. The CMLBD would then be an integrative domain in which the regulation of AtNHX1 by pH is coordinated to the regulation by AtCML18 and Ca^{2+}.

Our model was supported by complementation analyses, in which the D506N mutant of AtNHX1 was unable to suppress the yeast AXT3K sensitivity to HygB, whereas the H499L

mutant did. The fact that the double mutant H499L/D506N behaved as the single mutant D506N shows that this later mutation is epistatic over H499L. Also, Y2H assays were performed using as bait the CMLBD carrying mutations H499L or D506N, and AtCML18 as prey. As expected, the mutation of the D506N inhibited the interaction between CML18 and AtNHX1, while the H499L did not. This indicates that AtCML18 recognize and binds to the D506 residue in the C-terminal domain of AtNHX1, and that H499 has no effect other than enabling or not of this interaction according to the pH conditions of the medium by coordinating the D506 residue. In AtNHE3, the highly α-helical structure of the domain in which H479 and H499 are located overlaps with the CHP binding domain of HsNHE3 (Cha et al. 2003), and disruption of CHP binding drastically reduces Na^+/H^+ exchange activity (Pang et al. 2001). However, there are no studies on how the mutations generated affected the CHP binding to the protein at different pH.

If the model is correct, it will provide a mechanistic basis for the concerted regulation of exchanger activity by cytosolic pH and Ca2+-CAM binding that has been reported in plant and animal proteins alike. In other words, we may well provide a paradigm for the cross talk of cytosolic pH and Ca2+-sensing in the regulation of a wide range of eukaryotic cation-proton exchangers.

In accordance with the complementation assays with the yeast strain AXT3K, the AtNHX1 mutants with the D506N mutation in the CMLBD showed an acidic vacuolar pH, similar to the observed in the AXT3K strain, and much lower than the pH measured in the wild type W303. Our hypothesis indicates that mutant D506N is inactive because the CML18 is unable to bind to and activate the AtNHX1 protein. Mutations in the CaMBD of HsNHE1 however did not render the protein inactive, but produced a shift of the set point to a more alkaline pH (Ikeda et al. 1997; Shigeo Wakabayashi et al. 1997). This can be explained by the auto-inhibitory role that the CaMBD has in HsNHE1 through its direct interaction with a putative pH-sensor domain. When CaM binds the CaMBD, this fragment is separated from the pH-sensor domain and the NHE1 protein becomes activated (Shigeo Wakabayashi et al. 1997; Köster et al. 2011a). However, this mechanism is not supported by a new allosteric model, in which only H^+-transport sites are assumed to participate in the cooperative H^+-activation of NHE1, in a similar way as described for prokaryotic CPAs that lack the C-terminal tail of the eukaryotic counterparts (Lacroix et al. 2004). The CMLBD of AtNHX1 in this context is more similar to the CHP-binding domain (CHPBD) of HsNHE1, that has been described as essential for protein activity. Not only the deletion of the CHP binding region inhibited the NHE1 activity by inducing an acidic shift of intracellular pH dependence, but also single mutation of essential

residues within this domain (I534D, I534K and Ile537) has similar effects (Ammar et al. 2006). These findings suggest that CHP binding is required for both supporting the basal activity and regulating the pH-sensing of NHE1, as has been described for AtNHX1 and AtCML18 (Yamaguchi et al., 2005). It should be noted that the pH-sensor of HsNHE3 overlaps with the CHPBD (Cha et al. 2003). These models make evident the integration if pH and Ca^{2+} dependent regulation of eukaryotic CPA superfamily proteins through their C-terminal tail.

Residue H479 is equivalent to the conserved H479 of NHE3 protein, in which this residue is thought to be part of the pH-sensor (Cha et al. 2003). The lack of differences between the AtNHX1 wild-type allele and the H479L mutant with regard to pHvac in yeast was expected since no differences were observed in its biological activity in AXT3K cells under different saline or pH conditions. These results are evidence that this residue does not have a significant role in regulating AtNHX1 activity depending on pH. However, the AtNHX1 mutant alleles bearing the H499L substitution were expected to show differences. Previous results showed that the mutation H499L was detrimental for the growth of the yeast in liquid media in acidic pH (Figure 26) .

D.2.2. AtNHX1 and AtNHX2 regulation by phosphorylation

The existence of the phosphopeptide GFVPFVPG[pS]PTER belonging to an identical sequence at the C-terminal tail of AtNHX1 and AtNHX2 has been reported in proteomic studies (Whiteman et al. 2008b), but the protein kinases that phosphorylate the cytosolic C-termini of NHX proteins remained unknown. Qiu et al. (2004) reported that NHX activity in Arabidopsis is regulated by SOS2(CIPK24) in a SOS3(CBL4) independent manner. Apparently no phosphorylation was involved because CIPK24 could not phosphorylate AtNHX1 in vitro. Moreover, it has been demonstrated that SOS2 is able to stimulate the other tonoplast proteins without in vitro protein phosphorylation and through direct protein-protein interaction as, is the case of CAX1 (Cheng et al. 2004) and the V-ATPase (Batelli et al. 2007).

Unpublished results from our lab have shown that S526 of AtNHX1 and S532 of AtNHX2 are substrate for Mitogen Activated Protein Kinase6 (MPK6) phosphorylation, and that CIPK24 phosphorylates NHX2 at S539, a residue that is absent in AtNHX1 (FJ Quintero and JM Pardo, unpublished). These results explain in molecular terms the prior observation that CIPK24 regulates overall NHX activity at the tonoplast that is redundantly dominated by NHX1 and NHX2 (Andrés et al., 2014) while no phosphorylation of AtNHX1 by CIPK24 could be demonstrated (Qiu et al., 2004). Of note is that SOS1 is also substrate of MPK6 (Yu et al. 2010),

but no information about the physiological significance of this phosphorylation has been reported. MPK6 is activated by a phosphatidic acid produced under salt stress by Phospholipase Dα1 (PLDα1). Under salt stress PLDα/PA have been described to be important in different pathways. In guard cells, PA activity is essential in stomatal closing by binding NADPH oxidases AtRBOHDD and AtRBOHF that induce ROS elevation and stomatal closure, and also by binding the ABI1 protein phosphatase 2C (PP2C), a negative regulator in ABA signaling in stomata closure (Ma et al. 2012). Moreover, PLDs interact with both actin and tubulin regulating cytoskeleton reorganization, which is known to be rearranged by the hyperosmotic component of the salt stress (Kusner et al. 2002).. Also MPK6 and MPK4 in *Arabidopsis thaliana* have been related to cytoskeletal organization and remodelation (Takáč et al. 2016; Zhang et al. 2016). Last, a relation between AtNHX proteins and cytoskeletal reorganization under high K^+ and salt stress conditions has been described (Sun et al. 2008; McCubbin et al. 2014). Also, the interaction of HsNHE C-terminal tail with the cytoskeleton is already well known (Donowitz et al. 2009). All together, these results show that phosphorylation of AtNHX by MPK6 could be related to possible cytoskeleton interaction and reorganization under stress.

Also in unpublished results from our lab (Zaida Andrés, Thesis Dissertation, 2013), the interaction of AtNHX1 and AtNHX2 with different CIPKs was demonstrated by Y2H and BIFC assays. Interestingly, the results indicated strong interaction of AtNHX1 with CIPK23, and of AtNHX2 with CIPK23, CIPK24 and CIPK26. These three CIPKs have been related to the salt stress response (Halfter et al. 2000; Qiu et al. 2002; Quintero et al. 2002; Cheong et al. 2007; Thoday-Kennedy et al. 2015; Kurusu et al. 2015; Ragel et al. 2015)). It should be noted that these positive interactions did not include AtNHX1 and CIPK24 pair, in accordance with the negative in vitro phosphorylation results described before by Qiu et al (2004). In preliminary experiments not included in this dissertation, single mutant lines of each CIPK (*cipk23*, *cipk24* and *cipk26*), were analyzed to study the rate of loss of water by the gravimetric procedure. As previously shown (Barragán et al. 2012; Andres et al. 2014) Arabidospsis *nhx1 nhx2* double mutant have impaired hydric relationships, mainly due to the inability to open and close stomata properly. Accordingly, we found that the rate at which this mutant line loses water is much higher than Arabidopsis Col-0 wild-type. Having this phenotype as a control, the same assay was performed with Arabidopsis single mutant lines *cipk23, cipk24* and *cipk26*. The results showed that, in contrast to the *nhx1 nhx2* double mutant, these single mutant had a water-loss rates only slightly smaller than Col-0. These results indicate that *cipk* mutants may keep the stomata more closed than the wild-type.

According to BIFCs results, CIPK23 interacts with AtNHX1 and AtNHX2 at the tonoplast. CIPK23 is involved in the control of K^+ homeostasis at the plasma membrane under low-K^+ stress by regulating K^+ uptake activity by AKT1 and HAK5 in roots (Ragel et al., 2015), and in guard cell turgor regulation in aerial tissues (Xu et al. 2006; Li et al. 2006; Cheong et al. 2007; Nieves-Cordones et al. 2012). In addition, CIPK23 is involved in the stomatal function as a negative regulator of the ABA signaling in guard cells, and in fact *cipk23* mutants showed a more efficient stomatal closure in response to ABA than the wild type (Cheong et al. 2007; Nieves-Cordones et al. 2012). The ability of CIPK23 to phosphorylate NHX2 and K^+ fluxes at the tonoplast reinforces the role of CIPK23 in regulating cellular K+ homeostasis .

The weak phenotypes of *cipk23*, *cipk24* and *cipk26* single mutants could be due to redundancy in CIPK function. As an example, AtCIPK6 and AtCIPK16 both activate AtAKT1 (Luan 2009; Lee et al. 2007). Moreover, other pathways parallel to the CIPK/CBL might be contributing to stomatal closure, like the ABA signaling or ROS production (Pei et al. 1998; Li et al. 2000; Mustilli et al. 2002). As previously stated, AtNHX1 and AtNHX2 proteins seems to have at least differential Ca^+ dependent regulation by CIPKs, which can determine thatunder certain conditions, like in *cipk23*, *cipk24* and *cipk26* mutants linesone of these proteins is fully activated and the other not. Moreover, Andrés (2013, Thesis Dissertation) also showed that AtNHX1 and AtNHX2 form heterodimers in the tonoplast. The generation of hetero- and homodimers in other transporters has been shown to have effects in the activity rate of the protein (Rimon et al. 2007; Faraco et al. 2014). Phosphorylation of any of these proteins could affect the formation of the homo or heterodimers an thus modulate the antiporter activity across membrane.

D.3. pH variationin sensing in Arabidopsis roots upon saline stress

Maintaining cytoplasmic pH within a physiological range is essential for plant growth and survival. This is a ubiquitous trait among all biological kingdoms since many metabolic and enzymatic processes depend on specific pH conditions (Casey et al. 2010; Orij et al. 2011). This also determines that the cytosol is compartmented in organelles with different functions and pH requirement. Plant sessile lifestyle oblige them to be sensitive to their environment, integrating many signals to respond in an appropriate manner for survival. Alterartion in the environment like wounding and pathogen attack, water and nutrients availability or light changes in the soil are frequently presented in a localized manner altering these conditions

(Felle 2001; Roos et al. 2006; Kader and Lindberg 2010) There is also speculation that a change in pH may act as a signal (Pittman et al. 2005; Orij et al. 2011)

Soil salinity is a major environmental constrain to crop production, affecting millions of hectares of land throughout the world and costing billions of dollars every year (Munns 2005; Munns and Tester 2008; Shabala and Cuin 2008). The affected land has arisen from natural causes, such as rainfall, windblown salt from ocean, tsunamis, and rock weathering; but is also associated to land clearing by removal of deep root vegetation or irrigation practices, such as the use of water with high salt concentration. Saline soils are characterized by a high concentration of soluble salts, being NaCl is the most common. Most crop plants are glycophytes (salt-sensitive compared to salt-tolerant halophytes species) and can only tolerate relatively low concentrations of salt.

Plants are affected in three different ways by saline stress: a) osmotic stress, b) ionic toxicity and c) oxidative stress.

The increasing external osmotic pressure due to high salt in the soil reduce the soil water potential, affecting the capacity of root systems to uptake water and generating an internal water deficit that produce intracellular turgor reduction and decreased cell expansion that, together with ABA biosynthesis induction, leads to a decrease in stomatal aperture and conductance (Munns and Tester 2008; Pardo 2010; Roy et al. 2014). Consequently, there will be nutrient imbalance, decreased photosynthetic activity, growth imbalance. Studies of cytosolic pH variation in plants under saline stress have reported that osmotic stress does not affect this trait, either in intact Arabidopsis roots (Gao et al. 2004) , nor rice (Kader et al. 2007) or quince (D'Onofrio and Lindberg 2009) protoplasts.

The second component of the stress, ionic toxicity, arises from the accumulation of Na^+ and Cl^- ions in the plant cells, which at the same time inhibits uptake of K^+ ions which is an essential element for growth and development, decreasing the K^+/Na^+ ratio, which has become a key salt tolerance trait (Tester and Davenport 2003; Shabala and Pottosin 2014). The similar physicochemical properties between Na^+ and K^+ allows the first one to bind sites in key metabolic processes in the cytoplasm occupied for the second one, inhibiting the enzymes activity of many enzymes that require K^+ for functioning (Almeida et al. 2017). The movement of charged ion across the plasma membrane generate imbalances in the electrical gradient generated by the P- type H+-ATPase s which are translated into variations in the cytosolic pH, as has been noticed in several publications (Moseyko and Feldman 2001; Gao et al. 2004; Kader et al. 2007; D'Onofrio and Lindberg 2009). The reaction of the plant cells to

recover the previous conditions recruits P- ATPases and membrane transporters of the internal organelles, which in turn have repercussions in their luminal pH as well.

The third component, oxidative stress, is the effect induced by the production of reactive oxygen species (ROS) generated by both osmotic and ionic stresses beyond the plant's capacity for cellular oxidant detoxification. These molecules include singlet oxygen, superoxide anion, hydrogen peroxide and hydroxyl radical, and negatively affect cellular components (protein, lipids, DNA) and metabolism (Mansour 2014). Environmental stimuli are often highly localized and might be sensed by individual root tips, but the subsequent plant response is often elicited throughout the entire organism. The generated ROS species have a role in the tolerance mechanism in the propagation of the stress along the root and to the shoot (Jiang et al. 2012; Kurusu et al. 2015; Evans et al. 2016).

D.3.1. Generation of cytosolic pH-maps of Arabidopsis thaliana

Classical fluorescent dyes have been used to estimate pH in plants: fluorescein coupled to dextran allows pH recording in the close vicinity of roots or shoots (Monshausen et al. 2009, 2011; GEILFUS and MÜHLING 2012); or BCECF to measure plant vacuolar or cytosolic pH (Kader et al. 2007; D'Onofrio and Lindberg 2009; Krebs et al. 2010). But these approaches are invasive, and don't allow to measure pH in other structures. Genetically encoded pH sensors have been designed to overcome these limitations to visualize and analyse ion fluxes, signaling components, and metabolites. The huge interest and progress in the field is reflected is reflected in recent reviews (Germond et al. 2016; Walia et al. 2018), and even in more specifically, the use in pH sensing methods (Martinière et al. 2013b; Benčina 2013).

Even though cytosolic pH is tightly regulated, the before mentioned alterations in pumps and transporters proteins in different membranes of the cell, and in different tissues, may produce local changes in a transient manner in the cytosolic H^+ to act as a signal. Changes in pH are now widely accepted as a signaling mechanism in cells. Endomembrane system pH had already been obtained by genetically encoded sensors (Shen et al. 2013; Martinière et al. 2013a), and a pH map of these organelles was obtained. As a result, not only a more specific knowledge of the conditions of these compartments were obtained, but also a pH map of this system allowed to better understand the interactions and physiological functions each of them have. Moreover, it was possible to detect that, unlike the endomembrane of other

organisms (Casey et al. 2010; Ohgaki et al. 2011), the vacuole is not the more acidic compartment, but the TGN/EE. It was confirmed afterwards by Luo et al. (2015).

Generating a cytosolic pH map of Arabidopsis thaliana's root would allow to have a better understanding on how the cytosolic pH is affected by the cells activity in normal conditions of growth, as well as how it changes upon different external stimulus (like salt stress). Moreover, the specific detection of these pH variations in the surroundings of the different organelle membranes to study how the physiological activity of the proteins in the membranes of each organelle are affecting the cytosolic pH. To that end, Arabidopsis thaliana Col-0 lines expressing the pHGFP genetically encoded sensor were generated. These lines carried independent constructs in which the pHGFP (Moseyko and Feldman 2001) was translationally fused to protein markers of the different comparmtents of the endomembrane system, in such a manner that the pH sensor localized to the cytosolic side of the membrane of the specific organelle. The marker chosen were VTI11 (Zheng et al. 2014) for the tonoplasto and LTI6b (Cutler et al. 2000) for the plasma membrane. pHGFP was transformed alone to measure the cytosol pH.

Taking into consideration previous comments on how the measurement methodology could affect the final result (Gjetting et al. 2012), a previously described method was used to immobilizing Arabidopsis seedling roots for perfusion experiments which that not impair cell viability and allowed to follow changes of the cytosolic pH in root tissue (Waadt et al. 2017), so that it was possible to apply different treatments while recording in vivo the changes in cytosolic pH.

With the imaging experiments, it was first demonstrated that the pHGFP sensors expressed in the cytosol of Arabidopsis thaliana tissues were sensitive to pH changes in the media when treated with buffers at different pHs. These experiments were done with Arabidopsis' line expressing the pHGFP-VTI11 construct. Assuming that the seedlings cell's cytosolic pH was near neutrality, and that an increase in the pH would be reflected as an increase in the ΔR/R from the steady state at the beginning of the experiment, and a decrease in the pH as decreased ΔR/R, it can be conclude that the pH sensor was sensitive to the different pHs, as expected (Keinath et al. 2015). Since the pH variations were clearly visible at the tonoplasto localization, it was assumed that similar effects would be detected in the plasma membrane surroundings.

Based in these results, it was important to demonstrate that both, the plasma membrane and vacuolar membrane located sensors were sensitive to pH changes in probable

physiological situations, or in specific reaction that could take place in each location. As it has previously commented, H^+ATPases are the most important component of the cytosolic pH long-term regulation system in plant cells, and for that reason were the target proteins selected to do these experiments (Pittman 2012; Schumacher 2014).

In the plasma membrane, the P- type H^+-ATPase activity was altered with two known modulators: vanadate, an inhibitor of the P- type H+-ATPase protein; and fucicoccin, an activator. The inhibition of P- type H+-ATPase with vanadate did showed a decreased in the cytosolic pH compared with the initial situation, however the control treatment showed a diminution in the pH as well. In the case of the enhancement of the P- type H+-ATPase , fusicoccin, the expected increase in the cytosolic pH was observed, and in this case the control did not show the same behavior. This would mean that the pHGFP-LTI6b pH-sensor is sensitive to variations of the pH at physiological ranges. In previous studies in which not the cytosol pH, but the external pH variation was measure after the addition of these modulators were scored a clear change in pH due to alterations of the P- type H+-ATPase activity were observed: alcallinization of the media when the P- type H+-ATPase was challenged with vanadate, and acidification when was challenged with fusicoccin (Schaller and Oecking 1999; Faraco et al. 2014; Kriegel et al. 2015; Wigoda et al. 2017; Di et al. 2018; Camoni et al. 2018). Nontheless, the treatment with fusicoccin in Arabidopsis seedlings expressing pHGFP had been reported to acidify the cytosol (Moseyko and Feldman 2001). Fusicoccin binds to the complex formed by P- type H+-ATPase and the 14-3-3 protein that enhanced its activity, stabilizing this structure. Based in P- type H+-ATPase activity (extrusion of H^+ to the apopplast) and how fusicoccin affect its activity, it can be concluded that either the pH-sensor is not sensitive to low pH, or that the methology used by Moseyko and Feldman was not the right one to obtain a real result. As for the results obtained in this project, the fact that the control treatment decreased the root pH could be considered an artifact since in later assays this effect was not seen. The acidification induced by vanadate reached the same values as the negative control, although the decreased pH was reached faster. This could mean that there is inhibition of the ATPase by vanadate, which elicits a cytosolic acidification, but this variation is not so significant as expected. Wigoda et al. (2017) proposed that the low inhibition observed in media with low potassium (as is the case in this experiment) could be due to the requirement of high K^+ which can participate in secondary H^+-cotransport dissipating the protons.How low K^+ can affect these experiments was no tested. The inhibition of the P- type H+-ATPase inhibit the proton motiveforce generation, maybe inhibitn the influx of ios that made the cytosol more basic.

In the tonoplast, since V-PPase is the ATPase with larger effect on luminal pH (Kriegel et al. 2015), it was proposed to be the one to be challenged in order to obtain effects in the cytosolic pH. To that end, concanamycin A, an inhibitor of the V-ATPase activity, was used as the modulator. The inhibition of the V-ATPase with concA would acidify the cytosol. Although to my knowledge there are no other studies measuring cytosolic pH after inhibition of the V-ATPase using concA. These experiments either show increased vacuolar pH or malfunction of the protein (Wang et al. 2007; Krebs et al. 2010; Shen et al. 2013; Kriegel et al. 2015). Even so, although the results obtained in this here correspond to those expected, the acidification is masked by observing that the control treatment produces the same acidification in the cytosol pH. Once again, this effect may be due to deficiencies in the protocol. The intensity of the laser or the strength / composition of the medium on which it is carried out can affect the result, the stability of the fluorophore or the medium stability.

Further studies using the specific inhibitors of the plasma membrane and measuring the pH variation in the tonoplast, and vice versa, should be done. This would give an idea on how the specific activity of membrane proteins of one organelle is affecting the conditions and environment of the entire cell. It should be also noticed that the variation observed in all the tissues are taken into consideration, even though differences among tissues and cell type have already been reported (Kiegle et al. 2000).

D.3.2. Cytosolic pH variations upon saline stress.

The same Arabidopsis lines expressing pHGFP-VTI11 and pHGFP-L16b were challenged with increasing concentrations of NaCl. Imaging analyses of the root cell showed that, unlike previous assays in which a acidification of the cytosol was observed (Gao et al. 2004; Schulte et al. 2006; Kader et al. 2007; Monshausen et al. 2007; D'Onofrio and Lindberg 2009), there was a alkalinization of the cytosol. Looking closer to previous experiments some obvious differences are seen respect to the herein performed: most of them are carried out in single cell systems, such as guard cells, root hairs and pollen tubes, or protoplasts (Gao et al. 2004; Schulte et al. 2006; Kader et al. 2007; Monshausen et al. 2007; D'Onofrio and Lindberg 2009), where complex cell-to-cell communication are limited. Even though only a segment of the root was chosen to analyze the pH variation (MEZ) in the root imaging experiments done in this project, it includes all the tissues in this zone. As previously mentioned, the proteins involved in salt tolerance have distinctive expression patterns in space and time, and the overall pH measured in these assay does not take this into consideration. Although other

analyses have been done in intact roots, the analyses is generally based in the study of one cell type or tissue (Moseyko and Feldman 2001; Fasano et al. 2001; Monshausen et al. 2011; Gjetting et al. 2012), or if the complete seedling is used, the analyzed stimulus varies along the root and not across the tissues (Rincón-Zachary et al. 2010; Waadt et al. 2017) .

In accordance with this, complete seedling pH-maps showed a differential alkalinization between the vasculature and the ground tissue. According to these assays, the measured alkalinization takes place mainly in the vasculature of the root, while the ground tissue was acidified. These results make evident that the pH variations measured are generated by the extrusion of Na^+ outside the grown tissue of the root, that may be or not accompanied by a increments of H^+ concentration. The lack of a calibration curve does not allow to determine whether the acidified values correspond to a decrease pH compared to the seedlings in normal conditions, or just compared to the vasculature in the same conditions.

The strategies to overcome salinity stress by plants can be divided in three mechanisms: extrusion of Na^+ outside the roots, compartmentalization of toxic ions into the vacuole and metabolicpH regulation. There have been described two main proteins to be the responsible in the extrusion of Na^+ out of the cell in Arabidopsis: SOS1 and HKT1(Shi et al. 2002; Shi and Zhu 2002; Sunarpi et al. 2005; Pardo 2010; Kronzucker and Britto 2011; Conde et al. 2011). It had already been described by Shi et al. (2002) an accumulation of Na^+ in Arabidopsis wild-type stem, which wasn't observed in the *sos1* mutant.

Upon NaCl treatement Na^+ influx to epidermal cells depolarizes the plasma membrane activating Ca^{2+} channels that allow an influx of this ion to the cytosol where it is sensored by Ca^{2+}dependent proteins like CBL and Cam/CML. Different signaling pathways are activated among which the SOS pathway is included. The activity of SOS1 extrude Na^+ in exchange of H^+, which is translocated to the cytosol. This new situation would explain the acidification observed in single cell pH measurements under salt stress (Moseyko and Feldman 2001; Gao et al. 2004; Monshausen et al. 2007). The membrane depolarization enhances P- type H+-ATPase activity, and it hyperpolarizes the membrane potential. The proton motive force generated across maintain SOS1 activity. Due to the high concentration of Na^+, part of the toxic ions can reach the xylem, or they do it using the apoplastic via.

AtHKT1,1, which is highly expressed in the xylem parenchyma cells, is the main protein associated to Na+ retrieval from the xylem into the xylem parenchyma cells to avoid excessive Na+ accumulation in the shoots (Berthomieu et al. 2003; Sunarpi et al. 2005; DAVENPORT et al. 2007) and prevent excessive loading of Na+ into the transpiration stream. Disruption of

AtHKT1;1 causes a higher accumulation of Na+ in the shoots but reduced concentration in roots, with little effect on the net Na^+ uptake (Pardo 2010; Kronzucker and Britto 2011). It is also true for rice OsHKT1;5 (Horie et al. 2012; Cotsaftis et al. 2012) and wheat TmHKT1;5D (Munns et al. 2012).

Differential gene expression is an important defining trait of salt stress tolerance in glycophytes. Lower expression of HKT1;1 in *S. dolichostachya*, a salt resistant glycophyte, compared to *S. oleracea*, salt sensitive, in roots is accompanied by a higher expression of SOS1 in shoots as well as Na^+ levels (Katschnig et al. 2015). This would mean SOS1 in shoots is the responsible for Na^+ unloading. Something similar was also shown for differential expression of HKT, involved in Na+ exclusion from the leaf, of two solanaceous species (Solanum scabrum-tolerant and S. melongena-sensitive) (Assaha et al. 2015) and two rice cultivars (CFX18-tolerant and Juma67-sensitive, Ueda et al., 2013). This makes evident the role of SOS1 not only extruding Na^+ to the apoplast but also in loading of Na+ into the xylem, and directing Na^+ towards specialized cells for ion accumulation. In resistant halophyte Thellugiella salsuginea (halophyte) a higher ThSOS1 expression is nonetheless associated to a lower Na^+ accumulation in shoots and roots (Oh et al. 2009).

In Arabidopsis thaliana SOS1 is expressed in the epidermal cells of the root tip and in the inner tissues surrounding the vasculature. The high epidermal expression is thought to be a protection barrier actively extruding Na^+ so that this ions do not reach the meristematic cells at the root tip that lack large vacuoles for Na^+ compartmentation (Shi 2002). Efflux in the root tip has been demonstrated (Fujimaki et al. 2015; Hamam et al. 2016). This would turn the root tip more acidic, however in these experiments the root tip has shown mainly basic pH. In both treated and no treated seedlings.

SOS1 expression in the inner tissues surrounding the vasculature tissue of roots, hypocotyls, inflorescence stems, and leaves, mainly in the pericycle and in other parenchyma cells bordering xylem vessels. In stem it is restricted to the parenchyma suggesting an important role of SOS1 in regulating long-distance Na^+ transport (Shi 2002). The basic pH measured in the seedlings vasculature can be explained by an accumulation of Na^+ in these tissues. Under mild salt stress, AtSOS1 expressed in the xylem parenchyma, activity is , mainly loading Na^+ into the xylem (50 mM NaCl), and no accumulation of the ions takes place in the vasculature (Shi et al. 2002; Oh et al. 2010). In the results obtained herein, it seems that Arabidopsis is able to cope with this concentration since no accumulation of the ion is observed in the vasculature, maybe because the activity of SOS1 together with HKT1,1 is

enough to overcome this mild stress. However, high concentrations of NaCl, the activity of AtSOS1 might be reversed, as previously described by Shi and collegues (2002), and it would be retrieving ions from the xylem gap to the parenchyma cells, together with HKT1,1 , generating a high accumulation of these ions in the stele as observed in the results from seedling pH maps.

AtSOS1 role in loading Na^+ into the xylem sap is an accepted mechanism in both glycophytes and halophytes (Shi et al. 2002; Munns and Tester 2008). However, the unloading activity is theoretically energetically costly for the plants (Munns and Tester 2008), thus creating energy deficits for other metabolic processes and consequently growth impairment (Malagoli et al. 2008; Britto and Kronzucker 2015; Hamam et al. 2016). Nontheless, it has already been observed by (Lacan and Durand) in soybean roots treated with NaCl. Na^+ was reabsorbed from xylem vessels in exchange for K^+ by coupling Na^+/H^+ and K^+/H^+ antiport activities at the xylem/symplast boundary. These two parallel transport processes were strongly linked because Na^+ in the xylem sap enhanced K^+ release, whereas increased xylematic K^+ prompted Na^+ reabsorption. In Arabidopsis, AtSOS1 activity could be associated to AtHAK5 in the stele (Gierth et al. 2005)

It has previously been described for fission yeast Na^+/H^+ antiporters (SOD2) reversible bidirectional activity, regulated by Na^+ concentration. Whether AtSOS1 is capable of doing it still needs to studied. It should be noticed as well that, besides the regulation via SOS pathway of this antiporter, MPK6 also regulates its activity (Yu et al. 2010). No physiological or biological context has been described for this phosphorylation, neither the precise phosphorylated residue nor the effect on SOS1 activity was determined. Quintero et al (2011) proposed that the motif RIDSPSK of SOS1, in which the S1136 is phosphorylated by SOS2, is the target of the MPK6 protein as well, so the putative phosphorylation of S1136 by MPK6 would prevent activation by SOS2 and the constitution of the CBL4-CIPK24-SOS1 complex needed for Na^+ extrusion. Probably, the phosphorylation by MAPK6 enables SOS1 to translocate Na^+ in the opposite direction by itself or in coordination with other proteins in the plasma membrane. Similar situation had aready been described for P- type H+-ATPase in which the phosphorylation of S391 by the SnRK3 PKS5 inhibits the interaction with an activating 14–3-3 protein to the T947 (Fuglsang et al. 2007). HsNHE1 interaction with CaM is also is inhibited by the phosphorylation of an onsite Ser (S648) by an B/Akt protein (Shigeo Wakabayashi et al. 1997)

The fact that no differences are observed between the pHGFP-LTI6b and pHGFP-VTI11 Arabidopsis lines would mean either in the cytosolic pH variations generated by the previously mentioned mechanism is being measured in all intracellular space, or in the protein transport activities of each membrane are generating the same effect in the cytosol.

To determine of the first case scenario is true, the previous mentioned crossed-measurements should be performed, e.g: inhibit P- type H+-ATPase and measure pH at the vacuolar membrane.

In the tonoplast two main proteins are believed to have some roleinchanging the cytosolic pH: V-ATPase, which activity translocating H^+ to the vacuolar lumen would alkalinize the cytosolic pH, and AtNHX, which activity would acidify the cytosolic pH, either it is translocating Na^+ or K^+ to the vacuolar lumen in exchange for H^+. According to the previous results, AtNHX1 would be fully active when the cytosolic pH reaches values near neutrality, and in the presence of Ca^{2+}. According to the seedlings' pH-maps, that would make AtNHX1 and AtNHX2 fully active at the stele in the roots, but no in the epidermis, at least under high Na^+ concentration. Moreover, the probable acidification generated by AtNHX1 could be masked by the activity of K^+ channels activated to maintain the cytoplsmatic K^+/Na^+ ratio, mainly TPK1 or Ca^{2+} channels (Latz et al. 2013; Shabala and Pottosin 2014).

However, activity of these protein in other tissues cannot be ruled out. AtCIPK24 has been described to be involved in the activation of AtNHX1 and V-ATPase at the vacuolar lever in companion of the AtCBL10. In this project, it has been shown that it is not AtNHX1 but AtNHX2 the K^+/H^+ antiporter that is being phosphorylated by CIPK24, presumably previous AtCBL10 recruitment and activation. Moreover, Andrés (2013) showed that both proteins are phosphorylated by AtMPK6. No additive nor exclusive relationship has been established among the different regulations that AtNHX proteins are subjected to. More analyses have to be done with respect to this differential regulation. A possible gradual or tissue specific regulation of the protein could be taking place under salt stress or normal conditions.

D.3.3. Implications of SOS3 mutant in cytosolic pH variations under salt stress.

The expression of free pHGFP was used to measure the variations of cytosolic pH unassociated o any organelle. The cytosolic pH measurement in wilt-typeArabidopsis lines

resembled the before mentioned results. However, when the measurements were done in a *sos3* mutant background different results were seen.

SOS3 functions primarily in roots activating the SOS pathway upon Ca^{2+} sensing in the cytosol. Although during vegetative development under salt stress CBL10 also interacts with CIPK24 to initiate slat tolerance signaling pathways, this complex is formed in the tonoplasto, and due to differential expression pattern, the later CBL could no complement the lack of CBL4 (Quan et al., 2007; Zhu, 2016). CBL4-CIPK24 complex mediate Na^+ extrusion via the regulation of the H^+/Na^+ antiporter SOS1 at the plasma membrane, and CBL10-CIPK24 association results in Na^+ sequestration into the vacuole (Kim et al., 2007; Quan et al., 2007). This means that the signaling pathway is only affected in the root, but no in leaves, as can be seen in the results. On the other hand, Held et al. (2011) revealed that CBL4 interacts with CIPK6 to translocate AtAKT2 from the ER to the plasma membrane in the pholematic parenchyma stele. In this location, translocates K^+ across the plasma membrane loading the phloem, so the induced movement of nutrients and water from the shoots to the rootsavoids the latter to collapse (Szyroki et al. 2001; Deeken et al. 2002; Gajdanowicz et al. 2011; Sandmann et al. 2011; Held et al. 2011).

The la3ck of CBL4 render both, pathways inactive. In the first case, there would be no extrusion of Na^+ from the epidermis, which would in turn generate no H^+ gradient for P- type H+-ATPase to be activated. As a result, an alcalinization of the epidermis and cortex would take place, as it can be seen. The toxic concentrations of Na^+ that cannot be compartmentalized would arrive to the stele without any control, and to the xylem, with little to no retrvial to the xylem parenchyma cells, when arriving to the shoot, Na^+ generating the known toxic effect in plant shoots. The lack of alkalinization can also be explained by the lack of K^+ loading to the phloem directed by the CBL4-AtAKT2 (Deeken et al. 2002). Moreover, the accumulation of nutrients is also lost or diminished. Moreover, It should be observed that in the S1 if *sos3* mutants, the differences of pH among the different tossues seems to be completely lost, and cell have collapsed. The latter comple

x, which should avoid it is not working. In addition, in this zone (MEZ) the lack of the the casparian strip turns it more sensitive to the osmotic stress. In all the seedlings this segment seems to be crowded with swelling cells that have explode.

D.4. Phenotypation of *nhx3 nhx4* single and double mutants

The Arabidopsis genome encodes eight NHX homologs that have been grouped based on sequence similarity, subcellular location and function into three distinct classes: plasma membrane (NHX7/SOS1 and NHX8), endosomal (NHX5, NHX6), and vacuolar (NHX1, NHX2, NHX3, NHX4) (Brett et al. 2005a; Pardo 2010; McCubbin et al. 2014). Among the vacuolar ones, AtNHX1 and AtNHX2 have been the most studied due to their implication in K^+ homeostasis, salt resistance and stomatal movement. However, they have strong sequence homology with AtNHX3 and AtNHX4 (Yokoi et al. 2002). The quadruple mutant *nhx1 nhx2 nhx3 nhx4* has been studied by McCubbin et al. (2014), but these authors only reported that the quadruple mutant had a more pronounced phenotype than the double mutant *nhx1 nhx2*, and no specific description of *nhx3* and *nhx4* mutants was given. These results could mean that AtNHX3 and AtNHX4 have redundant functions with AtNHX1 and AtNHX2 and not to have a discernable activity per se. However, Liu et al. (2010) proposed that AtNHX4 is necessary for growth in low K^+ conditions, and they mentioned that no differences of the *nhx4* with the wild type were found under salt stress, but data was not shown. On the other hand, Li et al. (2009) reported that mutant *nhx3* was more resistant to salt stress. Because of these conflicting reports and considering the differential expression patterns of the vacuolar AtNHX members observed in other studies, we reasoned that NHX3 and NHX4 might have specific roles in different developmental stages (Yokoi et al. 2002; Wang et al. 2007; Li et al. 2009; LIU et al. 2010). To test this hypothesis, we generated and studied single and double *nhx3 nhx4* mutants to better understand the function of these proteins in Arabidospsis.

The Arabidopsis lines bearing single *nhx3* and *nhx4*, and double *nhx3 nhx4* mutations did not show differential germination in LAK medium supplemented with increasing concentrations of NaCl, but seedling survival after 21 days showed that the double mutant *nhx3 nhx4* and single mutant *nhx3* were less resistant to high NaCl concentrations, while the single mutant *nhx4* had the same phenotype as Col-0 wild-type. Root growth under salt treatment showed similar results (Figure 47). After 21 days growing in LAK medium with different concentrations of NaCl, mutant lines *nhx3* and *nhx3 nhx4* showed significant better performance than the wild-type Col-0 and the single mutant *nhx4* in control conditions. However, with increasing concentrations of NaCl, the resistance showed by the single mutant *nhx4* was significantly better than that of Col-0 and *nhx3*. The phenotype observed for the double mutant changed this time, and was more similar to *nhx4* mutant phenotype with increasing concentrations of NaCl.

In summary, according to our results the *nhx4* mutant is more resistant than wild-type Arabidopsis to salt stress conditions, while *nhx3* is more sensitive. This could be explained by the differential expression described for these proteins. In the case of AtNHX3, different patterns have been reported. Wang et al (2007) showed that AtNHX3 is mainly expressed in flowers, but Li et al (2009) showed a strong expression in 10-day-old seedlings and in stems. Thus, germination should not be affected by the *nhx3* mutation because the protein would not be expressed at this developmental stage. Survival of seedlings however could be affected by the lack of *AtNHX3* if this gene were expressed in Arabidopsis roots from day-20 onwards. The lack of the NHX3 protein could render seedlings sensitive to increasing NaCl treatment.

According to Wang et al (2007), *AtNHX4* is highly expressed in root vascular bundles during the early stages of the plant development, and in germinating seeds. Liu et al (2010) showed high expression in flowers, mainly in anther and pollen grains. Again, it would be expected that the lack of AtNHX4 rendered mutant seedlings sensitive to NaCl. Considering the expression patterns proposed by Wang et al. (2007) in which AtNHX3 is not expressed in root seedlings, in *nhx4* mutant lines only AtNHX1 and AtNHX2 would be functioning in the vacuole. According to previous publications, these proteins and AtNHX4, have functional redundancy (Barragán et al. 2012; McCubbin et al. 2014), moreover, Yokoi et al. (2002) reported that the expression of AtNHX4 was low, reason why the expected observed phenotype in this mutant line would be similar to the wild type, as observed in the germinations and survival assays. However, our results indicate an enhanced tolerance to NaCl. The difference observed with the wild-type line, could be explained by an increased expression of AtNHX1 and AtNHX2, which at the same time would be incremented by NaCl induction (Yokoi et al. 2002). Overexpression of AtNH1 have been largely studied and demonstrated to increase salt tolerance in arabidopsis and other species (Apse et al. 1999; Zhang and Blumwald 2001; Apse and Blumwald 2007; LIU et al. 2008; Wu et al. 2009; Kronzucker and Britto 2011), if its expression is being over-induced in the *nhx4* mutant line, it could be enhancing the plant resistance to NaCl Other possibility would be the proposed by Li et al (2009) for the resistant phenotype they observed in *nhx3* mutant. Applying their hypothesis in AtNHX4, in wild-type lines, this antiporter would be extruding Na from the vacuole to the cytosol. However, this is little probable since it has been demonstrated that AtNHX4 is stable and functional when expressed in onion cells, , making evident that the mechanism of action is the same as AtNHX1 and AtNHX2.

Li et al. (2009) had reported that the *nhx3* mutation conferred salt tolerance to Arabidopsis under salt stress. These results could not be confirmed here. The *nhx3* mutant phenotype is

similar to that of the wild-type (Figure 47). However, the experimental conditions are different. Altough the growth medium used by Li and colleagues was free of K^+, it was MS based modified medium (1/20-strength MS major salts and 1 ¥ MS minor salts) solidify with agarose. Morever, seeds were incubated in a growth under short-day conditions (12 h light/12 h dark). In our experimental setup, seeds were sawn in LAK medium with PhytAgar, and grown in long day conditions

When$^+$ when growing in low potassium medium, no significant differences were observed between the wild-type and the single mutants *nhx3 and nhx4*,or the double mutant *nh3 nhx4*.Root growth on the other hand show significant differences among mutants and col-0 either, maybe due to the previously mentioned redundancy expression and function with AtNHX1 and AtNHX2. Phenotypically the seedlings did not show any significant traits. The lack of phenotypes is not surprising. Previously, single mutants *nhx1* and *nhx2* had been shown to not have phenotypes maybe due to a redundancy of the vacuolar NHX function (Leidi et al. 2010). Moreover, Basil et al (2011) showed that the quadruple mutant *nhx1 nhx2 nhx3 nhx4* had enhanced phenotypes compared to the double mutant *nhx1 nhx2*, but this effect could be masked in the *nhx3 nhx4* mutant because the predominant role of the nearly ubiquitous and most abundant proteins AtNHX1 and AtNHX2 (Barragan et al, 2012).In any case, additional experiments are required to accurately demonstrate the expression pattern and regulation of AtNHX3 and AtNHX4, mainly in the early stages of development in order to better understand the phenotypes observed and their main function. The results reported herein previous publication (LIU et al. 2008, 2010; Li et al. 2009) show that these proteins seem to have evolved to have ans specific role in Arabidopsis.

D.4.1. Implication of NHX3 in flowering time and flower development.

Wang et al. (2007) reported that *AtNHX3* is mainly expressed in petals. In addition to this, the unusual behavior of this protein, which was unable to suppress the sensitivity of AXT3K cells to HygB and could not be expressed in onion cells as an GFP-translational fusion to determine subcellular localization (B. Cubero and JM Pardo, unpublished) indicated that this protein could have significant functional differences relative to other vacuolar AtNHXs. NHX proteins with specific expression in flowers or fruits have important roles in K^+ accumulation in their locations (Yamaguchi et al. 2001; Hanana et al. 2007; Yoshida et al. 2009). Specifically, in the case of *Ipomea nil* and *Ipomea tricolor*, the NHX1 protein is expressed in the vacuolar

membrane of petal limbs regulating vacuolar pH and petal color, an essential trait for the reproductive cycle of these plants. More interestingly, the activity of these proteins produced vacuolar alkalinization in petals, with a large pH shift of up to +1.1 units (Morita and Hoshino 2018). This is a large variation in comparison to the ones observed linked to AtNHX activity in Arabidopsis seedlings, that has been reported to account for pH shifts between 0.5 – 0.8 units by comparing the double mutant nhx1 nhx2 with wild-type plants (Bassil et al. 2011c; Andres et al. 2014; Reguera et al. 2015). Taking all this into consideration, we hypothesized that AtNHX3 could have a mechanism of action similar to *Ipomeoa's* NHX proteins with special function in flowering time or flower development. However, we demonstrated that neither *nhx3* and *nhx4* single mutants, nor the *nhx3 nhx4* double mutant had any effect in flowering time r flower opening. As previously described for *Ipomea nil*, the lack of expression of the vacuolar NHX did not inhibit cell expansion and flower opening (Yamaguchi et al. 2001; Pittman 2012), meaning even if AtNHX3 contributed to this process, other mechanisms are also involved. For instance, the reduced vacuolar NHX antiport activity in the *nhx1 nhx2* mutant was detrimental for the opening and closing of the stomata. However, reduced and delayed stomatal movements remained in the mutant that were proposed to be mediated by the influx of osmotically active solutes such as sugars and organic acids (Andrés et al., 2014). The double mutant *nhx1 nhx2* has been described to display significant phenotypes in their reproductive organs (Bassil et al. 2011c), but rather than related to flower opening or petal size they were more related to reproductive traits, such as low number of siliques with few or no seeds, shorter and narrower flowers, stamens with shorter filaments, o non-dehiscent anthers.

To determine if AtNHX3 or AtNHX4 contributed to turgor generation for cell expansion in petals, the area of the petals was measured in *nhx3* and *nhx4* mutants. Although the result showed that the petal size of the single mutants *nhx3* and *nhx4* did not significantly differ from the wild type Col-0, the double mutant showed significantly largerpetal area then the wild-type and single mutant lines. Unfortunately, it was no possible to study weather this difference was due to a variation in the cells size or cell number in petals. However, there is no previous evidence that vacuolar NHX proteins could affect the number of cells in petals, but the nhx1 nhx2 mutant showed reduced cell sizes in leaves (Barragán et al., 2012). Therefore, we suggest that the difference observed is due to increased cell/vacuolar size in the double *nhx3 nhx4* mutant. Whether the lack of expression of AtNHX3 and AtNHX4 in flowers might induce the expression of other solute transporters that help in petal extension and flower opening should be studied. In guard cells the main solutes involved in the

osmoregulation process are sucrose, K^+, and accompanying anions (malate and chloride), depending on the environmental conditions and time of the day (Andres et al. 2014), and it can be assumed that these would be implicated in petals expansion as well. The Arabidopsis CHX20 is a putative K+/H+ exchanger that appears to play a role in guard cell osmoregulation through K+ fluxes and possibly pH modulation (Padmanaban et al. 2007). Little is known about the function of most CHX proteins, but it should be no ruled out the possibility of their implication in petal extension because they are expressed in flower organs and in pollen where they contribute to extension of the pollen tube (Sze et al. 2004)

Considering that the main function of Ipomea's NHX1 in flower development is the change in vacuolar pH, pHvac was measured in Arabidopsis petals using the BCECF method. The results showed that *nhx3* single mutant and double mutant *nhx3 nhx4* had a more acidic pH in comparison with the wild-type line. Moreover, *nhx4* single and the *nhx1 nhx2* double mutant had intermediate pH values. This in accordance to the expected results considering the expression of *AtNHX3* in flowers (Wang et al. 2007). The abscense of AtNHX3 would diminish K+ influx into the vacuole in petals, being these cells unable to alkalinize the lumen. The phenotype observed in the double mutant *nhx1 nhx2* could be explained by the reported expression of *AtNHX1* and *AtNHX2* in the stomata of petals, which might me altering somehow the size of petals (Shi and Zhu 2002; Barragán et al. 2012). Apse and Blumwald (2003) also identified *AtNHX1* mRNA in petal epidermis, but no reference to the cell type in which it was expressed or their size was given. A similar situation was described for *Ipomoea nil* and *Ipomoea tricolor.* In the *nhx1* mutant of *I.nil*, the petals reddish-purple buds become purple open flowers instead of blue flowers, and the cells' vacuolar pH have a partial increase, indicating that there must be genes other than InNHX1 that mediate vacuolar alkalization in the flowers (Yamaguchi et al. 2001). Ohnishi et al. (2005) showed that in *I. nil* the protein InNHX2, which is expressed mainly in leaves, stems and roots, has a low and time limited expression in petals before flower opening. This protein accumulates Na^+ and K^+ in the vacuole, being the responsible for the partial alcalinization observed in the *nhx1* mutant. Based in this, it is probable that other vacuolar AtNHX o AtCHX have a role in the pHvac of petals, which could explain the intermediate pHvac of XXX. However, AtNHX3 seems to be InNHX1 orthologue which has evolved to specifically modify petals pH, with a pollination and reproduction role (Morita and Hoshino 2018). In summary, our results indicate that AtNHX3 is the most critical protein responsible for the control of the vacuolar pH in the petals of Arabidopsis.

CONCLUSIONS

1- The topological and ternary models of AtNHX1 indicate that this plant protein conserves the structural features characteristic of microbial and mammalian members of the CPA superfamily, consisting of cytosolic N- and C-terminal ends, twelve transmembrane segments arranged in an antiparallel manner and the distinctive Nha-fold at the active center.

2- Several conserved amino acids that are essential for the activity of AtNHX1 have been identified at the active site and the Nha-fold. These residues are the T156 and D157 of the TD-motif in TM4, D185 of the ND-motif in TM5,, and arginines R353 and R390 in in TM10 and TM11, respectively. Residue N184 at the ND-motif that is highly conserved in electroneutral antiporters of the CPA1 family is not essential for the activity of AtNHX1, at least in the heterologous system used to validate the functionality of mutated AtNHX1 proteins.

3- In agreement with the proposed function in planta, AtNHX1 can regulate vacuolar pH in yeasts cells, and the expression of mutant mutant in the conserved amino acids of the Nha-fold generate pH differences in the yeast vacuole.

4- Calmodulin-binding domains that mediate interaction with CML18 have been identified at the C-terminal cytosolic extensions of AtNHX1 and AtNHX2, to two major K+/H+ exchangers in Arabidopsis vacuoles. This interaction takes places in the cytosol and not in the vacuolar lumen as previously reported.

5- The calmodulin-binding domain of AtNHX1 is essential for protein activity. The highly conserved residue D506, but not H499, at the core of the calmodulin binding domain is essential for the interaction of AtNHX1 and CML18 and for protein activity.

6- A model is proposed in which the calmodulin binding domain of AtNHX1 integrates a cis-regulation by cytosolic pH and the trans-regulation by CML18 and calcium. According to this model, CML18 binding stimulates K+/H+ antiport at the tonoplast as long as the cytosolic pH is not exceedingly acidic, in which case protonation of H499 promotes the formation of a salt bridge with D506, thereby hindering the binding of CML18 to restrain further ion exchange and the release of protons into the cytosol.

7- Genetically encoded ratiometric pH-sensors based on pHGFP fused to markers of different cellular membranes is a suitable to generate cytosolic pH-maps of Arabidopsis thaliana seedling that excellent resolution in time and space.

8- The SOS3/CBL4 is generally regarded as a critical sensor protein of salinity stress, and the pH-maps of sos3 mutant demonstrate that dynamic variations of cytosolic pH induced by salinity in wild-type seedlings are largely absent in the mutant.

9- AtNHX3 and AtNHX4 are vacuolar proteins with specific roles in Arabidopsis development. AtNHX3 has an important role in the regulation of vacuolar pH of petals cells.

ANNEXES

Annex 1

Abbreviations

ABA	Abcisic acid
AD	Activation domain
AP	Arginine phosphate medium
APS	Amonic perfulphate
ATP	Adenosine-5'-triphosphate
Asn or N	Asparragine
Arg or R	Arginine
Asp or D	Aspartic acid
BCECF-AM	(2',7'-Bis-(2-Carboxyethyl)-5-(and-6)-Carboxyfluorescein, Acetoxymethyl Ester)
BD	Binding domain
BiFC	Bimolecular fluorescence complementation
bp	Basepair
BSA	Bovine serum albumin
BTP	Bis-tris propane buffer
Ca^{2+}	Calcium
cDNA	Complementary deoxyribonucleic acid
CDS	Coding sequence
cm	Centimetre
Col-0	*Arabidopsis thaliana* cv Columbia wild type
CTAB	Hexadecyltrimethylammonium bromide
DEPC	Diethil pirocarbonate
DNA	Deoxyribonucleic acid
dNTP	Deoxynucleotide triphosphates
DTT	Dithiothreitol
EDTA	Ethylenediaminetetraacetic acid
ER	Endoplasmic reticulum
g	Gram
GFP	Green fluorescent protein
Glu or E	Acid glutamic
GST	Glutathione S-transferase
GUS	Beta-glucuronidase
GTE	Glucose-Tris-EDTA
h	Hour
H^+	Hydrogen or protons
His	Histidine
Hyg	Hygromycin
IC	Intracellular
IPTG	Isopropil-d-D-tiogalactopiranosid
K^+	Potassium
Kan	Kanamycin

Ka	Dissociaton constant
kb	Kilobase
kDa	Kilodalton
KIRC	Inward-rectifier K^+ channel
KO	*Arabidopsis thaliana nhx1-2 nhx2-1* mutant line
KORC	Outward-rectifier K^+ channel
kV	Kilovolts
L	Litre
LAK	Modified Long Ashton mineral solution
LB	Luria-Bertani medium for bacteria growth
Leu	Leucine
Lys or K	Lysine
m	Meter
mA	Milliampere
MES	2-(*N*-morpholino)ethanesulfonic acid
mg	Milligram
min	Minute
mL	Millilitre
mm	Millimetre
mM	Millimolar
MS	Murashige & Skoog medium for plant growth
mV	Millivolts
MVBs	Multivesicular bodies
N	Normal
Na^+	Sodium
NADPH	Nicotinamide adenine dinucleotide phosphate
NH_4^+	Amonium
nm	nanometre
nM	Nanomolar
NO_3^-	Nitrate
OD	Optical density
PCR	Polymerase chain reaction
PEG	Polyethylene glycol
PLATE	Solution for yeast transformation (PEG-lithium acetate-Tris-EDTA)
PM	Plasma membrane
PM-ATPase	Plasma membrane atpase
PM-PPase	Plasma membrane pirophosphatase
PMSF	Phenylmethylsulfonyl fluoride
PVC	Pre-vacuolar compartment
RNase	Ribonulclease
RNA	Ribonucleic acid
rpm	Revolutions per minute
ROS	Reactive oxygen species
RT-PCR	Reverse transcription polymerase chain reaction

s	Second
SDS	sodium dodecyl sulfate
SDS-PAGE	SDS polyacrylamide gel electrophoresis
Ser or S	Serine
SOB	Super optimal broth medium
SOC	Super optimal broth with catabolite repression medium
TAE	Tris acetate-sodium acetate-EDTA
Taq polymerase	DNA polymerase isolated from the bacterium *Thermus aquaticus*
TBS	Tris-buffered saline
T-DNA	Transfer DNA
TE	Tris:EDTA
TEMED	Tetramethylethylenediamine
TGN	Trans-Golgi network
Thr or T	Threonine
Tm	Melting temperature
TM	Transmembrane domain
Thr	Threonine
Trp	Tryptophan
Ura	Uracil
U	Enzyme unit
V	Volts
v	Volume
V-ATPase	Vacuolar atpase
V-PPase	Vacuolar pirophosphatase
w	weight
Y2H	Yeast two-hybrid
YEP	Yeast Extract Peptone medium for *Agrobacterium* growth
YFP	Yellow fluorescent protein
YNB	Yeast-nitrogen-base medium for yeast growth
YPD	Yeast-peptone-dextrose medium for yeast growth
X-Gluc	5-bromo-4-chloro-3-indolyl glucuronide
µL	Microliter
µM	Micromolar
µmol	Micromol

Annex 2

1- Vectors used:

Cloning Vectors				
Vector	**Reference**	**Organism**	**Slection marker**	**Use**
pBluescript II SK (+/-)	Stratagene	Bacteria	Ampicilin	Gene clonation and conservation. Template for point mutations and deletion PCR
pSparkI	Canvax Biotech	Bacteria	Ampicilin	

Expression vectors					
Vector	**Reference**	**Organism**	**Selection marker**	**Promotor/ Terminator**	**Use**
pGEX2TK	GE healthcare	Bacteria	Ampiciline	*TAC/TAC*	GST fusioned protein expression in bacteria
pCDF-Duet	Novagen (EMD Millipore)	Bacteria	Streptomycin/ Spectinomycin	*T7/T7*	RGS6xHis fusioned protein expression inbacteria
pDR195	Rentsch *et al*., 1995	Yeast (multicopy) /bacteria	URA3/ Ampicilin	*PMA1*/ *ADH1*	Gene expresion in *S. cerevisiae*
pGADT7	Clontech	Yeast (multicopy) /bacteria	LEU2/ Amplicilin	*ADH1/ ADH1*	Y2H assay
pGBKT7	Clontech	Yeast (multicopy) /bacteria	TRP1/ Kanamycin	*ADH1/ ADH1*	Y2H assay

Binary vectors

Vector	Reference	Organism	Selection marker	Promotor/ Terminator	Use
pSPYNE173	Waadt et al. (2008)	Plantas/ Bacterias	Kanamycin	*CaMV35S*/ *NOS*	Transient expression in Nicothiana benthamiana. BIFC assay
pSPYCE (M)	Waadt et al. (2008)	Plantas/ Bacterias	Kanamycin	*CaMV35S*/ *NOS*	Transient expression in Nicothiana benthamiana. BIFC assay

2- Constructions generated and used:

Y2H assay

Vector	Reference	Replicaction	Selection marker	Promotor/ Terminator
pSpark-NHX1ct	Present work	Bacteria	Ampicilin	T7/T7
pSpark-NHX1ΔBDct	Present work	Bacteria	Ampicilin	T7/T7
pSpark-CML18	Present work	Bacteria	Ampicilin	T7/T7
pGADT7-CML18	Present work	Yeast (multicopy)/ bacteria	LEU2/ Amplicilin	ADH1/ADH1
pGBKT7-NHX1ct	Present work	Yeast (multicopy)/ bacteria	TRP1/ Kanamycin	ADH1/ADH1
pGBKT7-nhx1ΔC5ct	Present work	Yeast (multicopy)/ bacteria	TRP1/ Kanamycin	ADH1/ADH1
pGBKT7- nhx1ΔC6ct	Present work	Yeast (multicopy)/ bacteria	TRP1/ Kanamycin	ADH1/ADH1
pGBKT7- NHX2ct	Andrés, Z (2013). Thesis dissertation	Yeast (multicopy)/ bacteria	TRP1/ Kanamycin	ADH1/ADH1
pGBKT7-nhx1ΔBDct	Present work	Yeast (multicopy)/	TRP1/	ADH1/ADH1

		bacteria	Kanamycin	
pGBKT7-NHX1D506Nct	Present work	Yeast (multicopy)/ bacteria	TRP1/ Kanamycin	ADH1/ADH1
pGBKT7-NHX1H499Lct	Present work	Yeast (multicopy)/ bacteria	TRP1/ Kanamycin	ADH1/ADH1
p53	Clontech	Yeast (multicopy)/ bacteria	LEU2/ Amplicilin	ADH1/ADH1
pSV40	Clontech	Yeast (multicopy)/ bacteria	TRP1/ Kanamycin	ADH1/ADH1

BIFC assay

Vector	**Reference**	**Replicaction**	**Selection marker**	**Promotor/ Terminator**
pSPark-NHX1ΔBD	Present work	Plant/ Bacteria	Ampicilin	
pSPYCE(M)-CML18	Present work	Plant/ Bacteria	Kanamycin	*CaMV35S*/*NOS*
pSPYNE173-CML18	Present work	Plant/ Bacteria	Kanamycin	*CaMV35S*/*NOS*
pSPYCE(M)-NHX1	Andrés, Z. (2013). Thesis dissertation	Plant/ Bacteria	Kanamycin	*CaMV35S*/*NOS*
pSPYCE(M)-NHX2	Andrés, Z. (2013). Thesis dissertation	Plant/ Bacteria	Kanamycin	*CaMV35S*/*NOS*
pSPYNE173-NHX1	Andrés, Z. (2013). Thesis dissertation	Plant/ Bacteria	Kanamycin	*CaMV35S*/*NOS*
pSPYNE173-NHX2	Andrés, Z. (2013). Thesis dissertation	Plant/ Bacteria	Kanamycin	*CaMV35S*/*NOS*
pSPYNE173-nhx1ΔBD	Present work	Plant/ Bacteria	Kanamycin	*CaMV35S*/*NOS*

Vector	Reference	Replicaction	Selection marker	Promotor/ Terminator
pSK-NHX1-RGS6xHis	Present work	Bacteria	Ampicilin	
pDR-NHX1-RGS6xHis	Present work	Yeast (multicopy)/ bacteria	URA3/Ampicilin	*PMA1*/ *ADH1*
pSPark-nhx1ΔBD-RGS6xHis	Present work	Bacteria	Ampicilin	
pDR-ABD	Present work	Yeast (multicopy)/ bacteria	URA3/Ampicilin	*PMA1*/ *ADH1*
pDR-AtNHX1 mutant alleles generated for the present work. Detailled in Materials and methods (section)				
pGEX-nhx1BD fragment	Present work	Detailled in Materials and methods (section M.4.1)		
pCDFDuet-CML18	Present work	Detailled in Materials and methods (section M.4.1)		

Annex 3

Oligos used.

1- Genotipation PCR

Primer	Sequence	Gene
gen_NHX3-FW	GCTGGATTGCTCAGTGCTTT	AtNHX3
gen_NHX3-RV	TTGTAGTTCACGGATCAAAACC	AtNHX3
gen_NHX4-FW	CGTGGTGAAATAGGTCGCTG	AtNHX4
gen_NHX4-RV	CACACCAAAGGACATGATGG	AtNHX4
LBa1	TGGTTTCACGTAGTGGGCCATCG	T-DNA of pROK
LB3	TAGCATCTGAATTTCATAACCAATCTCGATACAC	T-DNA of pDAP101

2- Cloning and mutagenesis

Primer	Sequence	Gene
NHX1-BD BamHI FW	GGATCCCACCAGAACGCCACC	AtNHX1-BD
NHX1-BD NotI nonstop RV	GCGGCCGCACCTCCAAAGACGG	AtNHX1-BD
CML18 EcoRI FW	GAATTCGATGAGCTGCGACGGAGGC	AtCML18
CML18 NotI nonstop RV	GCGGCCGCACCCCAAGCATTATC	AtCML18
NHX1ct EcoRI FW	GAATTCACCAAACCACTCATAAGC	AtNHX1ct
NHX1 BamHI RV	GGATCCTCACCTTACTAAGATCAGGAG	AtNHX1
NHX1 FW SpeI	ACTAGTATGTTGGATTCTCTAGTG	AtNHX1
NHX1 nonStop XhoI RV	CTCGAGCCTTACTAAGATCAGGAG	AtNHX1
NHX1 BD deletion FW	ACACGGCCCACTCGAGGTCGTGGCTTTGTA	AtNHX1ABD
NHX1 BD deletion RV	TACAAAGCCACGACCTCGAGTGGGCCGTGT	AtNHX1ABD
CML18 EcoRI Fw	CGGAATTCATGAGCTGCACGGAGGC	AtCML18
CML18 BamHI Rv	CGGGATCCTCAACCCCAAGCATTATCAAAGGC	AtCML18
NHX1 SpeI FW	ACTAGTATGTTGGATTCTCTAGTG	AtNHX1
NHX1 XhoI nonStop RV	CTCGAGCCTTACTAAGATCAGGAG	AtNHX1
CML18 SpeI FW	ACTAGTATGAGCTGCGACGGAGGC	AtCML18
CML18 KpnII nonstop RV	GGTACCACCCCAAGCATTATC	AtCML18

Annex 4..

Pairwaise alignments of AtNHX1 with the best fitting templates from SwissModel.

AtNHX1 PaNhaP_4cza.1.A (CLUSTAL pairwise)

```
NHX1_seq      MLDSLVSKLPSLSTSDHASVVALNLFVALLCACIVLGHLLEENRWMNESITALLIGLGTG   60
4cza.1.A      ----------------------------LILFTGVISMLISRRTG-ISYVPIFILTGLVIG   32
                                                  TM-I           TM-II

NHX1_seq      VTILLISKGKSSHLLVFSEDLFFIYLLPPIIFNAGFQVKKKQFFRNFVTIMLFGAVGTII   120
4cza.1.A      PLLKLIPRD----LAHEIFDFVRVFGLVIILFTEGHNLSWRLLKKNMPTIVTLDTIGLIL   88
                      TM-III                                  TM-IV

NHX1_seq      SCTIISLGVTQFFKKLDIGTFDLGDYLAIGAIFAATDSVCTLQVLNQDETP-LLYSLVFG   179
4cza.1.A      TALIAGFIFKVVFN------SSFLLGFLFGAIIGATDPATLIPLFRQYRVKQDIETVIVT   142
                                          TM-V

NHX1_seq      EGVVNDATSVVVFNAIQSFDLTHLNHEAAFH-----------LLGNFLYLFLLSTLLGAA   228
4cza.1.A      ESIFNDPLGIVLTLIAISMLVPGYGGGI-FSTLSEKLGIYAGGVIYFLYNVSVSISLGIF   201
                 TM-VI                                       TM-VII

NHX1_seq      TGLISAYVIKKLYFGRHSTDREVALMMLMAYLSYMLAELFDLSGILTVFFCGIVMSHYTW   288
4cza.1.A      LGILGYKFIKRTGIF--DFPEIEAFSLSLAFLGFFIGERLDASGYLVATVTGIVLGNYKL   259
                TM-VIII                                 TM-IX

NHX1_seq      HNVTESSRI---------TTKHTFATLSFLAETFIFLYVGMDALDIDKWRSVSDTPGTSI   339
4cza.1.A      LKPRENIRILKRLQRAIEKEVHFNDTLAALATIFIFVLLGAEMN-LEVIWSN-------L   311
                                        TM-X

NHX1_seq      AVS-SILMGLVMVGRAAFVFPLSFLSNLAKKNQSEKINFNMQVVIWWSGLMRGAVSMALA   398
4cza.1.A      GKGLLVALGVMILARPLATLPLLK----------WWNFREYLFIALEG-PRGVVPSALA   359
                  TM-XI                                     TM-XII

NHX1_seq      YNKFT-----RAGHTDVRGNAIMITSTITVCLFSTVVFGMLT    435
4cza.1.A      SLPLSLALKYKSPLLTVHWGEIIMATVVITVLTSVIVETLW-    400
                             TM-XIII
```

AtNHX1 MjNhaP1_4cz81b (CLUSTAL pairwise)

```
NHX1      MLDSLVSKLPSLSTSDHASVVALNLFV-ALLCACIVLGHLLEENRWMNESITALLIGLGT  59
NhaP      ----------------------SLAEALFLILFTGVISMLISRRTG-ISYVPIFILTGLVI  42
                                 TM-Ia              TM-Ib

NHX1      GVTILLISKGKSSHLLVFSEDLFFIYLLPPIIFNAGFQVKKKQFFRNFVTIMLFGAVGTI 119
NhaP      GPLLKLIPRD----LAHEIFDFVRVFGLVIILFTEGHNLSWRLLKKNMPTIVTLDTIGLI  98
                           TM-II                        TM-III

NHX1      ISCTIISLGVTQFFKKLDIGTFDLGDYLAIGAIFAATDSVCTLQVLNQDETP-LLYSLVF 178
NhaP      LTALIAGFIFKVVF------NSSFLLGFLFGAIIGATDPATLIPLFRQYRVKQDIETVIV 152
                                       TM-IV

NHX1      GEGVVNDATSVVVFNAIQSFDLTHLNHEAAFHL-LG----------NFLYLFLLSTLLGA 227
NhaP      TESIFNDPLGIVLTLIAISMLVPGYGG-GIFSTLSEKLGIYAGGVIYFLYNVSVSISLGI 211
                TM-V                                    TM-VI

NHX1      ATGLISAYVIKKLYFGRHSTDR--EVALMMLMAYLSYMLAELFDLSGILTVFFCGIVMSH 285
NhaP      FLGILGYKFIKRTG----IFDFPEIEAFSLSLAFLGFFIGERLDASGYLVATVTGIVLGN 267
                                    TM-VII               TM-VIII

NHX1      YTWHNVT--ESSRI-------TTKHTFATLSFLAETFIFLYVGMDALDIDKWRSVSDTPG 336
NhaP      YKLLKPRENIRILKRLQRAIEKEVHFNDTLAALATIFIFVLLGAEMN-LEVIW----S-- 320
                              TM-IX

NHX1      TSIAVSSILMGLVMVGRAAFVFPLSFLSNLAKKNQSEKINFNMQVVIWWSGLMRGAVSMA 396
NhaP      NLGKGLLVALGVMILARPLATLP-LL-----K----WWN-FREYLFIALEG-PRGVVPSA 368
                     TM-X                                TM-XI

NHX1      LAYNKFT-----RAGHTDVRGNAIMITSTITVCLFSTVVFGMLTKPLISYLLPHQNATTS 451
NhaP      LASLPLSLALKYKSPLLTVHWGEIIMATVVITVLTSVIVETLWIPILKDKLDV------- 421
                                    TM-XII

NHX1      MLSDDNTPKSIHIPLLDQDSFIEPSGNHNVPRPDSIRGFLTRPTRTVHYYWRQFDDSFMR 411
NhaP      ------------------------------------------------------------

NHX1      PVFGGRGFVPFVPGSPTERNPPDLSKA 538
NhaP      ---------------------------
```

AtNHX1 vs NapA_4bwz (CLUSTAL pairwise)

```
NHX1_seq  ALNLFVALLCACIVLGHLLEENRWMNESITALLIGLGTGVTILLISKGKSSHLLVFSEDL 81
4bwz.1.A  ----IFYLLLAAQVCAFIFKRLN-QPVVIGEVLAGVLVGPALLGL--VHEGE----ILEF 58
                 TM-I1                TM-I

NHX1_seq  FFIYLLPPIIFNAGFQVKKKQFFRNFVTIMLFGAVGTIISCTIISLGVTQFFKKLDIGTF 141
4bwz.1.A  LAELGAVFLLFMVGLETRLKDILAVGKEAFLVAVLGVALPFLGGY-LYGLEI------GF 111
               TM-II                          TM-III

NHX1_seq  DLGDYLAIGAIFAATDSVCTLQVLNQDE-TP-LLYSLVFGEGVVNDATSVVVFNAIQSFD 199
4bwz.1.A  ETLPALFLGTALVATSVGITARVLQELGVLSRPYSRIILGAAVIDDVLGLIVLACVNGVA 171
                     TM-IV                              TM-V

NHX1_seq  LTH-LNHEAAFHLLGNFLYLFLLSTLLGAATGL-ISAYVIKKLYFGRHSTDREVALMMLM 257
4bwz.1.A  ETGQVEVGA---ITRLIV-LSVVFVGLAVFLSTLIARLPLERL-----PVGSPLGFALAL 222
                         TM-VI                                   TM-VII

NHX1_seq  AYLSYMLAELFDLSGILTVFFCGIVMSHYTWHNVTESSRITTKHTFATLSFLAETFIFLY 317
4bwz.1.A  GVGMAALAASIGLAPIVGAFLGGMLLSEVR-----EKYRL--EEPIFAIESFLAPIFFAM 275
                               TM-VIII                      TM-IX

NHX1_seq  VGMDALDIDKWRSVSDTPGTSIA--VSSILMGLVMVGRAAFVFPLSFLSNLAKKNQSEKI 375
4bwz.1.A  VGVRL-ELSALA-------SPVVLVAGTVVTVIAILGKVLGGFLGALT----Q-----GV 318
                                        TM-X

NHX1_seq  NFNMQVVIWWSGLMRGAVSMALAYNKFTRAGHTDVRGNAIMITSTITVCLFSTVVFGMLT 435
4bwz.1.A  R--SALTVGCGMAPRGEVGLIVAALGLK-AG---AVN-EEEYAIVLFMVVFTTLFAPFAL 371
                    TM-XI                                TM-XII

NHX1_seq  KPLISYL 442
4bwz.1.A  KPLIAW- 377
```

AtNHX1 vs NhaA_4au5 (CLUSTAL pairwise)

```
NHX1_seq  MLDSLVSKLPSLSTSDHASVVALNLFVALLCACIVLGHLLEENRWMNESITALLIGLGTG 60
4au5.1.A  ------------------------------------------------------------

NHX1_seq  VTILLISKGKSSHLLVFSEDLFFIYLLPPIIFNAGFQVK-------KKQFFRNFVTIMLF 113
4au5.1.A  -------------------LWINDALMAVFFLLVGLEVKRELMQGSLASLRQAAFP-VIA 100
                                TM-II                            TM-III

NHX1_seq  GAVGTIISCTIISLGVTQFFKKLDIGTFDLGDYLAIGAIFAATDSVCTLQVLNQD--ETP 171
4au5.1.A  AIGGMIVPALLY-----LAF------NYADPITREGWAIPAATDIAFALGVLALLGSRVP
                                                  TM-IV

NHX1_seq  -LLYSLVFGEGVVNDATSVVVFNAIQSFDLTHLNHEAAFHLLGNFLYLFLLSTLLGAATG 230
4au5.1.A  LALKIFLMALAIIDDLGAIIIIALFYTN---DL----------SMASL------GVAAVA 149
               TM-V                                              TM-VI

NHX1_seq  LISAYVIKKLYFGRHSTDREVALMMLMAYLSYMLAELFDLSGILTVFFCGIVMSHYTWHN 290
4au5.1.A  IAVLAVLNLCGA----RRTGV-Y-ILVGVVLWTAVLKSGVHATLAGVIVGFFIPLKEKHG 244
                                  TM-VII              TM-VIII

NHX1_seq  VTESSRITTKHTFAT-LSFLAETFIFLYVGMDALDIDKWRSVSDTPGTSIAVSSILMGLV 349
4au5.1.A  RSPAKRL-EHVLHPWVAYLILPLFAFANAGVSLQGVT-LDGLT-S----I-LPLGIIAGL 296
              TM-IX

NHX1_seq  MVGRAAFVFPLSFLSNLAKK-NQSEKINFNMQVVIWW-SGLMRGAVSMALAYNKFTRAGH 407
4au5.1.A  LIGKPLGISLFCWLALRLKLAHLPEGTTYQQIMVVGILCG-IGFTMSIFIA--------- 346
               TM-X                               TM-XI

NHX1_seq  TDVRGNAIMITSTITVCLFSTVVFGMLTKPLISYLLPHQNATTSMLSDDNTPKSIHIPLL 467
4au5.1.A  ------------------------------------------------------------


NHX1_seq  DQDSFIEPSGNHNVPRPDSIRGFLTRPTRTVHYYWRQFDDSFMRPVFGGRGFVPFVPGSP 527
4au5.1.A  ------------------------------------------------------------

NHX1_seq  TERNPPDLSKA 538
4au5.1.A  -----------
```

Annex 5

Modeling of of AtNHX1 active center using as template the structures of MjNhaP1 and TtNapA.

NHX1 based on MjNhaP1

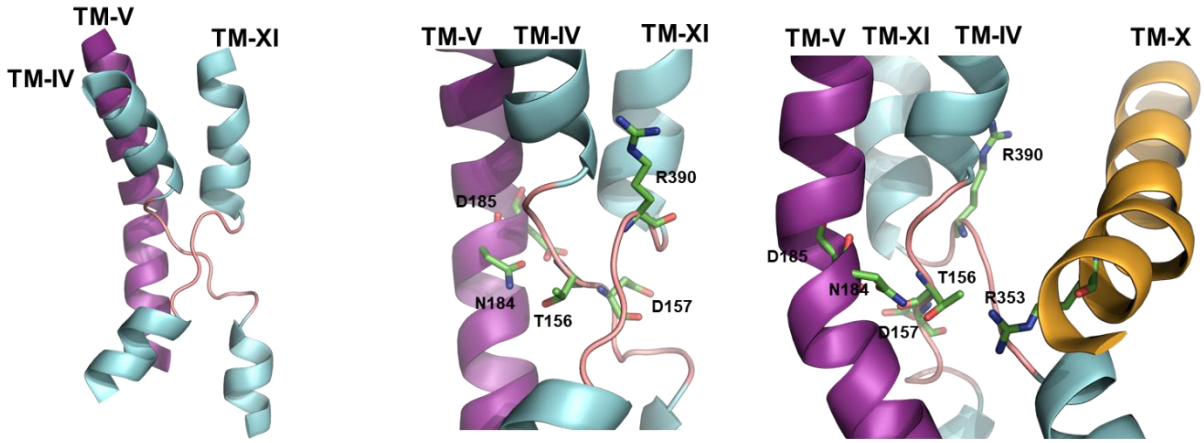

NHX1 based on NapA

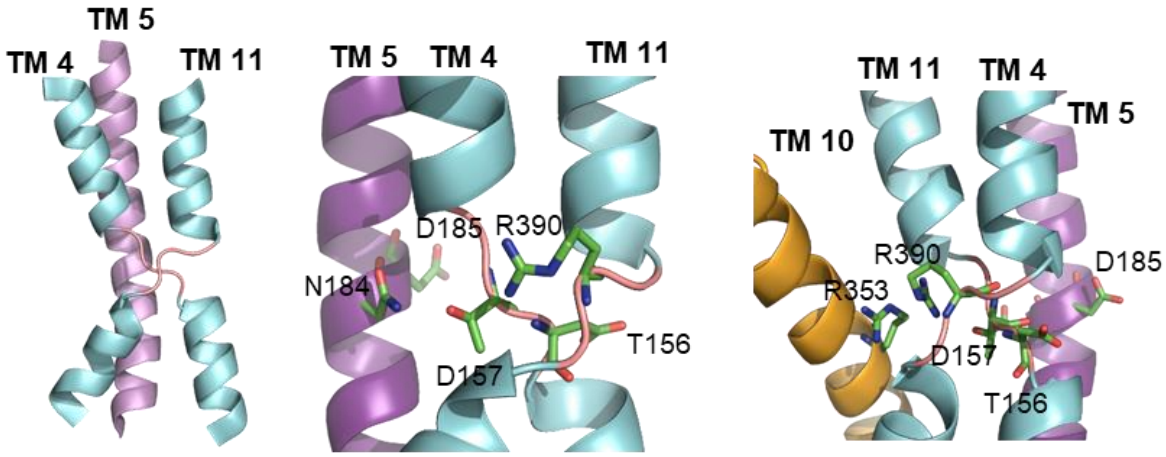

Annex 6.

In vitro verification of NHX1 tridimensional structure using as templeates the structures of MjNhaP1, TtNapA and EcNhaA.

- Positive-inside rule

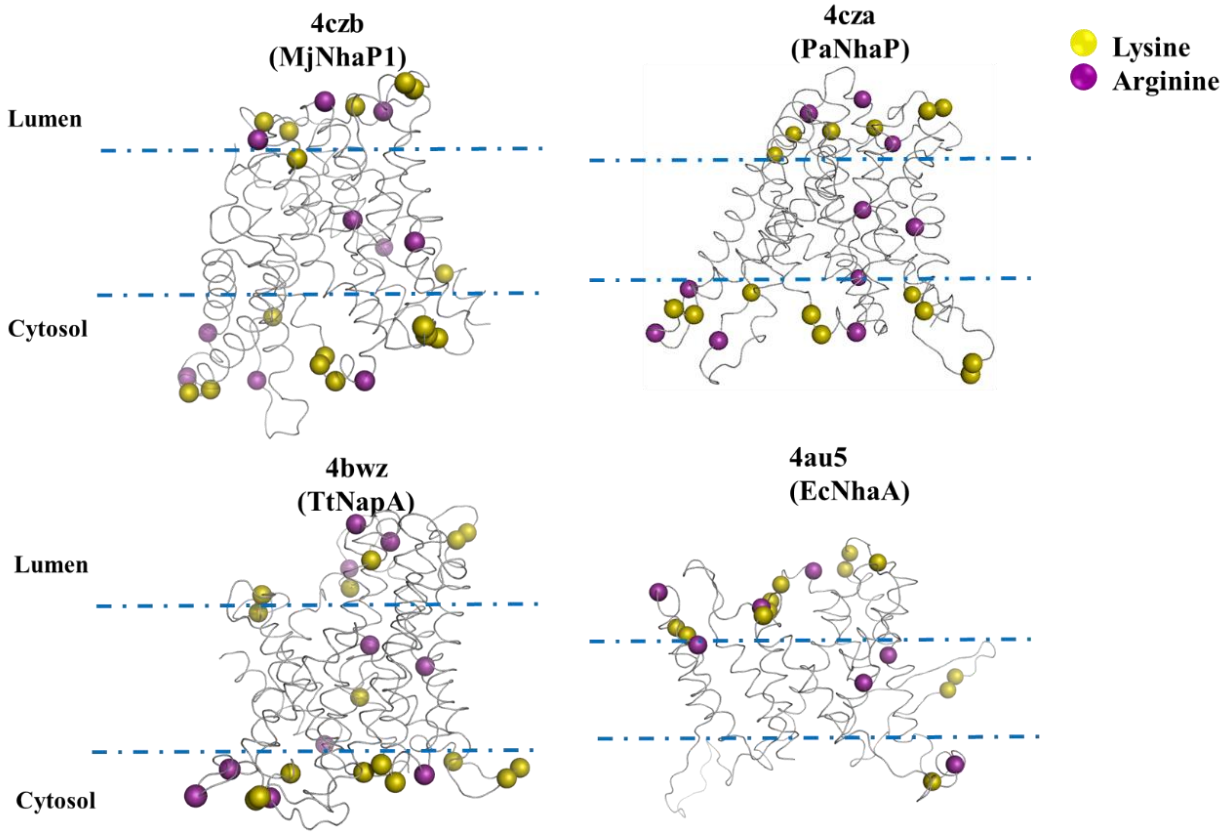

- Hidrophobcity analysis.

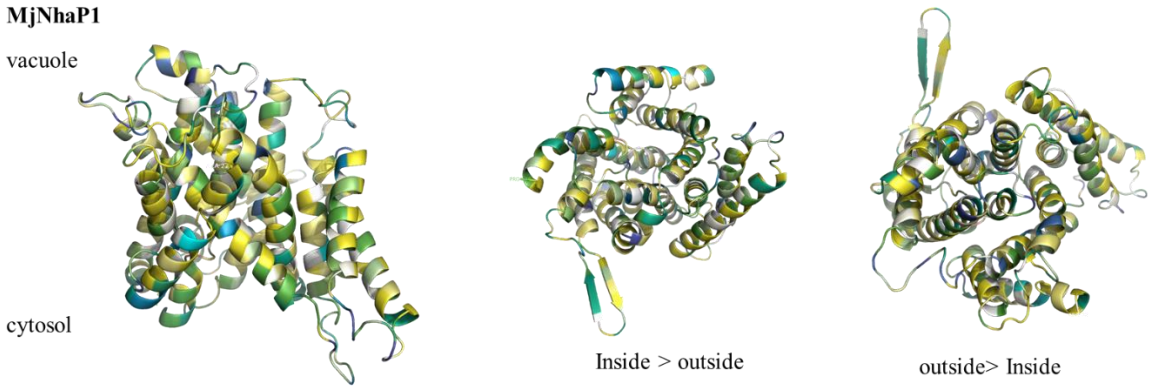

TtNapA

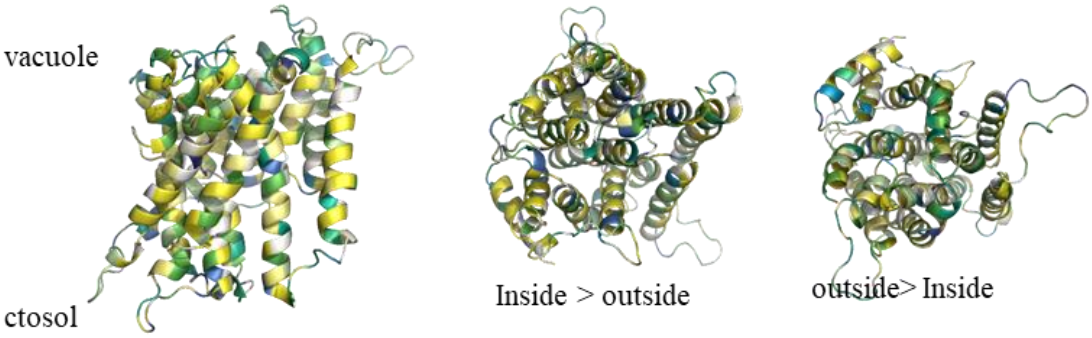

- <u>Residues Conservation.</u>

MjNhaP1

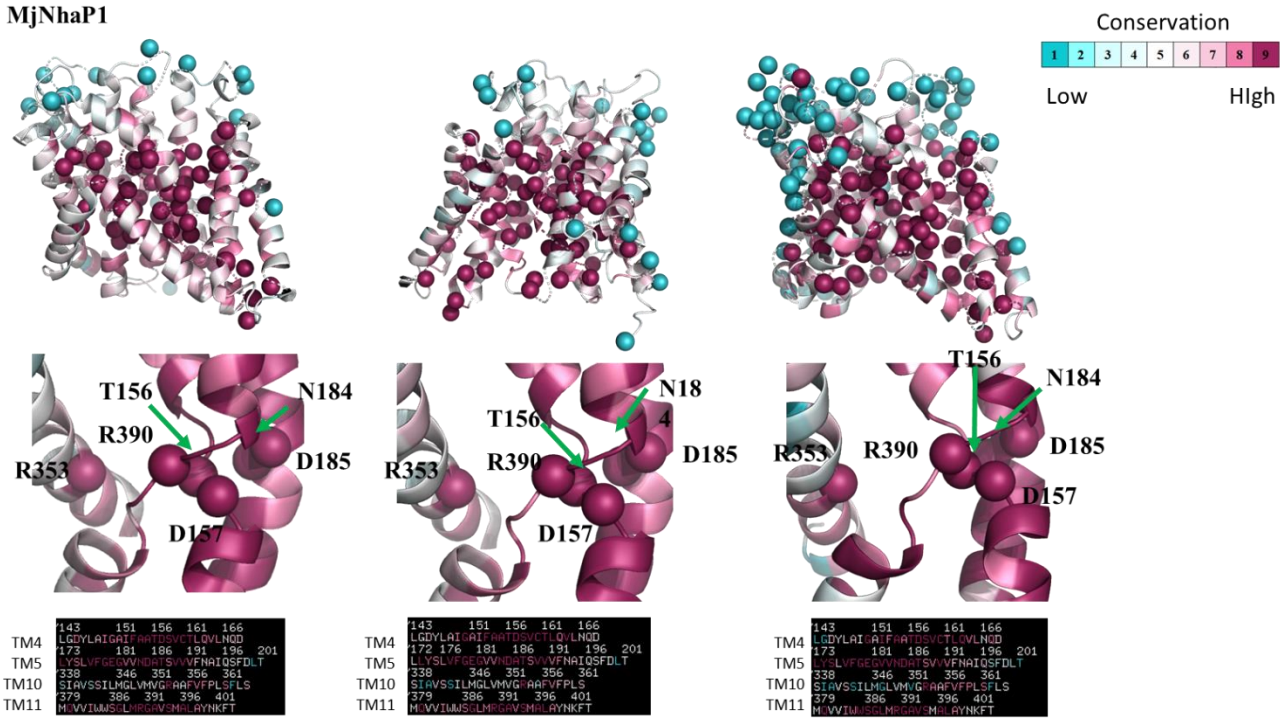

TtNapA

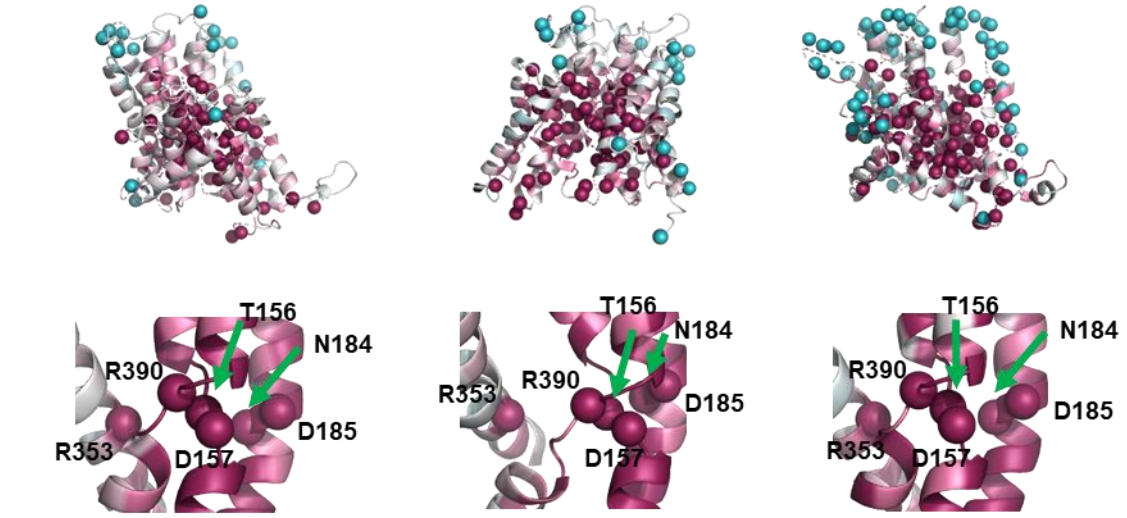
T156
N184
R390
D185
R353
D157
T156
N184
R390
R353
D185
D157
T156
N184
R390
D185
R353
D157


TM-IV
TM-V
TM-X
TM-XI


TM-IV
TM-V
TM-X
TM-XI

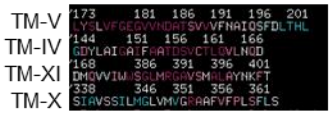
TM-V
TM-IV
TM-XI
TM-X

Annex 7

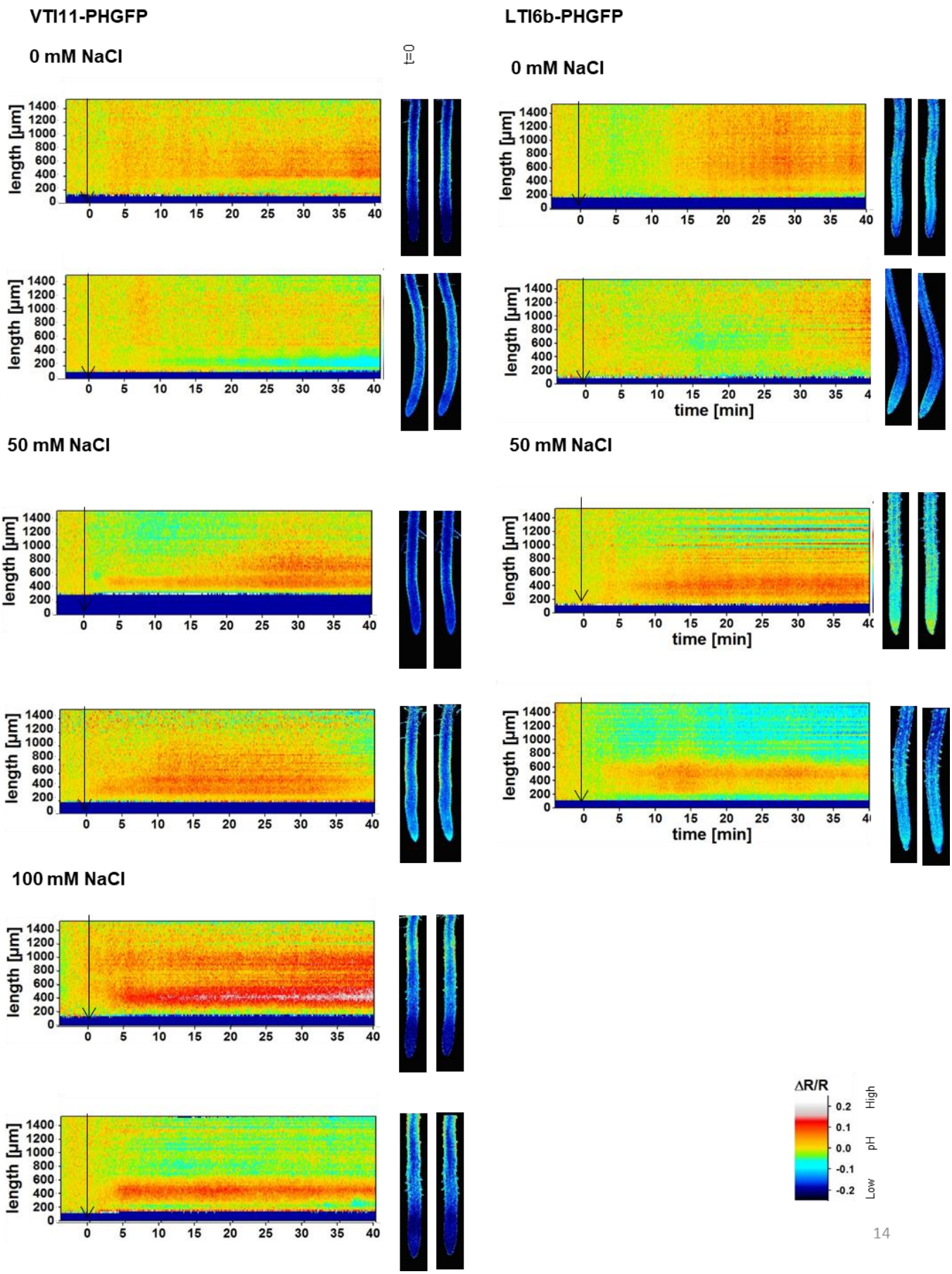
VTI11-PHGFP
LTI6b-PHGFP
0 mM NaCl
t=0
0 mM NaCl
50 mM NaCl
50 mM NaCl
100 mM NaCl
length [µm]
time [min]
ΔR/R
0.2
0.1
0.0
-0.1
-0.2
High
pH
Low

Annex 8

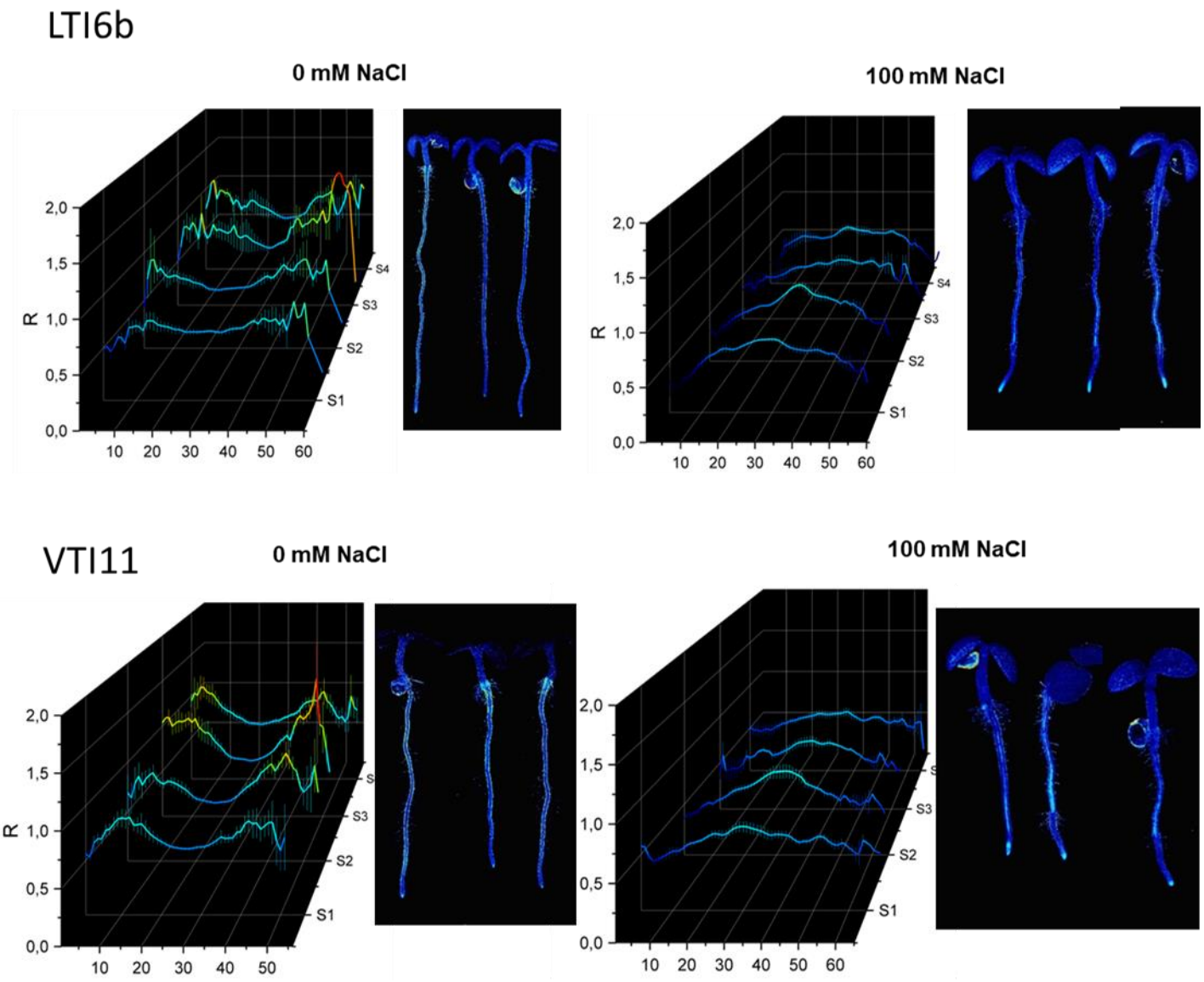
LTI6b
0 mM NaCl
100 mM NaCl
R
S1
S2
S3
S4
VTI11
0 mM NaCl
100 mM NaCl

Annex 9

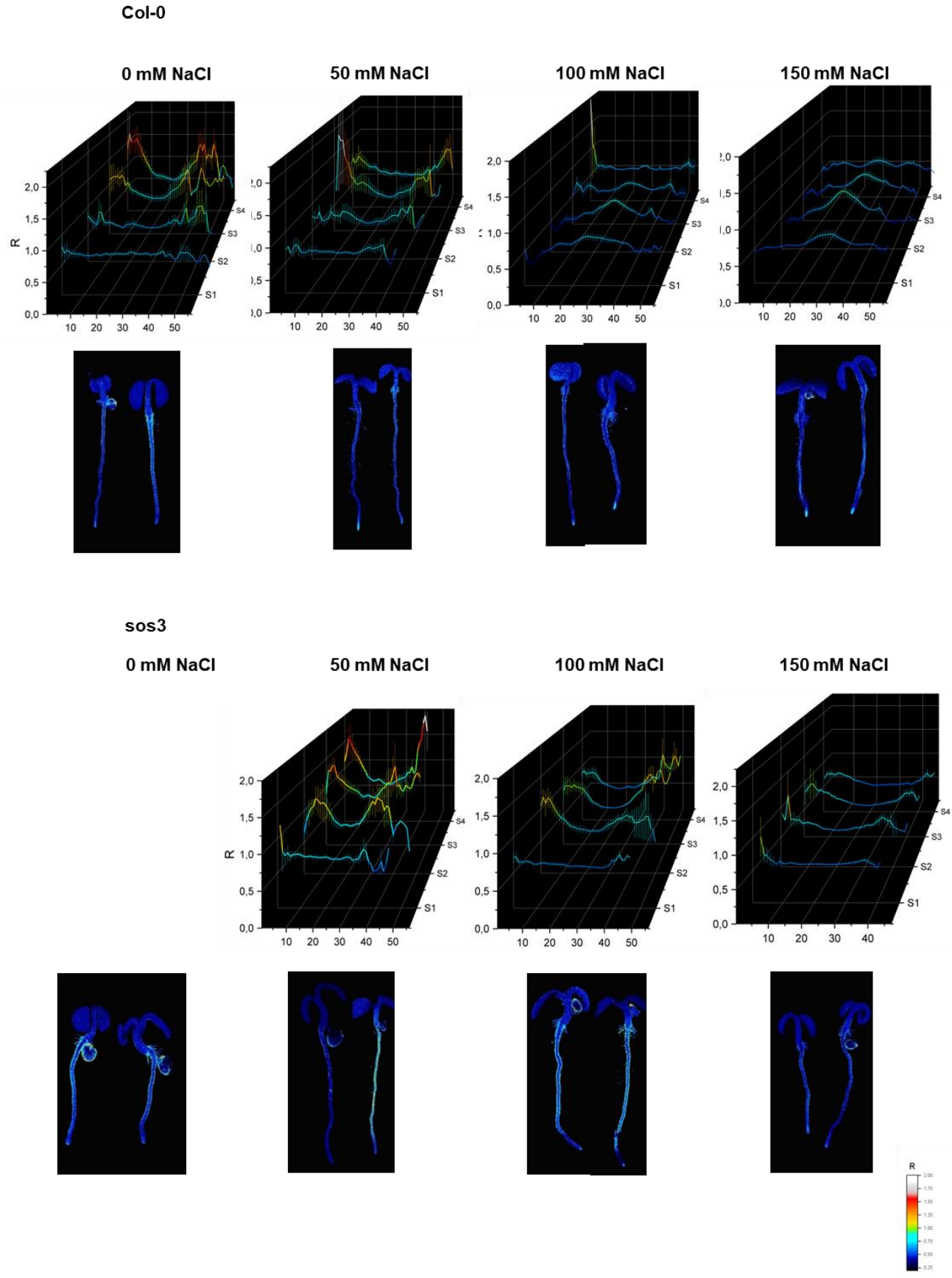
Col-0
0 mM NaCl
50 mM NaCl
100 mM NaCl
150 mM NaCl
sos3
0 mM NaCl
50 mM NaCl
100 mM NaCl
150 mM NaCl
R
S1
S2
S3
S4

BIBLIOGRAPHY

Aharon GS, Apse MP, Duan S, et al (2003) Characterization of a family of vacuolar Na $^{+}$ /H $^{+}$ antiporters in Arabidopsis thaliana. Plant Soil 253:245–256. doi: 10.1023/A:1024577205697

Albuquerque CP, Smolka MB, Payne SH, et al (2008) A multidimensional chromatography technology for in-depth phosphoproteome analysis. Mol Cell Proteomics 7:1389–96. doi: 10.1074/mcp.M700468-MCP200

Aleman F, Nieves-Cordones M, Martinez V, Rubio F (2011) Root K+ Acquisition in Plants: The Arabidopsis thaliana Model. Plant Cell Physiol 52:1603–1612. doi: 10.1093/pcp/pcr096

Alexander RT, Grinstein S (2009) Tethering, recycling and activation of the epithelial sodium-proton exchanger, NHE3. J Exp Biol 212:1630–7. doi: 10.1242/jeb.027375

Ali R, Brett CL, Mukherjee S, Rao R (2004) Inhibition of sodium/proton exchange by a Rab-GTPase-activating protein regulates endosomal traffic in yeast. J Biol Chem 279:4498–506. doi: 10.1074/jbc.M307446200

Almeida DM, Oliveira MM, Saibo NJM, et al (2017) Regulation of Na+ and K+ homeostasis in plants: towards improved salt stress tolerance in crop plants. Genet Mol Biol 40:326–345. doi: 10.1590/1678-4685-gmb-2016-0106

Altschul SF, Madden TL, Schäffer AA, et al (1997) Gapped BLAST and PSI-BLAST: a new generation of protein database search programs. Nucleic Acids Res 25:3389–402

Amith SR, Vincent KM, Wilkinson JM, et al (2017) Defining the Na+/H+ exchanger NHE1 interactome in triple-negative breast cancer cells. Cell Signal 29:69–77. doi: 10.1016/j.cellsig.2016.10.005

Ammar Y Ben, Takeda S, Hisamitsu T, et al (2006) Crystal structure of CHP2 complexed with NHE1-cytosolic region and an implication for pH regulation. EMBO J 25:2315–25. doi: 10.1038/sj.emboj.7601145

Amtmann A, Armengaud P, Volkov V (2018) Potassium Nutrition and Salt Stress. In: Annual Plant Reviews. John Wiley & Sons, Ltd, Chichester, UK, pp 328–379

An R, Chen Q-J, Chai M-F, et al (2007) AtNHX8, a member of the monovalent cation:proton antiporter-1 family in Arabidopsis thaliana, encodes a putative Li+/H+ antiporter. Plant J 49:718–728. doi: 10.1111/j.1365-313X.2006.02990.x

Andres Z, Perez-Hormaeche J, Leidi EO, et al (2014) Control of vacuolar dynamics and regulation of stomatal aperture by tonoplast potassium uptake. Proc Natl Acad Sci 111:E1806–E1814. doi: 10.1073/pnas.1320421111

Apse MP, Aharon GS, Snedden WA, Blumwald E (1999) Salt tolerance conferred by overexpression of a vacuolar Na+/H+ antiport in Arabidopsis. Science 285:1256–8. doi: 10.1126/SCIENCE.285.5431.1256

Apse MP, Blumwald E (2007) Na $^{+}$ transport in plants. FEBS Lett 581:2247–2254. doi: 10.1016/j.febslet.2007.04.014

Apse MP, Sottosanto JB, Blumwald E (2003) Vacuolar cation/H $^{+}$ exchange, ion homeostasis, and leaf development are altered in a T-DNA insertional mutant of *AtNHX1* , the

Arabidopsis vacuolar Na + /H + antiporter. Plant J 36:229–239. doi: 10.1046/j.1365-313X.2003.01871.x

Aronson PS, Nee J, Suhm MA (1982) Modifier role of internal H+ in activating the Na+-H+ exchanger in renal microvillus membrane vesicles. Nature 299:161–3

Ashnest JR, Huynh DL, Dragwidge JM, et al (2015) Arabidopsis Intracellular NHX-Type Sodium-Proton Antiporters are Required for Seed Storage Protein Processing. Plant Cell Physiol 56:pcv138. doi: 10.1093/pcp/pcv138

Assaha DVM, Mekawy AMM, Ueda A, Saneoka H (2015) Salinity-induced expression of HKT may be crucial for Na+ exclusion in the leaf blade of huckleberry (Solanum scabrum Mill.), but not of eggplant (Solanum melongena L.). Biochem Biophys Res Commun 460:416–421. doi: 10.1016/j.bbrc.2015.03.048

Assaha DVM, Ueda A, Saneoka H, et al (2017) The Role of Na+ and K+ Transporters in Salt Stress Adaptation in Glycophytes. Front Physiol 8:509. doi: 10.3389/fphys.2017.00509

Ausubel FM, Brent R, Kingston RE, et al (1996) Current protocols in molecular biology. Greene Pub. Associates

Bairoch A, Apweiler R, Wu CH, et al (2005) The Universal Protein Resource (UniProt). Nucleic Acids Res 33:D154-9. doi: 10.1093/nar/gki070

Barragán V, Leidi EO, Andrés Z, et al (2012) Ion exchangers NHX1 and NHX2 mediate active potassium uptake into vacuoles to regulate cell turgor and stomatal function in Arabidopsis. Plant Cell 24:1127–42. doi: 10.1105/tpc.111.095273

Bassil E, Blumwald E (2014) The ins and outs of intracellular ion homeostasis: NHX-type cation/H+transporters. Curr Opin Plant Biol. doi: 10.1016/j.pbi.2014.08.002

Bassil E, Krebs M, Halperin* S, et al (2013) Fluorescent Dye Based Measurement of Vacuolar pH and K+. BIO-PROTOCOL 3:. doi: 10.21769/BioProtoc.810

Bassil E, Ohto M, Esumi T, et al (2011a) The Arabidopsis intracellular Na+/H+ antiporters NHX5 and NHX6 are endosome associated and necessary for plant growth and development. Plant Cell 23:224–39. doi: 10.1105/tpc.110.079426

Bassil E, Tajima H, Liang Y-C, et al (2011b) The Arabidopsis Na+/H+ Antiporters NHX1 and NHX2 Control Vacuolar pH and K+ Homeostasis to Regulate Growth, Flower Development, and Reproduction. Plant Cell Online 23:3482–3497. doi: 10.1105/tpc.111.089581

Bassil E, Tajima H, Liang Y-C, et al (2011c) The Arabidopsis Na+/H+ antiporters NHX1 and NHX2 control vacuolar pH and K+ homeostasis to regulate growth, flower development, and reproduction. Plant Cell 23:3482–97. doi: 10.1105/tpc.111.089581

Batelli G, Verslues PE, Agius F, et al (2007) SOS2 promotes salt tolerance in part by interacting with the vacuolar H+-ATPase and upregulating its transport activity. Mol Cell Biol 27:7781–90. doi: 10.1128/MCB.00430-07

Batistic O, Kudla J (2004) Integration and channeling of calcium signaling through the CBL calcium sensor/CIPK protein kinase network. Planta 219:915–924. doi: 10.1007/s00425-

004-1333-3

Belver A, Olías R, Huertas R, Rodríguez-Rosales MP (2012) Involvement of SlSOS2 in tomato salt tolerance. Bioengineered 3:298–302. doi: 10.4161/bioe.20796

Benčina M (2013) Illumination of the spatial order of intracellular pH by genetically encoded pH-sensitive sensors. Sensors (Basel) 13:16736–58. doi: 10.3390/s131216736

Bender KW, Snedden WA (2013) Calmodulin-related proteins step out from the shadow of their namesake. Plant Physiol 163:486–95. doi: 10.1104/pp.113.221069

Berthomieu P, Conéjéro G, Nublat A, et al (2003) Functional analysis of AtHKT1 in Arabidopsis shows that Na(+) recirculation by the phloem is crucial for salt tolerance. EMBO J 22:2004–14. doi: 10.1093/emboj/cdg207

Bienert S, Waterhouse A, de Beer TAP, et al (2017) The SWISS-MODEL Repository—new features and functionality. Nucleic Acids Res 45:D313–D319. doi: 10.1093/nar/gkw1132

Blumwald E (1987) Tonoplast vesicles as a tool in the study of ion transport at the plant vacuole. Physiol Plant 69:731–734. doi: 10.1111/j.1399-3054.1987.tb01993.x

Blumwald E, Poole RJ (1985) Na/H Antiport in Isolated Tonoplast Vesicles from Storage Tissue of Beta vulgaris. Plant Physiol 78:163–7

Blundell CD, Mahoney DJ, Cordell MR, et al (2007) Determining the molecular basis for the pH-dependent interaction between the link module of human TSG-6 and hyaluronan. J Biol Chem 282:12976–88. doi: 10.1074/jbc.M611713200

Bowers K, Levi BP, Patel FI, Stevens TH (2000) The Sodium/Proton Exchanger Nhx1p Is Required for Endosomal Protein Trafficking in the Yeast *Saccharomyces cerevisiae*. Mol Biol Cell 11:4277–4294. doi: 10.1091/mbc.11.12.4277

Bowers K, Stevens TH (2005) Protein transport from the late Golgi to the vacuole in the yeast Saccharomyces cerevisiae. Biochim Biophys Acta - Mol Cell Res 1744:438–454. doi: 10.1016/J.BBAMCR.2005.04.004

Bowie JU (2005) Solving the membrane protein folding problem. 438:581–589. doi: 10.1038/nature04395

Bowman JL, Smyth DR, Hill JP, et al (1994) Flowers. In: Arabidopsis - An atlas of Morphology and Development. Springer New York, New York, NY, pp 133–273

Boyes DC, Zayed AM, Ascenzi R, et al (2001) Growth Stage-Based Phenotypic Analysis of Arabidopsis: A Model for High Throughput Functional Genomics in Plants

Bradford MM (1976) A rapid and sensitive method for the quantitation of microgram quantities of protein utilizing the principle of protein-dye binding. Anal Biochem 72:248–254. doi: 10.1016/0003-2697(76)90527-3

Brett CL, Donowitz M, Rao R (2005a) Evolutionary origins of eukaryotic sodium/proton exchangers. Am J Physiol Physiol 288:C223–C239. doi: 10.1152/ajpcell.00360.2004

Brett CL, Kallay L, Hua Z, et al (2011) Genome-wide analysis reveals the vacuolar pH-stat of Saccharomyces cerevisiae. PLoS One 6:e17619. doi: 10.1371/journal.pone.0017619

Brett CL, Tukaye DN, Mukherjee S, Rao R (2005b) The yeast endosomal Na+K+/H+ exchanger Nhx1 regulates cellular pH to control vesicle trafficking. Mol Biol Cell 16:1396–405. doi: 10.1091/mbc.E04-11-0999

Brini F, Hanin M, Lumbreras V, et al (2007) Overexpression of wheat dehydrin DHN-5 enhances tolerance to salt and osmotic stress in Arabidopsis thaliana. Plant Cell Rep 26:2017–2026. doi: 10.1007/s00299-007-0412-x

Britto DT, Kronzucker HJ (2015) Sodium efflux in plant roots: What do we really know? J Plant Physiol 186–187:1–12. doi: 10.1016/j.jplph.2015.08.002

Byrt CS, Zhao M, Kourghi M, et al (2017) Non-selective cation channel activity of aquaporin AtPIP2;1 regulated by Ca^{2+} and pH. Plant Cell Environ 40:802–815. doi: 10.1111/pce.12832

Caballero F, Botella MA, Rubio L, et al (2012) A Ca2+-Sensitive System Mediates Low-Affinity K+ Uptake in the Absence of AKT1 in Arabidopsis Plants. Plant Cell Physiol 53:2047–2059. doi: 10.1093/pcp/pcs140

Călinescu O, Dwivedi M, Patiño-Ruiz M, et al (2017) Lysine 300 is essential for stability but not for electrogenic transport of the Escherichia coli NhaA Na+/H+ antiporter. J Biol Chem 292:7932–7941. doi: 10.1074/jbc.M117.778175

Călinescu O, Linder M, Wöhlert D, et al (2016) Electrogenic Cation Binding in the Electroneutral Na+/H+ Antiporter of Pyrococcus abyssi. J Biol Chem 291:26786–26793. doi: 10.1074/jbc.M116.761080

Călinescu O, Paulino C, Kühlbrandt W, Fendler K (2014) Keeping it simple, transport mechanism and pH regulation in Na+/H+ exchangers. J Biol Chem 289:13168–76. doi: 10.1074/jbc.M113.542993

Camoni L, Barbero F, Aducci P, Maffei ME (2018) Spodoptera littoralis oral secretions inhibit the activity of Phaseolus lunatus plasma membrane H+-ATPase. PLoS One 13:e0202142. doi: 10.1371/journal.pone.0202142

Casey JR, Grinstein S, Orlowski J (2010) Sensors and regulators of intracellular pH. Nat Rev Mol Cell Biol 11:50–61. doi: 10.1038/nrm2820

Cha B, Oh S, Shanmugaratnam J, et al (2003) Two histidine residues in the juxta-membrane cytoplasmic domain of Na +/H+ exchanger isoform 3 (NHE3) determine the set point. J Membr Biol 191:49–58. doi: 10.1007/s00232-002-1044-2

Chanchevalap S, Yang Z, Cui N, et al (2000) Involvement of histidine residues in proton sensing of ROMK1 channel. J Biol Chem 275:7811–7

Chanroj S, Padmanaban S, Czerny DD, et al (2013) K+ Transporter AtCHX17 with Its Hydrophilic C Tail Localizes to Membranes of the Secretory/Endocytic System: Role in Reproduction and Seed Set. Mol Plant 6:1226–1246. doi: 10.1093/mp/sst032

Chanroj S, Wang G, Venema K, et al (2012) Conserved and diversified gene families of monovalent cation/h(+) antiporters from algae to flowering plants. Front Plant Sci 3:25. doi: 10.3389/fpls.2012.00025

Cheng N-H, Pittman JK, Zhu J-K, Hirschi KD (2004) The protein kinase SOS2 activates the Arabidopsis H(+)/Ca(2+) antiporter CAX1 to integrate calcium transport and salt tolerance. J Biol Chem 279:2922–6. doi: 10.1074/jbc.M309084200

Cheong YH, Pandey GK, Grant JJ, et al (2007) Two calcineurin B-like calcium sensors, interacting with protein kinase CIPK23, regulate leaf transpiration and root potassium uptake in Arabidopsis. Plant J 52:223–239. doi: 10.1111/j.1365-313X.2007.03236.x

Conde A, Chaves MM, Geros H (2011) Membrane Transport, Sensing and Signaling in Plant Adaptation to Environmental Stress. Plant Cell Physiol 52:1583–1602. doi: 10.1093/pcp/pcr107

Coonrod EM, Graham LA, Carpp LN, et al (2013) Homotypic vacuole fusion in yeast requires organelle acidification and not the V-ATPase membrane domain. Dev Cell 27:462–8. doi: 10.1016/j.devcel.2013.10.014

Cotsaftis O, Plett D, Shirley N, et al (2012) A Two-Staged Model of Na+ Exclusion in Rice Explained by 3D Modeling of HKT Transporters and Alternative Splicing. PLoS One 7:e39865. doi: 10.1371/journal.pone.0039865

CRAIG PLETT D, MØLLER IS (2010) Na $^{+}$ transport in glycophytic plants: what we know and would like to know. Plant Cell Environ 33:612–626. doi: 10.1111/j.1365-3040.2009.02086.x

Cutler SR, Ehrhardt DW, Griffitts JS, Somerville CR (2000) Random GFP::cDNA fusions enable visualization of subcellular structures in cells of Arabidopsis at a high frequency. Proc Natl Acad Sci 97:3718–3723. doi: 10.1073/pnas.97.7.3718

Czerny DD, Padmanaban S, Anishkin A, et al (2016) Protein architecture and core residues in unwound α-helices provide insights to the transport function of plant AtCHX17. Biochim Biophys Acta - Biomembr 1858:1983–1998. doi: 10.1016/j.bbamem.2016.05.008

D'Onofrio C, Lindberg S (2009) Sodium induces simultaneous changes in cytosolic calcium and pH in salt-tolerant quince protoplasts. J Plant Physiol 166:1755–1763. doi: 10.1016/J.JPLPH.2009.05.006

DAVENPORT RJ, MUÑOZ-MAYOR A, JHA D, et al (2007) The Na $^{+}$ transporter AtHKT1;1 controls retrieval of Na $^{+}$ from the xylem in Arabidopsis. Plant Cell Environ 30:497–507. doi: 10.1111/j.1365-3040.2007.01637.x

Davis SJ, Vierstra RD (1998) Soluble, highly fluorescent variants of green fluorescent protein (GFP) for use in higher plants. Plant Mol Biol 36:521–528. doi: 10.1023/A:1005991617182

Deeken R, Geiger D, Fromm J, et al (2002) Loss of the AKT2/3 potassium channel affects sugar loading into the phloem of Arabidopsis. Planta 216:334–344. doi: 10.1007/s00425-002-0895-1

Dettmer J, Hong-Hermesdorf A, Stierhof Y-D, Schumacher K (2006) Vacuolar H+-ATPase Activity Is Required for Endocytic and Secretory Trafficking in Arabidopsis. PLANT CELL ONLINE 18:715–730. doi: 10.1105/tpc.105.037978

Di T, Afzal MR, Yoshihashi T, et al (2018) Further insights into underlying mechanisms for the

release of biological nitrification inhibitors from sorghum roots. Plant Soil 423:99–110. doi: 10.1007/s11104-017-3505-5

Diakov TT, Kane PM (2010) Regulation of vacuolar proton-translocating ATPase activity and assembly by extracellular pH. J Biol Chem 285:23771–8. doi: 10.1074/jbc.M110.110122

Diakov TT, Tarsio M, Kane PM (2013) Measurement of vacuolar and cytosolic pH in vivo in yeast cell suspensions. J Vis Exp. doi: 10.3791/50261

Donowitz M, Mohan S, Zhu CX, et al (2009) NHE3 regulatory complexes. J Exp Biol 212:1638–46. doi: 10.1242/jeb.028605

Dragwidge JM, Scholl S, Schumacher K, Gendall AR (2018) NHX-type Na+(K+)/H+ antiporter activity is required for endomembrane trafficking and ion homeostasis in Arabidopsis thaliana. bioRxiv 382663. doi: 10.1101/382663

Du L, Poovaiah BW (2005) Ca2+/calmodulin is critical for brassinosteroid biosynthesis and plant growth. Nature 437:741–745. doi: 10.1038/nature03973

Duby G, Boutry M (2009) The plant plasma membrane proton pump ATPase: a highly regulated P-type ATPase with multiple physiological roles. Pflügers Arch - Eur J Physiol 457:645–655. doi: 10.1007/s00424-008-0457-x

Eddy SR (1996) Hidden Markov models. Curr Opin Struct Biol 6:361–365. doi: 10.1016/S0959-440X(96)80056-X

Edgar RC (2004) MUSCLE: multiple sequence alignment with high accuracy and high throughput. Nucleic Acids Res 32:1792–7. doi: 10.1093/nar/gkh340

Edwards K, Johnstone C, Thompson C (1991) A simple and rapid method for the preparation of plant genomic DNA for PCR analysis. Nucleic Acids Res 19:1349

Elble R (1992) A simple and efficient procedure for transformation of yeasts. Biotechniques 13:18–20

Evans MJ, Choi W-G, Gilroy S, Morris RJ (2016) A ROS-Assisted Calcium Wave Dependent on the AtRBOHD NADPH Oxidase and TPC1 Cation Channel Propagates the Systemic Response to Salt Stress. Plant Physiol 171:1771–84. doi: 10.1104/pp.16.00215

Fan L, Zhao L, Hu W, et al (2018) Na^+,K^+/H^+ antiporters regulate the pH of endoplasmic reticulum and auxin-mediated development. Plant Cell Environ 41:850–864. doi: 10.1111/pce.13153

Faraco M, Spelt C, Bliek M, et al (2014) Hyperacidification of Vacuoles by the Combined Action of Two Different P-ATPases in the Tonoplast Determines Flower Color. Cell Rep 6:32–43. doi: 10.1016/J.CELREP.2013.12.009

Fasano JM, Swanson SJ, Blancaflor EB, et al (2001) Changes in root cap pH are required for the gravity response of the Arabidopsis root. Plant Cell 13:907–21

Felle HH (2001) pH: Signal and Messenger in Plant Cells. Plant Biol 3:577–591. doi: 10.1055/s-2001-19372

Ferrándiz C, Pelaz S, Yanofsky MF (1999) Control of Carpel and Fruit Development in

Arabidopsis. Annu Rev Biochem 68:321–354. doi: 10.1146/annurev.biochem.68.1.321

Fleishman SJ, Ben-Tal N (2006) Progress in structure prediction of α-helical membrane proteins. Curr Opin Struct Biol 16:496–504. doi: 10.1016/J.SBI.2006.06.003

Fritz R, Stiasny K, Heinz FX (2008) Identification of specific histidines as pH sensors in flavivirus membrane fusion. J Cell Biol 183:353–61. doi: 10.1083/jcb.200806081

Fuglsang AT, Guo Y, Cuin TA, et al (2007) Arabidopsis protein kinase PKS5 inhibits the plasma membrane H+ -ATPase by preventing interaction with 14-3-3 protein. Plant Cell 19:1617–34. doi: 10.1105/tpc.105.035626

Fujimaki S, Maruyama T, Suzui N, et al (2015) Base to Tip and Long-Distance Transport of Sodium in the Root of Common Reed [Phragmites australis (Cav.) Trin. ex Steud.] at Steady State Under Constant High-Salt Conditions. Plant Cell Physiol 56:943–950. doi: 10.1093/pcp/pcv021

Fukada-Tanaka S, Inagaki Y, Yamaguchi T, et al (2000) Colour-enhancing protein in blue petals. Nature 407:581–581. doi: 10.1038/35036683

Fukuda A, Nakamura A, Hara N, et al (2011) Molecular and functional analyses of rice NHX-type Na+/H+ antiporter genes. Planta 233:175–188. doi: 10.1007/s00425-010-1289-4

Fukuda A, Nakamura A, Tagiri A, et al (2004) Function, Intracellular Localization and the Importance in Salt Tolerance of a Vacuolar Na+/H+ Antiporter from Rice. Plant Cell Physiol 45:146–159. doi: 10.1093/pcp/pch014

Fukuda A, Nakamura A, Tanaka Y (1999) Molecular cloning and expression of the Na+/H+ exchanger gene in Oryza sativa. Biochim Biophys Acta - Gene Struct Expr 1446:149–155. doi: 10.1016/S0167-4781(99)00065-2

Gajdanowicz P, Michard E, Sandmann M, et al (2011) Potassium (K+) gradients serve as a mobile energy source in plant vascular tissues. Proc Natl Acad Sci U S A 108:864–9. doi: 10.1073/pnas.1009777108

Galili L, Rothman A, Kozachkov L, et al (2002) Trans membrane domain IV is involved in ion transport activity and pH regulation of the NhaA-Na+/H+ antiporter of Escherichia coli. Biochemistry 41:609–617. doi: 10.1021/bi011655v

Gao D, Knight MR, Trewavas AJ, et al (2004) Self-reporting Arabidopsis expressing pH and [Ca2+] indicators unveil ion dynamics in the cytoplasm and in the apoplast under abiotic stress. Plant Physiol 134:898–908. doi: 10.1104/pp.103.032508

GAO S, YUAN L, ZHAI H, et al (2012) Overexpression of SOS Genes Enhanced Salt Tolerance in Sweetpotato. J Integr Agric 11:378–386. doi: 10.1016/S2095-3119(12)60022-7

Gaxiola RA, Rao R, Sherman A, et al (1999) The Arabidopsis thaliana proton transporters, AtNhx1 and Avp1, can function in cation detoxification in yeast. Proc Natl Acad Sci U S A 96:1480–5. doi: 10.1073/PNAS.96.4.1480

GEILFUS C-M, MÜHLING KH (2012) Transient alkalinization in the leaf apoplast of Vicia faba L. depends on NaCl stress intensity: an in situ ratio imaging study. Plant Cell Environ 35:578–587. doi: 10.1111/j.1365-3040.2011.02437.x

Gerchman Y, Olami Y, Rimon A, et al (1993) Histidine-226 is part of the pH sensor of NhaA, a Na+/H+ antiporter in Escherichia coli. Proc Natl Acad Sci U S A 90:1212–6

Gerchman Y, Rimon A, Padan E (1999) A pH-dependent conformational change of NhaA Na+/H+antiporter of Escherichia coli involves loop VIII-IX, plays a role in the pH response of the protein, and is maintained by the pure protein in dodecyl maltoside. J Biol Chem 274:24617–24624. doi: 10.1074/jbc.274.35.24617

Germond A, Fujita H, Ichimura T, Watanabe TM (2016) Design and development of genetically encoded fluorescent sensors to monitor intracellular chemical and physical parameters. Biophys Rev 8:121–138. doi: 10.1007/s12551-016-0195-9

Gierth M, Mäser P, Schroeder JI (2005) The potassium transporter AtHAK5 functions in K(+) deprivation-induced high-affinity K(+) uptake and AKT1 K(+) channel contribution to K(+) uptake kinetics in Arabidopsis roots. Plant Physiol 137:1105–14. doi: 10.1104/pp.104.057216

Gjetting KSK, Ytting CK, Schulz A, Fuglsang AT (2012) Live imaging of intra-and extracellular pH in plants using pHusion, a novel genetically encoded biosensor. J Exp Bot 63:3207–3218. doi: 10.1093/jxb/ers040

Goswami P, Paulino C, Hizlan D, et al (2011) Structure of the archaeal Na+/H+antiporter NhaP1 and functional role of transmembrane helix 1. EMBO J 30:439–449. doi: 10.1038/emboj.2010.321

Gruhler A, Olsen J V, Mohammed S, et al (2005) Quantitative phosphoproteomics applied to the yeast pheromone signaling pathway. Mol Cell Proteomics 4:310–27. doi: 10.1074/mcp.M400219-MCP200

Guthrie C, Fink GR (1991) Guide to yeast genetics and molecular biology. Academic Press

Halfter U, Ishitani M, Zhu J-K (2000) The Arabidopsis SOS2 protein kinase physically interacts with and is activated by the calcium-binding protein SOS3. Proc Natl Acad Sci 97:3735–3740. doi: 10.1073/pnas.97.7.3735

Hamada a, Hibino T, Nakamura T, Takabe T (2001) Na+/H+ antiporter from Synechocystis species PCC 6803, homologous to SOS1, contains an aspartic residue and long C-terminal tail important for the carrier activity. Plant Physiol 125:437–46. doi: 10.1104/pp.125.1.437

Hamaji K, Nagira M, Yoshida K, et al (2009) Dynamic aspects of ion accumulation by vesicle traffic under salt stress in arabidopsis. Plant Cell Physiol 50:2023–2033. doi: 10.1093/pcp/pcp143

Hamam AM, Britto DT, Flam-Shepherd R, Kronzucker HJ (2016) Measurement of Differential Na(+) Efflux from Apical and Bulk Root Zones of Intact Barley and Arabidopsis Plants. Front Plant Sci 7:272. doi: 10.3389/fpls.2016.00272

Hanana M, Cagnac O, Yamaguchi T, et al (2007) A Grape Berry (Vitis vinifera L.) Cation/Proton Antiporter is Associated with Berry Ripening. Plant Cell Physiol 48:804–811. doi: 10.1093/pcp/pcm048

Hanin M, Ebel C, Ngom M, et al (2016) New Insights on Plant Salt Tolerance Mechanisms and

Their Potential Use for Breeding. Front Plant Sci 7:1787. doi: 10.3389/fpls.2016.01787

Haro R, Garciadeblas B, Rodriguez-Navarro A (1991) A novel P-type ATPase from yeast involved in sodium transport. FEBS Lett 291:189–191. doi: 10.1016/0014-5793(91)81280-L

He C, Yan J, Shen G, et al (2005) Expression of an Arabidopsis Vacuolar Sodium/Proton Antiporter Gene in Cotton Improves Photosynthetic Performance Under Salt Conditions and Increases Fiber Yield in the Field. Plant Cell Physiol 46:1848–1854. doi: 10.1093/pcp/pci201

Held K, Pascaud F, Eckert C, et al (2011) Calcium-dependent modulation and plasma membrane targeting of the AKT2 potassium channel by the CBL4/CIPK6 calcium sensor/protein kinase complex. Cell Res 21:1116–30. doi: 10.1038/cr.2011.50

Hellmer J, Teubner A, Zeilinger C (2003a) Conserved arginine and aspartate residues are critical for function of MjNhaP1, a Na+/H+ antiporter of M. jannaschii. FEBS Lett 542:32–6. doi: 10.1016/S0014-5793(03)00332-6

Hepworth SR, Klenz JE, Haughn GW (2006) UFO in the Arabidopsis inflorescence apex is required for floral-meristem identity and bract suppression. Planta 223:769–778. doi: 10.1007/s00425-005-0138-3

Hima Kumari P, Anil Kumar S, Ramesh K, et al (2018) Genome-Wide Identification and Analysis of Arabidopsis Sodium Proton Antiporter (NHX) and Human Sodium Proton Exchanger (NHE) Homologs in Sorghum bicolor. Genes (Basel) 9:. doi: 10.3390/genes9050236

Himabindu Y, Chakradhar T, Reddy MC, et al (2016) Salt-tolerant genes from halophytes are potential key players of salt tolerance in glycophytes. Environ Exp Bot 124:39–63. doi: 10.1016/J.ENVEXPBOT.2015.11.010

Hirsch RE, Lewis BD, Spalding EP, Sussman MR (1998) A role for the AKT1 potassium channel in plant nutrition. Science 280:918–21. doi: 10.1126/SCIENCE.280.5365.918

Ho SN, Hunt HD, Horton RM, et al (1989) Site-directed mutagenesis by overlap extension using the polymerase chain reaction. Gene 77:51–59. doi: 10.1016/0378-1119(89)90358-2

Horie M, Fujita K, Kato H, et al (2012) Association of the physical and chemical properties and the cytotoxicity of metal oxide nanoparticles: metal ion release, adsorption ability and specific surface area. Metallomics 4:350. doi: 10.1039/c2mt20016c

Hu C-D, Chinenov Y, Kerppola TK (2002) Visualization of interactions among bZIP and Rel family proteins in living cells using bimolecular fluorescence complementation. Mol Cell 9:789–98. doi: 10.1016/S1097-2765(02)00496-3

Hunte C, Screpanti E, Venturi M, et al (2005a) Structure of a Na+/H+ antiporter and insights into mechanism of action and regulation by pH. Nature 435:1197–1202. doi: 10.1038/nature03692

Hunte C, Screpanti E, Venturi M, et al (2005b) Structure of a Na+/H+ antiporter and insights into mechanism of action and regulation by pH. Nature 435:1197–1202. doi: 10.1038/nature03692

Huss M, Ingenhorst G, König S, et al (2002) Concanamycin A, the specific inhibitor of V-ATPases, binds to the Vo subunit c Downloaded from. JBC Papers in Press

Ikeda T, Schmitt B, Pouysségur J, et al (1997) Identification of cytoplasmic subdomains that control pH-sensing of the Na+/H+exchanger (NHE1): pH-maintenance, ATP-sensitive, and flexible loop domains. J Biochem 121:295–303. doi: 10.1093/oxfordjournals.jbchem.a021586

Inoue H, Noumi T, Tsuchiya T, Kanazawa H (1995) Essential aspartic acid residues, Asp-133, Asp-163 and Asp-164, in the transmembrane helices of a Na^+/H^+ antiporter (NhaA) from *Escherichia coli*. FEBS Lett 363:264–268. doi: 10.1016/0014-5793(95)00331-3

James-Kracke MR (1992) Quick and accurate method to convert BCECF fluorescence to pHi: Calibration in three different types of cell preparations. J Cell Physiol 151:596–603. doi: 10.1002/jcp.1041510320

Jeong E-Y, Seo PJ, Woo JC, Park C-M (2015) AKIN10 delays flowering by inactivating IDD8 transcription factor through protein phosphorylation in Arabidopsis. BMC Plant Biol 15:110. doi: 10.1186/s12870-015-0503-8

Ji H, Pardo JM, Batelli G, et al (2013) The Salt Overly Sensitive (SOS) Pathway: Established and Emerging Roles. Mol Plant 6:275–286. doi: 10.1093/mp/sst017

Jiang C, Belfield EJ, Mithani A, et al (2012) ROS-mediated vascular homeostatic control of root-to-shoot soil Na delivery in Arabidopsis. EMBO J 31:4359–70. doi: 10.1038/emboj.2012.273

Jiang X, Leidi EO, Pardo JM (2010) How do vacuolar NHX exchangers function in plant salt tolerance? Plant Signal Behav 5:792–795

Jin X, Sun T, Wang X, et al (2016) Wheat CBL-interacting protein kinase 25 negatively regulates salt tolerance in transgenic wheat. Sci Rep 6:28884. doi: 10.1038/srep28884

Julkowska MM, Testerink C (2015) Tuning plant signaling and growth to survive salt. Trends Plant Sci 20:586–94. doi: 10.1016/j.tplants.2015.06.008

Kader MA, Lindberg S (2010) Cytosolic calcium and pH signaling in plants under salinity stress. Plant Signal Behav 5:233–238. doi: 10.4161/psb.5.3.10740

Kader MA, Lindberg S, Seidel T, et al (2007) Sodium sensing induces different changes in free cytosolic calcium concentration and pH in salt-tolerant and -sensitive rice (Oryza sativa) cultivars. Physiol Plant 130:99–111. doi: 10.1111/j.1399-3054.2007.00890.x

Kane PM (2016) Proton Transport and pH Control in Fungi. Adv Exp Med Biol 892:33–68. doi: 10.1007/978-3-319-25304-6_3

Kardash E, Bandemer J, Raz E (2011) Imaging protein activity in live embryos using fluorescence resonance energy transfer biosensors. Nat Protoc 6:1835–1846. doi: 10.1038/nprot.2011.395

Katschnig D, Bliek T, Rozema J, Schat H (2015) Constitutive high-level SOS1 expression and absence of HKT1;1 expression in the salt-accumulating halophyte Salicornia dolichostachya. Plant Sci 234:144–154. doi: 10.1016/j.plantsci.2015.02.011

Keinath NF, Waadt R, Brugman R, et al (2015) Live Cell Imaging with R-GECO1 Sheds Light on flg22- and Chitin-Induced Transient [Ca(2+)]cyt Patterns in Arabidopsis. Mol Plant 8:1188–200. doi: 10.1016/j.molp.2015.05.006

Kiegle E, Moore CA, Haseloff J, et al (2000) Cell-type-specific calcium responses to drought, salt and cold in the Arabidopsis root. Plant J 23:267–278. doi: 10.1046/j.1365-313x.2000.00786.x

Koncz C, Schell J (1986) The promoter of TL-DNA gene 5 controls the tissue-specific expression of chimaeric genes carried by a novel type of Agrobacterium binary vector. MGG Mol Gen Genet 204:383–396. doi: 10.1007/BF00331014

Kondapalli KC, Hack A, Schushan M, et al (2013) Functional evaluation of autism-associated mutations in NHE9. Nat Commun 4:2510. doi: 10.1038/ncomms3510

Köster S, Pavkov-Keller T, Kühlbrandt W, et al (2011a) Structure of human Na +/H + exchanger NHE1 regulatory region in complex with calmodulin and Ca 2+. J Biol Chem 286:40954–40961. doi: 10.1074/jbc.M111.286906

Köster S, Pavkov-Keller T, Kühlbrandt W, Yildiz Ö (2011b) Structure of human Na+/H+ exchanger NHE1 regulatory region in complex with calmodulin and Ca2+. J Biol Chem 286:40954–61. doi: 10.1074/jbc.M111.286906

Krebs M, Beyhl D, Gorlich E, et al (2010) Arabidopsis V-ATPase activity at the tonoplast is required for efficient nutrient storage but not for sodium accumulation. Proc Natl Acad Sci 107:3251–3256. doi: 10.1073/pnas.0913035107

Kriegel A, Andrés Z, Medzihradszky A, et al (2015) Job Sharing in the Endomembrane System: Vacuolar Acidification Requires the Combined Activity of V-ATPase and V-PPase. Plant Cell 27:3383–3396. doi: 10.1105/tpc.15.00733

Kronzucker HJ, Britto DT (2011) Sodium transport in plants: a critical review. New Phytol 189:54–81. doi: 10.1111/j.1469-8137.2010.03540.x

Kudla J, Batistic O, Hashimoto K (2010) Calcium signals: the lead currency of plant information processing. Plant Cell 22:541–63. doi: 10.1105/tpc.109.072686

Kurusu T, Kuchitsu K, Tada Y (2015) Plant signaling networks involving Ca2+ and Rboh/Nox-mediated ROS production under salinity stress. Front Plant Sci 6:427. doi: 10.3389/fpls.2015.00427

Kusner DJ, Barton JA, Wen K-K, et al (2002) Regulation of phospholipase D activity by actin. Actin exerts bidirectional modulation of Mammalian phospholipase D activity in a polymerization-dependent, isoform-specific manner. J Biol Chem 277:50683–92. doi: 10.1074/jbc.M209221200

Kwiatkowska D (2008) Flowering and apical meristem growth dynamics. J Exp Bot 59:187–201. doi: 10.1093/jxb/erm290

Kwiatkowska D (2006) Flower primordium formation at the Arabidopsis shoot apex: quantitative analysis of surface geometry and growth. J Exp Bot 57:571–580. doi: 10.1093/jxb/erj042

Lacan D, Durand M Na+-K+ Exchange at the XylemlSymplast Boundary Its Significance in the Salt Sensitivity of Soybean

Lacroix J, Poët M, Maehrel C, Counillon L (2004) A mechanism for the activation of the Na/H exchanger NHE-1 by cytoplasmic acidification and mitogens. EMBO Rep 5:91–6. doi: 10.1038/sj.embor.7400035

Landau M, Herz K, Padan E, Ben-Tal N (2007) Model structure of the Na+/H+ exchanger 1 (NHE1): Functional and clinical implications. J Biol Chem 282:37854–37863. doi: 10.1074/jbc.M705460200

Landau M, Mayrose I, Rosenberg Y, et al (2005) ConSurf 2005: the projection of evolutionary conservation scores of residues on protein structures. Nucleic Acids Res 33:W299-302. doi: 10.1093/nar/gki370

Latz A, Mehlmer N, Zapf S, et al (2013) Salt stress triggers phosphorylation of the Arabidopsis vacuolar K+ channel TPK1 by calcium-dependent protein kinases (CDPKs). Mol Plant 6:1274–1289. doi: 10.1093/mp/sss158

Lee BL, Sykes BD, Fliegel L (2013a) Structural and functional insights into the cardiac Na + /H + exchanger. J Mol Cell Cardiol 61:60–67. doi: 10.1016/j.yjmcc.2012.11.019

Lee C, Kang HJ, von Ballmoos C, et al (2013c) A two-domain elevator mechanism for sodium/proton antiport. Nature 501:573–577. doi: 10.1038/nature12484

Lee C, Yashiro S, Dotson DL, et al (2014) Crystal structure of the sodium–proton antiporter NhaA dimer and new mechanistic insights. J Gen Physiol 144:529–544. doi: 10.1085/jgp.201411219

Leidi EO, Barragán V, Rubio L, et al (2010) The AtNHX1 exchanger mediates potassium compartmentation in vacuoles of transgenic tomato. Plant J 61:495–506. doi: 10.1111/j.1365-313X.2009.04073.x

Lena Kozachkov, Katia Herz and, Padan* E (2007) Functional and Structural Interactions of the Transmembrane Domain X of NhaA, Na+/H+ Antiporter of Escherichia coli, at Physiological pH†. doi: 10.1021/BI602393S

Lew RR (1991) Electrogenic Transport Properties of Growing Arabidopsis Root Hairs1 The Plasma Membrane Proton Pump and Potassium Channels

Li H-T, Liu H, Gao X-S, Zhang H (2009) Knock-out of Arabidopsis AtNHX4 gene enhances tolerance to salt stress. Biochem Biophys Res Commun 382:637–641. doi: 10.1016/J.BBRC.2009.03.091

Li J, Wang XQ, Watson MB, Assmann SM (2000) Regulation of abscisic acid-induced stomatal closure and anion channels by guard cell AAPK kinase. Science 287:300–3. doi: 10.1126/SCIENCE.287.5451.300

Li L, Kim B-G, Cheong YH, et al (2006) A Ca(2)+ signaling pathway regulates a K(+) channel for low-K response in Arabidopsis. Proc Natl Acad Sci U S A 103:12625–30. doi: 10.1073/pnas.0605129103

LIU H, TANG R, ZHANG Y, et al (2010) AtNHX3 is a vacuolar K+/H+ antiporter required for low-

potassium tolerance in Arabidopsis thaliana. Plant Cell Environ 33:1989–1999. doi: 10.1111/j.1365-3040.2010.02200.x

LIU H, WANG Q, YU M, et al (2008) Transgenic salt-tolerant sugar beet (*Beta vulgaris* L.) constitutively expressing an *Arabidopsis thaliana* vacuolar Na $^{+}$ /H $^{+}$ antiporter gene, *AtNHX3* , accumulates more soluble sugar but less salt in storage roots. Plant Cell Environ 31:1325–1334. doi: 10.1111/j.1365-3040.2008.01838.x

Long J, Barton MK (2000) Initiation of Axillary and Floral Meristems in Arabidopsis. Dev Biol 218:341–353. doi: 10.1006/DBIO.1999.9572

Luan S (2009) The CBL–CIPK network in plant calcium signaling. Trends Plant Sci 14:37–42. doi: 10.1016/j.tplants.2008.10.005

Luan S, Kudla J, Rodriguez-Concepcion M, et al (2002) Calmodulins and calcineurin B-like proteins: calcium sensors for specific signal response coupling in plants. Plant Cell 14 Suppl:S389-400. doi: 10.1105/TPC.001115

Luo Y, Scholl S, Doering A, et al (2015) V-ATPase activity in the TGN/EE is required for exocytosis and recycling in Arabidopsis. Nat plants 1:15094. doi: 10.1038/nplants.2015.94

Ma L, Zhang H, Sun L, et al (2012) NADPH oxidase AtrbohD and AtrbohF function in ROS-dependent regulation of Na+/K+ homeostasis in Arabidopsis under salt stress. J Exp Bot 63:305–317. doi: 10.1093/jxb/err280

Maathuis FJM (2014) Sodium in plants: Perception, signalling, and regulation of sodium fluxes. J Exp Bot. doi: 10.1093/jxb/ert326

Maathuis FJM, Ahmad I, Patishtan J (2014) Regulation of Na+ fluxes in plants. Front Plant Sci 5:467. doi: 10.3389/fpls.2014.00467

Maathuis FJM, Sanders D (2001) Sodium Uptake in Arabidopsis Roots Is Regulated by Cyclic Nucleotides 1. doi: 10.1104/pp.010502

Maes M, Rimon A, Kozachkov-Magrisso L, et al (2012) Revealing the ligand binding site of NhaA Na+/H+ antiporter and its pH dependence. J Biol Chem 287:38150–7. doi: 10.1074/jbc.M112.391128

Mager T, Rimon A, Padan E, Fendler K (2011) Transport mechanism and pH regulation of the Na+/H+ antiporter NhaA from Escherichia coli: an electrophysiological study. J Biol Chem 286:23570–81. doi: 10.1074/jbc.M111.230235

Malagoli P, Britto DT, Schulze LM, Kronzucker HJ (2008) Futile Na+ cycling at the root plasma membrane in rice (Oryza sativa L.): kinetics, energetics, and relationship to salinity tolerance. J Exp Bot 59:4109–17. doi: 10.1093/jxb/ern249

Manishankar P, Wang N, Köster P, et al (2018) Calcium signaling during salt stress and in the regulation of ion homeostasis. J Exp Bot 69:4215–4226. doi: 10.1093/jxb/ery201

Mansour MMF (2014) The plasma membrane transport systems and adaptation to salinity. J Plant Physiol 171:1787–1800. doi: 10.1016/j.jplph.2014.08.016

Mao J, Manik SMN, Shi S, et al (2016) Mechanisms and Physiological Roles of the CBL-CIPK

Networking System in Arabidopsis thaliana. Genes (Basel) 7:. doi: 10.3390/genes7090062

Marshansky V (2007) The V-ATPase a2-subunit as a putative endosomal pH-sensor. Biochem Soc Trans 35:1092–1099. doi: 10.1042/BST0351092

Martínez-Atienza J, Jiang X, Garciadeblas B, et al (2007) Conservation of the salt overly sensitive pathway in rice. Plant Physiol 143:1001–12. doi: 10.1104/pp.106.092635

Martínez-Muñoz GA, Kane P (2008) Vacuolar and plasma membrane proton pumps collaborate to achieve cytosolic pH homeostasis in yeast. J Biol Chem 283:20309–19. doi: 10.1074/jbc.M710470200

Martinière A, Bassil E, Jublanc E, et al (2013a) In vivo intracellular pH measurements in tobacco and Arabidopsis reveal an unexpected pH gradient in the endomembrane system. Plant Cell 25:4028–43. doi: 10.1105/tpc.113.116897

Martinière A, Desbrosses G, Sentenac H, Paris N (2013b) Development and properties of genetically encoded pH sensors in plants. Front Plant Sci 4:523. doi: 10.3389/fpls.2013.00523

Mäser P, Hosoo Y, Goshima S, et al (2002) Glycine residues in potassium channel-like selectivity filters determine potassium selectivity in four-loop-per-subunit HKT transporters from plants. Proc Natl Acad Sci U S A 99:6428–33. doi: 10.1073/pnas.082123799

Mäser P, Thomine S, Schroeder JI, et al (2001) Phylogenetic relationships within cation transporter families of Arabidopsis. Plant Physiol 126:1646–67

Mayrose I, Mitchell A, Pupko T (2005) Site-Specific Evolutionary Rate Inference: Taking Phylogenetic Uncertainty into Account. J Mol Evol 60:345–353. doi: 10.1007/s00239-004-0183-8

McCubbin T, Bassil E, Zhang S, Blumwald E (2014) Vacuolar Na+/H+ NHX-Type Antiporters Are Required for Cellular K+ Homeostasis, Microtubule Organization and Directional Root Growth. Plants 3:409–426. doi: 10.3390/plants3030409

Mendoza I, Rubio F, Rodriguez-Navarro A, Pardo JM (1994) The protein phosphatase calcineurin is essential for NaCl tolerance of Saccharomyces cerevisiae. J Biol Chem 269:8792–6

Miesenböck G, De Angelis DA, Rothman JE (1998) Visualizing secretion and synaptic transmission with pH-sensitive green fluorescent proteins. Nature 394:192–195. doi: 10.1038/28190

Mishima M, Wakabayashi S, Kojima C (2007) Solution structure of the cytoplasmic region of Na+/H+ exchanger 1 complexed with essential cofactor calcineurin B homologous protein 1. J Biol Chem 282:2741–51. doi: 10.1074/jbc.M604092200

Monshausen GB, Bibikova TN, Messerli MA, et al (2007) Oscillations in extracellular pH and reactive oxygen species modulate tip growth of Arabidopsis root hairs. Proc Natl Acad Sci U S A 104:20996–1001. doi: 10.1073/pnas.0708586104

Monshausen GB, Bibikova TN, Weisenseel MH, Gilroy S (2009) Ca2+ regulates reactive oxygen species production and pH during mechanosensing in Arabidopsis roots. Plant Cell 21:2341–56. doi: 10.1105/tpc.109.068395

Monshausen GB, Miller ND, Murphy AS, Gilroy S (2011) Dynamics of auxin-dependent Ca2+ and pH signaling in root growth revealed by integrating high-resolution imaging with automated computer vision-based analysis. Plant J 65:309–318. doi: 10.1111/j.1365-313X.2010.04423.x

Morita Y, Hoshino A (2018) Recent advances in flower color variation and patterning of Japanese morning glory and petunia. Breed Sci 68:128–138. doi: 10.1270/jsbbs.17107

Moseyko N, Feldman LJ (2001) Expression of pH-sensitive green fluorescent protein in Arabidopsis thaliana. Plant Cell Environ 24:557–63. doi: 10.1046/j.1365-3040.2001.00703.x

Munns R (2005) Genes and salt tolerance: bringing them together. New Phytol 167:645–663. doi: 10.1111/j.1469-8137.2005.01487.x

Munns R, James RA, Läuchli A (2006) Approaches to increasing the salt tolerance of wheat and other cereals. J Exp Bot 57:1025–1043. doi: 10.1093/jxb/erj100

Munns R, James RA, Xu B, et al (2012) Wheat grain yield on saline soils is improved by an ancestral Na+ transporter gene. Nat Biotechnol 30:360–364. doi: 10.1038/nbt.2120

Munns R, Tester M (2008) Mechanisms of Salinity Tolerance. Annu Rev Plant Biol 59:651–681. doi: 10.1146/annurev.arplant.59.032607.092911

Mustilli A-C, Merlot S, Vavasseur A, et al (2002) Arabidopsis OST1 protein kinase mediates the regulation of stomatal aperture by abscisic acid and acts upstream of reactive oxygen species production. Plant Cell 14:3089–99. doi: 10.1105/TPC.007906

Nieves-Cordones M, Caballero F, Martínez V, Rubio F (2012) Disruption of the Arabidopsis thaliana Inward-Rectifier K+ Channel AKT1 Improves Plant Responses to Water Stress. Plant Cell Physiol 53:423–432. doi: 10.1093/pcp/pcr194

Ogunrinde A, Munro K, Davidson A, et al (2017) Arabidopsis Calmodulin-Like Proteins, CML15 and CML16 Possess Biochemical Properties Distinct from Calmodulin and Show Non-overlapping Tissue Expression Patterns. Front Plant Sci 8:2175. doi: 10.3389/fpls.2017.02175

Oh D-H, Lee SY, Bressan RA, et al (2010) Intracellular consequences of SOS1 deficiency during salt stress. J Exp Bot 61:1205–13. doi: 10.1093/jxb/erp391

Oh D-H, Leidi E, Zhang Q, et al (2009) Loss of halophytism by interference with SOS1 expression. Plant Physiol 151:210–22. doi: 10.1104/pp.109.137802

Ohgaki R, van IJzendoorn SCD, Matsushita M, et al (2011) Organellar Na^+/H^+ Exchangers: Novel Players in Organelle pH Regulation and Their Emerging Functions. Biochemistry 50:443–450. doi: 10.1021/bi101082e

Ohnishi M, Fukada-Tanaka S, Hoshino A, et al (2005) Characterization of a Novel Na+/H+ Antiporter Gene InNHX2 and Comparison of InNHX2 with InNHX1, Which is Responsible

for Blue Flower Coloration by Increasing the Vacuolar pH in the Japanese Morning Glory. Plant Cell Physiol 46:259–267. doi: 10.1093/pcp/pci028

Orij R, Brul S, Smits GJ (2011) Intracellular pH is a tightly controlled signal in yeast. Biochim Biophys Acta - Gen Subj 1810:933–944. doi: 10.1016/j.bbagen.2011.03.011

Orij R, Urbanus ML, Vizeacoumar FJ, et al (2012) Genome-wide analysis of intracellular pH reveals quantitative control of cell division rate by pH(c) in Saccharomyces cerevisiae. Genome Biol 13:R80. doi: 10.1186/gb-2012-13-9-r80

Ottmann C, Marco S, Jaspert N, et al (2007) Structure of a 14-3-3 coordinated hexamer of the plant plasma membrane H+ -ATPase by combining X-ray crystallography and electron cryomicroscopy. Mol Cell 25:427–40. doi: 10.1016/j.molcel.2006.12.017

Padan E (2014) Functional and structural dynamics of NhaA, a prototype for Na+ and H+ antiporters, which are responsible for Na+ and H+ homeostasis in cells. Biochim Biophys Acta - Bioenerg 1837:1047–1062. doi: 10.1016/J.BBABIO.2013.12.007

Padan E, Kozachkov L, Herz K, Rimon A (2009) NhaA crystal structure: functional-structural insights. J Exp Biol 212:1593–603. doi: 10.1242/jeb.026708

Padan E, Michel H (2015) NhaA: A unique structural fold of secondary active transporters. Isr J Chem 55:1233–1239. doi: 10.1002/ijch.201500044

Padmanaban S, Chanroj S, Kwak JM, et al (2007) Participation of endomembrane cation/H+ exchanger AtCHX20 in osmoregulation of guard cells. Plant Physiol 144:82–93. doi: 10.1104/pp.106.092155

Pang T, Su X, Wakabayashi S, Shigekawa M (2001) Calcineurin homologous protein as an essential cofactor for Na+/H+ exchangers. J Biol Chem 276:17367–72. doi: 10.1074/jbc.M100296200

Pardo JM (2010) Biotechnology of water and salinity stress tolerance. Curr Opin Biotechnol 21:185–196. doi: 10.1016/J.COPBIO.2010.02.005

Pardo JM, Cubero B, Leidi EO, Quintero FJ (2006) Alkali cation exchangers: roles in cellular homeostasis and stress tolerance. J Exp Bot 57:1181–1199. doi: 10.1093/jxb/erj114

Paulino C, Wöhlert D, Kapotova E, et al (2014) Structure and transport mechanism of the sodium/proton antiporter MjNhaP1. Elife 3:1–21. doi: 10.7554/eLife.03583

Pei ZM, Ghassemian M, Kwak CM, et al (1998) Role of farnesyltransferase in ABA regulation of guard cell anion channels and plant water loss. Science 282:287–90. doi: 10.1126/SCIENCE.282.5387.287

Pittman JK (2012) Multiple Transport Pathways for Mediating Intracellular pH Homeostasis: The Contribution of H(+)/ion Exchangers. Front Plant Sci 3:11. doi: 10.3389/fpls.2012.00011

Pittman JK, Shigaki T, Hirschi KD (2005) Evidence of differential pH regulation of the *Arabidopsis* vacuolar Ca^{2+} /H^{+} antiporters CAX1 and CAX2. FEBS Lett 579:2648–2656. doi: 10.1016/j.febslet.2005.03.085

Plant PJ, Manolson MF, Grinstein S, Demaurex N (1999) Alternative mechanisms of vacuolar

acidification in H+-ATPase-deficient yeast. J Biol Chem 274:37270–37279. doi: 10.1074/jbc.274.52.37270

Platten JD, Cotsaftis O, Berthomieu P, et al (2006) Nomenclature for HKT transporters, key determinants of plant salinity tolerance. Trends Plant Sci 11:372–4. doi: 10.1016/j.tplants.2006.06.001

Pope BJ, Zierler-Gould KM, Kühne R, et al (2004) Solution structure of human cofilin: actin binding, pH sensitivity, and relationship to actin-depolymerizing factor. J Biol Chem 279:4840–8. doi: 10.1074/jbc.M310148200

Pouysségur J (1994) Mutation of calmodulin-binding site renders the Na+/H+ exchanger (NHE1) highly H(+)-sensitive and Ca2+ regulation-defective Hypoxia, nutrient deprivation & cancer Metabolism View project. Artic J Biol Chem

Preibisch S, Saalfeld S, Tomancak P (2009) Globally optimal stitching of tiled 3D microscopic image acquisitions. Bioinformatics 25:1463–1465. doi: 10.1093/bioinformatics/btp184

Proft M, Struhl K (2004) MAP Kinase-Mediated Stress Relief that Precedes and Regulates the Timing of Transcriptional Induction. Cell 118:351–361. doi: 10.1016/j.cell.2004.07.016

Pyo YJ, Gierth M, Schroeder JI, Cho MH (2010) High-Affinity K+ Transport in Arabidopsis: AtHAK5 and AKT1 Are Vital for Seedling Establishment and Postgermination Growth under Low-Potassium Conditions. PLANT Physiol 153:863–875. doi: 10.1104/pp.110.154369

Qiu Q-S (2016a) Plant endosomal NHX antiporters: Activity and function. Plant Signal Behav 11:e1147643. doi: 10.1080/15592324.2016.1147643

Qiu Q-S (2016b) AtNHX5 and AtNHX6: Roles in protein transport. Plant Signal Behav 11:e1184810. doi: 10.1080/15592324.2016.1184810

Qiu Q-S, Guo Y, Dietrich MA, et al (2002) Regulation of SOS1, a plasma membrane Na+/H+ exchanger in Arabidopsis thaliana, by SOS2 and SOS3. Proc Natl Acad Sci U S A 99:8436–41. doi: 10.1073/pnas.122224699

Qiu QS, Guo Y, Quintero FJ, et al (2004) Regulation of Vacuolar Na+/H+Exchange in Arabidopsis thaliana by the Salt-Overly-Sensitive (SOS) Pathway. J Biol Chem 279:207–215. doi: 10.1074/jbc.M307982200

Quattrocchio F, Verweij W, Kroon A, et al (2006) PH4 of Petunia is an R2R3 MYB protein that activates vacuolar acidification through interactions with basic-helix-loop-helix transcription factors of the anthocyanin pathway. Plant Cell 18:1274–91. doi: 10.1105/tpc.105.034041

Quintero FJ, Blatt MR, Pardo JM (2000) Functional conservation between yeast and plant endosomal Na^+/H^+ antiporters [1]. FEBS Lett 471:224–228. doi: 10.1016/S0014-5793(00)01412-5

Quintero FJ, Martinez-Atienza J, Villalta I, et al (2011) Activation of the plasma membrane Na/H antiporter Salt-Overly-Sensitive 1 (SOS1) by phosphorylation of an auto-inhibitory C-terminal domain. Proc Natl Acad Sci U S A 108:2611–6. doi: 10.1073/pnas.1018921108

Quintero FJ, Ohta M, Shi H, et al (2002) Reconstitution in yeast of the Arabidopsis SOS signaling pathway for Na+ homeostasis. Proc Natl Acad Sci U S A 99:9061–6. doi: 10.1073/pnas.132092099

Ragel P, Ródenas R, García-Martín E, et al (2015) The CBL-Interacting Protein Kinase CIPK23 Regulates HAK5-Mediated High-Affinity K+ Uptake in Arabidopsis Roots. Plant Physiol 169:2863–73. doi: 10.1104/pp.15.01401

Rajan S, Wischmeyer E, Xin Liu G, et al (2000) TASK-3, a novel tandem pore domain acid-sensitive K+ channel. An extracellular histiding as pH sensor. J Biol Chem 275:16650–7. doi: 10.1074/jbc.M000030200

Ranty B, Aldon D, Galaud J-P (2006) Plant calmodulins and calmodulin-related proteins: multifaceted relays to decode calcium signals. Plant Signal Behav 1:96–104

Reddy GV, Heisler MG, Ehrhardt DW, Meyerowitz EM (2004) Real-time lineage analysis reveals oriented cell divisions associated with morphogenesis at the shoot apex of Arabidopsis thaliana. Development 131:4225–37. doi: 10.1242/dev.01261

Reeves PH, Coupland G (2001) Analysis of Flowering Time Control in Arabidopsis by Comparison of Double and Triple Mutants 1

Reguera M, Bassil E, Tajima H, et al (2015) pH Regulation by NHX-Type Antiporters Is Required for Receptor-Mediated Protein Trafficking to the Vacuole in Arabidopsis. Plant Cell 27:1200–1217. doi: 10.1105/tpc.114.135699

Rimon A, Dwivedi M, Friedler A, Padan E (2018) Asp133 Residue in NhaA Na+/H+ Antiporter Is Required for Stability Cation Binding and Transport. J Mol Biol 430:867–880. doi: 10.1016/J.JMB.2018.01.014

Rimon A, Gerchman Y, Olami Y, et al (1995) Replacements of histidine 226 of NhaA-Na+/H+ antiporter of Escherichia coli. Cysteine (H226C) or serine (H226S) retain both normal activity and pH sensitivity, aspartate (H226D) shifts the pH profile toward basic pH, and alanine (H226A) inactivates the carrier at all pH values. J Biol Chem 270:26813–7. doi: 10.1074/JBC.270.45.26813

Rimon A, Tzubery T, Padan E (2007) Monomers of the NhaA Na+/H+ antiporter of Escherichia coli are fully functional yet dimers are beneficial under extreme stress conditions at alkaline pH in the presence of Na+ or Li+. J Biol Chem 282:26810–21. doi: 10.1074/jbc.M704469200

Rincón-Zachary M, Teaster ND, Sparks JA, et al (2010) Fluorescence resonance energy transfer-sensitized emission of yellow cameleon 3.60 reveals root zone-specific calcium signatures in Arabidopsis in response to aluminum and other trivalent cations. Plant Physiol 152:1442–58. doi: 10.1104/pp.109.147256

Rodríguez-Navarro A, Ramos J (1984) Dual system for potassium transport in Saccharomyces cerevisiae. J Bacteriol 159:940–5

Rodríguez-Rosales MP, Gálvez FJ, Huertas R, et al (2009) Plant NHX cation/proton antiporters. Plant Signal Behav 4:265–276. doi: 10.4161/psb.4.4.7919

Rodriguez-Rosales MP, Jiang X, Gálvez FJ, et al (2008) Overexpression of the tomato K+/H+

antiporter LeNHX2 confers salt tolerance by improving potassium compartmentalization. New Phytol 179:366–77

Roos W, Viehweger K, Dordschbal B, et al (2006) Intracellular pH signals in the induction of secondary pathways – The case of Eschscholzia californica. J Plant Physiol 163:369–381. doi: 10.1016/J.JPLPH.2005.11.012

Roy SJ, Negrão S, Tester M (2014) Salt resistant crop plants. Curr Opin Biotechnol 26:115–124. doi: 10.1016/j.copbio.2013.12.004

Rubio F, Alemán F, Nieves-Cordones M, Martínez V (2010) Studies on Arabidopsis athak5, atakt1 double mutants disclose the range of concentrations at which AtHAK5, AtAKT1 and unknown systems mediate K+ uptake. Physiol Plant 139:220–228. doi: 10.1111/j.1399-3054.2010.01354.x

Rubio F, Nieves-Cordones M, Alemán F, Martínez V (2008) Relative contribution of AtHAK5 and AtAKT1 to K^+ uptake in the high-affinity range of concentrations. Physiol Plant 134:598–608. doi: 10.1111/j.1399-3054.2008.01168.x

Sambrook J, Fritsch EF, Maniatis T (1989) Molecular cloning : a laboratory manual, 2nd ed. Cold Spring Harbor Laboratory, Cold Spring Harbor N.Y.

Sanders D, Pelloux J, Brownlee C, Harper JF (2002) Calcium at the crossroads of signaling. Plant Cell 14 Suppl:S401-17. doi: 10.1105/TPC.002899

Sandmann M, Skłodowski K, Gajdanowicz P, et al (2011) The K (+) battery-regulating Arabidopsis K (+) channel AKT2 is under the control of multiple post-translational steps. Plant Signal Behav 6:558–62. doi: 10.4161/PSB.6.4.14908

Saponaro A, Porro A, Chaves-Sanjuan A, et al (2017) Fusicoccin Activates KAT1 Channels by Stabilizing Their Interaction with 14-3-3 Proteins. 29:2570–2580. doi: 10.1105/tpc.17.00375

Sato Y, Sakaguchi M (2005) Topogenic properties of transmembrane segments of Arabidopsis thaliana NHX1 reveal a common topology model of the Na+/H+ exchanger family. J Biochem 138:425–431. doi: 10.1093/jb/mvi132

Schaller A, Oecking C (1999) Modulation of Plasma Membrane H-ATPase Activity Differentially Activates Wound and Pathogen Defense Responses in Tomato Plants

Schindelin J, Arganda-Carreras I, Frise E, et al (2012) Fiji: an open-source platform for biological-image analysis. Nat Methods 9:676–82. doi: 10.1038/nmeth.2019

Schubiger CB, Mourin M, Resch CT, et al (2017) Mutations of a Single Glycine in Vc-NhaP2, a Cation-Proton Antiporter in Vibrio cholerae, Confer the Ability to Exchange Li+ for H+. J Mol Biol Biotechnol 2:

Schulte A, Lorenzen I, Böttcher M, Plieth C (2006) A novel fluorescent pH probe for expression in plants. Plant Methods 2:7. doi: 10.1186/1746-4811-2-7

Schumacher K (2014) pH in the plant endomembrane system-an import and export business. Curr Opin Plant Biol 22:71–76. doi: 10.1016/j.pbi.2014.09.005

Schushan M, Xiang M, Bogomiakov P, et al (2010) Model-guided mutagenesis drives

functional studies of human NHA2, implicated in hypertension. J Mol Biol 396:1181–96. doi: 10.1016/j.jmb.2009.12.055

Sekler I, Kobayashi S, Kopito RR (1996) A cluster of cytoplasmic histidine residues specifies pH dependence of the AE2 plasma membrane anion exchanger. Cell 86:929–35

Shabala S, Cuin TA (2008) Potassium transport and plant salt tolerance. Physiol Plant 133:651–669. doi: 10.1111/j.1399-3054.2007.01008.x

Shabala S, Demidchik V, Shabala L, et al (2006) Extracellular Ca2+ ameliorates NaCl-induced K+ loss from Arabidopsis root and leaf cells by controlling plasma membrane K+ -permeable channels. Plant Physiol 141:1653–65. doi: 10.1104/pp.106.082388

Shabala S, Mackay A (2011) Ion Transport in Halophytes. Adv Bot Res 57:151–199. doi: 10.1016/B978-0-12-387692-8.00005-9

Shabala S, Pottosin I (2014) Regulation of potassium transport in plants under hostile conditions: implications for abiotic and biotic stress tolerance. Physiol Plant 151:257–279. doi: 10.1111/ppl.12165

Shabala S, Wu H, Bose J (2015) Salt stress sensing and early signalling events in plant roots: Current knowledge and hypothesis. Plant Sci 241:109–119. doi: 10.1016/j.plantsci.2015.10.003

Sharma N, Xin R, Kim D-H, et al (2016) NO FLOWERING IN SHORT DAY (NFL) is a bHLH transcription factor that promotes flowering specifically under short-day conditions in Arabidopsis. Development 143:682–90. doi: 10.1242/dev.128595

Shen J, Zeng Y, Zhuang X, et al (2013) Organelle pH in the Arabidopsis Endomembrane System. Mol Plant 6:1419–1437. doi: 10.1093/MP/SST079

Shi H (2002) The Putative Plasma Membrane Na+/H+ Antiporter SOS1 Controls Long-Distance Na+ Transport in Plants. PLANT CELL ONLINE 14:465–477. doi: 10.1105/tpc.010371

Shi H, Ishitani M, Kim C, Zhu JK (2000) The Arabidopsis thaliana salt tolerance gene SOS1 encodes a putative Na+/H+ antiporter. Proc Natl Acad Sci U S A 97:6896–901. doi: 10.1073/pnas.120170197

Shi H, Lee B, Wu S-J, Zhu J-K (2003) Overexpression of a plasma membrane Na+/H+ antiporter gene improves salt tolerance in Arabidopsis thaliana. Nat Biotechnol 21:81–85. doi: 10.1038/nbt766

Shi H, Quintero FJ, Pardo JM, Zhu J-K (2002) The putative plasma membrane Na(+)/H(+) antiporter SOS1 controls long-distance Na(+) transport in plants. Plant Cell 14:465–77. doi: 10.1105/TPC.010371

Shi H, Zhu J-K (2002) Regulation of expression of the vacuolar Na+/H+ antiporter gene AtNHX1 by salt stress and abscisic acid. Plant Mol Biol 50:543–50

Shigeo Wakabayashi *, Toshitaro Ikeda, Takahiro Iwamoto, et al (1997) Calmodulin-Binding Autoinhibitory Domain Controls “pH-Sensing” in the Na+/H+ Exchanger NHE1 through Sequence-Specific Interaction†. doi: 10.1021/BI9715472

Slepkov ER, Rainey JK, Sykes BD, Fliegel L (2007) Structural and functional analysis of the Na +

/H + exchanger. Biochem J 401:623–633. doi: 10.1042/BJ20061062

Smyth DR, Bowman JL, Meyerowitz EM (1990) Early Flower Development in Arabídopsis. American Society of Plant Physiologists

Snabaitis AK, Cuello F, Avkiran M (2008a) Protein Kinase B/Akt Phosphorylates and Inhibits the Cardiac Na+/H+ Exchanger NHE1. Circ Res 103:881–890. doi: 10.1161/CIRCRESAHA.108.175877

Snabaitis AK, Cuello F, Avkiran M (2008b) Protein kinase B/Akt phosphorylates and inhibits the cardiac Na+/H+ exchanger NHE1. Circ Res 103:881–90. doi: 10.1161/CIRCRESAHA.108.175877

Snedden WA, Fromm H (2001) Calmodulin as a versatile calcium signal transducer in plants. New Phytol 151:35–66. doi: 10.1046/j.1469-8137.2001.00154.x

Sondergaard TE, Schulz A, Palmgren MG, et al (2004) Energization of Transport Processes in Plants. Roles of the Plasma Membrane H+-ATPase. PLANT Physiol 136:2475–2482. doi: 10.1104/pp.104.048231

Srivastava J, Barber DL, Jacobson MP (2007) Intracellular pH Sensors: Design Principles and Functional Significance. Physiology 22:30–39. doi: 10.1152/physiol.00035.2006

Sun F, Zhang W, Hu H, et al (2008) Salt modulates gravity signaling pathway to regulate growth direction of primary roots in Arabidopsis. Plant Physiol 146:178–88. doi: 10.1104/pp.107.109413

SUN J, WANG M-J, DING M-Q, et al (2010) H2O2 and cytosolic Ca2+ signals triggered by the PM H+-coupled transport system mediate K+/Na+ homeostasis in NaCl-stressed Populus euphratica cells. Plant Cell Environ 33:943–958. doi: 10.1111/j.1365-3040.2010.02118.x

Sunarpi, Horie T, Motoda J, et al (2005) Enhanced salt tolerance mediated by AtHKT1 transporter-induced Na+ unloading from xylem vessels to xylem parenchyma cells. Plant J 44:928–938. doi: 10.1111/j.1365-313X.2005.02595.x

Swanson SJ, Jones RL, Cervantes-Cervantes M, et al (1996) Gibberellic Acid Induces Vacuolar Acidification in Barley Aleurone. PLANT CELL ONLINE 8:2211–2221. doi: 10.1105/tpc.8.12.2211

Sze H, Chanroj S (2018) Plant Endomembrane Dynamics: Studies of K+/H+ Antiporters Provide Insights on the Effects of pH and Ion Homeostasis. Plant Physiol 177:875–895. doi: 10.1104/pp.18.00142

Sze H, Padmanaban S, Honys D, et al (2004) Expression Patterns of a Novel AtCHX Gene Family Highlight Potential Roles in Osmotic Adjustment and K 1 Homeostasis in Pollen Development 1[w]. doi: 10.1104/pp.104.046003

Szyroki A, Ivashikina N, Dietrich P, et al (2001) KAT1 is not essential for stomatal opening. Proc Natl Acad Sci U S A 98:2917–21. doi: 10.1073/pnas.051616698

Takáč T, Vadovič P, Pechan T, et al (2016) Comparative proteomic study of Arabidopsis mutants mpk4 and mpk6. Sci Rep 6:28306. doi: 10.1038/srep28306

Tarsio M, Zheng H, Smardon AM, et al (2011) Consequences of loss of Vph1 protein-containing

vacuolar ATPases (V-ATPases) for overall cellular pH homeostasis. J Biol Chem 286:28089–96. doi: 10.1074/jbc.M111.251363

Tester M, Davenport R (2003) Na+ tolerance and Na+ transport in higher plants. Ann Bot 91:503–27. doi: 10.1093/AOB/MCG058

Thoday-Kennedy EL, Jacobs AK, Roy SJ (2015) The role of the CBL–CIPK calcium signalling network in regulating ion transport in response to abiotic stress. Plant Growth Regul 76:3–12. doi: 10.1007/s10725-015-0034-1

Thompson AN, Posson DJ, Parsa P V, Nimigean CM (2008) Molecular mechanism of pH sensing in KcsA potassium channels

Tian F, Chang E, Li Y, et al (2017) Expression and integrated network analyses revealed functional divergence of NHX-type Na+/H+ exchanger genes in poplar. Sci Rep 7:2607. doi: 10.1038/s41598-017-02894-8

Tidow H, Nissen P (2013) Structural diversity of calmodulin binding to its target sites. FEBS J 280:5551–5565. doi: 10.1111/febs.12296

Törnroth-Horsefield S, Wang Y, Hedfalk K, et al (2006) Structural mechanism of plant aquaporin gating. Nature 439:688–694. doi: 10.1038/nature04316

Uzdavinys P, Coinçon M, Nji E, et al (2017) Dissecting the proton transport pathway in electrogenic Na + /H + antiporters. Proc Natl Acad Sci 114:E1101–E1110. doi: 10.1073/pnas.1614521114

Vahisalu T, Kollist H, Wang Y-F, et al (2008) SLAC1 is required for plant guard cell S-type anion channel function in stomatal signalling. Nature 452:487–91. doi: 10.1038/nature06608

Venema K, Belver A, Marin-Manzano MC, et al (2003) A novel intracellular K+/H+ antiporter related to Na+/H+ antiporters is important for K+ ion homeostasis in plants. J Biol Chem 278:22453–9. doi: 10.1074/jbc.M210794200

Venema K, Quintero FJ, Pardo JM, Donaire JP (2002) The arabidopsis Na+/H+ exchanger AtNHX1 catalyzes low affinity Na+ and K+ transport in reconstituted liposomes. J Biol Chem 277:2413–8. doi: 10.1074/jbc.M105043200

Verslues PE, Agarwal M, Katiyar-Agarwal S, et al (2006) Methods and concepts in quantifying resistance to drought, salt and freezing, abiotic stresses that affect plant water status. Plant J 45:523–539. doi: 10.1111/j.1365-313X.2005.02593.x

Véry A-A, Sentenac H (2003) M OLECULAR M ECHANISMS AND R EGULATION OF K $^{+}$ T RANSPORT IN H IGHER P LANTS. Annu Rev Plant Biol 54:575–603. doi: 10.1146/annurev.arplant.54.031902.134831

Viehweger K, Dordschbal B, Roos W (2002) Elicitor-activated phospholipase A(2) generates lysophosphatidylcholines that mobilize the vacuolar H(+) pool for pH signaling via the activation of Na(+)-dependent proton fluxes. Plant Cell 14:1509–25. doi: 10.1105/TPC.002329

Viotti C, Krüger F, Krebs M, et al (2013) The endoplasmic reticulum is the main membrane source for biogenesis of the lytic vacuole in Arabidopsis. Plant Cell 25:3434–49. doi:

10.1105/tpc.113.114827

Voinnet O, Rivas S, Mestre P, Baulcombe D (2003) Retracted: An enhanced transient expression system in plants based on suppression of gene silencing by the p19 protein of tomato bushy stunt virus. Plant J 33:949–956. doi: 10.1046/j.1365-313X.2003.01676.x

Waadt R, Krebs M, Kudla J, Schumacher K (2017) Multiparameter imaging of calcium and abscisic acid and high-resolution quantitative calcium measurements using R-GECO1-mTurquoise in Arabidopsis. New Phytol 216:303–320. doi: 10.1111/nph.14706

Waadt R, Kudla J (2008) In plant visualization of protein interactions using bimolecular fluorescence complementation (BiFC). Cold Spring Harb Protoc 3:pdb.prot4995-pdb.prot4995. doi: 10.1101/pdb.prot4995

Wakabayashi S, Fafournoux P, Sardet C, Pouysségur J (1992) The Na+/H+ antiporter cytoplasmic domain mediates growth factor signals and controls "H(+)-sensing". Proc Natl Acad Sci U S A 89:2424–8

Walia A, Waadt R, Jones AM (2018) Genetically Encoded Biosensors in Plants: Pathways to Discovery. Annu Rev Plant Biol 69:497–524. doi: 10.1146/annurev-arplant-042817-040104

Wallin E, von Heijne G (1998) Genome-wide analysis of integral membrane proteins from eubacterial, archaean, and eukaryotic organisms. Protein Sci 7:1029–38. doi: 10.1002/pro.5560070420

Wang D, Balkovetz DF, Warnock DG (1995) Mutational analysis of transmembrane histidines in the amiloride-sensitive Na+/H+ exchanger. Am J Physiol 269:C392-402. doi: 10.1152/ajpcell.1995.269.2.C392

Wang J, Zuo K, Wu W, et al (2003) Molecular Cloning and Characterization of a New Na^+/H^+ Antiporter Gene from *Brassica napus*. DNA Seq 14:351–358. doi: 10.1080/10855660310001596211

Wang L, Feng X, Zhao H, et al (2014) Functional Analysis of the Na+,K+/H+ Antiporter PeNHX3 from the Tree Halophyte Populus euphratica in Yeast by Model-Guided Mutagenesis. PLoS One 9:e104147. doi: 10.1371/journal.pone.0104147

Wang W, Li Y, Zhang Y, et al (2007) Comparative expression analysis of three genes from the Arabidopsis vacuolar Na+/H+ antiporter (AtNHX) family in relation to abiotic stresses. Chinese Sci Bull 52:1754–1763. doi: 10.1007/s11434-007-0278-x

Wang W, Malcolm BA (1999) Two-Stage PCR Protocol Allowing Introduction of Multiple Mutations, Deletions and Insertions Using QuikChange ^{TM} Site-Directed Mutagenesis. Biotechniques 26:680–682. doi: 10.2144/99264st03

Waterhouse A, Bertoni M, Bienert S, et al (2018) SWISS-MODEL: homology modelling of protein structures and complexes. Nucleic Acids Res 46:W296–W303. doi: 10.1093/nar/gky427

Webb AAR, McAinsh MR, Taylor JE, Hetherington AM (1996) Calcium Ions as Intracellular Second Messengers in Higher Plants.

Whiteman S-A, Nühse TS, Ashford DA, et al (2008a) A proteomic and phosphoproteomic analysis of *Oryza sativa* plasma membrane and vacuolar membrane. Plant J 56:146–156. doi: 10.1111/j.1365-313X.2008.03578.x

Whiteman S-A, Serazetdinova L, Jones AME, et al (2008b) Identification of novel proteins and phosphorylation sites in a tonoplast enriched membrane fraction of Arabidopsis thaliana. Proteomics 8:3536–3547. doi: 10.1002/pmic.200701104

Wigoda N, Grunwald Y, Sade N, et al (2017) Bundle-sheath cells are leaf "water valves" controlled via xylem acidification by H +-ATPase One-sentence summary: Cells enwrapping the leaf veins control the leaf hydraulic conductance by xylem sap pH regulated by a proton-pump

Wöhlert D, Kühlbrandt W, Yildiz Ö (2014) Structure and substrate ion binding in the sodium/proton antiporter PaNhaP. Elife 3:e03579. doi: 10.7554/eLife.03579

Wu C, Gao X, Kong X, et al (2009) Molecular Cloning and Functional Analysis of a Na+/H+ Antiporter Gene ThNHX1 from a Halophytic Plant Thellungiella halophila. Plant Mol Biol Report 27:1–12. doi: 10.1007/s11105-008-0048-1

Wu SJ, Ding L, Zhu JK (1996) SOS1, a Genetic Locus Essential for Salt Tolerance and Potassium Acquisition. Plant Cell 8:617–627. doi: 10.1105/tpc.8.4.617

Würtele M, Jelich-Ottmann C, Wittinghofer A, Oecking C (2003) Structural view of a fungal toxin acting on a 14-3-3 regulatory complex. EMBO J 22:987–94. doi: 10.1093/emboj/cdg104

Xia T, Apse MP, Aharon GS, Blumwald E (2002) Identification and characterization of a NaCl-inducible vacuolar Na+/H+ antiporter in Beta vulgaris. Physiol Plant 116:206–212. doi: 10.1034/j.1399-3054.2002.1160210.x

Xu H, Jiang X, Zhan K, et al (2008) Functional characterization of a wheat plasma membrane Na+/H+ antiporter in yeast. Arch Biochem Biophys 473:8–15. doi: 10.1016/j.abb.2008.02.018

Xu J, Li H-D, Chen L-Q, et al (2006) A protein kinase, interacting with two calcineurin B-like proteins, regulates K+ transporter AKT1 in Arabidopsis. Cell 125:1347–60. doi: 10.1016/j.cell.2006.06.011

Yamaguchi T, Aharon GS, Sottosanto JB, Blumwald E (2005) Vacuolar Na+/H+ antiporter cation selectivity is regulated by calmodulin from within the vacuole in a Ca2+- and pH-dependent manner. Proc Natl Acad Sci U S A 102:16107–12. doi: 10.1073/pnas.0504437102

Yamaguchi T, Apse MP, Shi H, Blumwald E (2003) Topological analysis of a plant vacuolar Na+/H+ antiporter reveals a luminal C terminus that regulates antiporter cation selectivity. Proc Natl Acad Sci U S A 100:12510–5. doi: 10.1073/pnas.2034966100

Yamaguchi T, Fukada-Tanaka S, Inagaki Y, et al (2001) Genes Encoding the Vacuolar Na+/H+ Exchanger and Flower Coloration. Plant Cell Physiol 42:451–461. doi: 10.1093/pcp/pce080

Yamniuk AP, Vogel HJ (2005) Structural investigation into the differential target enzyme

regulation displayed by plant calmodulin isoforms. Biochemistry 44:3101–3111. doi: 10.1021/bi047770y

Ye C-Y, Zhang H-C, Chen J-H, et al (2009) Molecular characterization of putative vacuolar NHX-type Na^+/H^+ exchanger genes from the salt-resistant tree *Populus euphratica*. Physiol Plant 137:166–174. doi: 10.1111/j.1399-3054.2009.01269.x

Yokoi S, Quintero FJ, Cubero B, et al (2002) Differential expression and function of Arabidopsis thaliana NHX Na+/H+ antiporters in the salt stress response. Plant J 30:529–539. doi: 10.1046/j.1365-313X.2002.01309.x

Yoshida K, Kawachi M, Mori M, et al (2005) The Involvement of Tonoplast Proton Pumps and Na+(K+)/H+ Exchangers in the Change of Petal Color During Flower Opening of Morning Glory, Ipomoea tricolor cv. Heavenly Blue. Plant Cell Physiol 46:407–415. doi: 10.1093/pcp/pci057

Yoshida K, Kondo T, Okazaki Y, Katou K (1995) Cause of blue petal colour. Nature 373:291–291. doi: 10.1038/373291a0

Yoshida K, Miki N, Momonoi K, et al (2009) Synchrony between flower opening and petal-color change from red to blue in morning glory, Ipomoea tricolor cv. Heavenly Blue. Proc Jpn Acad Ser B Phys Biol Sci 85:187–97. doi: 10.2183/PJAB.85.187

Yu HQ, Yong TM, Li HJ, et al (2015) Overexpression of a phospholipase Dα gene from Ammopiptanthus nanus enhances salt tolerance of phospholipase Dα1-deficient Arabidopsis mutant. Planta 242:1495–1509. doi: 10.1007/s00425-015-2390-5

Yu L, Nie J, Cao C, et al (2010a) Phosphatidic acid mediates salt stress response by regulation of MPK6 in Arabidopsis thaliana. New Phytol 188:762–773. doi: 10.1111/j.1469-8137.2010.03422.x

Yu L, Nie J, Cao C, et al (2010b) Phosphatidic acid mediates salt stress response by regulation of MPK6 in Arabidopsis thaliana. New Phytol 188:762–773. doi: 10.1111/j.1469-8137.2010.03422.x

Zhang H-X, Blumwald E (2001) Transgenic salt-tolerant tomato plants accumulate salt in foliage but not in fruit. Nat Biotechnol 19:765–768. doi: 10.1038/90824

Zhang T, Chen S, Harmon AC (2016) Protein-protein interactions in plant mitogen-activated protein kinase cascades. J Exp Bot 67:607–618. doi: 10.1093/jxb/erv508

Zhang Y, Pines G, Kanner BI (1994) Histidine 326 is critical for the function of GLT-1, a (Na+ + K+)-coupled glutamate transporter from rat brain. J Biol Chem 269:19573–7

Zheng J, Han SW, Rodriguez-Welsh MF, Rojas-Pierce M (2014) Homotypic Vacuole Fusion Requires VTI11 and Is Regulated by Phosphoinositides. Mol Plant 7:1026–1040. doi: 10.1093/mp/ssu019